Studies on the frost resistance of natural stone

Wessman, Lubica

1997

LUNDS TEKNISKA HÖGSKOLA
Byggnadsmaterial

LUND UNIVERSITY
LUND INSTITUTE OF TECHNOLOGY
Division of Building Materials

Studies on the frost resistance of natural stone

Lubica Wessman

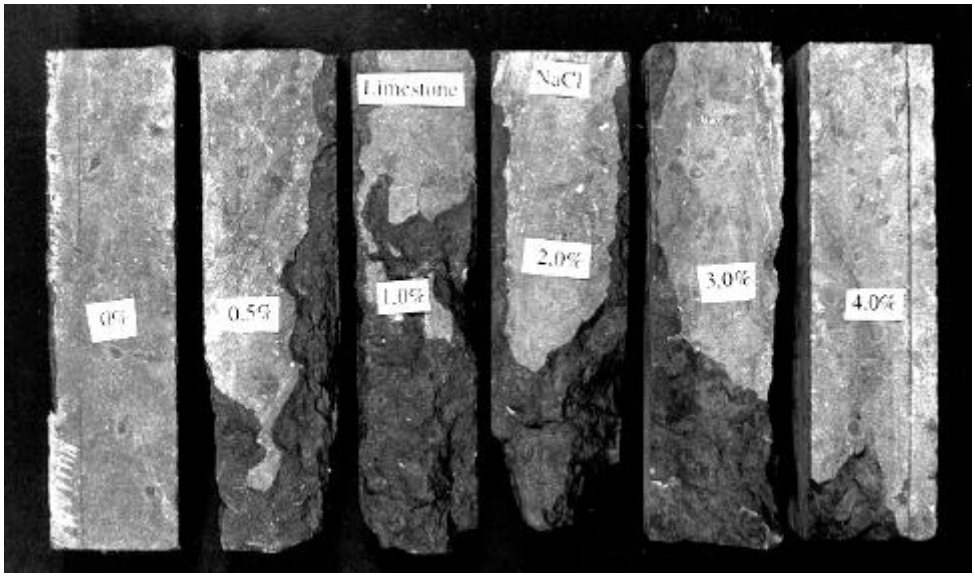

Report TVBM-3077
Lund 1997

LUNDS TEKNISKA HÖGSKOLA
Byggnadsmaterial

LUND UNIVERSITY
LUND INSTITUTE OF TECHNOLOGY
Division of Building Materials

Studies on the frost resistance of natural stone

Lubica Wessman

Report TVBM-3077 Licentiate Thesis
Lund 1997

ISRN: LUTVDG/TVBM--97/3077--SE(1-199)
ISSN: 0348-7911 TVBM

Lund Institute of Technology
Division of Building Materials
Box 118
S-221 00 Lund, Sweden

Printed in Sweden
KFS AB, Lund
Lund 1997

Preface

This work was performed at the Division of Building Materials, Lund Institute of Technology, under the supervision of Professor Göran Fagerlund. The project was financially supported by the Central Board of National Antiquities.

I would like to thank Professor Göran Fagerlund for initiating this project and for guidance and valuable and interesting discussions. I would also like to thank Dr Runo Löfvendahl at the Central Board of National Antiquities for advice and help concerning the stone species. I thank Dr. Wojciech Roszak for performing the experiments with the cup method and Dr Göran Hedenblad for evaluating the results from these experiments. I thank Annika Wirje for the work on obtaining the porosity and density data of limestone from Borghamn and Thomas Carlsson for help with the thin section microscopy. I also thank all other people working at the Division of Building Materials: laboratory personnel, secretaries and doctoral students as well as researchers for help and support. A special thank you to my roommate Mårten Janz for always trying to answer all my questions.

Contents

Summary

This work deals with the effects of freeze-thawing on the deterioration of some types of natural stone, especially stones frequently used in old buildings in Sweden. Laboratory studies were performed mainly on Gotland sandstone from the Gotland Island in the Baltic Sea. This stone has been widely used in old buildings in the whole Baltic region, and it is often badly deteriorated. A granite from Bohuslän Province in Sweden was studied as well, as there are problems with degradation of the granite rock carvings from the Bronze Age. The Gotland sandstone studied here is very porous and highly water absorptive. Its porosity sometimes exceeds 20%, whereas the granite is extremely dense with a porosity of 0.6%. In order to include stones with intermediate porosities, limestones from the island Öland and the village Borghamn, with porosities of about 2 to 3%, were studied. These types of limestone have also been widely used in old buildings in Sweden.

It is important to have some knowledge about the internal structure of the stones in order to be able to understand the degradation mechanism. The total open porosity was measured by weighing stone prisms under dry and water-saturated conditions in air and submerged in water. The pore structure was studied with thin section microscopy. Sorption isotherms were also measured, and a complementary study with mercury porosimetry was done.

In the freezing process, as well as in almost all other processes concerning deterioration of stone, water plays a very important role. Therefore, the moisture behaviour of the stones was studied by conventional methods such as the capillary suction and the cup method, which give information about the moisture permeability of the stone at different moisture levels. Many of the stones became completely saturated after a relatively short time of capillary suction, which is a rather unusual property in a building material and a property that makes the stones vulnerable to frost when the porosity is high such as in sandstone.

Several freeze-thaw tests of different types were performed on the stones in order to study the effects of water content and internal and external salt solutions on their frost resistance. The salts used were NaCl and Na_2SO_4, which are both often found as efflorescence on building facades.

To see the effects of salt solutions and concentrations so-called salt-scaling tests were performed. After repeated freeze-thaw cycles with stone prisms completely submerged in salt solutions of different concentrations, the damage was measured as a weight loss caused by surface scaling and as a loss in dynamic modulus of elasticity. The loss in dynamic modulus of elasticity is a measure of internal damage caused by formation of micro-cracks and loss of cohesion. Also very low salt concentrations, especially NaCl in combination with freezing and thawing of the limestone Öland B1 studied here, had a marked aggravating effect on scaling. When different concentrations of the solution inside the pore system of the stone and in the surrounding solution were studied, the internal solution had a negligible effect compared to the effect the external solution had.

The effects of water content expressed in terms of degree of water saturation were studied with dilatation tests. Moisture conditioned specimens were exposed to one single freeze-thaw cycle. The damage was measured as a dilatation during the freezing phase or as a permanent dilatation after thawing. Only the sandstone was porous enough to be studied with this method. The damage increased exponentially with the degree of saturation. The critical degree

of saturation, defined as the highest degree of saturation for which the dilatation does not exceed zero, was about 0.85 for all sandstones. The effect of salt on the critical degree of saturation was studied as well. Salt did not change the critical degree of saturation, but at high degrees of saturation, the effect of salt in combination with freezing and thawing was worse than the effect of pure water.

Critical degrees of water saturation of sandstone were also determined by repeated freeze-thawing of moisture-sealed specimens. Stone prisms with different degrees of saturation were frozen and thawed for several cycles, and the damage was measured as a loss in dynamic modulus of elasticity. The values found with this method were somewhat higher, about 0.9, compared to the values of about 0.85 found in the dilatation test. The exact value of the critical degree of saturation is, however, determined by the definition of what is acceptable damage. If this is supposed to correspond to a dilatation equal to the tensile strain capacity, the values of the critical degree of saturation determined with the two different methods might be almost the same.

Calorimetric studies were performed to quantify the amount of ice formed in the pore system at different temperatures, which is important for understanding the mechanism causing frost damage. Ice formation could be observed for all stones tested, but the amount of ice formed was too small to be quantified in an ordinary Differential Scanning Calorimeter (DSC), in which very small samples are used. The amount of ice formed in saturated sandstone at freezing could be quantified in another type of calorimeter, in which larger samples could be used. Almost all the water in the pore system of sandstone froze.

A relevant question is whether the stones are likely to reach a degree of saturation high enough to cause damage under natural conditions. For sandstone, the degree of saturation reaches a value of about 0.8 after capillary suction for one week. This degree of saturation is not, according to the dilatation tests and S_{crit}-tests, enough to cause damage at freezing. On the other hand, it was found that the critical value of the degree of saturation was clearly exceeded after some weeks of water absorption. This might happen in practice during very moist conditions such as when a stone constantly sucks in ground water or when a stone is exposed to a leaking drain pipe. The granite and limestones were completely saturated after capillary suction for one week; however, no considerable damage was observed when these stones were freeze-thaw tested in pure water under saturated conditions. When the limestone Öland B1 was exposed to weak salt solutions, which might very well occur in practice, severe scaling occurred.

The main conclusion, therefore, is that much of the damage observed on buildings and monuments made of these stone types — sandstone and certain types of limestone, and possibly granite as well — might depend on freeze-thaw action. Another conclusion is that low salt concentrations at the surface of the stone severely aggravate the effect of frost attack on some types of stones. This might be a reason why stone damage seems to have increased in intensity during the last decades; because of air pollution, salts have been deposited on the surface of buildings and monuments, which has gradually made the stone more sensitive to surface scaling from frost.

Notations

A_s	Surface area (m^2/kg)
A_w	Sorption coefficient ($kg/m^2s^{1/2}$)
B	Water penetration coefficient ($m/s^{1/2}$)
C	Concentration by mass of salt (kg/kg)
CF_d	Correction factor for E-modulus of dry specimens
CF_w	Correction factor for E-modulus of wet specimens
D_f	Coefficient of moisture transport (different units, depending on f)
E_{d0}	Dynamic modulus of elasticity of dry specimen before freeze-thaw test (Pa)
E_{w0}	Dynamic modulus of elasticity of wet specimen before freeze-thaw test (Pa)
E_{dn}	Dynamic modulus of elasticity of dry specimen after freeze-thaw test (Pa)
E_{wn}	Dynamic modulus of elasticity of wet specimen after freeze-thaw test (Pa)
f_{d0}	Fundamental resonant frequency of dry specimen before freeze-thaw test (Hz)
f_{w0}	Fundamental resonant frequency of wet specimen before freeze-thaw test (Hz)
f_{dn}	Fundamental resonant frequency of dry specimen after freeze-thaw test (Hz)
f_{wn}	Fundamental resonant frequency of wet specimen after freeze-thaw test (Hz)
ΔH	Molar heat of fusion of liquid (J/mole)
h	Suction height (m)
K	Permeability ($m^4/Pa \cdot s$)
k	Constant in BET equation
M_w	Molar weight of water, $M_w = 0.018$ kg/mole
m_s	Mass of absorbed water per area of suction surface (kg/m^2)
n	Number of specimens
P	Porosity (m^3/m^3)
p_l	Pore water pressure (Pa)
$p_s(T)$	Water vapour pressure at saturation at the temperature T (Pa)
p	Pressure (Pa)
Q	Required weight (kg)
Q_0	Specimen weight at start of freeze-thaw test (kg)
Q_a	Weight of vacuum-saturated specimen in air (kg)
$Q_{d(50)}$	Weight of specimen dried at 50 °C (kg)
$Q_{d(105)}$	Weight of specimen dried at 105 °C (kg)
Q_{d0}	Weight of dry specimen before freeze-thaw test (kg)
Q_{dn}	Weight of dry specimen after freeze-thaw test (kg)
Q_{ds}	Dry weight of scaled-off material (kg)
Q_n	Specimen weight at end of freeze-thaw test (kg)
Q_w	Weight of vacuum-saturated specimen in water (kg)
q	Moisture flow (kg/m^2s)
R	Gas constant, $R = 8.314$ J / (mol · K)
r	Pore radius (m)
r_K	Radius of the water meniscus in the pore (m), $r_K \approx r$
r_a	Pore radius (m) corresponding to the freezing point -ΔT (K)
$\bar{r}$	Mean pore radius (m)
S	Degree of saturation
S_0	Degree of saturation at start of the freeze-thaw test or capillary suction test
S_k	Degree of saturation at the nick-point in capillary suction test
S_n	Degree of saturation at end of the freeze-thaw test

S_r	Required degree of saturation
s_p	Standard deviation of the porosity (m^3/m^3)
s_r	Standard deviation of the bulk density (kg/m^3)
T	Temperature (K)
T_0	Freezing point of bulk liquid (K)
ΔT	Freezing point depression (K)
t	Time (s)
t_a	Thickness of adsorbed liquid layer (m)
t_k	Time at the nick-point in capillary suction test (h or s)
V	Total pore volume (m^3/kg)
V_a	Amount of absorbed water (kg/kg material)
V_m	Amount of absorbed water corresponding to a monolayer covering the whole surface area (kg/kg material)
x	Distance of flow (m)
z	Penetration depth (m)
β_t	True amount of salt (kg)
β_c	Calculated amount of salt (kg)
γ	Surface tension of mercury (0.00485 N/m)
δ_v	Moisture permeability (m^2/s)
η	Coefficient of viscosity of fluid (Pa·s)
θ	Wetting angle
ρ_b	Bulk density (kg/m^3)
ρ_s	Solid density (kg/m^3)
ρ_w	Density of water, $\rho_w \approx 1000$ (kg/m^3)
σ	Surface tension of water, $\sigma = 0.073$ N/m
φ	Moisture state. When the conditions are isothermal, φ can be the mass of water per volume of material (w [kg/m^3]), the mass of water per mass of material (u [kg/kg]), the relative humidity (ϕ [%]), the partial pressure (p [Pa]) or the humidity by volume of air (v [kg/m^3]).
ϕ	Relative humidity (%)
ψ	Kirchhoff potential (kg/m·s)

1 Introduction

Man has been using natural stone as a building material and to create monuments and other structures for thousands of years. Natural stone is used in many various kinds of buildings, like churches, castles and magnificent houses in the cities, as well as in simple country houses. Natural stone is used because it is considered a durable material with high aesthetic value, but not even rock is a material that lasts forever. Degradation of natural stone is a natural process influenced by, for example, temperature changes, erosion, growth of lichen and moss, salt crystallisation and frost. These natural, organic and physical degradation processes are often called *weathering*. Probably, the most important type of weathering in the Nordic climate is frost action. This is the main problem treated in this report.

During the last decades, attention has been paid to the seemingly increasing deterioration of old buildings and monuments made of natural stone. The problem is by now rather well documented. It is suspected that this increase is the result of human action causing air pollution through the burning of fossil fuels because the deterioration of stone seems to have become more severe since the start of industrialisation. Therefore, much of the research done concerning this subject has been focused on the chemical reaction between stone and the products of air pollution.

Various degradation processes, natural as well as artificial, interact with each other in a complicated way. The damage caused by two various degradation processes acting together at the same time is not necessarily the same as the sum of two degradation processes acting separately. The effects of two or several processes acting together can be one of the following:

1) Additive, that is, the total effect is equal to the sum of the separate effects.

2) Antagonistic, that is, the total effect is smaller than the sum of the separate effects.

3) Synergetic, that is, the total effect is larger than the sum of the separate effects.

There are several examples of synergetic effects on the deterioration of natural stone. One example is the way in which frost changes the pore structure of the stone by enlarging the internal surface area and increasing the permeability, thus making the inner parts of the stone more available to various chemical reactions. Another example the way in which frost in combination with salt causes more severe damage than frost does by itself, even though no salt crystallisation occurs. This last synergetic effect is one of the main subjects treated in this report. This work shows that the frost-salt synergism is very powerful.

The deterioration of old stone buildings and monuments is causing owners all over the world considerable cost, as it is considered important to preserve these relics of the past for future generations. To be able to do this in an adequate way, knowledge of how stone deteriorates must be increased. Hopefully, this report will be a contribution to such knowledge.

2 General background

2.1 Introduction

This chapter deals with subjects that are of some importance understanding deterioration of natural stone, especially frost deterioration. In this chapter, natural stone and rock are described in general, and then various types of deterioration processes caused by weathering or chemical reaction are mentioned and briefly described, with a special emphasis on frost deterioration. The last section covers conservation and restoration.

2.2 Natural stone and rock

2.2.1 Introduction

In order to understand the degradation mechanisms of natural stone, it is important to know something about the structure of the stone and of what it is composed. Natural stone is a more or less porous, brittle material composed of mineral grains. These grains, generally composed of one single mineral, but sometimes composed of different minerals adhering to each other, form species of stone.

Although thousands of minerals are known, most common natural stones can be adequately described in terms of a few minerals. The most common minerals are quartz (SiO_2), the feldspars (for example, orthoclase ($KAlSi_3O_8$) and anorthite ($CaAl_2Si_2O_8$)), the micas, and clay and chlorite minerals (Holmes, A., 1965). The various minerals are physically characterised by their colour and hardness.

The empty spaces between the grains in a species of stone make them porous. This porosity can vary from less than 1% (for example, some granites) to more than 20% (for example, some sandstones). The porosity, pore structure and pore size distribution are important factors because they influence the durability and degradation of the stone. These qualities determine how the material and the moisture will interact, what degrees of saturation that will occur and how likely it is that water will freeze. The availability of water determines most mechanisms for the degradation of stone.

The earth's crust consists of a large number of various kinds of rock, but only a few of them are common (Handbook of Stone, 1986). Rock species are divided into three main groups according to the process by which they formed: igneous rocks (for example, granite, diorite and gabbro), sedimentary rocks (for example, sandstone and limestone) and metamorphic rocks (for example, marble and gneiss). The following text describes the origin of these three main groups of rock species and discusses the use of stone in ancient buildings.

2.2.2 Sedimentary rock

Sedimentary rock is normally formed on the bottom of prehistoric seas. Sandstone consists of more or less rounded grains of sand similar in appearance to the sand on a beach. Sandstone differs from deposits of modern sand only in being coherent instead of loose. The sandstone grains are fragments of metamorphic and igneous rock such as granite. Most of the grains are quartz, but other minerals such as feldspar can also be present. The grains are cemented together by calcite or silica. Calcite is the most common cementing material, and it gives rise to a rather loose stone. When the cementing material is silica, which has crystallised as

quartz, the sandstone becomes harder. Such hard, siliceous sandstone with low porosity, which is mostly white in colour, is often referred to as *quartzite*. Sandstone is easily quarried, and it has therefore been used frequently for building purposes.

The sandstone from Gotland Island in the Baltic Sea that is studied in this report is one of the predominate materials in buildings of historic interest in the Baltic region. It was often used in sculptural decorations, as it is soft and therefore easy to work, but it is also used in facings, mostly from the 17th century. The problems with deterioration of this stone are very extensive.

Limestones are composed principally of calcium carbonate (calcite). They are normally deposits formed from dissolved material from sea water and accumulations of organic remains. They consist of lime shells of various forms and sizes from prehistoric marine animals, embedded in an extremely fine-grained matrix. In some limestones fossils, from for example trilobites and ortoceratites, frequently occur. The colour of limestone varies widely; all shades of white, yellow, brown, grey, green and red limestones can be found.

Limestones are sometimes commercially known as ‘marble’ when they can be effectively polished and used for decorative purposes. To the geologist, however, the term *marble* is restricted to limestone that has been completely re-crystallised by metamorphic processes. Limestone of suitable quality has been widely used for stones in buildings since the 17th century, because of the ease with which it can be worked, and limestone is still used in modern buildings. The problems with deterioration are extensive.

2.2.3 Igneous rock

Igneous rocks normally crystallise from a molten state in the deeper parts of the earth. The crystals are disordered. Igneous rocks are in turn divided into two groups containing finer-grained *volcanic* rock like lavas and *plutonic* rock like granite, which has been slowly cooled and therefore has medium to coarse crystal grains. Granite is essentially composed of quartz, feldspar and mica.

Granite is hard, so worked granite was not used frequently in buildings until the middle of the 19th century when the technique for working granite was developed. At the turn of the century, granite reached its most popular period as a building material in Sweden. There are seldom problems with deterioration of granite in buildings, but there are problems with ancient rock carvings from the Bronze Age, as well as with granite rune stones.

2.2.4 Metamorphic rock

Metamorphic rock is igneous or sedimentary rock that has been re-crystallised by high temperature and pressure during its burial in the earth’s crust. The minerals are often oriented in planes. The metamorphic equivalent of granite is gneiss, and the metamorphic equivalent of limestone is marble.

Marble has been used for building purposes and for sculptures ever since the time of the ancient Greeks, or even before.

2.3 Weathering

2.3.1 Introduction

Weathering is a common word for natural physical degradation processes like erosion and degradation caused by climatic temperature changes. These processes have always been active as a part of the natural deterioration of stone. The surfaces of some stone materials sometimes become even more beautiful by this ageing, acquiring a noble patina. The ageing can protect the stone to some extent from further attack. This is a well-known phenomenon in metals, but it also applies to other materials such as some types of stone (Conservation Institute of National Antiquities, 1990).

Weathering is often negatively affected by changes in the environment, such as an increase in air pollution. Scientists all over the world have maintained over and over during the last decades that the rate at which those parts of our cultural heritage exposed to the atmosphere are being damaged is increasing. They claim that attack has become gradually more severe, and the materials have become eroded and weakened to a considerable depth. The main reason for the increased rate of attack is normally said to be chemical reaction between the stone and the air pollutants. The hypothesis treated in this report is that a just as important reason is frost attack, possibly in creased by pollutants.

Frost action is also a type of weathering. It is treated separately in Chapter 2.4, as it is the main subject of this report.

2.3.2 Moisture

Moisture is the single factor that has perhaps the most influence on deterioration of stone, as it takes part in almost all destructive mechanisms. Moisture reaches a porous building material from the ground by suction of ground water, by rain and snow, or by diffusion of vapour from the air. Even when no precipitation occurs, the air still contains moisture, which is transported into or out of the stone until an equilibrium between the stone and the air is reached. Moisture is transported in the pores by diffusion of the vapour phase and by capillary transport of the liquid phase. In some cases the moisture can be transported by a pressure gradient caused by wind or by water pressure. The moisture content and moisture distribution in the stone at any given time is decided not only by the conditions of the outer environment but also by the properties of the material, such as hygroscopicity, porosity, pore structure and pore size distribution, as well as by the ‘moisture history’ of the material. Hygroscopic salts in the pore system can also affect the moisture content and moisture distribution in the stone.

The moisture content of a porous material can be expressed either as mass of water per volume of material (w [kg/m^3]), as mass of water per mass of material (u [kg/kg]) or as volume of water per volume of material (m^3/m^3). A fourth way of expressing moisture content is by using degree of saturation, S. When the material is completely saturated, that is, $S = 1$, all open pores are completely filled with water. The relationship between S and w is

$$S = \frac{w}{P \cdot \rho_w} \tag{2.3.1}$$

where

S degree of saturation (m^3/m^3);

w mass of water per volume of material (kg/m^3);

P porosity (m^3/m^3);

ρ_w density of water (kg/m^3).

Capillarity

There are mainly two kinds of attraction forces involved when a liquid is sucked into a capillary pore. One of these is the attraction force between the molecules of the liquid, here called the *cohesion*, which is the same in a pore as in free bulk liquid. The other force exerted on the liquid is the attraction force between the liquid and the wall of the pore, here called the *adhesion*. In a big vessel, adhesion can be neglected. In a small vessel, such as in a capillary pore, adhesion is greater per liquid molecule, as the wall area per liquid molecule is greater.

The capillary transport in a capillary tube is due to both adhesion and cohesion. As long as the forces causing capillary transport are greater than are the counteracting forces acting on the liquid column, the liquid column will continue to grow. The counteracting force is friction when horizontal transport occurs and friction and gravity combined when vertical transport occurs. Finally, a steady state is reached when the counteracting force is equal to the force causing capillary transport. (In the horizontal case, the water transport theoretically continues infinitely, as the friction is proportional to the velocity, but the velocity asymptotically approaches zero.) This phenomenon is possible only if the cohesion is great enough to make the liquid retain its liquid state, that is, if the tensile strength of the liquid is great enough.

When a slice of porous material of limited height is placed with one surface in water (Figure 2.3.1.a), capillary transport of water will take place. When the mass of water per area of suction surface, m_s (kg/m^3), in the porous material is plotted against the square root of time, the result is similar to that shown in Figure 2.3.1.b. Before the nick-point, t_k, the water sorption will follow the equation

$$z = B\sqrt{t} \tag{2.3.2}$$

where

z is the penetration depth (m)

B is the water penetration coefficient ($m/\sqrt{s}$)

t is the time (s)

The sorption coefficient A_w ($kg/m^3 \cdot s^{1/2}$) is calculated by the formula

$$A_w = \frac{\Delta m_s}{\sqrt{\Delta t}} \approx \frac{m_s - m_0}{\sqrt{t}} \tag{2.3.3}$$

where Δm_s is the water absorption in the time interval Δt, m_s is the mass of water per area of suction surface and m_0 is the mass of water per area of suction surface at start of suction. The sorption coefficient is only calculated for the process before the knick-point.

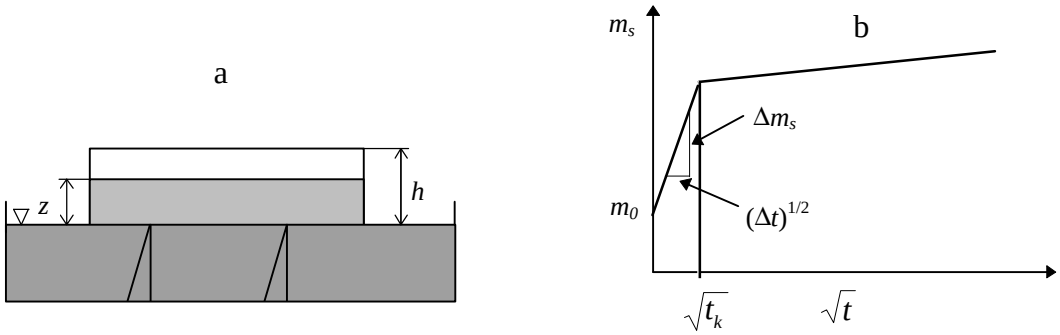

Figure 2.3.1. Principles of a capillary suction test. The results are presented as water sorption versus square root of time.

This equation is followed until the water front reaches the upper surface, which is represented by the knick-point in Figure 2.3.1. Sometimes m_s increases even after the knick-point is reached, which depends on that the pores are further filled with water when air in enclosed bubbles, contained in pores bigger than about 1 μm, is dissolved (Fagerlund, 1994b). Instead of using mass of water per area of suction surface, the lateral axis can be expressed in terms of moisture ratio, moisture content or degree of saturation. If some of these latter units are to be used, it is important to be aware of that the moisture distribution is uneven in the sample before the knick-point is reached, as there is a moisture front in the sample. Thus, the lower parts of the sample can contain a lot of moisture when the upper parts are almost dry, but the moisture ratio, moisture content and degree of saturation are calculated as a mean value for the whole sample.

Adhesion causes the surface of a water column in a capillary to have a concave shape if the wall is hydrophilic. If the wall is hydrophobic the surface will have a convex shape (see Figure 2.3.2). The wetting angle q is a measure of the attraction force between the wall and the liquid, that is, the adhesion. The smaller the angle, the greater the adhesion.

Figure 2.3.2. Water column in a hydrophilic (left) and a hydrophobic (right) capillary.

The capillary rise of water in a hydrophobic material is negative; the wall of the pore actually repels water because of the retentive force between the water molecules and the hydrophobic walls. Such a case occurs, for example, in a stone treated by hydrophobing agents, such as silicone, silane and similar.

Sorption isotherms

When an equilibrium state is reached between a porous material and the surrounding air containing a given relative humidity, the material will contain a certain amount of moisture. The graph describing the equilibrium moisture content as a function of the relative humidity is called the *sorption isotherm* or *moisture equilibrium curve.* The moisture content at equilibrium varies, depending on whether the material was wet or dry from the start, which

gives rise to different sorption isotherms for desorption and absorption. In that case, the moisture content of the desorption isotherm is always higher than is the moisture content of the absorption isotherm. This phenomenon is called *sorption hysteresis.*

Sorption isotherms give information about the moisture equilibrium at various relative humidities, which in itself is an important and interesting information, and in addition they give information about the pore structure. There are some methods for obtaining information about the pore structure from the sorption isotherm. One method is based on the Kelvin equation:

$$p_l = p_s(T) + \frac{R T \rho_w}{M_w} \cdot \ln(\varphi) \tag{2.3.4}$$

where

p_l	pore water pressure (Pa);
$p_s(T)$	water vapour pressure at saturation at the temperature T (Pa);
R	gas constant, R= 8,314 (J / (mol · K));
T	temperature (K);
ρ_w	density of water, ($\rho_w \approx 1000$ (kg/m^3));
M_w	molar weight of water, (M_w = 0,018 kg/mole);
φ	relative humidity.

and on the relationship

$$p_l = p_s(T) - \frac{2\sigma \cos\theta}{r_K} \tag{2.3.5}$$

where

σ	surface tension of water, (σ = 0.073 N/m at 20 °C);
θ	wetting angle, defined by Figure 3.2;
r_K	radius of the water meniscus in the pore (m). This is almost equal to the pore radius for the relatively large pores of the stones studied in this report.

$p_s(T)$ in the Kelvin equation can be neglected as it is small compared to the other term. The wetting angle θ is set to 0 (perfect wetting). Now, all values needed to get a correlation between the radius r and the relative humidity φ are known:

$$r_K = \frac{-0.92 \cdot 10^{-9}}{\ln\varphi} \tag{2.3.6}$$

It is only possible to use this method at relative humidities high enough to form water menisci, that is, above about 45%. At lower relative humidities, only a layer of water molecules of various thicknesses, the size of which depend on the RH, covers the pore wall. This is the theoretical basis from which the internal surface area is calculated with the so-called BET method:

$$\frac{V_a}{V_m} = \frac{k \cdot \varphi}{(1-\varphi) \cdot (1 + k \cdot \varphi - \varphi)} \tag{2.3.7}$$

where

V_a amount of adsorbed water at the relative humidity φ (kg/kg material);

V_m amount of adsorbed water corresponding to a monolayer covering the whole surface area (kg/kg material);

k a constant depending on the heat of condensation, or heat of adsorption, of the first adsorbed layer;

φ relative humidity.

k is normally about 20 for mineral-based building materials (Fagerlund, 1995). This implies that one monolayer is covering the total pore surface (that is, $V_a=V_m$) at a relative humidity of about 18%. Knowing the equilibrium moisture content at this single value of relative humidity makes it possible to calculate specific surface area A_s (m^2/kg) of the material. A densely packed monolayer is assumed to be present and the water molecules are assumed to be spherical and to have diameter of 0.35 nm. Then,

$$A_s = 3.5 \cdot 10^6 \cdot V_m \tag{2.3.8}$$

If all pores are assumed to be spherical and of the same size, a mean pore radius $\bar{r}_s$ can be calculated using the following equation:

$$\bar{r}_s = \frac{3P}{\rho_b A_s} \tag{2.3.9}$$

If all pores are assumed to be cylindrical and of the same size, a mean pore radius $\bar{r}_c$ can be calculated using the following equation:

$$\bar{r}_c = \frac{2P}{\rho_b A_s} \tag{2.3.10}$$

where

$\bar{r}$ pore radius (m);

P porosity (m^3/m^3);

ρ_b bulk density of the porous material (kg/m^3);

A_s surface area (m^2/kg).

Moisture flow and permeability

The moisture flow through a porous material can be described by

$$g = -D_\varphi \frac{\partial \varphi}{\partial x} \tag{2.3.11}$$

where

g moisture flow ($kg/(m^2 s)$);

D_φ coefficient of moisture transport (various units, depending on φ);

x distance of flow (m);

φ moisture state. When the conditions are isothermal, φ can be the mass of water per volume of material (w [kg/m^3]), the mass of water per mass of material (u [kg/kg]), the

relative humidity (j [%]), the partial vapour pressure (p [Pa]) or the humidity per volume of air (v [kg/m^3]) (Arfvidsson, 1994).

When f is the humidity by volume of air, D_f is the moisture permeability, written as δ_v.

The moisture flow can also be expressed in terms of the Kirchhoff potential, y (Arfvidsson, 1994).

$$y = \int D_f \nabla f \tag{2.3.12}$$

$$q = -\frac{\nabla y}{\nabla x} \tag{2.3.13}$$

2.3.3 Salt

Various soluble salts are often found as efflorescence or crystals on stone surfaces. The origin of the salts is ground water rising through the stone from the soil, air-borne salts from sea spray, air pollution or dissolved minerals from the stone itself or from products of chemical reactions. Salt crystals that are formed inside the pores in a porous material can, under certain conditions, exert a pressure on the pore walls. This can make the material rupture. Salts also have secondary effects on deterioration, for example, by affecting the equilibrium state of humidity of the porous material. Salts that have various hydration states, for example, some sulphates, are especially dangerous, as each state is characterised by a certain specific volume (Amoroso & Fassina, 1983). Each time the relative humidity changes the salt changes its hydration state. This gives rise to rhythmic contraction and pressure on the pore walls, which sometimes results in damage to the stone.

Lewin (1982) proposed a salt destruction mechanism in which salt crystallisation occurs at a certain distance from the surface where the rate of evaporation and the rate of re-supply of solution is in dynamic balance. This forming and growing of salt crystals causes exfoliation.

According to a study made on medieval brick by Larsen & Nielsen (1990), thermal expansion and hygroscopic shrinkage of a stone containing salt crystals increases as the NaCl content increases, which might lead to internal strains and fracturing.

Salt affects frost destruction as well (see Chapter 2.4).

2.3.4 Temperature

A stone surface exposed to the blazing sun can reach a fairly high temperature. This causes a temperature gradient between the surface and the inner parts of the stone. In consequence, because of the coefficient of thermal expansion, a thin outer shell expands and tends to pull away from the cooler layer within. Under perfectly dry conditions, the stresses that thus develop are insufficient to fracture fresh massive stone, but in the presence of water, repeated alterations of heating and cooling eventually lead to rupture (Holmes, 1965).

Some species of stone that are composed of calcite, for example, marble, are especially sensitive to temperature alterations. An internationally well-known example is the bend marble panels of the facade cladding of the Finlandia Hall in Helsinki. Calcareous stone is probably sensitive to temperature changes because the thermal expansion coefficient of calcite changes according to the direction in the crystal. Between 18 and 50 °C the thermal

expansion coefficients are $25.1 \cdot 10^{-6}$ °C^{-1} in one direction in the crystal and $-4.9 \cdot 10^{-6}$ °C^{-1} perpendicular to that direction. The different signs mean that an increase in temperature causes the crystal to expand in one direction and to contract in the perpendicular direction. Such movements cause a loosening of the grain boundaries, thereby increasing the porosity and water absorption of the material (Amoroso & Fassina, 1983; Widhalm et al, 1994).

2.3.5 Wind

When dust particles, driving rain, hail or snow blow against the surface of a material, they cause abrasion and erosion. Wind also influences the deterioration of natural stone by affecting the moisture conditions; wind increases drying, but it can also increase the moisture content by forcing rainwater into the pores.

2.3.6 Biological growth

Various micro-organisms and plants, such as some algae, bacteria, lichen, moss and climbing plants, can grow on stone surfaces. Dirt and dust on the surface can serve as nourishment for these organisms. Sometimes the minerals of the stone itself provide nourishment to the organisms. Biological growth is often considered to be part of the natural ageing process of stone and becomes part of the patination of the material. However, biological growth can also be destructive; the root system and other parts of the plants can contribute to the deterioration of the stone by penetrating into the pore system, thereby causing fracture and breaking of the stone surface. The biological growth can also change the physico-chemical properties in the stone by increasing the wetting time after rain and by changing the pH and chemical composition of the pore water. Change in the atmospheric composition through air pollution changes the conditions for the organisms and plants. In some cases this is of advantage to the stone, but in other cases, it is a disadvantage.

2.4 Frost action

2.4.1 Introduction

When water freezes in a porous, brittle material, the material can be damaged. The most frequent types of damage are surface scaling and exfoliation, but deep cracking can also occur (Amoroso & Fassina, 1983).

A large number of studies have been made on the subject of freezing of porous solids during the last decades. Most of these studies concern concrete and brick (for example, Collins, 1944; Powers, 1949; Verbeck & Klieger, 1957; Fagerlund, 1972), as these are materials of great commercial interest, but studies have also been made on natural stone. A great number of various investigation methods have been used, most with the purpose of getting some kind of measure of the general durability level of the material. The purpose of some studies, however, has been to get a better understanding of the mechanisms that cause frost destruction.

2.4.2 Freezable water

The freezing temperature of water in a small pore is lower than that of bulk water; the smaller the pore, the lower the freezing point, according to a modified Kelvin equation (Defay et al, 1966; Fagerlund, 1993a).

$$r_q = \frac{-2 \cdot s \cdot M_w}{r_w \cdot \Delta H \cdot \ln(\frac{T_0 - \Delta T}{T_0})} + t_a \qquad (2.4.1)$$

Where

r_q is the pore radius of a cylindrical pore, corresponding to the freezing point T_0-ΔT;
s is the surface tension water-air (N/m);
M_w is the molecular weight of water (kg/mole);
r_w is the density of bulk water (kg/m^3);
T_0 is the freezing point of bulk water (K);
ΔT is the freezing point depression (K);
ΔH is the molar heat of fusion of water (J/mole) (ΔH is a function of temperature);
t_a is the thickness of the adsorbed unfrozen water layer (m).

The freezing point depression occurs because the attraction force between the liquid and the wall of the pore is greater per liquid molecule in a small pore than in a big vessel, as the wall area per liquid molecule is greater. This adhesive attraction force keeps the liquid molecules from forming an orderly solid crystal structure, which is the most stable configuration at the freezing temperature of bulk water. The low temperature is acting as a driving force for freezing, and at a certain point, this force is great enough to cause freezing. However, there will be an adsorbed, liquid-like layer nearest the wall that will never freeze. (Also free ice has a liquid-like layer, a few hundred molecules thick, that exists at temperatures well below 0 °C (Hobbs, 1974)). Therefore, at each temperature below zero, there exists a certain minimum pore size below which water in the pore does not freeze, that is, in a fine-porous material, at each temperature below zero a certain amount of water remains nonfreezable. Theoretically calculated correlations between pore radii and freezing point depressions according to Equation 2.4.1 are shown in Table 2.4.1.

Table 2.4.1 Correlation between pore radii and freezing point depressions (Fagerlund, 1993b).

Radius (nm)	22	14	10	8	6
Freezing point (°C)	-6	-10	-15	-20	-30

2.4.3 Critical degrees of water saturation

Fagerlund (1972) found that critical degrees of water saturation existed for all porous, brittle materials treated in his study (various kinds of brick, lime silica brick, cellular concrete, asbestos cement and cement mortar). Fagerlund froze and thawed sealed specimens of the materials, containing various amounts of water, that is, with varying degrees of water saturation. After a number of cycles, the damage was measured as a relative loss in dynamic modulus of elasticity. The results showed that samples with a degree of water saturation higher than a certain critical value were all damaged, whereas samples with less water were almost undamaged. Fagerlund also performed studies in which the damage to pre-conditioned, sealed specimens was measured as a maximum length-deviation after one single freeze-thaw cycle. The results of the critical degree of saturation from the two test methods were normally almost the same, but the critical degree of saturation of the length-deviation tests was somewhat lower than that of the multi-cycle tests.

2.4.4 Internal hydrostatic pressure

Chatterji and Christensen (1979) studied frost damaged limestone nodules in gravel pits in Denmark. They found that nodules smaller than 8 to 10 mm in size were not damaged. Larger nodules were either fractured into a few, comparatively large pieces or they were surface

pitted. The results from the fractured nodules gave rise to a theory regarding the development of hydrostatic pressure during freezing. The theory was that hydrostatic pressure develops when the outer surface of a porous, wet material is initially frozen. As freezing continues, ice also forms in the inner parts of the material, but since the outer shell is sealed with ice, it cannot expand. If the hydrostatic pressure thus developed exceeds the tensile strength of the ice-limestone composite in the shell, the material breaks. The theory was further studied in laboratory investigations in which water was frozen in plastic forms of various volumes. Initial freezing was continued until enough ice had formed to allow the ice shapes to be removed from the forms. When the freezing process was then completed, it was observed that the larger volumes of 100 ml were shattered, while smaller volumes of 6 ml were intact after freezing. In addition, 'porous' and 'dense' limestone nodules were frozen and thawed in various volumes of water. The porosity of the stones is not specified in the report, but in general, dense nodules frozen in large quantities of water developed only surface pop-outs, although some of the dense nodules frozen in large quantities of water were broken into a few large pieces. The porous nodules were always broken into large pieces, irrespective of the thickness of the water layer.

It can be shown theoretically that a maximum — or critical — size of the types found by Chatterji and Christensen (1979) will also be predicted by the hydraulic pressure theory as described by Powers (1949) (see Equation 2.4.2 below). In fact, such critical sizes were found experimentally by Fagerlund (1981) for cement pastes frozen and thawed under saturated conditions. Therefore, in theory, no ice crust outside the stone is required in order to predict the existence of a maximum material size that is not harmed by frost.

2.4.5 Frost action with salt

The freezing temperature of a solution is lower than that of pure water. The reason is basically the same as that for the freezing point depression in a small pore; the ions or molecules of the solute attract the water molecules in the same qualitative way that the pore wall does.

The solubility of a salt normally decreases with decreasing temperature, and salts can form various hydrates. This is shown in a 2-phase diagram, where the temperature T versus the concentration x of the mixture between two substances is shown. A 2-phase diagram of NaCl in water is shown in Figure 2.4.1. The data are from the Handbook of Chemistry and Physics (1980-1990).

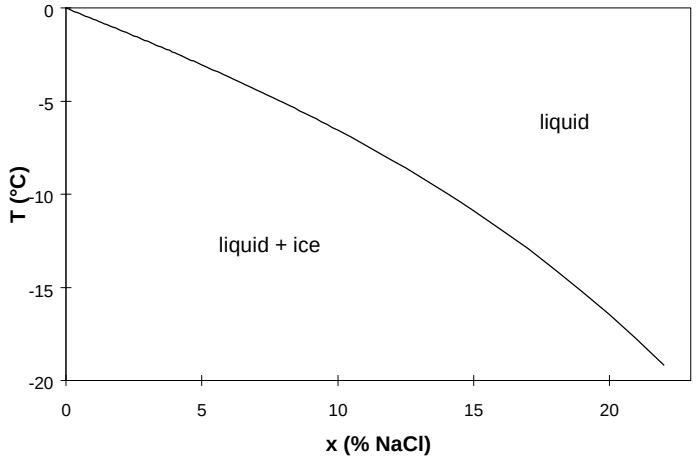

Figure 2.4.1. 2-phase diagram of NaCl in water. Data are from the Handbook of Chemistry and Physics (1980-1990).

When a salt solution is cooled below the freezing point, many small ice crystals caused by heterogeneous nucleation are formed (Hobbs, 1974), and a salt solution with a higher concentration than the first is trapped in the cavities between the crystals. The reason for this is that foreign substances, such as salts, normally do not incorporate into the ice structure.

It is known that materials like concrete are damaged more by salt solutions than by pure water when they are frozen and thawed, and that weak solutions cause more damage than stronger ones do. No theory is yet fully established to explain this phenomenon.

Arnfelt (1941) was the first scientist to draw attention to the fact that pessimum concentrations exist when various de-icers are used at freezing and thawing. Arnfelt's study was performed on concrete, brick and sandstone, and he tested solutions of calcium chloride, sodium chloride, ethanol and urea. He froze pieces of material completely submerged in solution for 12 hours at -25 °C, and then he thawed the pieces still submerged in the same solution at 20 °C for 12 hours. The freezing and thawing was repeated until the damage was great enough. He found that the pessimal concentration of concrete freeze-thaw-tested in $CaCl_2$ solution was 2% by weight, with an accuracy of one percentage unit. The effects of sodium chloride, ethanol and urea were similar, although the studies with these solutions were not as accurate as those with $CaCl_2$. Sandstone and brick samples tested in water and $CaCl_2$ solutions of concentrations ranging between 1% and 20% by weight were more damaged by pure water than by the solutions. A similar study was made on air-entrained and non-air-entrained concrete (Verbeck & Klieger, 1957). Slabs (7.5 cm in depth and 15 by 38 cm in area) were frozen with 250 ml water on the surface for 18 hours at -29 °C. The slabs were then thawed at 21 °C for 6 hours with de-icer applied to the ice. After thawing, the resulting solution was removed, the surface was rinsed and 250 ml of water were placed on the surface for the next freeze portion of the cycle. De-icers used were the same as those used in Arnfelt's study, that is, calcium chloride, sodium chloride, ethanol and urea. The fact that air-entrained concrete is more freeze-thaw resistant than is non-air-entrained concrete was already known by then. Specimens exposed to various concentrations of de-icers were subjected to surface scaling tests. The damage was visually examined and rated as to extent and depth of scaling on six levels. The results of the experimental study showed that relatively low concentrations, on the order of 2 to 4 percent by weight, of the de-icer produced more surface scaling than did higher concentrations or absence of de-icer. Lindmark (1993) has performed additional studies and found that the concentration of solute (NaCl) inside the pores of concrete specimen has less effect on scaling than has the concentration of the solution surrounding the test specimen during freezing and thawing.

Several interactions can occur between the phases present when a salt solution freezes in a porous solid. Three main phases exist:

- ice, which does not incorporate salt in its crystals;
- salt solution, consisting of water and solved salt ions (the salt does not normally crystallise because of the low concentrations);
- the solid, porous material.

This complex system makes it difficult to describe quantitatively in detail what is actually happening when a salt solution freezes inside or on top of a porous solid and thus to explain the occurrence of a pessimal salt concentration.

2.4.6 Mechanisms

Freezing of a porous solid is a complicated phenomenon, even when no salt is present, and includes several various mechanisms that sometimes interact with each other. Several theories have been presented. Some of the most recognised theories are briefly described below.

The volumetric expansion theory

The volumetric expansion theory is based on the fact that the volume of ice, depending on its crystal structure, is 109% of that of water. When water freezes in a porous medium, the growth of ice crystals puts pressure on the pore walls. If this pressure exceeds the strength of the pore walls, they will break. A consequence of this theory is that frost damage will only occur when the air-filled pore space before freezing is less than 9% of the volume of the freezable water. It has, however, been found in numerous studies that frost damage almost always occurs when the degree of saturation is below the value 0.917 predicted by the volumetric expansion theory.

The ice lens growth theory

The volume expansion of water upon freezing is not the only explanation for the effect of frost. In laboratory tests, effects similar to those caused by ice have been obtained on frozen clay saturated with nitrobenzene, which freezes with a decrease in volume (Taber, 1930). This implies that it is the growth of the crystal, caused by transport of the liquid to the solid crystal, rather than the volume expansion itself, that causes the damage. This fact lies behind the so-called ice lens growth theory.

Frost heave in the ground is caused by formation of growing ice lenses. Two conditions must be met before an ice lens can be formed; free water must be available (water source), and there must also be a suction caused by unfrozen water adsorbed in small pores or at the surface of small soil particles (Knutsson, 1995). This is the case when soil consisting of fine-grained particles is cooled unidirectionally from the air above. Ice is then formed at a certain level where the temperature is low enough for freezing to occur and unfrozen water is available from the thermally insulated underlying soil. The process is also governed by the water permeability of the soil. When ice is formed, heat is emitted, as ice formation is an exothermic process. When the sum of the heat emitted and the heat transported to the freezing zone with the unfrozen water is equal to the heat withdrawn from the freezing zone, thermal equilibrium is reached, and the temperature will be zero (or somewhat below zero) at a constant level. An ice lens will develop at this level, perpendicular to the heat flow, which in turn will cause frost heave. A new ice lens can then develop at another level where the conditions are right. The ice lens will continue to grow as long there is a temperature gradient and water is available, and no outer load of sufficient magnitude is applied.

The frost destruction of porous solids can be explained by microscopic ice lens formation, which is basically the same mechanism as the one described above, that is, the mechanism that causes frost heave (Collins, 1944; Powers & Helmuth, 1953). When the temperature in a porous solid is lowered, ice will first be formed in coarser pores (see Chapter 2.4.2). Water will then be withdrawn from a water source to make the ice crystal grow. The water source can be either unfrozen water in finer neighbouring pores, or an unfrozen salt solution surrounding the porous material. The process continues as long as the energy level of the ice is lower than the energy level of the water in the finer pores or in the surrounding salt solution. Microscopic ice lenses inside individual pores will develop, causing damage.
Ice lenses will grow in all pores where ice is present. In coarse pores that are partly water-filled (ice-filled) and partly air-filled, the ice lens can grow without causing pressure. Ice lens

growth in such pores will be promoted at the expense of ice lens growth in completely ice-filled pores. Therefore, the pressure, and thereby the risk of frost damage, is reduced when the material is only partly filled with water.

If there is no salt solution at the surface of the porous material, ice lenses can only be formed if there is a pore size distribution of both small pores with unfrozen water and large pores with ice. Otherwise no water source is available. Concrete, for which the microscopic ice lens theory was originally developed, has a pore size distribution of both small pores with unfrozen water and large pores where ice is formed. In most species of natural stone, though, the pore size distribution is more narrow, and all pores are of almost the same size and fairly coarse. Therefore, there is almost no unfrozen water inside the stone that can serve as a source for ice lens growth.

When the only water source is in small pores (for example, in concrete), the ice lens growth will cause a drying out of the finer pore structure, and because of the capillary underpressure caused by drying, the free energy of the remaining unfrozen water will be lowered and the ice lens growth will eventually stop (Powers & Helmuth, 1953). In such a case, the supply of water is limited, but if there is a solution at the surface of the material, this can serve as a relatively unlimited water source, as the freezing point of the solution is low (see Chapter 2.4.5) (Lindmark, 1996). If there is pure water instead of a solution at the surface, this will freeze, and no water source will be available.

The hydraulic pressure theory
One theory often mentioned in the literature to explain frost destruction is the hydraulic pressure theory (Powers, 1945 and 1949). This theory is based on Darcy´s law, which says that the flow q is proportional to the pressure gradient dP/dx and the permeability K_p of the material and inversely proportional to the viscosity η of the fluid.

$$q = \frac{K_p}{\eta} \cdot \frac{dp}{dx} \tag{2.4.2}$$

where

p pressure (Pa);
η coefficient of dynamic viscosity of fluid (Pa·s);
q fluid flow (kg/m^{2}s);
K_p permeability (kg/m);
x distance of flow (m).

Flow is generated at the point of freezing because of the 9% increase in volume that occurs when water is transformed into ice. The higher the rate of ice formation, the more rapid the generation of flow and the higher the pressure (see Equation 2.4.2). The material fractures when the pressure exceeds the cohesion of the material.

Powers (1953) presented data from some experimental studies to prove his theory about the development of hydraulic pressures in cement paste during freezing. He measured the corresponding values of expansion and temperature of hardened Portland cement pastes with and without entrained air.
The importance of the hydraulic pressure mechanism will probably vary in different porous materials. The theory was originally developed for concrete, which contains cement paste.

The cement paste contains large air voids and smaller capillary pores surrounded by cement gel with very small gel pores about 2 nm across (Powers & Brownyard, 1947; Powers, 1962). The size of the capillary pores is 5 to 100 nm (Concrete Handbook, 1994). Therefore, capillary pores can contain ice, but ice is not formed in the gel pores, as these are too small. The capillaries, which are pockets isolated by layers of gel, are of such a size that they are readily filled with water. When ice is formed in the capillary pores, water is expelled through the gel, which has a low permeability to water. The low permeability makes the hydraulic pressure high.

If a porous material, such as natural stone, has another microstructure, the hydraulic flow mechanism will have another validity. Natural stone consists of mineral grains (crystals) impermeable to water and connected to each other. Between the grains are pores, which can contain water. The pores in many species of natural stone are of the same order of size, or larger, as the capillary pores in cement paste. With the exception of argillaceous rock types, marbles and certain granites, the majority of pore spaces in rocks are greater than 15 nm in diameter (J. P. Lautridou and J. C. Ozouf). In certain sandstones, the pores can be as large as 0.1 mm in diameter (Wessman, 1995). The larger pores in natural stone are not as readily filled with water as are the capillary pores in cement paste, but on the other hand, almost all water in the pores is freezable.

According to Powers (1949), the resistance to flow through the capillary pores containing unfrozen water in cement paste is negligible compared to the resistance to flow through the barriers of gel. However, permeability in the capillary pores, as well as in stone pores, becomes lower as freezing progresses because of the ice formed. In his calculations, Powers assumed that the permeability of the cement paste did not change during freezing, but in natural stone the reduction in permeability might be substantial. Therefore, even though the permeability of the unfrozen stone is high, it might be so low in the frozen stone that the hydraulic pressure mechanism could be a cause of destruction.

Results from the laboratory tests presented by Taber (1930), in which destruction effects similar to those caused by water were obtained with clay saturated with nitrobenzene, which freezes with a decrease in volume, cannot be explained by the hydraulic pressure theory. This situation, however, can be explained by the frost heave theory, that is, the ice lens growth theory described above.

2.5 Deterioration influenced by air pollution

2.5.1 Introduction

Human activities influence the quality of the atmosphere, but taken on a world-wide basis, the total mass of air pollutants emitted by ‘nature itself’, for example, volcanic emissions, still exceeds that emitted by man. The exception is sulphur dioxide, which is the most destructive air pollutant when stone deterioration caused by chemical reaction is considered, and for which artificial pollution sources are greater than natural ones (Amoroso & Fassina, 1983). In urban areas and near large emission sources and traffic, air can be considerably polluted. Culturally valuable objects are frequently located in these areas.

Air pollution can occur in the form of gas, aerosols or solutes. Air pollution can also form salts. Natural stone can react in various ways with all these forms of air pollution.

Below, the most significant processes treated in the literature are mentioned.

2.5.2 Formation of gypsum

The formation of gypsum on calcareous stone is the most important chemical reaction involving air pollutants to cause stone degradation. When gypsum is formed on sandstone, the porous sandstone disintegrates to a powdered material, while limestone and marble develop thick crusts instead (Conservation Institute of National Antiquities, 1991).

Gypsum is formed when calcite in calcite-cemented sandstone, limestone and marble react with sulphur trioxide in the presence of water, according to the simplified reaction formula

$$CaCO_3 + SO_3 + 2H_2O \rightarrow CaSO_4 \cdot 2H_2O + CO_2 \qquad (2.5.1)$$

This reaction is increased when NO_2 is present, probably because NO_2 acts as a catalyst for the oxidation of SO_2 to SO_3 on the stone surface (Johansson, Lindqvist & Mangio, 1988). SO_2, mainly from oil- or coal-fuelled power plants, industry and others, and NO_2, mainly from traffic, are considered to be the most damaging gases.

2.5.3 Black layers and scabs

Thin, hard black layers or scabs often occur on non-calcareous rock such as quartz-cemented sandstone, granite and others. The dark colour is mainly due to some chemical compounds like iron-oxide-hydroxides in combination with soot and dirt (Conservation Institute of National Antiquities, 1991).

When ornamental details on a stone facade channel the flow of rain water onto dirty sections of the stone, the discoloration from the dirt is partly washed away. Lighter strips occur on the otherwise dark surface, which is called ‘white washing’. ‘Dirt washing’ occurs when the flowing water causes dirt to accumulate on other parts of the stone (Lala et al, 1989).

2.5.4 Dissolution

Water can cause damage by dissoluting minerals without co-acting with other processes. For example, calcite ($CaCO_3$) has a solubility that is great enough to affect the deterioration of stone with high capillarity, such as calcareous sandstone (Fagerlund, 1994a). This effect is increased when the rain water becomes acid through dissolution of air pollutants, such as sulphur dioxide (SO_2), as the solubility of calcite increases with decreasing pH.

SO_2 is oxidised to form SO_3 by various rather complicated processes, and in the presence of water, SO_3 immediately reacts to form sulphuric acid.

$$SO_3 + H_2O \rightarrow H_2SO_4 \qquad (2.5.2)$$

H_2SO_4 is one of the strongest acids known ($pK_a \approx -2$), and it is considered to be the main contributor to acidification.

In addition, when CO_2 is dissolved in rainwater, the pH decreases. This is a consequence of the acid-base equilibriums $H^+ + HCO_3^- \leftrightarrow H_2CO_3$ and $H^+ + CO_3^{2-} \leftrightarrow HCO_3^-$. However, both H_2CO_3 and HCO_3^- are rather weak acids (pK_a = 6.37 and 10.33, respectively), and their effect on the pH of rainwater is perhaps negligible. The increase of dissolution of calcite

caused by CO_2 is sometimes said to be caused by the formation of calcium bicarbonate, according to the formula

$$CaCO_3 + CO_2 \cdot H_2O \rightarrow Ca(HCO_3)_2 \qquad (2.5.3)$$

According to Amoroso & Fassina (1983), calcium bicarbonate is about one hundred times more soluble than calcium carbonate. According to Hägg (1984), $Ca(HCO_3)_2$ is actually unknown as a substance, so this mode of expressing the increased dissolution is perhaps inappropriate.

The solubility of CO_2 in water, and as a consequence, the dissolved amount of $CaCO_3$, is strongly temperature dependent; the lower the temperature of the water, the more soluble the CO_2. Water at a temperature near the freezing point dissolves almost twice the quantity of CO_2 that it does near 25 °C.

CO_2 gas is a natural constituent of air, but because of its increase in concentration during the last decades, it may be regarded as an air pollutant. Prior to 1900, that is, before industrialisation, the average atmospheric concentration of CO_2 in the Northern Hemisphere was 290 ppm, but now, the concentration is more than 350 ppm as a result of the burning of fossil fuels. In polluted air in urban and industrial regions, the concentration can be as high as 400 ppm (Amoroso & Fassina, 1983).

2.6 Conservation and restoration

This chapter is based on certain parts of the publication *Degradation of Materials and the Swedish Heritage* (Central Board of National Antiquities, 1992-1995), and on an interview (Asp, 1996).

There are many various types of damage occurring to ancient stone buildings and monuments. When one speaks about ‘damage’ in these cases, one mainly means aesthetic deterioration, such as gypsum crusts, exfoliation, scaling, discoloration from soot and dirt and black scabs. The aim of conservation is often to prevent further attack rather than to restore an object to its original shape. Most conservation methods have, by tradition, been developed by experience and ‘trial and error’ rather than by scientific knowledge and facts, although the more scientific points of view have gained more terrain lately.

When a damaged stone is going to be restored, the first thing that has to be done is to document its present condition. This is done by making a written description of it and photographing it.

Sometimes the stone surface is so damaged that the slightest touch causes loss of the material. Before cleaning can be carried out on these areas, the surface has to be pre-consolidated with, for example, silicic acid ester. Cleaning has to be carefully performed so as not to increase the damage. When a very damaged, sensitive object is to be cleaned, it is cleaned by hand with soft brushes. Pure water is normally used, but sometimes, such as when graffiti is to be removed, stronger chemicals have to be used. Salts can be removed with a damp clay covering or by moist compresses. Salts migrate into the clay or compress and precipitate there. After the clay has dried, it falls off the surface or can easily be removed from it.

When washing is completed, the restoration is continued by mending any loose stone pieces. Holes and cracks are covered with mortar. Seriously damaged parts that cannot be mended are replaced by new stone. Replacement of parts that have fallen off completely is not always performed, as the aim of conservation normally is to prevent further attack rather than to restore the object to its original condition.

The new material and the mortar and glue that is used to fix the new parts to the old parts have to be compatible with the old material. The thermal coefficients have to be of the same order of size, and the shrinkage and swelling caused by moisture variation have to be similar, in order not to cause even worse damage after the restoration. The permeability to water also has to be high enough to make drying possible so that moisture doesn't accumulate in the original material. Thus, a good moisture balance must be restored after repair, which is often complex to arrange.

Porous stones, like sandstone, that are easily powdered, are often consolidated in order to improve their strength. This is done with various special chemicals, such as silicone esters. There are a considerable number of consolidating materials on the market today, and there has also been a lot of research done to improve the performance of these materials Not only does there have to be good compatibility with the underlying stone but the adhesion between the stone and the synthetic treatment has to be good as well. It is desirable that the treatment covers only the pore walls so that the pore system remains permeable to vapour and the stone can dry. If the outer stone surface is completely covered and the surface pores are clogged, the water content of the stone would most probably increase and the damage could be disastrous. When the surface is covered, water can still reach the pore system either by capillary suction from the soil or by cracks in the covering surface. When drying is not possible, or reduced, water will accumulate. The treatment also has to be durable and resistant against various atmospheric agitations.

Hydrophobing of stone with various chemical treatments was previously performed on stones in Sweden, as it at least temporarily decreases the capillary suction of the material. As mentioned before, moisture is the single factor with the most influence on deterioration, as it affects almost all other destruction mechanisms. Now, however, this treatment has been almost totally abandoned, until further evaluation of the consequences can be carried out. Hydrophobing is not reversible, so it cannot be removed if it proves harmful. The hydrophobing agents are similar to consolidating agents in the way they bind to the pore surface of the stone material, but they also have a hydrophobic polymer tail that limits capillary transport. Even if the hydrophobic surface is permeable to vapour diffusion, which it mostly is, hydrophobing agents can be harmful to the stone if moisture reaches the internal parts of the stone through capillary suction from the soil or through cracks in the hydrophobed surface. This is because drying of an untreated porous material occurs through both capillary transport and diffusion.

To avoid harmful levels of moisture, changing the environment is often the only possible measure. This can be done by protecting the stone from rain, such as with rainwater pipes or pent-roofing. However, this is often in conflict with the aesthetic value of a building or a facade. To avoid damage caused by freezing of valuable bronze age rock carvings during the wintertime, it has been proposed that mats with electrical heating might be used.

3 Experimental work

3.1 Introduction

In this chapter, different experiments performed to increase the understanding and knowledge of freezing of natural stone are described. The pore structure of the tested materials was studied, as well as the moisture behaviour of the material. Finally some different types of freeze-thaw tests were performed. The freeze-thaw tests are the central part of this study.

3.2 Types of stones

The following materials were tested:

1) Calcite-bound sandstone from Gotland: Types Botvide, Uddvide, Valar and X:1.
2) Limestone from Öland: Types Öland B1, (Öland G1, Öland G2 and Öland Flammig).
3) Limestone from Borghamn, grey from the north quarry.
4) Granite from Bohuslän: Type Bohus red Bratteby.

The physical properties of the different stones are shown in Appendix A.

3.3 Pore structure

3.3.1 Thin section microscopy

Thin section microscopy is a method used to study the structure of pores larger than about 20 μm. A very thin (about 25 μm) slice of the porous material is mounted between two microscope glass slides. The porous material is normally impregnated with epoxy coloured with a fluorescent dye. This makes the sample more coherent and stable, and it also makes it easier to study and analyse the image under the microscope.

Method
One thin section for each kind of stone was prepared. Stone pieces with the dimensions 25 × 25 × 8 mm were dried in an air-circulated oven at a temperature of 50 °C for 24 h. The dried pieces were glued onto a glass slide, a so-called working glass that was later thrown away, with UV-setting glue. The hardened samples were impregnated with de-aired epoxy, which fills the pores of the material. The epoxy contained a yellow, fluorescent dye. Before they were impregnated with the epoxy, the samples were held at a pressure of 4 mbar for 4 h. After the epoxy was applied to the samples, the low pressure was maintained for another 10 minutes before being slowly increased to atmospheric pressure over a time interval of 5 to 10 min. The samples were then allowed to harden for two days. The hardened samples were surface ground and polished with a special polishing wheel with pellets studded with small (25 to 30 μm) natural diamonds. After washing the samples in an ultrasonic bath and drying them, the procedure was repeated once more: impregnation, grinding, polishing, washing and drying.

A microscope slide was glued onto the polished side of each sample. The samples were sawed with a diamond saw to a thickness of about 1 mm, and the working glass was thrown away. Then the surface was ground until the samples were about 50 μm thick. The final

grinding and polishing was continued until the samples were 25 μm thick. The thickness of the samples was determined from the colour of the quartz grains in polarised light. The samples were washed and dried before the other microscope slides were glued onto them with UV-setting glue.

The final thin section was studied under a microscope. Automatic image analysis normally makes it possible to quantitatively evaluate porosity, pore-size distribution, pore shape and continuity, but unfortunately, this was not possible with the materials studied here. The curvature of the grains gave rise to various shades of yellow between the epoxy-filled pores and the somewhat transparent grains, which meant that the colour contrast between the grains and the pores was not sharp enough. For this reason, only a qualitative evaluation could be made.

Results
Photographs of the thin sections are shown in Appendix B.

Sandstones
The colour of the calcite-bound sandstones from Gotland is light grey, normally with no tints in it. No strata can be seen with the naked eye, except in the type Valar, which sometimes contains light brown lines parallel to the bedding. These lines contain more clay minerals than do the light grey parts. The thin section microscopy (Appendix B) of the stones shows that they consist almost entirely of quartz grains with empty spaces between them making them porous. The cementing calcite is not visible, probably because the amount is too small; that is, the calcite layers between the quartz grains are too thin. The size of the grains is 0.1 to 0.2 mm in Botvide and Uddvide and 0.05 to 0.15 mm in Valar. Clay minerals are visible as brown rods, 0.2 to 0.4 mm in length, normally oriented in the same direction, parallel to the bedding.

Limestones
Two different types of limestone from the island Öland in the Baltic Sea were studied with thin section microscopy: a patchy stone from Gillberga, Öland Flammig, and a brown-red one from Horns Udde, Öland B1. In both types, fossils, often rod-shaped, are frequently present, although somewhat more in the Gillberga-stone than in the Horns Udde-stone. Strata can be seen.

In the stone from Gillberga, the fossils are 0.05 to 0.15 mm in size, and the calcite grains are 10 to 150 μm in size. The larger calcite grains consist of fossils. The fossils of Öland B1 are 0.05 to 0.40 mm or even longer, and the calcite grains are about 7 μm in size. Under thin section microscopy with polarised light (Figure B:6, Appendix B), one can sometimes see small holes, which probably emanate from loosened fossils, but no pores are visible. In the Gillberga stone, cracks of about 5 to 6 mm in length and only a few micrometers in width occur. It is not possible to know if the holes and cracks were formed when the sample was prepared. Making a rough estimate based on visible holes and cracks in the thin sections, the porosity is considerably less than 1% for both limestones. This means that such visible cracks and holes cannot alone explain the total porosity of the stones, which is 1.7% for the Gillberga stone and 3.6% for Öland B1. Therefore, the porosity of these stones must be caused by very small pores that are either invisible in thin section microscopy (less than 20 μm in size) or invisible because of other complications in interpreting the thin section, or the porosity must be caused by cracks so thinly distributed that they are not readily ‘caught’ in a thin section of only 25 × 25 mm. A combination of these two is also possible.

Granite

The granite Red Bratteby from Bohuslän has a grey to light pink colour. It is essentially composed of grains of quartz and feldspar 2 to 8 mm in diameter. Flakes of mica can also be seen. The individual mineral grains are densely packed side by side. Between the grains, tiny cracks in a net-shaped pattern are visible under thin section microscopy (Figure A:8, Appendix A). Sometimes cracks are also present within the grains, mainly in the quartz grains. It is difficult to evaluate the porosity caused by these visible cracks, but a rough estimation indicates that the porosity of 0.6% in the granite could be caused solely by these kinds of cracks.

3.3.2 Porosity and density

The porosity and density of a porous material can be measured by weighing a specimen under both dry conditions and vacuum-saturated conditions. The volume of the specimen is measured according to Archimedes' principle by weighing a water-saturated sample completely immersed in water. The desired properties can be calculated using Equations 3.3.1 to 3.3.3.

Method

Stone prisms with the dimensions 2 × 2 × 15 cm or 3 × 3 × 12 cm were sawed from a block with the dimensions 15 × 15 × 30 cm. The prisms were dried in an air-circulated oven, until no more weight loss caused by moisture evaporation occurred, that is, for at least four days. The drying temperature was either 50 °C or 105 °C. The different temperatures made no difference in the porosity and density of the specimens. The dried specimens were allowed to cool in a desiccator with silica gel before they were evacuated for 3 h at a residual pressure of less than 2 mbar. Water was then let into the vacuum chamber until the specimens were completely covered with water. The pump was run for 1 h with water in the vacuum chamber before the pressure was increased to normal atmospheric pressure. The water-saturated samples were then weighed while immersed in water. The surface of the specimens was wiped with a moist sponge before their weight in air was determined. Finally, when the first drying temperature was 50 °C, the dry weight of the specimens was determined after drying in an air-circulated oven at a temperature of 105 °C for at least four days and then cooling them in a desiccator with silica gel. The following can then be calculated:

$$P = \frac{Q_a - Q_{d(105)}}{Q_a - Q_w} \tag{3.3.1}$$

$$\rho_b = \frac{Q_{d(105)} \cdot \rho_w}{Q_a - Q_w} \tag{3.3.2}$$

$$\rho_s = \frac{Q_{d(105)} \cdot \rho_w}{Q_{d(105)} - Q_w} \tag{3.3.3}$$

where

P	porosity (m^3/m^3);
ρ_b	bulk density (kg/m^3);
ρ_s	solid density (kg/m^3);
Q_a	weight of vacuum saturated specimen in air (kg);
$Q_{d(105)}$	weight of specimen dried in 105 °C (kg);
Q_w	weight of vacuum saturated specimen in water (kg);

ρ_w density of water (1000 kg/m^3).

Results
All materials were investigated. The results are shown in Appendix A, Table A:1.

Comments
The calculation of the porosity and the solid density by this method requires that the pore system is actually completely filled with water. That this is so can be checked by comparing the solid density with the density measured with another method, such as with a helium pycnometer, in which the pore system of the pre-dried material is filled with the small atoms of helium gas. This was done for the sandstones Botvide, Uddvide and Valar and for the limestone Öland B1. The values were 2672, 2660, 2683 and 2726 kg/m^3 respectively, which is in very good agreement with the values calculated with the weighing method. The difference is less than 0.6%.

The pore system of the dense Borghamn limestone was not completely filled after the vacuum treatment, as it continued to suck water even after terminated vacuum saturation procedure.

3.3.3 Mercury porosimetry

Mercury porosimetry is a classical method of obtaining the pore size distribution of a porous material. The mercury is forced into the pores by pressure. The higher the pressure, the smaller the pores that are penetrated. Knowing of the intrusion volume of mercury at each pressure makes it possible to find the pore size distribution. The pore radius r corresponding to a certain pressure is calculated by the Washburn equation:

$$r = \frac{-2 \cdot \gamma \cdot \cos\theta}{p} \tag{3.3.4}$$

where
r pore radius (m);
γ surface tension of mercury (0.00485 N/m);
θ wetting angle (in this case (mercury) θ = 130° (Micromeritics, 1987));
p pressure (Pa).

Method
A piece of the stone with the dimensions 1 × 5 × 10 cm was washed for 15 min in an ultrasonic bath. The sample was dried at 105 °C for 12 h. After cooling it over silica gel, the sample was crushed into smaller pieces with a hammer. About 1 g of the crushed material was tested in the mercury porosimeter *Penetrometer number 5* in the Department of Chemical Technology, Lund Institute of Technology.

The instrument calculates the bulk density from the sample weight and the sample volume at the initial mercury filling pressure (Micromeritics, 1987). The solid density is calculated from the bulk density and the pore volume measured at the maximum pressure attained during the run. The calculation of the surface area is based on the assumption of cylindrical pores with radii corresponding to the different pressures and volumes corresponding to the intrusion volume at each pressure.

Results

Only the Botvide sandstone was investigated. In Figures 3.3.1 and 3.3.2, the results from the mercury porosimetry test are shown as the percent cumulative and incremental pore volume versus the pore diameter in micrometers. The results show that a large majority of the pores are about 10 μm in diameter, which correspond well to what is qualitatively seen under thin section microscopy.

The run also gave the following data:

Total intrusion volume: 0,1224 cm^3/g
Bulk density (ρ_b): 1852 kg/m^3
Solid density (ρ_s): 2394 kg/m^3
Surface area (A_s): 1060 m^2/kg

The porosity P can be calculated by

$$P = 1 - \frac{\rho_b}{\rho_s} \tag{3.3.5}$$

This gives P=22.6%.

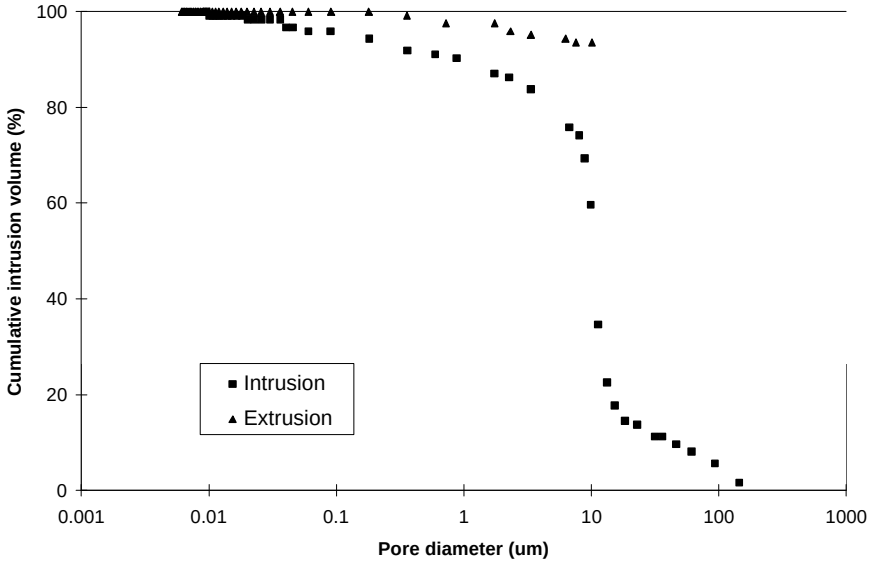

Figure 3.3.1. Result from a run with a mercury porosimeter on Botvide sandstone. Cumulative pore volume (%) versus pore diameter (μm).

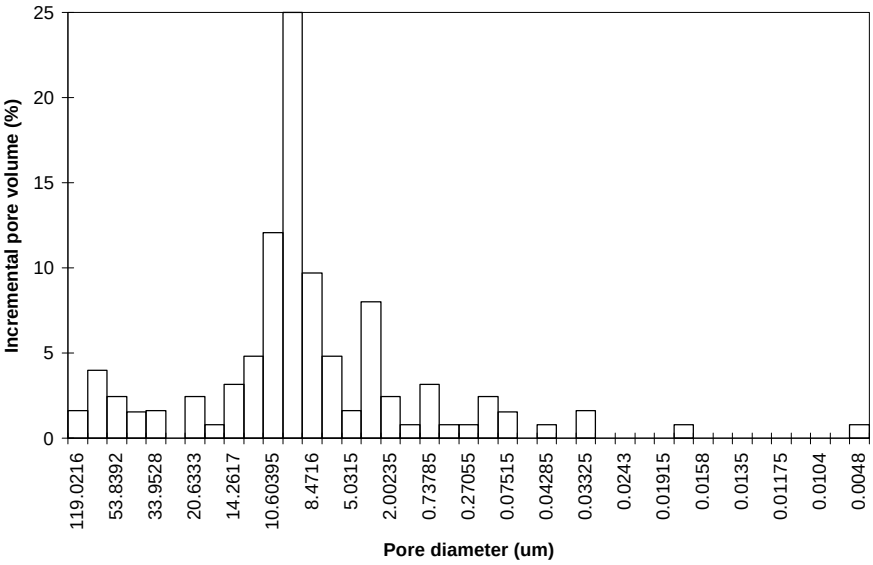

*Figure 3.3.2. Result from a run with a mercury porosimeter on Botvide sandstone. Incremental pore volume (%) versus pore diameter (*m*m).*

Discussion
The bulk density and the solid density values from the mercury porosimetry test are lower than the densities measured by weighing dry and water-saturated specimens in water and in air (see Appendix A, Table A:1). However, the porosity value is in good agreement with the porosity measured with that method, which indicates that all pores were penetrated in the mercury porosimetry test.

As the porosity values agree well but the density values do not, the pore volume measured by the mercury porosimeter was probably correct, but either the sample volume measured by the mercury porosimeter at the initial mercury filling pressure was larger than the correct value or the weight of the sample told to the calculating computer was smaller than the correct value. This is not very likely, though, and the problem remains unsolved.

3.3.4 Moisture equilibrium curves

Sorption isotherms - Method
Sorption isotherms were determined for the three Gotland sandstones Botvide, Uddvide and Valar, for the limestone Öland B1 and for the granite Bohus Red Bratteby. Crushed stone was placed on glass dishes in climate boxes containing air with various constant relative humidities. The various relative humidities were obtained by solutions saturated with various salts that were allowed to reach equilibrium with the air in the box. The salts used and the corresponding values of relative humidity (RH) were LiCl - 11%, $MgCl_2$ - 33%, NaBr - 59%, NaCl - 76%, KCl - 85%, KNO_3 - 95%, K_2SO_4 - 98%. (LiCl - 11% was used only for the sandstones.) The air in each box was mixed with a fan. Each dish with its stone sample was weighed every month until no change in weight occurred from one month to another, and at that time equilibrium was considered to have been reached. Equilibrium was reached after about four months for all stones.

Sorption isotherms - Results and discussion

As an example, the sorption isotherm of the sandstone Uddvide is shown in Figure 3.3.3. The sorption isotherms of the other stones, that is, the sandstones Botvide and Valar, the limestone Öland B1 and the granite Bohus Red Bratteby, are shown in Appendix C. The isotherms for absorption and desorption are almost the same for all of the stones. Thus, almost no sorption hysteresis for the stones tested was found.

The sorption isotherms of the two sandstones and the limestone are quite equal in shape. However, a much larger part of the pore system of the limestone is filled when the moisture content is the same; for example, when the moisture content is 10 kg/m^3, corresponding to about 80% RH, the degree of saturation is 0.30 for the limestone, but only 0.05 for the sandstone Botvide (calculated according to Equation 2.3.1). This indicates a finer pore system in the limestone, which is also seen in the thin sections (see Chapter 3.3.1). The pore system of the limestone becomes filled with water to 88% at an RH of 95%, which is the highest RH tested here. This corresponds well to the capillary suction test, which shows that the pore system of Öland limestone becomes completely filled at the 'nick-point' after suction of free water. For the granite, the degree of saturation is about 66% at 95% RH and about 33% at 80% RH.

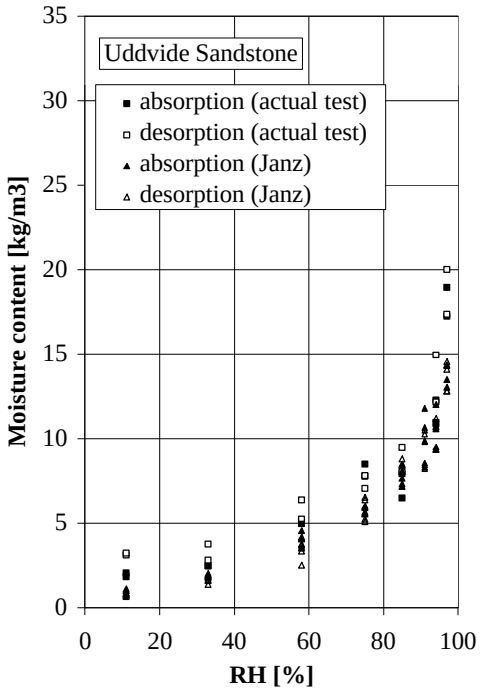

Figure 3.3.3. Sorption isotherm of the sandstone Uddvide. The values measured by Janz (1995) are made on thin slices (thickness 4 mm or 25 mm, diameter = 64 mm). The reason why the values determined by Janz are somewhat lower can be that the piece of stone is taken from another part of the quarry and therefore has a somewhat different pore structure.

Moisture equilibrium curves at high moisture contents

At high relative humidities, the values of the equilibrium moisture content are very uncertain. The difference in relative humidity between 97% and 100% often corresponds to a large moisture content interval. As an example, the moisture content of the sandstone Uddvide increases from 14 kg/m^3 to 160 kg/m^3 when the relative humidity rises from 97% to 100%.

100% RH means suction of free water. A different technique has to be used in this high RH range. One such technique is the use of a *pressure plate extractor*. With this apparatus, water is forced out from a capillary-saturated sample by a well-defined outer pressure.

Thus, by establishing a relationship between the amount of water retained in the sample and the outer pressure, which equals the inner capillary pressure, a so-called moisture equilibrium curve is obtained. This can also be translated into a sorption isotherm in the high RH interval from about 93%, corresponding to a pressure of 10 MPa to 100% corresponding to zero pressure. The relationship between the pore water pressure and the relative humidity is given by the Kelvin equation (Equation 2.3.4).

Moisture equilibrium curves were determined only for the Uddvide sandstone. This was done in another study in our department (Janz 1997). In that report, the theory and the method of using the pressure plate extractor is described in more detail. The results are shown in Figure 3.3.4.

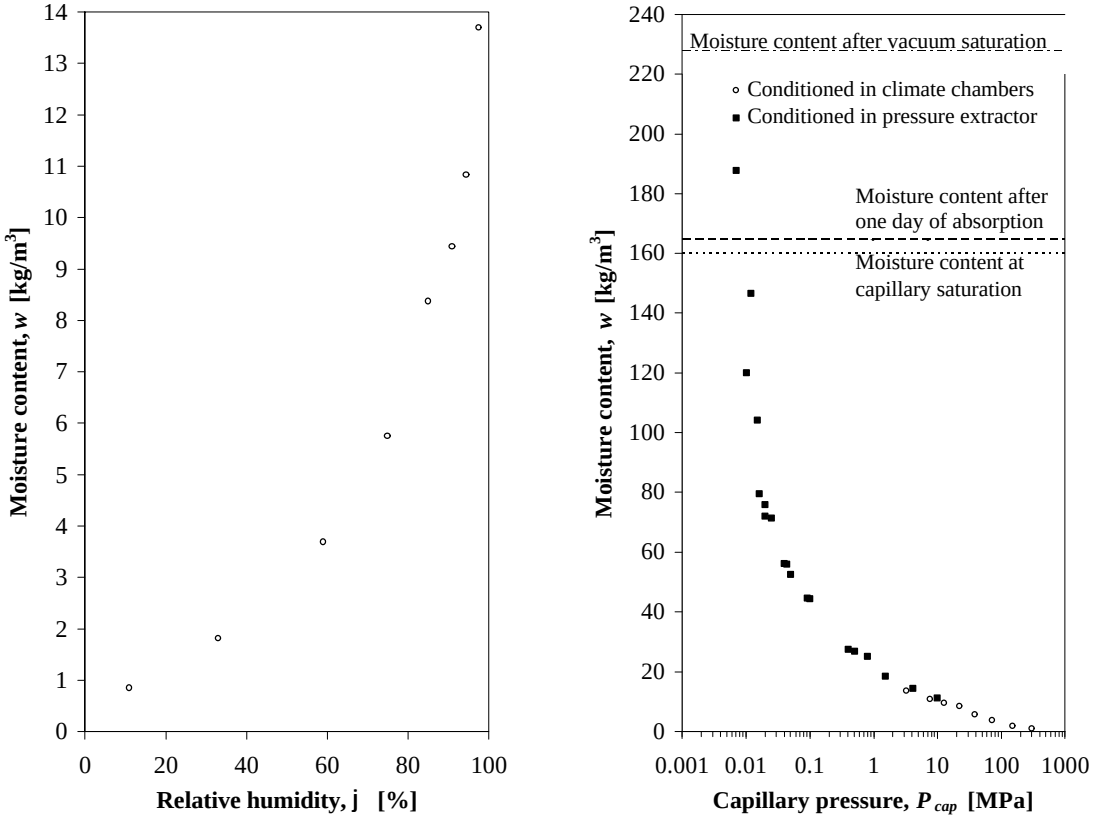

Figure 3.3.4. The left graph shows a conventional sorption isotherm of the sandstone Uddvide (mean value of 5 slices, see Figure 3.3.3. above). These values are recalculated into a capillary pressure according to the Kelvin equation and plotted in the right graph together with values from a pressure plate extractor (Janz, 1997).

Discussion

A pore size distribution can be obtained from the sorption isotherm according to the methods described in Chapter 2.3.2 (Equation 2.3.4). The principle is basically the same as the one for mercury intrusion porosimetry, which is based on the same theory (Equation 3.3.4). The values in the right graph in Figure 3.3.4 can be recalculated to give the cumulative pore volume versus pore diameter. This has been done in Figure 3.3.5. A comparison with values

from a test using mercury intrusion porosimetry is shown in the figure as well, which shows that the two methods agree well.

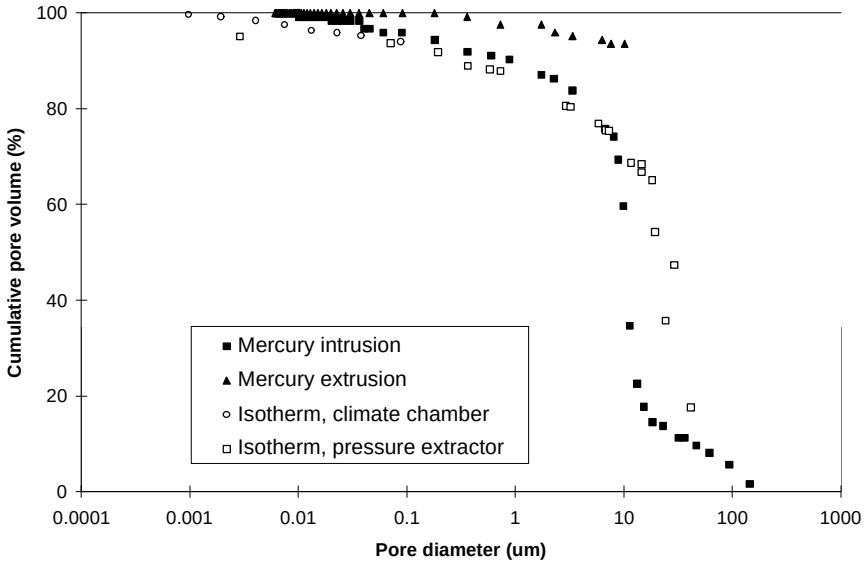

Figure 3.3.5. Pore size distribution acquired from two different methods.

From the moisture content at 18% RH (see Chapter 2.3.2) the internal surface area of the materials can be calculated according to the equation

$$A_s = 3.5 \cdot 10^6 \cdot \frac{m_{18\%}}{\rho_b} \tag{3.3.6}$$

where
A_s surface area (m^2/kg);
$m_{18\%}$ moisture content at 18% RH (kg/m^3);
ρ_b density of the porous material (kg/m^3).

The equation is basically the same as Equation 2.3.8 in Chapter 2.3.2. The pore radius, assuming all pores are of the same size, can be calculated as well, according to

$$r = \frac{a \cdot P}{3.5 \cdot 10^6 \cdot m_{18\%}} \tag{3.3.7}$$

where P is the porosity and a = 3 when spherical pores are assumed and a = 2 when cylindrical pores are assumed. The equation is basically the same as Equations 2.3.9 and 2.3.10 in Chapter 2.3.2.

The values of the moisture content at 18% RH, density, porosity and calculated values of surface area and pore radii are shown in Table 3.3.1.

Table 3.3.1. Surface area and pore radii calculated from sorption isotherms.

	$m_{18\%}$ (kg/m^3)	ρ_b (kg/m^3)	P	A_s (m^2/kg)	*r (sphere)* (nm)	*r (cyl.)* (nm)
Botvide	3	2080	0.222	5097	63	42
Uddvide	2	2069	0.227	3416	96	64
Valar	4.5	2220	0.174	7163	33	22
Öland B1	2	2639	0.034	2678	14	10
Granite	0.8	2637	0.0061	1072	6	4

The value of 5097 m^2/kg for the surface area from water sorption of the sandstone Botvide can be compared to the value obtained of 1060 m^2/kg from the mercury intrusion porosimetry test. Considering the many approximations made, the values are still in good agreement, as they are in the same order of magnitude. However, it is of interest here to mention that the surface area measured with nitrogen near its condensation point, which is the conventional method of measuring surface area, normally gives a smaller value of surface area than does a measurement with water vapour (Mikhail & Abo-El-Enein, 1972). The much smaller values for pore radii, compared to the values obtained from the mercury intrusion porosimetry test and thin section microscopy, probably mainly result from the erroneous assumption of one single pore size.

3.4 Sorption enthalpies

When water is adsorbed on a surface, heat is emitted. This heat can be registered by an isothermal micro-calorimeter. Sorption enthalpies of sandstone have been investigated with this method. The results from this investigation are presented in Appendix D, which is based on a study by Wadsö (1994).

3.5 Moisture mechanics

3.5.1 Capillary suction

The ability of the stones to absorb water under natural conditions is an important factor in deterioration, especially frost deterioration. Capillary suction tests give a hint about how the stone will behave during suction of ground water or rainwater.

Method

The principles of a capillary suction test are shown in Figure 2.3.1. Dried stone prisms with the dimension 3 × 3 × 12 cm were placed with one long side on a grid a few millimetres below the water surface. The pre-drying temperature before water absorption was 50 °C, except for granite, which was dried at both 50 °C and 105 °C. The prisms were weighed during the water absorption test at longer and longer time intervals. Before a prism was weighed, the wet surface was wiped with a moist sponge to remove surface water. The results from the capillary suction tests are expressed as degree of saturation versus square root of time. For all stones except the granite the degree of saturation S_t at each suction time t is calculated as

$$S_t = \frac{Q_t - Q_{d(105)}}{Q_a - Q_{d(105)}} \tag{3.5.1}$$

where

Q_t weight of the specimen at the suction time t (kg);
Q_a weight of a vacuum-saturated specimen (kg);
$Q_{d(105)}$ weight of a specimen dried at 105 °C (kg).

S_t for granite is calculated as

$$S_t = \frac{(Q_t - Q_{d(105)}) \cdot \rho_b}{Q_{d(105)} \cdot P \cdot \rho_w} \tag{3.5.2}$$

where ρ_b is the bulk density of the material (kg/m^3), P is the porosity of the material (m^3/m^3) and ρ_w is the density of water (1000 kg/m^3).

From the graphs some quantities can be evaluated; t_k is the time at the nick-point (h), S_k is the degree of saturation at the nick-point (m^3/m^3) and A_w (kg/m^3·s$^{1/2}$) is the sorption coefficient. The penetration coefficient B ($m / \sqrt{s}$) is explained in Chapter 2.3.2 (Equation 2.3.2) and is evaluated from t_k and the specimen thickness h:

$$B = \frac{h}{\sqrt{t_k}} \tag{3.5.3}$$

In this case, h = 0.03 m.

A_w is calculated according to Equation 3.5.4 below:

$$A_w = \frac{(S_k - S_0) \cdot 1000 \cdot P \cdot h}{\sqrt{t_k}} \tag{3.5.4}$$

where S_0 is the degree of saturation at start of suction (m^3/m^3), 1000 is the density of water (kg/m^3) and P is the porosity (m^3/m^3).

Results
In Appendix E, the results from the capillary suction tests are plotted. They are expressed as degree of saturation versus the square root of time. This makes it possible to compare the moisture content directly with the freeze-thaw tests; the dilatation tests (Chapter 3.7) and the 'S_{crit}-tests' (Chapter 3.8). Note, however, that S-values for suction times lower than t_k are fictitious since S is based on the total pore volume in the specimen, and only a fraction of the specimen is penetrated by moisture. Therefore, for the wet part of the specimen, S is just as high as S_k or even higher because of the dissolution of air in the pores. In Table 3.5.1, t_k, S_k, B ($m / \sqrt{s}$) and A_w (kg/m^3·s$^{1/2}$) are presented for each of the tested stones. t_k is the time at the nick-point (h) and S_k is the degree of saturation at the nick-point (m^3/m^3). For comparison with other building materials, data for concrete, brick and lime silica brick are also presented in the table. The t_k-value depends on the thickness of the specimen and is therefore not shown.

Table 3.5.1. Capillarity of specimens with the suction height 3 cm.

Stone	t_k (h)	S_k	B (m/(s)$^{1/2}$)	A_w (kg/m^{2}s$^{1/2}$)
Sandstone Botvide	0.19	0.68	$1.1 \cdot 10^{-3}$	0.16
Sandstone Uddvide	0.11	0.69	$1.5 \cdot 10^{-3}$	0.23
Sandstone Valar	2.11	0.68	$0.34 \cdot 10^{-3}$	0.038
Limestone Öland B1	74.7	1	$5.8 \cdot 10^{-5}$	$1.8 \cdot 10^{-3}$
Limestone Öland G1	148.2	1	$4.1 \cdot 10^{-5}$	$0.6 \cdot 10^{-3}$
Limestone Öland G2	57.6	1	$6.6 \cdot 10^{-5}$	$2.2 \cdot 10^{-3}$
Limestone Öland Flammig	167.8	1	$3.9 \cdot 10^{-5}$	$0.5 \cdot 10^{-3}$
Borghamn Limestone	121	1	$4.5 \cdot 10^{-5}$	$7.4 \cdot 10^{-4}$
Granite dried at 50°C	16	0.9	10^{-4}	$3 \cdot 10^{-7}$
Granite dried at 105°C	16	0.7	10^{-4}	$5 \cdot 10^{-7}$
Concrete		0.71-0.88(1	10^{-4} - 10^{-3}(2	0.01-0.03(3
Brick		0.32(4-1(5	10^{-3}(3	0.09-0.37(3
Lime silica brick		0.76-0.81(4	$3 \cdot 10^{-4}$(6	0.07-0.08(6

(1 Data from Hedenblad & Nilsson (1985)
(2 Data from Concrete Handbook (1994)
(3 Data from Nevander & Elmarsson (1994)
(4 Data from Fagerlund (1972)
(5 Sandin, K., Personal communication (1997)
(6 Janz, M., Personal communication (1997)

Discussion

The *sandstones* have a quick initial suction, especially the more porous Botvide and Uddvide. From this point of view, the sandstone almost behaves like a sponge. After the 'nick-point' the pore system continues to fill for a long time until it becomes completely saturated. This is probably because enclosed air bubbles slowly dissolve into the water (Fagerlund, 1994b). Complete saturation for the sample dimension studied here occurs after about 3 months. The time for complete saturation is obtained by extrapolation of the capillary suction curves, and it is also confirmed by the dilatation tests presented in Chapter 3.7, where sandstone prisms of the dimension 2 × 2 × 15 cm were completely saturated after having been submerged in salt solutions for 3 months.

The *limestones* have a slower suction than the sandstones, but the pore system becomes completely filled at S_k, which is a rather unusual and risky property for a porous material from the point of view of resisting frost deterioration.

The *granite* has no clear nick-point, which is why the values calculated in the table are approximate. The granite becomes completely saturated after a suction time equal to the t_k of limestone.

Some of the values of S exceed 1, which must mean that the weighing of the specimens was not accurate or that there is actually more water in the pore system after capillary suction than after vacuum saturation. For the granite, these excessive values are explained by the approximate calculation of the degree of saturation and the low porosity, which makes it difficult to weigh accurate enough.

3.5.2 Moisture permeability

Method
The moisture permeability of the sandstones Uddvide and Valar, the limestone Öland B1 and the granite Bohus Red Bratteby was studied using the so-called *cup method* (Figure 3.5.2). Slices of the stones were used as covers on cups. The relative humidities on the outside of the cups and inside the cups were different. This caused moisture to flow through the porous material from the side with higher relative humidity to the side with lower relative humidity. The moisture flow was obtained by weighing the cups at various times when steady state was reached.

The variation of the moisture permeability as a function of RH between about 35% to 100% was investigated. The RH outside the cups was about 35%, and the RH values inside the cups were about 60, 75, 82, 85, 90, 95, 98, and 100%. These RH values were obtained using saturated solutions of the following salts respectively: NaBr, NaCl, KBr, KCl, KNO_3 and K_2SO_4. Pure water was used to obtain RH 100%. Triple cups were used for each RH. The thickness of the sample was chosen so that the moisture transport was satisfactory, that is, so that the weight loss was high enough to be measurable within one week.

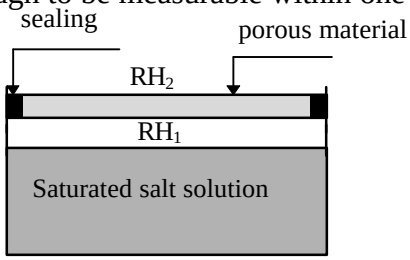

Figure 3.5.2. The cup method for determination of moisture permeability.

The bottom of the cup was removable so that the salt solution could be refilled. This made it possible to keep the distance between the liquid surface and the bottom surface of the sample almost constant. If the distance between the liquid sample and the bottom of the sample increases too much, the RH at the bottom of the sample will be lower than intended because of the diffusion resistance of the air. This has an especially large effect for materials with a high open porosity, like sandstone. The diffusion resistance of the air between the liquid surface and the bottom surface of the sample is, however, taken into account when evaluating the results.

Results and discussion
In Appendix F, the results from the cup method are shown both as the Kirchhoff-potential ψ (kg/m·s), defined by Equation 2.3.12, and as the moisture permeability δ_v (m^2/s), defined by Equation 2.3.11 with ϕ as the vapour concentration in air ρ (kg/m^3), as a function of the relative humidity inside the cup. The graph showing δ_v as a function of the relative humidity is the derivative of the graph showing ψ as a function of the relative humidity. ψ and δ_v are described in more detail in Chapter 2.3.2.

δ_v increases with increasing porosity of the different stones, which is what is expected. The sudden increase in moisture permeability that appears at a relative humidity of approximately 65% for the sandstones and the limestone and at about 97% for the granite occurs because the capillary transport of moisture in the liquid phase becomes active at this point. At lower relative humidities most of the moisture transport occurs as diffusion of vapour.

3.6 Unsealed multi-cycle freeze-thaw tests - Scaling tests

3.6.1 Introduction - overview of all tests

It has been known for some decades that salt solutions cause more severe surface damage to concrete in freeze-thaw tests than does pure water. It is also a general opinion that a pessimal salt concentration exits, which is considered to be about 3% by weight for NaCl (Arnfelt, 1941; Verbeck & Klieger, 1957; Lindmark 1993). The tests described here were performed to show whether this is also true for natural stone.

In the so-called Unsealed multi-cycle freeze-thaw test or Scaling test undamaged stone prisms, that is, unweathered stone, were frozen and thawed a number of cycles while completely submerged in salt solutions of various concentrations. The damage was measured as weight loss or scaling. Internal damage, that is, internal crack formation and loss of cohesion, was measured as a loss in fundamental frequency of transverse vibration or as a calculated dynamic modulus of elasticity (see Appendix G).

A: Tests with the same salt concentration inside and outside the stone

Tests with sandstones

The three sandstones from Gotland, Botvide, Uddvide and Valar, were freeze-thaw tested in NaCl solutions of various concentrations. Three tests were performed with only small differences between the tests. The results from these tests are presented in Chapter 3.6.2. In Chapter 3.6.3, a discussion about the salt transport into the pore system is presented. The sandstone Uddvide was also treated in various concentrations of Na_2SO_4. These results are shown in Chapter 3.6.4.

Tests with limestones

The red limestone B1 from Öland and a limestone from Borghamn were freeze-thaw tested in solutions of NaCl and Na_2SO_4 of various concentrations. These results are shown in Chapter 3.6.4.

Test with granite

In Chapter 3.6.5, the results from a freeze-thaw test with granite are presented. This was only a pre-test, but as the granite was almost undamaged, it was not tested further.

In all the tests mentioned above, the stone samples were capillary saturated before the start of the test with the same solution as they were submerged in during the freezing and thawing. The term ‘capillary saturated’ indicates that the stone samples had been stored in the solution at least until the nick-point had been reached.

B: Tests with different initial salt concentrations inside and outside the stone

In the tests presented in Chapter 3.6.6, the prisms were saturated with a solution of a concentration different from the one they were submerged in during the freeze-thaw test. This was done because it was previously known for concrete that the internal concentration plays a small or even negligible role in scaling (Lindmark, 1993), and this may be valid for natural stone as well. Various combinations of internal and external salt concentrations were tested. One sandstone (Valar) and one limestone (Öland B1) were tested using the two different salts NaCl and Na_2SO_4. In the tests described under A (above), the damage was measured only at the end of the test. In the actual tests damage was also measured at certain intervals during the test.

3.6.2 Sandstone tested in NaCl solution

The aim of these tests was mainly to see if a pessimal, or most dangerous, salt concentration exists. The three sandstones from Gotland: Botvide, Uddvide and Valar were freeze-thaw tested in NaCl solutions of various concentrations. Three different test series were performed. The different test variables in the three test series can be seen in Table 3.6.1. The drying temperature (50 °C-105 °C) and the time in solution before the freeze-thaw test (4-10 days) probably did not influence the results.

Method

Sawed stone prisms of the three sandstones from Gotland: Botvide, Uddvide and Valar, with the dimensions 3 × 3 × 12 cm were pre-dried in an air-circulated oven until no more weight loss caused by moisture evaporation occurred, that is for about four days. The bedding of the Gotland sandstone is not visible to the naked eye, so it is not possible to know if the prisms were sawed parallel or perpendicular to the bedding. One prism for each sandstone and salt concentration was tested. The prisms were weighed after cooling them over silica gel, and in test series 3, the fundamental resonant frequency at transverse vibration was measured. The method of measuring the resonant frequency and of calculating the dynamic modulus of elasticity is explained in more detail in Appendix G. Measuring the loss in the dynamic modulus of elasticity is a way of measuring the internal damage. In tests series 1 and 2, the resonant frequency was measured with an older piece of equipment that was found to be so inaccurate that the results have limited relevancy.

The prisms were placed in a standing position in vessels containing salt solutions of various concentrations, one vessel for each specimen. The vessels contained about 850 ml of solution, and the upper surface of the stone prism was about 1 cm below the surface of the solution. The specimens were kept completely submerged in the solution long enough to be capillary saturated before the freeze-thaw test started. Before the freeze-thaw test started, the capillary-saturated prisms were weighed, and in test series 3, the fundamental resonant frequency at transverse vibration was measured once again. The vessels with their specimens were placed in a freeze-thaw cabinet with an automatic freeze-thaw cycle.

Dummies, treated equally to the prisms but containing a thermocouple in a drilled hole in their centres, were also placed in the freezer in a vessel filled with solution. These dummies were used to measure the temperature to ensure that the entire prisms reached the desired temperature condition during the freeze-thaw cycling. The freeze-thaw cycles are shown in Appendix H. It must be noted that in 10 of the freeze-thaw cycles in test series 1, the inner parts of the stone prisms were not completely frozen.

After the freeze-thaw test, the fragments that had loosened, or that could easily be loosened from the specimen with the fingers, were collected in a filter paper. The papers with the fragments were then dried for four days and were weighed after cooling them over silica gel. The stone ‘torsos’ left were weighed, and in test series 3, the fundamental resonant frequency at transverse vibration was measured both before and after drying.

Results

Photographs of the tested specimens are shown in Appendix I. All data for the tested specimens are presented in Appendix P1.

Table 3.6.1. Characterisation of different freeze-thaw series of sandstones in NaCl solution.

	Series 1	Series 2	Series 3
Concentration of NaCl (% by weight)	0%; 2.5%; 5.0%; 10.0%	0%; 2.0%; 4.0%; 6.0%; 8.0%; 10.0%	0%; 0.5%; 1.0%; 1.5%; 2.0%; 2.5%; 3.0%; 3.5%
Drying temperature before pre-saturation	95 °C	105 °C	50 °C
Time in solution before freeze-thaw test	4 days	10 days	4 days
Number of cycles	20	7	20
Freeze-thaw cycle	Figures H:1-H:3	Figure H:4	Figure H:5
Measuring of resonant frequency	no	no	yes

Figure 3.6.1 shows that the sandstone Valar is more sensitive to freezing and thawing in salt solution than are the other two sandstones. The pessimal salt concentration is somewhere between 0% and 4% by weight.

According to Figure 3.6.2, the pessimal salt concentration seems to be less than 0.5% by weight for the sandstone Valar. Some of the stone prisms tested at lower salt concentrations (series 3; Botvide 0%, 0.5%, and 1.0%; Uddvide 0%) were divided into two pieces during the test. In some of these cases, the smaller piece was very badly scaled or rather crumbled. However, from the test series 1 and 2, it is known that the weight loss for specimens freeze-thaw tested in pure water is less than that for specimens freeze-thaw tested in 2% NaCl solution.

Figure 3.6.3 shows that the internal damage as determined by the dynamic E-modulus is independent of the salt concentration. The reduction in the E-modulus is rather high, however.

Discussion

All these sandstones have a rather low degree of frost resistance when tested in weak salt solutions. For concrete, a maximum weight loss corresponding to 0.2 mm scaling depth after 56 freeze-thaw cycles is accepted (Bro 94, 1994). This corresponds to about 0.07 mm after 20 freeze-thaw cycles, which corresponds to about 1% weight loss for the actual stones at evenly distributed scaling. Most stones have a larger scaling than that, especially as the scaling is concentrated to only a part of the surface.

All test series show that the denser sandstone Valar was more damaged than the more porous stones Botvide and Uddvide. The difference between the types Botvide and Uddvide is small, but there is a tendency for Uddvide to be more damaged than Botvide during the same freeze-thaw conditions. The pessimal salt concentration is not very distinct for the more porous sandstones Botvide and Uddvide. In test series 1, the pessimal salt concentration for Valar is shown to be within the interval 0 to 4.5%, which is confirmed by test series 2; the interval in this test is 0 to 4%. In test series 3, the pessimal salt concentration is shown to be within the interval 0 to 0.5%. For the specimens in test series 3 that fractured, salt scaling was not the predominant destruction mechanism, but internal damage was. The results from the different tests cannot be quantitatively compared to each other, as the freeze-thaw cycles differ. The reason the samples were more damaged in test series 3 than in test series 1 is probably because the internal parts of the samples were not completely frozen during the first

10 cycles in test series 1, so the actual number of freeze-thaw cycles in test series 1 was 10 and not 20.

It is interesting to note that the scaling is clearly dependent on the salt concentration, whereas the internal damage is not, although the salt solution also reaches the internal pore system (see Chapter 3.6.3). This implies that the salt scaling is governed by a process that is active only at the surface of the specimen in contact with the solution. This phenomenon can be explained by the mechanism proposed by Lindmark (1996), in which ice lenses near the surface grow at the expense of the solution. It seems reasonable to believe that the internal damage is governed solely by the degree of saturation, which is probably almost equal in all specimens of the same kind in the same test, as they are allowed to suck solution for an equally long time until they reach capillary saturation. The difference between the internal damage measured by the loss in E-modulus on dry and wet samples can be explained by the relatively large porosity of the sandstones; when the pore system is filled with water, the sandstone actually becomes a different material or a different composite from the one it is when it is filled with air.

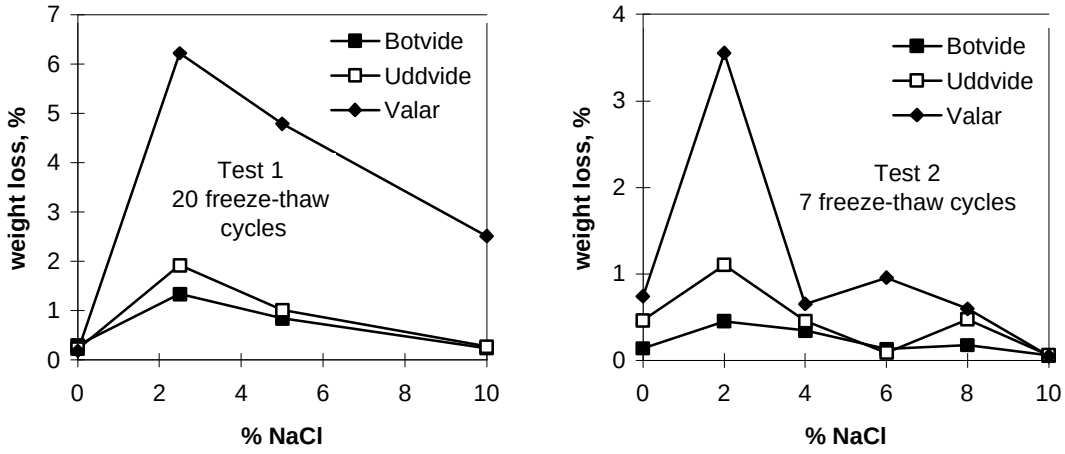

Figure 3.6.1. Weight loss as a percentage of the original weight of sandstones freeze-thaw tested in NaCl solution versus the salt concentration. Test series 1 and 2.

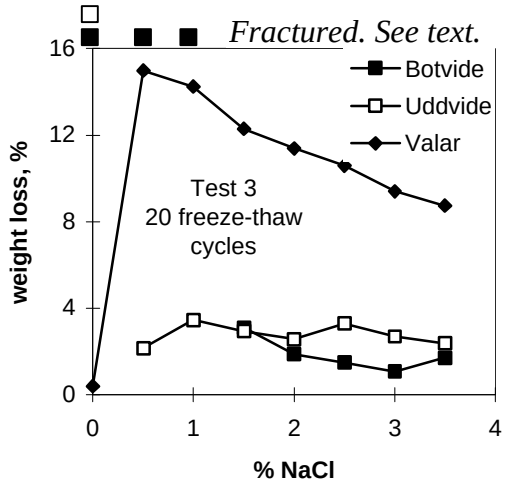

Figure 3.6.2. Weight loss as a percentage of the original weight of sandstones freeze-thaw tested in NaCl solution, versus the salt concentration. Test series 3.

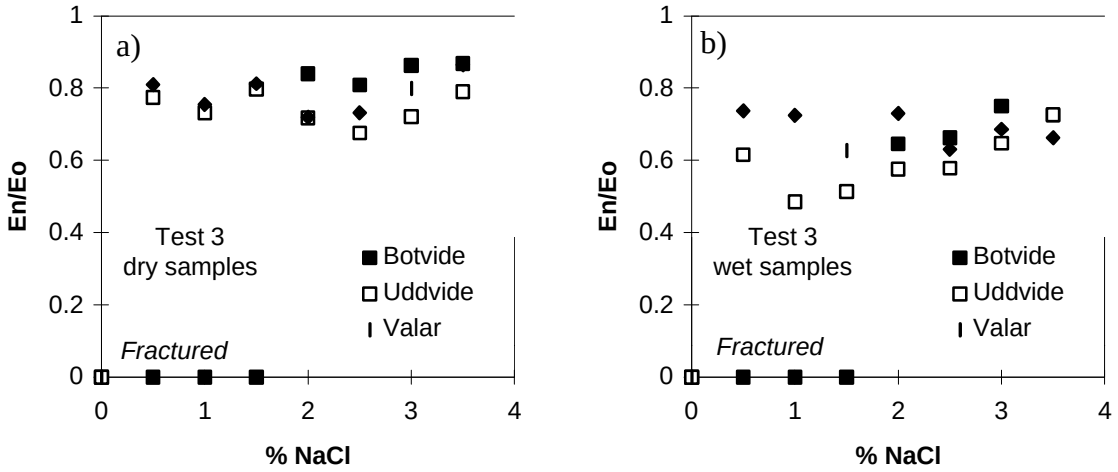

Figure 3.6.3. The relative loss in dynamic modulus of elasticity of sandstones freeze-thaw tested in NaCl solution, versus the salt concentration. E_0 is the dynamic modulus of elasticity before freeze-thaw test. E_n is the dynamic modulus of elasticity after a freeze-thaw test. a) E measured on dry samples. b) E measured on wet samples.

Here, it should also be mentioned that a solution of 1% by weight is realistic in a sandstone saturated with solution and exposed to air pollution. This is based on calculations using data from field measurements (Löfvendahl & Asp, 1995).

3.6.3 Estimation of the salt content of the freeze-thaw specimens

A question that could be asked in connection with these tests is whether salt is really transported into the pore system together with the water sucked in. It is a well-known fact that concrete obstructs the intake of Cl^- ions, partly because the diffusion is hindered by the small pores, partly because there might be an ion exchange in which Cl^- ions replace OH^- ions in the pore solution and partly because Cl^- bind to the pore walls. In the actual sandstones, these effects are probably much smaller because the pores are much bigger, the pore water is neutral and probably no binding sites exist.

The transport of salt could be detected by the weighing performed in the scaling test series 1 and 2 described in Chapter 3.6.2. This could not be done in any other of the tests described in this report, as the salt quantity was too small to be detected by weighing, either because the salt concentration was too low or because the material was too dense (limestone and granite). Scaling test series 3 for sandstone could not be used for this purpose because the salt concentration was too low and the scaling was too large, which made the accuracy of the weights too low.

The 'true' amount of salt can be calculated from the weights. As the samples freeze-thaw tested in pure water had decreased somewhat in weight, possibly because of leaching, the 'true' amount of salt inside the specimen, b_t, must be compensated for by using the following equation:

$$Q_{dn}^{(0\%)} + Q_{ds}^{(0\%)} - Q_{d0}^{(0\%)} = -a \tag{3.6.1}$$

$$b_t = Q_{dn} + Q_{ds} - Q_{d0} + a \tag{3.6.2}$$

where

-a weight loss from possible leaching in samples freeze-thaw tested in pure water (g);

b_t 'true' amount of salt (g);

Q_{dn} weight of a dry sample after a freeze-thaw test (g);

Q_{ds} dry weight of scaled off material (g);

Q_{d0} weight of a dry sample before a freeze-thaw test (g).

'(0%)' indicates freezing and thawing in pure water.

The calculated amount of salt in the specimen, b_c, (g) is

$$b_c = (Q_n + Q_{ds} - Q_{d0}) \cdot C \tag{3.6.3}$$

where Q_n is the weight of a wet sample after a freeze-thaw test (g) and C is the concentration by mass of salt (g/g).

The results of this calculation are shown in Figure 3.6.4. The agreement is good between the 'true' amount of salt and the salt that should be transported into the specimen by suction if salt transport is not hindered. This indicates that the outer and the inner salt concentrations were almost the same.

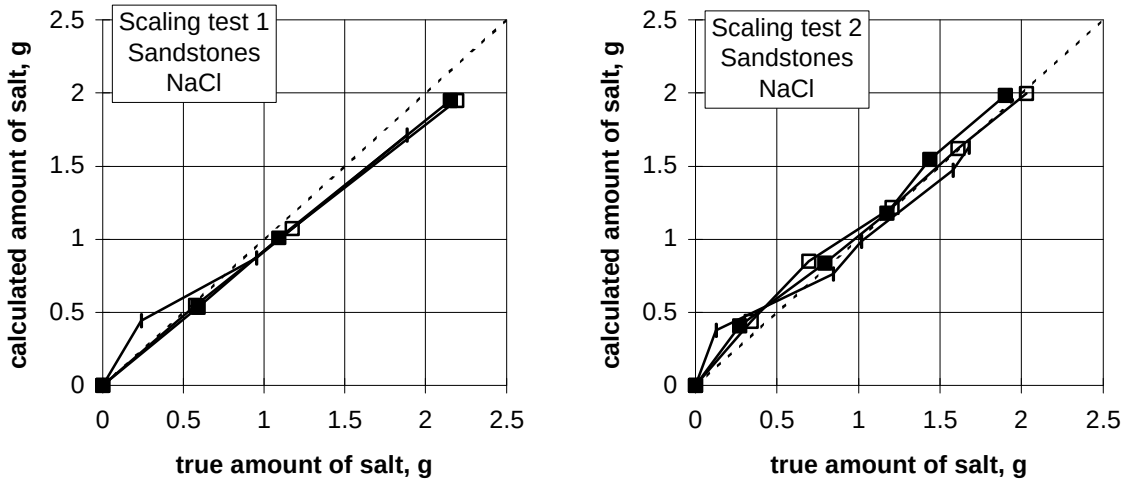

Figure 3.6.4. Relationship between the true amount of salt and the calculated amount of salt based on the absorption of solution in specimens after freeze-thaw test series 1 and 2 (described in Chapter 3.6.2). The linear relationships show that salt is transported into the pore system together with water sucked in.

3.6.4 Limestone tested in NaCl and Na_2SO_4 solution and sandstone Uddvide tested in Na_2SO_4 solution

In this test the effects of different salts and different salt concentrations were investigated in freeze-thaw tests of some natural stones. The idea of comparing the different salts based on the concentration by weight comes from the results of the study made by Verbeck and Klieger (1953), in which they found that a pessimal concentration of about 2% by weight was valid for several different solutes used for freeze-thaw testing concrete.

Method

The test procedure, with the exception of some minor details mentioned below, was the same as that in test series 3 described in Chapter 3.6.2 (above). The limestones were sawed with the bedding direction parallel to the long side of the prisms. The bedding direction of the Gotland sandstone is not visible to the naked eye, so it is not possible to know if the prisms were sawed parallel or perpendicular to the bedding. The salt concentrations used were 0%, 0.5%, 1.0%, 2.0%, 3.0% and 4.0% by weight of the salts NaCl and $Na_2SO_4 \cdot 10H_2O$ and Na_2SO_4. The salts $Na_2SO_4 \cdot 10H_2O$ and Na_2SO_4 are, of course, the same solute, but their concentrations differ by a factor of 2.27; that is, the concentration of Na_2SO_4 is 2.27 times higher than that for $Na_2SO_4 \cdot 10H_2O$ when the percentage by weight is the same. The drying temperature before and after freezing and thawing was 105 °C for Öland limestone tested in NaCl and $Na_2SO_4 \cdot 10H_2O$ and for sandstone tested in $Na_2SO_4 \cdot 10H_2O$. It was 50 °C for Borghamn limestone, Öland limestone tested in NaCl and for all stones tested in Na_2SO_4. The drying temperature is not supposed to influence the results, because there is no reason to believe that the drying temperature has any marked effect on the structure of the stones in question. Limestone tested in NaCl was exposed to only 4 freeze-thaw cycles because of the huge weight loss. All other stones were exposed to 20 freeze-thaw cycles.

Results - External damage

External damage was determined by measurements of the weight loss. Photographs of the specimens tested are shown in Appendix I. All test data and calculated properties for the tested specimens are shown in Appendix P2.

In Figures 3.6.5-3.6.9 below, the results are presented as external damage versus the salt concentration. The external damage is expressed as weight loss as a percentage of the original weight (Figures 3.6.5-3.6.6).

Figure 3.6.5. shows that the Öland limestone tested in NaCl is more scaled when it is freeze-thaw tested in intermediate NaCl concentrations within the range 0.5% and 3% than when it is tested in pure water or in a concentration of 4%. However, a dummy specimen tested in 4% NaCl solution was completely destroyed after 20 cycles. Figure 3.6.5.b shows that the Öland limestone in the weaker Na_2SO_4 solution, expressed as percentage by weight of $Na_2SO_4 \cdot 10H_2O$, is almost unscaled. The stronger Na_2SO_4 solution, expressed as percentage by weight of Na_2SO_4, gives more scaling, but the scaling in this solution is still less than the scaling that occurs in a NaCl solution of the same percentage by weight. It is possible, though, that since the stronger and weaker solutions differ only by a factor of about 2, this difference might be caused by differences in the stone quality, for example, the stones were from different deliveries and therefore had somewhat different properties.

Figure 3.6.5.c shows that the Borghamn limestone has low scaling and that no significant effect from either of the salts can be noted.

Figure 3.6.5.d shows that, like the Öland limestone, the sandstone is more scaled when it is tested in NaCl solution than when it is tested in Na_2SO_4 solution, but the difference between the effects of the two salts is considerably smaller for the sandstone than it is for the limestone. The results of the freeze-thaw test of the sandstone in NaCl are taken from test series 3 described in Chapter 3.6.2. For the sandstone, none of the Na_2SO_4 concentrations used gave significantly more scaling than pure water did.

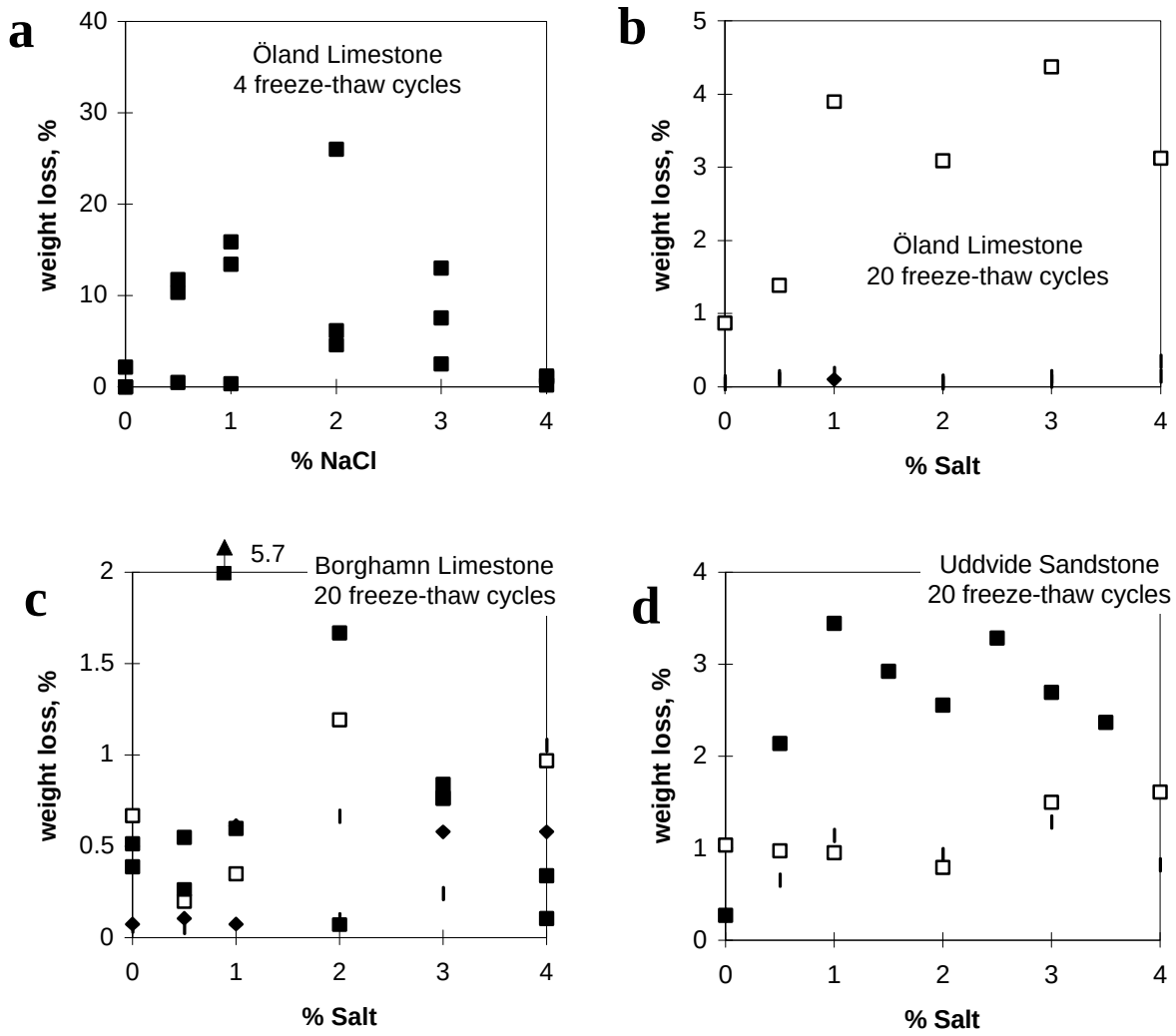

Figure 3.6.5. Weight loss as a percentage of original weight versus the salt concentration. Symbols: ■ = NaCl, □ = Na_2SO_4, ♦ = $Na_2SO_4 \cdot 10H_2O$. *Note: different scales in different figures. The concentration is expressed as % by weight of the actual salt; i.e. a certain concentration of pure* Na_2SO_4 *is 2.27 times as strong when it is expressed as %* Na_2SO_4 *than when it is expressed as %* $Na_2SO_4 \cdot 10H_2O$. *a) Öland Limestone B1 exposed to 4 freeze-thaw cycles in NaCl solution. b) Öland limestone B1 exposed to 20 freeze-thaw cycles in* Na_2SO_4 *solution. c) Borghamn limestone exposed to 20 freeze-thaw cycles in different salt solutions. d) Uddvide sandstone exposed to 20 freeze-thaw cycles in different salt solutions.*

Results - Internal damage

The internal damage was determined by measurements of the fundamental frequency of transverse vibration. For calculation of the dynamic modulus of elasticity from the fundamental frequency, the loss of material at the surface must be taken into account. The theory for this correction is described in Appendix G, and the correction factor is shown in Appendix P2. The internal damage is expressed in Figure 3.6.7 as the relative loss in dynamic modulus of elasticity measured on wet and dry samples.

Figures 3.6.7 a1 and a2 show that the Öland limestone is more damaged when it is freeze-thaw tested in NaCl solution, irrespective of the salt concentration, than it is when it is tested in pure water.

For Öland limestone freeze-thaw tested in Na_2SO_4 solution (Figures 3.6.7 b1 and b2) no clear effect of the salt concentration can be seen.

The Borghamn limestone is undamaged in all salts and concentrations, both externally and internally (Figures 3.6.7. c1 and c2.)

For the Uddvide sandstone (Figures 3.6.7. d1 and d2), there is no clear dependency on either on the salt type or the concentration. The difference between the internal damage measured by the same method on dry and wet samples can be explained by the relatively large porosity of the sandstones; when the pore system is filled with water it is actually a different material or a different composite from what it is filled with air.

The internal and external damage are independent of each other for all stones. This can be seen for the Öland limestone B1 freeze-thaw tested in NaCl solution in Figure 3.6.6.

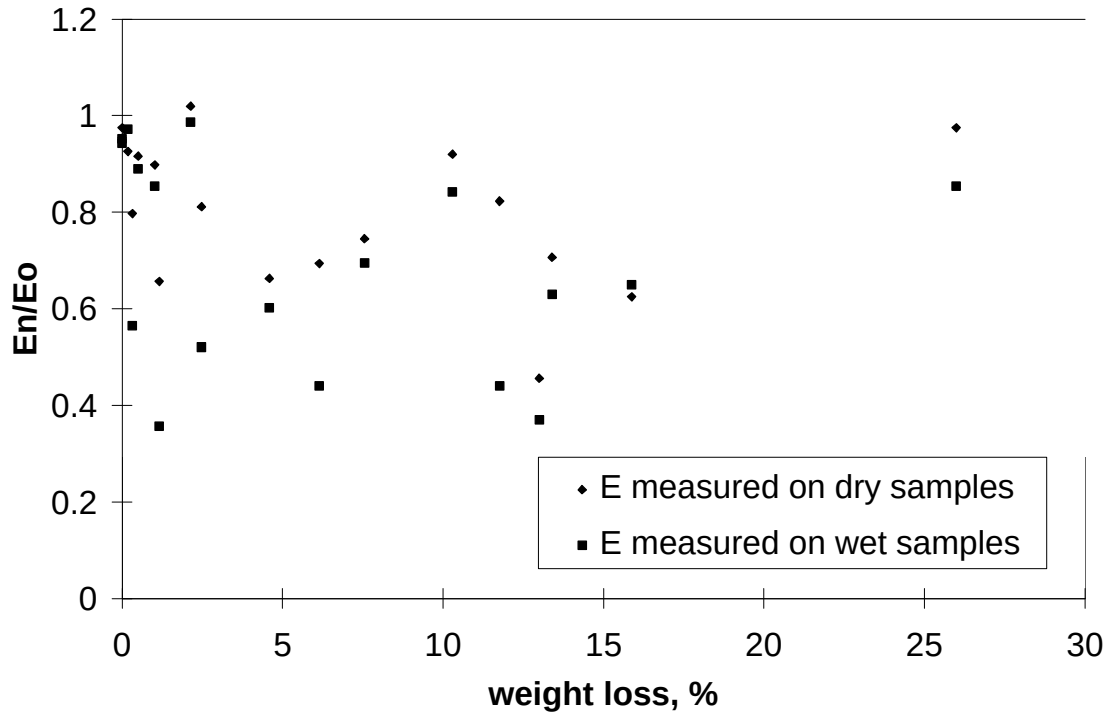

Figure 3.6.6. The correlation between the internal damage, expressed as a relative loss in dynamic modulus of elasticity, versus the external damage expressed as weight loss for the Öland limestone B1 freeze-thaw tested in NaCl solution.

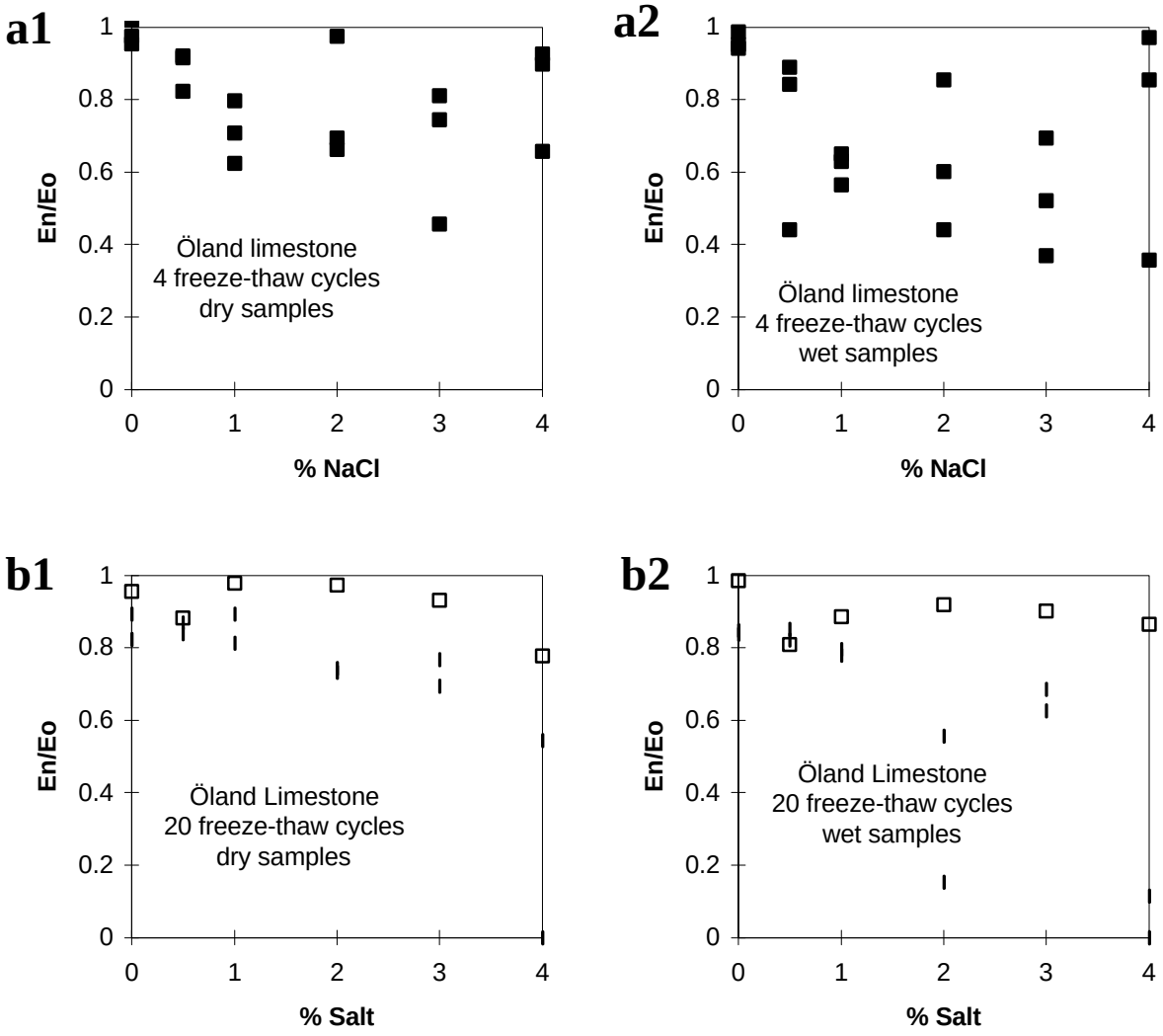

Figure 3.6.7 a1-b2. Loss in the dynamic modulus of elasticity versus the salt concentration. Symbols: ■ = NaCl, □ = Na_2SO_4, ♦ = $Na_2SO_4 \cdot 10H_2O$. *The concentration is expressed as % by weight of the actual salt; that is, a certain concentration of pure* Na_2SO_4 *is 2.27 times as strong when it is expressed as %* Na_2SO_4 *than when it is expressed as %* $Na_2SO_4 \cdot 10H_2O$. *Dry samples means that E was measured on dry specimens. Wet samples means that E was measured on wet specimens. a1) Öland Limestone B1 exposed to 4 freeze-thaw cycles in NaCl solution, E measured on wet samples. a2) Öland Limestone B1 exposed to 4 freeze-thaw cycles in NaCl solution, E measured on dry samples. b1) Öland limestone B1 exposed to 20 freeze-thaw cycles in* Na_2SO_4 *solution, E measured on dry samples. b2) Öland limestone B1 exposed to 20 freeze-thaw cycles in* Na_2SO_4 *solution, E measured on wet samples.*

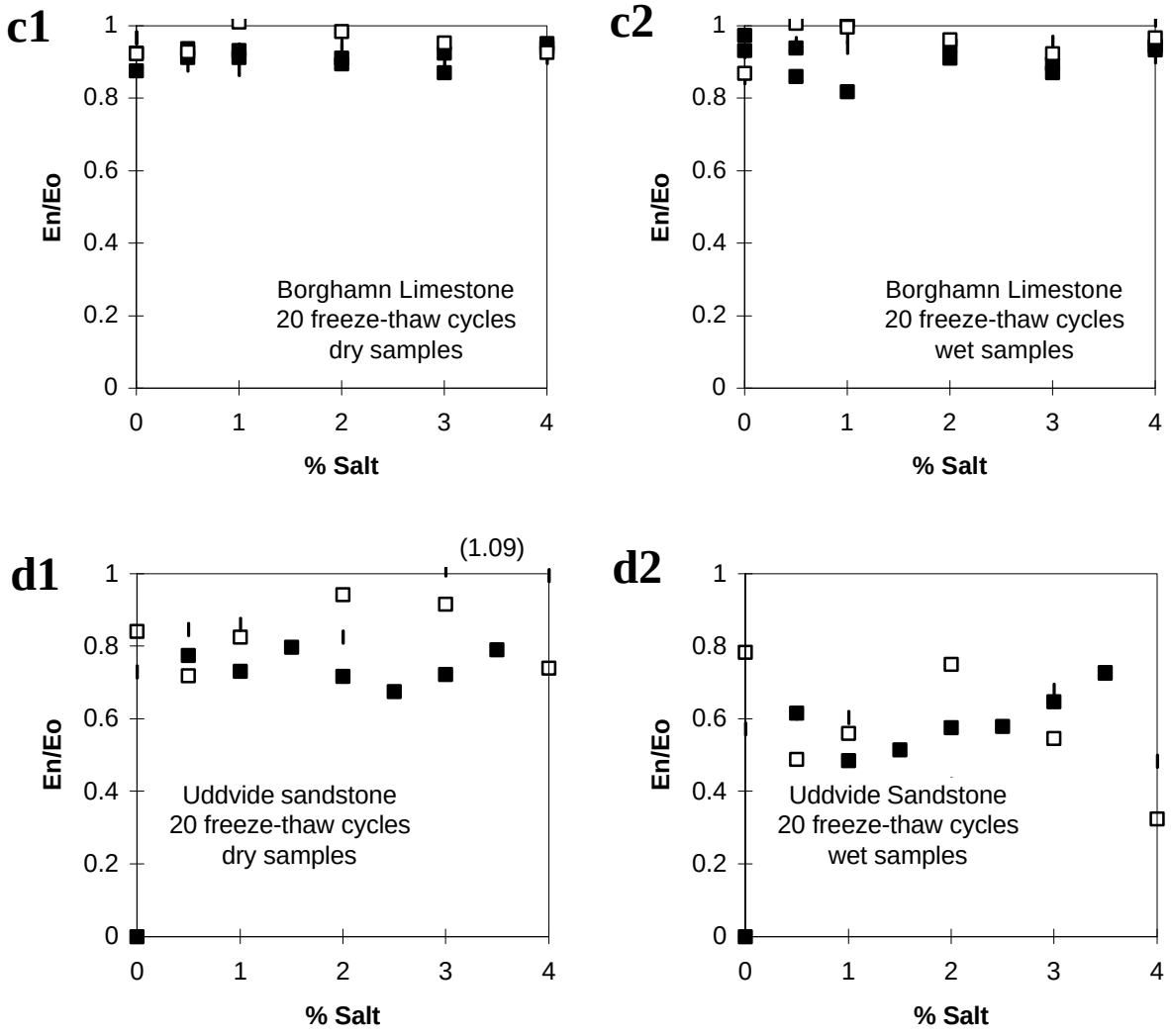

Figure 3.6.7 c1-d2. Loss in the dynamic modulus of elasticity versus the salt concentration. Symbols: ■ = NaCl, □ = Na_2SO_4, ♦ = $Na_2SO_4 \cdot 10H_2O$. *The concentration is expressed as % by weight of the actual salt; that is, a certain concentration of pure* Na_2SO_4 *is 2.27 times as strong when it is expressed as %* Na_2SO_4 *than when it is expressed as %* $Na_2SO_4 \cdot 10H_2O$. *Dry samples means that E was measured on dry specimens. Wet samples means that E was measured on wet specimens. c1) Borghamn limestone exposed to 20 freeze-thaw cycles in different salt solutions, E measured on dry samples. c2) Borghamn limestone exposed to 20 freeze-thaw cycles in different salt solutions, E measured on wet samples. d1) Uddvide sandstone exposed to 20 freeze-thaw cycles in different salt solutions, E measured on dry samples. d2) Uddvide sandstone exposed to 20 freeze-thaw cycles in different salt solutions, E measured on wet samples.*

3.6.5 Granite tested in solutions of NaCl and Na_2SO_4

Method

Sawed stone prisms with the dimensions 3 × 3 × 12 cm were dried in an air-circulated oven at a temperature of 50 °C until no more weight loss caused by moisture evaporation occurred (that is, for four days). The prisms were weighed after cooling them over silica gel. The prisms were then either vacuum saturated by the actual solution or left in the solution for ten days before the vessels containing prisms and solution were placed in the freezer. The vessels contained about 850 ml of solution and the upper surface of the stone prism was about 1 cm below the surface of the solution. Only pure water and one concentration of 2% by weight was used for each of the salts NaCl and $Na_2SO_4 \cdot 10H_2O$. The resonant frequency of transverse vibration was measured for the prisms under dry and wet conditions before and after the freezing and thawing. The freeze-thaw cycle is shown in Appendix H. As can be seen, it is very similar to the cycle in series 3 described in Chapter 3.6.2 (see Appendix H). The granite was exposed to 35 such cycles.

Results

All test data and calculated properties of the tested specimens are shown in Appendix P3. The weight loss is also shown in Figure 3.6.8. No internal damage was detected since the loss in the dynamic modulus of elasticity was negligible. The weight loss is presented in Figure 3.6.8 as a percentage of the original weight. The granite had a relatively small weight loss after 35 freeze-thaw cycles. It is therefore hard to see any difference between the effects of the different salts or between capillary and vacuum-saturated specimens. The weight loss was mainly caused by loosened flakes of mica.

Discussion

The effect of frost was small but measurable despite the fact that the granite had only 0.6% porosity. It is therefore possible that weathered granite surfaces, for example, granite rock carvings from the Bronze Age, which is more porous because of selective dissolution of some minerals or because of chemical attack (Sjöberg et al, 1992), is even more sensitive to frost attack than the unweathered granite used in this test is.

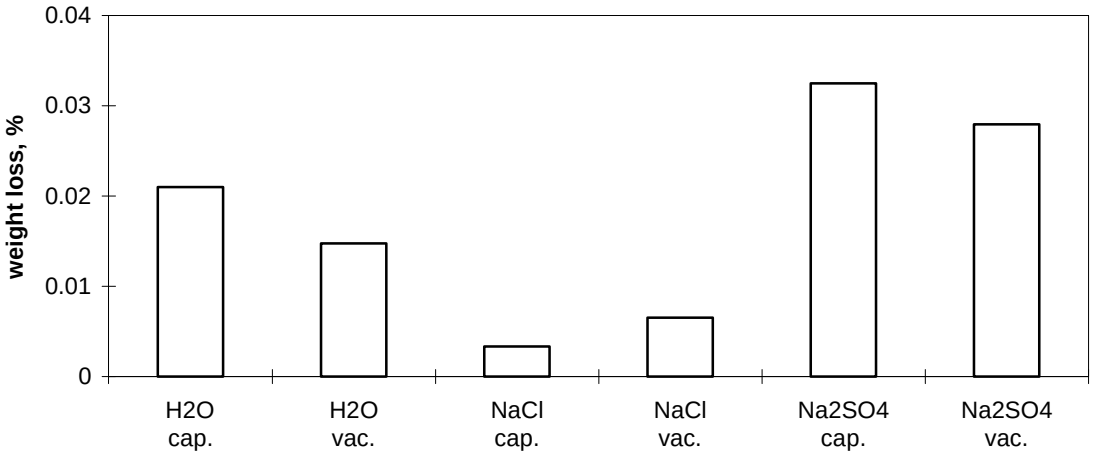

*Figure 3.6.8. Weight loss, expressed as a percentage of original weight, of granite after 35 cycles of freeze-thaw in pure water and 2% salt solutions of NaCl and $Na_2SO_4 \cdot 10H_2O$. The specimens were either capillary (*cap.*) or vacuum (*vac.*) saturated before the start of the test.*

3.6.6 Tests with different initial internal and external salt concentrations

Method
Prisms of the sandstone Valar and the limestone Öland B1 with the dimensions 3 × 3 × 12 cm were sawed. The limestone was sawed with the bedding direction parallel to the long side of the prisms. The bedding direction of the Gotland sandstone is not visible to the naked eye, so it is not possible to know if the prisms were sawed parallel or perpendicular to the bedding. The prisms were dried in an air-circulated oven at a temperature of 105 °C until no more weight loss caused by moisture evaporation occurred (that is, for at least four days). After cooling them over silica gel, the prisms were weighed and the fundamental frequency of transverse vibration was measured.

The prisms were then placed in salt solutions of various concentrations for 19 weeks to be capillary saturated by the solution. Four concentrations of each salt (NaCl and $Na_2SO_4 \cdot 10H_2O$) were used: 0%, 0.25%, 0.5% and 1.0% by weight. The concentration of the solution by which the pore systems of the specimens were saturated is called the *internal concentration*.

After storage in solution, the weight and resonant frequency of the samples was again measured. The prisms were then placed in vessels containing solutions with different concentrations, called the *external concentration*. The external concentrations were also 0%, 0.25%, 0.5% and 1.0% by weight. This makes 16 various combinations of internal and external concentrations for each stone type and salt type.

The prisms were then frozen and thawed without removing them from the solution. After 3 to 22 freeze-thaw cycles, depending on the degree of scaling, the prisms were removed from the vessels and weighed, at which time the resonant frequency was measured. The fragments that had loosened, or could easily be loosened from the specimen with the fingers, were collected in a filter paper. Sometimes the samples were broken into two pieces. In such cases, it was a matter of judgement if the smaller pieces should be considered as scaled material, or if they should be freeze-thaw tested further together with the larger piece. The fragments were then dried at a temperature of 105 °C for at least four days before weighing. The cumulative weight of these fragments gives the cumulative weight loss.

The specimen were put back into the vessels containing new solutions, and the freezing and thawing was continued for another 1 to 22 cycles. This was repeated 3 to 4 times until a total of 10 to 52 cycles were completed.

Dummies, treated equally to the prisms but containing a thermocouple in a drilled hole in their centres, were also placed in vessels in the freezer. These dummies were used to measure the temperature to ensure that the entire prisms reached the desired temperature condition during the freeze-thaw cycling. The freeze-thaw cycle used is shown in Appendix H. As can be seen, it is very similar to the cycle in series 3 described in Chapter 3.6.2 (see Appendix H).

Results
The measured and calculated values of weight loss and E-modulus of the tested specimens are shown in Appendix P4. The external damage or scaling is presented as cumulative weight loss versus number of cycles in Appendix J and in Figures 3.6.9-3.6.11 below. The internal

damage is expressed as a relative decrease in dynamic modulus of elasticity (E_n/E_0 in Appendix J and in Figures 3.13-3.16 below).

The external damage was almost independent of the internal concentration but very dependent on whether the outer solution contained salt. Therefore, the external damage is expressed as a mean value of the samples having different internal concentrations in Figures 3.6.9-3.6.11 below. According to these figures, it is evident that external pure water generally caused considerably less damage than did external salt solutions. The difference between 0.25%, 0.5%, and 1.0% was relatively small. This is qualitatively the same result that has been previously observed for concrete (e.g., Lindmark (1993)).

Generally, the internal damage was independent of both internal and external concentration. Some representative examples of the internal damage versus the number of cycles are shown in Figures 3.6.13-3.6.16.

Appendix J contains additional comments on the results.

Comments
Damage, both internal and external, increases with increasing number of freeze-thaw cycles. There is a general trend that an increased scaling also corresponds to increased reduction in E-modulus., as can be seen in Figure 3.6.17.

The external concentration has considerably more effect on the weight loss than on the internal damage. External pure water gives almost no weight loss compared to an external salt solution. There is a very small difference between the concentrations 0.25%, 0.5% and 1.0.

Normally neither the internal nor the external concentration has any effect on the internal damage. The only exception from this rule is the case of sandstone freeze-thaw tested in pure water, which incurs less internal damage than the sandstone tested when surrounded by NaCl solution.

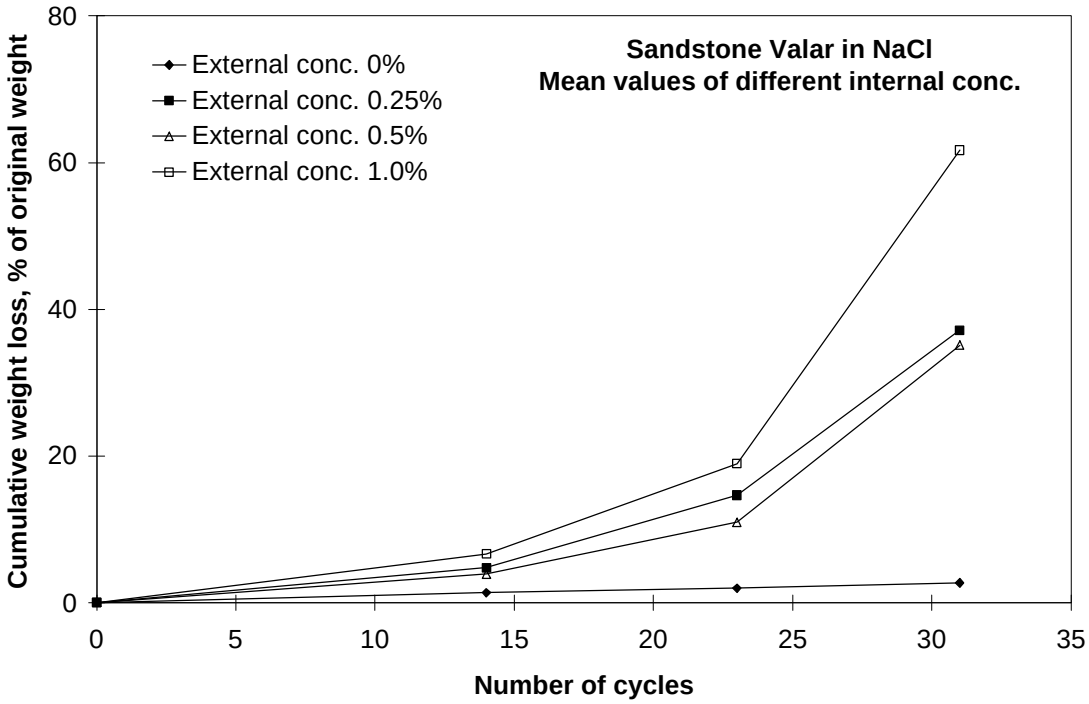

Figure 3.6.9. Cumulative weight loss versus the number of freeze-thaw cycles of sandstone tested with different external NaCl concentrations. The results show mean values of different internal concentrations.

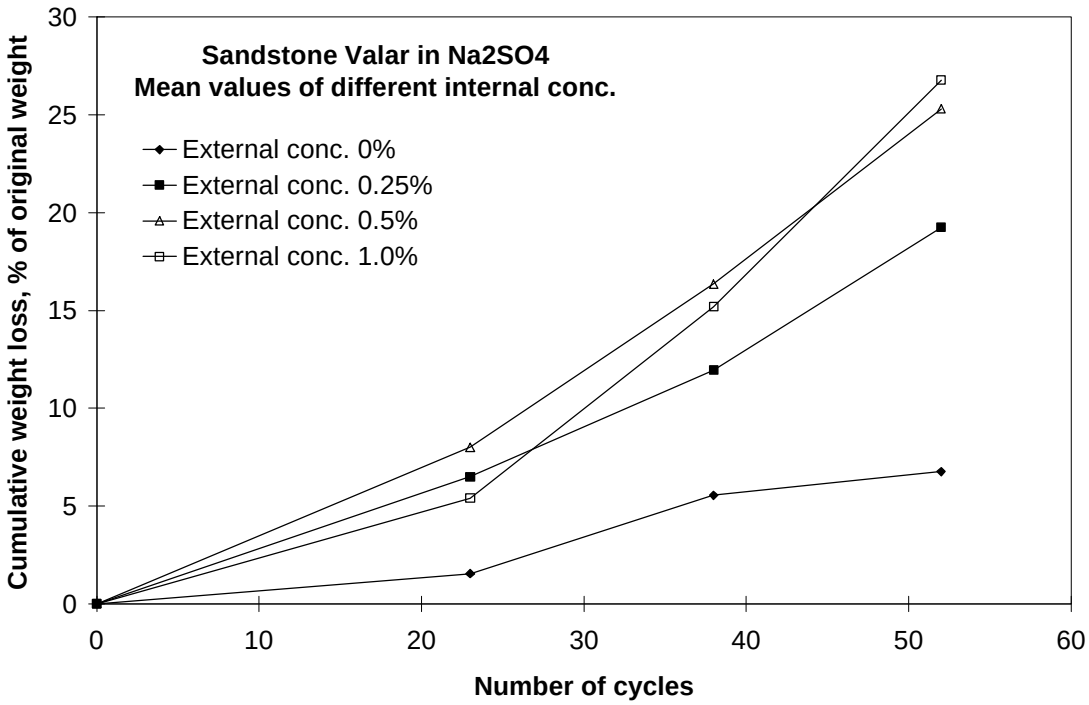

Figure 3.6.10. Cumulative weight loss versus the number of freeze-thaw cycles of sandstone tested with different external concentrations of $Na_2SO_4 \cdot 10H_2O$. The results show mean values of different internal concentrations.

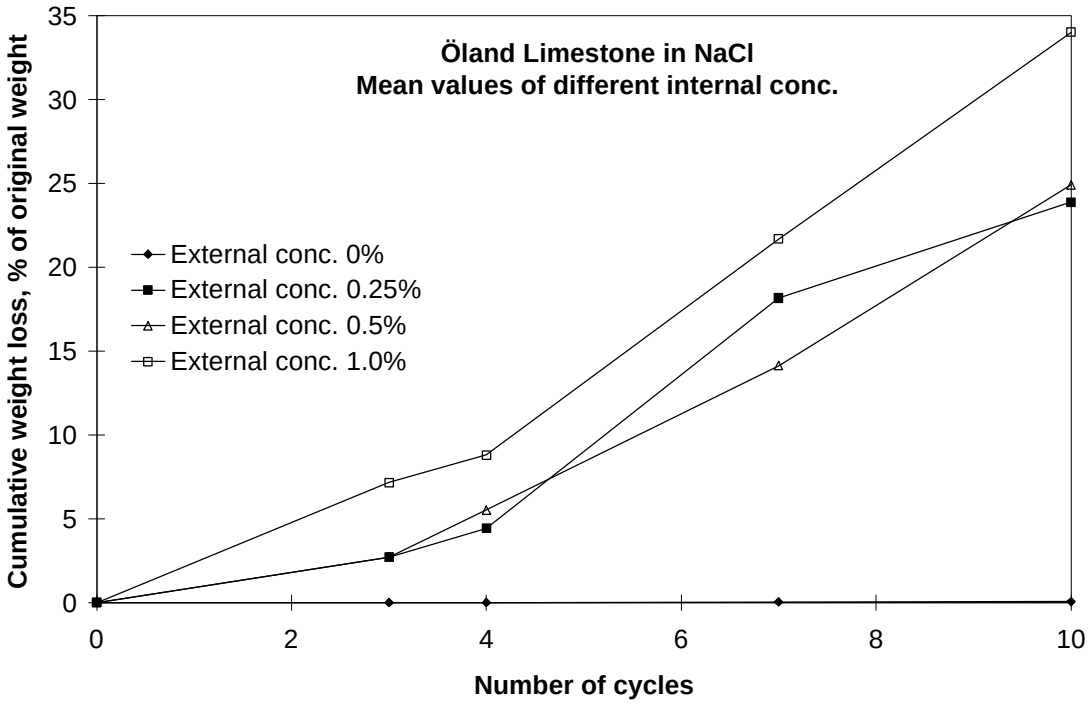

Figure 3.6.11. Cumulative weight loss versus the number of freeze-thaw cycles of limestone tested with different external NaCl concentrations. The results show mean values of different internal concentrations.

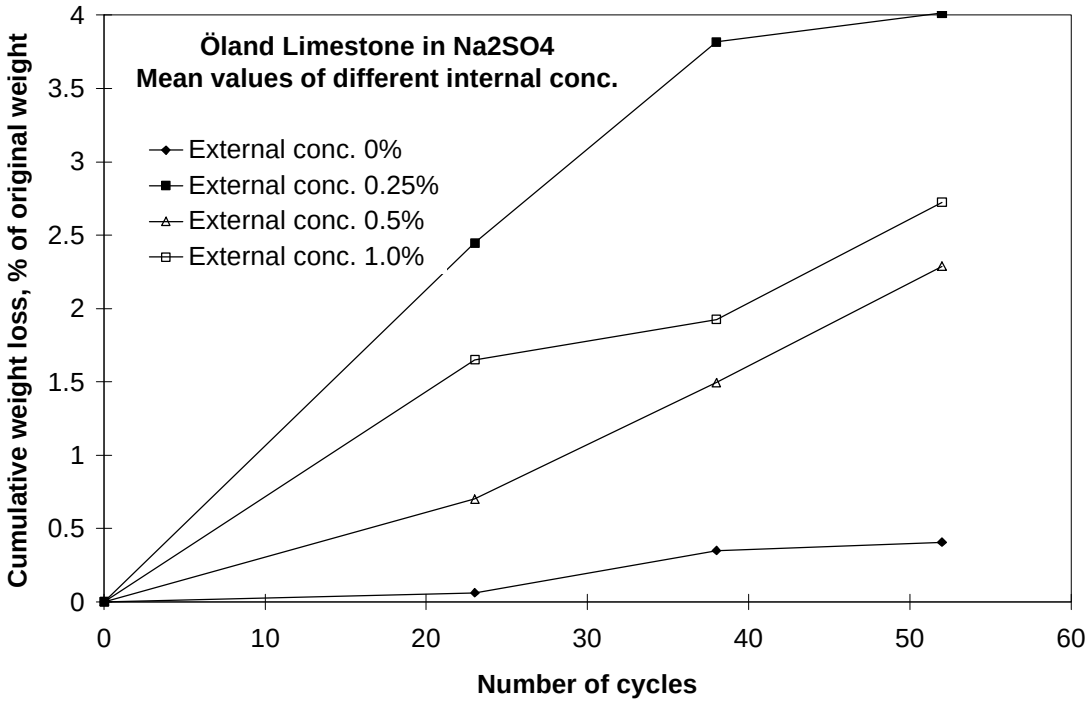

Figure 3.6.12. Cumulative weight loss versus the number of freeze-thaw cycles of limestone tested with different external concentrations of $Na_2SO_4 \cdot 10H_2O$. The results show mean values of different internal concentrations.

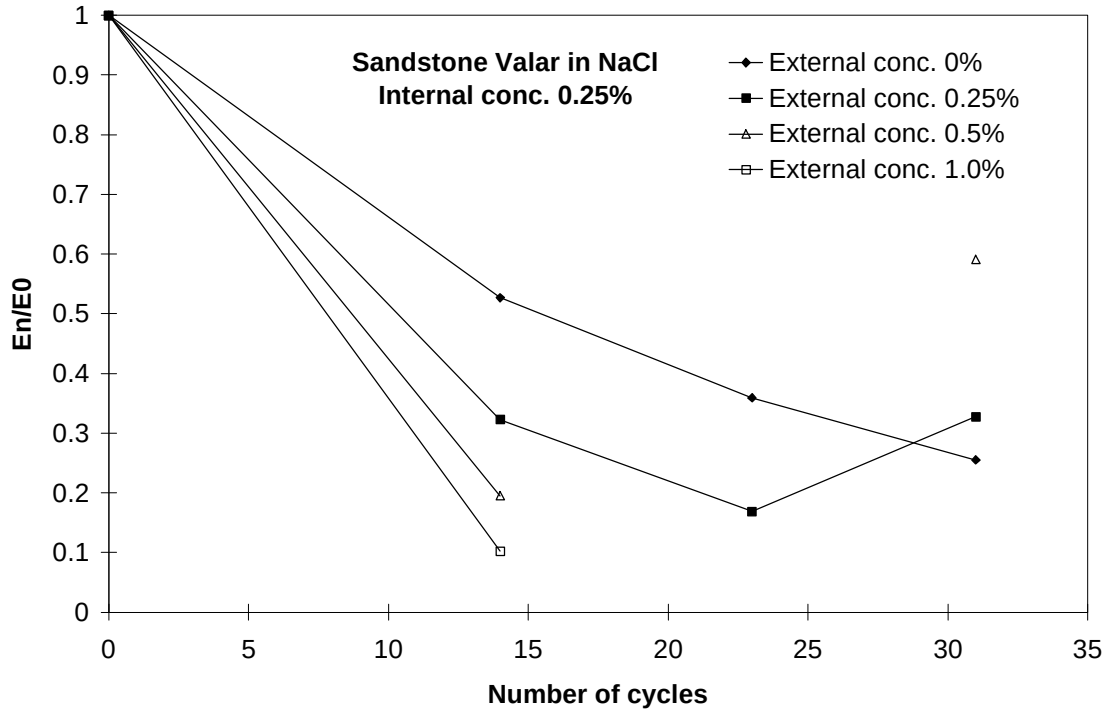

Figure 3.6.13. Loss in dynamic modulus of elasticity versus number of freeze-thaw cycles of the sandstone Valar tested in NaCl solution. The internal concentration in this example is 0.25%, but the results look similar for all internal concentrations tested (see Appendix J).

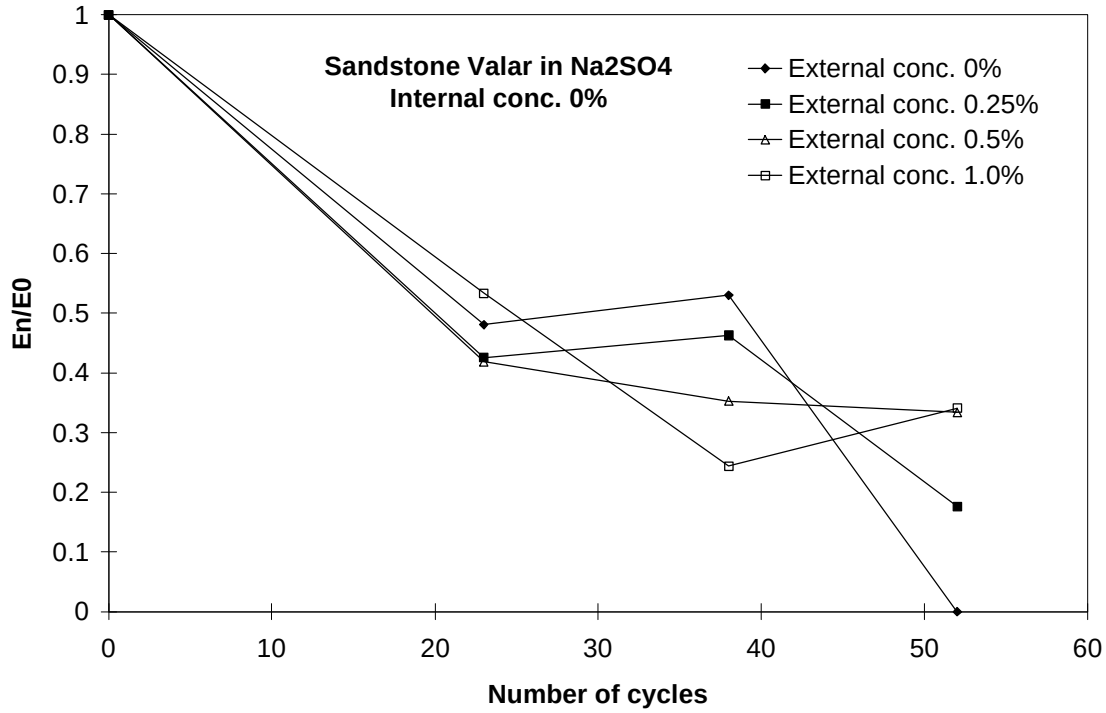

Figure 3.6.14. Loss in dynamic modulus of elasticity versus number of freeze-thaw cycles of the sandstone Valar tested in solutions of $Na_2SO_4 \cdot 10H_2O$. The internal solution in this example is pure water, but the results look similar for all internal concentrations tested (see Appendix J).

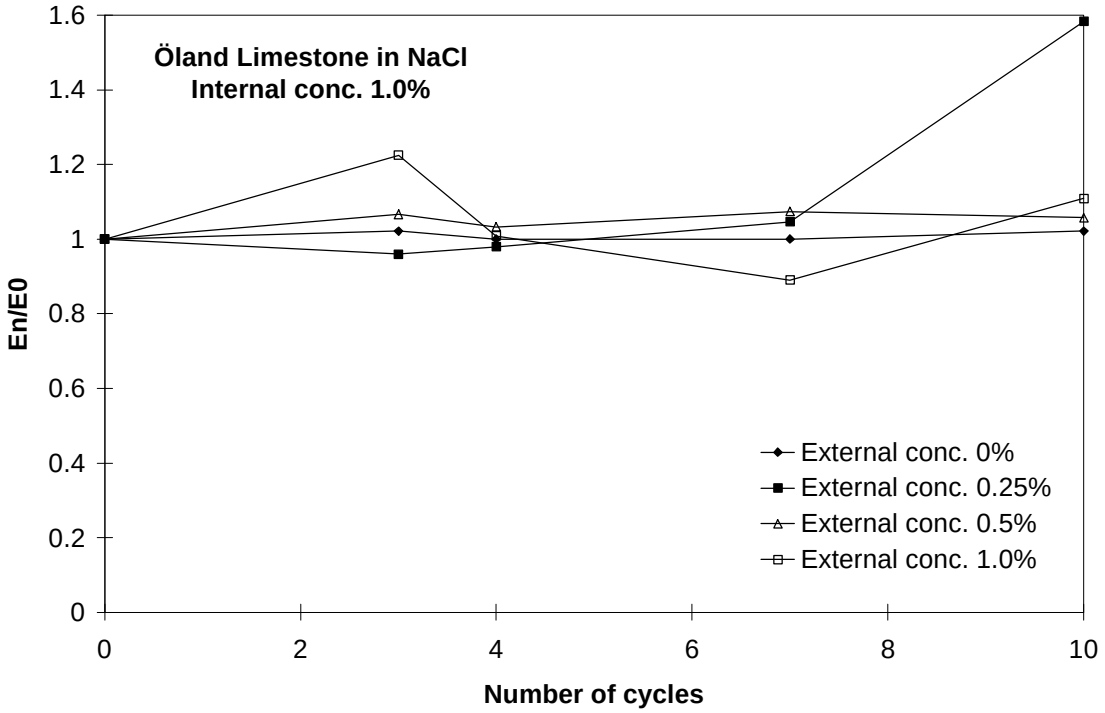

Figure 3.6.15. Loss in dynamic modulus of elasticity versus number of freeze-thaw cycles of the limestone Öland B1 tested in NaCl-solution. The internal concentration in this example is 1%, but the results look similar for all internal concentrations tested (see Appendix J).

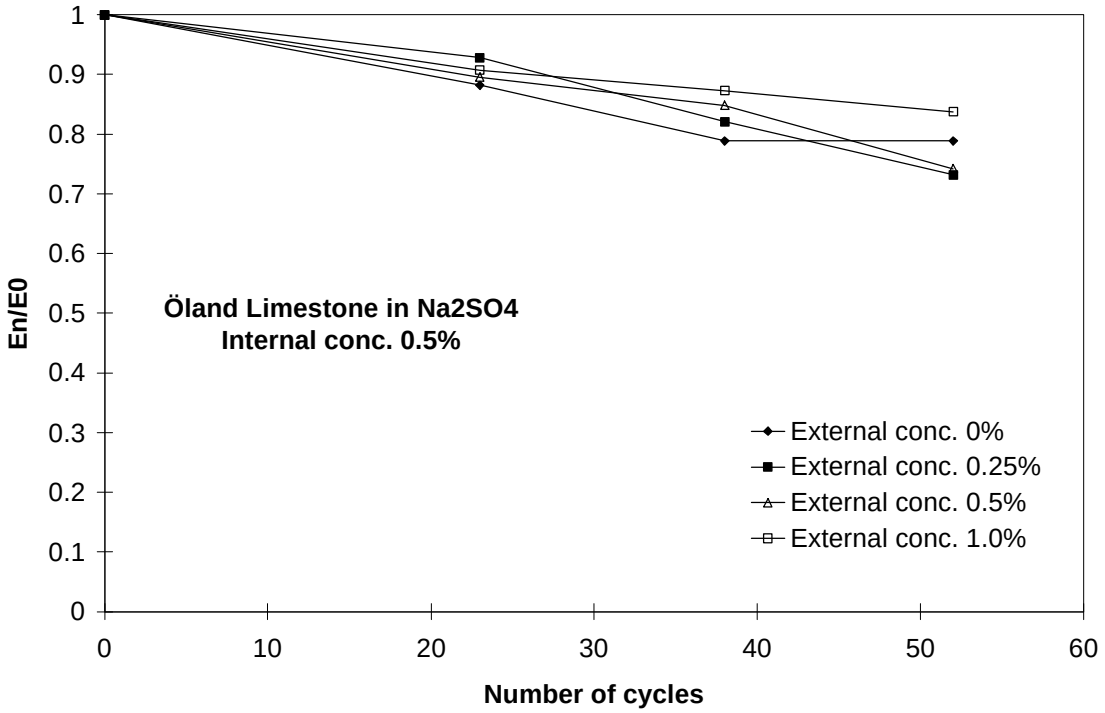

Figure 3.6.16. Loss in dynamic modulus of elasticity versus number of freeze-thaw cycles of the limestone Öland B1 tested in solutions of $Na_2SO_4 \cdot 10H_2O$. The internal concentration in this example is 0.5%, but the results look similar for all internal concentrations tested (see Appendix J).

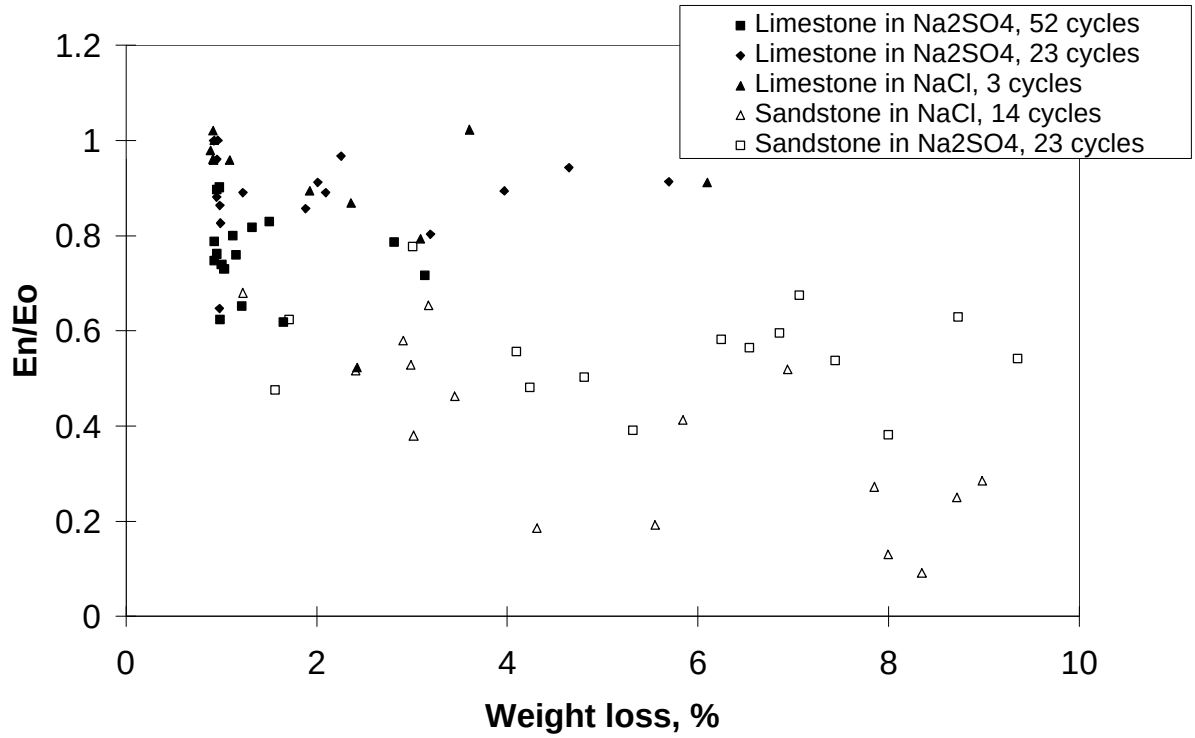

Figure 3.6.17. Example of the correlation between the internal damage, expressed as a relative loss in dynamic modulus of elasticity, versus the external damage, expressed as weight loss.

Discussion

The scaling in salt solution is very large compared to the Swedish standard of freeze-thaw resistance of concrete (SS 13 72 44), for which the maximal allowed scaling for an acceptable concrete is 1 kg/m^2 after 56 cycles. In the standard test method for concrete, a 3% NaCl solution is used. The freeze-thaw cycle in the actual test of natural stone follows the cycle recommended in the concrete standard method rather well. Thirty percent by weight in the test described here corresponds to about 5 kg/m^2.

The results, which indicate that samples surrounded by pure water are less scaled than samples surrounded by salt solution, independent of the concentration, are in good agreement with the theory proposed by Lindmark (1996) (see Chapter 2.4.6). According to the hypothesis, internal salt should reduce scaling, but it is difficult to predict how large this reduction should be. It might be that the concentration of the solutions in the pore system in this study actually has an effect on scaling but that it is too small to be detectable.

When sandstone was freeze-thaw tested surrounded by pure water, the internal damage was less than when it was surrounded by NaCl solution during freezing. This might be explained by the 'drying' of the pore system that might take place during freezing; ice outside the pore system consumes water from the pores. This phenomenon is not seen in the limestone, perhaps because the huge weight loss that occurred made it difficult to measure the internal damage.

3.7 Sealed single-cycle freeze-thaw tests - Dilatation tests

3.7.1 Introduction

The principal aim of this test was to measure the length changes of preconditioned specimens during one freeze-thaw cycle in order to discover the values of the so-called critical degrees of saturation. This method was originally published in Fagerlund (1972). Another aim of this test was to see if salt solutions had other effects on the length changes or critical degrees of saturation of these specimens than pure water did.

3.7.2 Method

The Gotland sandstones Botvide, Uddvide, Valar and X:1 were tested. The sandstone X:1 came from a newly opened quarry. The Öland limestone B1 and the granite from Bohuslän were also tested. Sawed stone prisms with the dimensions 2 × 2 × 15 cm were provided with measuring knobs at the ends. As the bedding direction of sandstone and granite is not visible to the naked eye, it was not possible to know in what direction the prisms were sawed. The bedding direction of the limestone was parallel to the long side of the prism. The prisms were then pre-dried in an air-circulated oven at a temperature of 105 °C, until no more weight loss caused by moisture evaporation occurred (that is, for at least four days). The prisms were weighed after cooling them over silica gel. The sandstone prisms were then conditioned to contain various amounts of solution. For limestone and granite, only completely saturated samples were tested as the porosity and thus the dilatation of these stones was small. Pure water and two different concentrations, 0.5% and 1.0% by weight, for each of the salts NaCl and $Na_2SO_4 \cdot 10\,H_2O$ were used.

The resonant frequency of transverse vibration was measured for the prisms under dry and wet conditions before and after the freezing and thawing. This was done to make it possible to calculate the loss in dynamic modulus of elasticity, which is a way of measuring internal damage. This is explained in more detail in Appendix G.

The amount of solution inside the specimens was expressed in terms of degree of saturation. Completely saturated samples, for which the degree of saturation was 1, were vacuum saturated at a residual pressure of 2 mbar after the pre-drying. The specimens containing pure water were vacuum saturated in the same manner and then dried to the desired degree of saturation. The drying was performed in an air-circulated oven of 50 °C and with a blow-dryer. To reach the desirable degree of saturation of salt solution, lower than 1, the dry samples were either allowed to suck solution for various time intervals, or they were ‘vacuum-saturated’ by sucking the solution into their pore system after a pre-treatment consisting of evacuation to various residual pressures. Table 3.7.1 shows the method of moisture conditioning and the approximate degree of saturation reached by each pre-treatment. The numbers in the left-hand column are used in the graphs shown in Appendix K.

Table 3.7.1. Moisture conditioning of dilatation samples.

Number	Treatment	Approximate degree of saturation
1	Submerged in solution for 1 day	0.69
2	Submerged in solution for 7 days	0.82
3	Submerged in solution for 21 days	0.88
4	Submerged in solution for 3 months	S~1.0
5	Absorption following evacuation to about 280 mbar	0.94
6	Absorption following evacuation to about 250 mbar	0.97
7	Absorption following evacuation about 1 mbar (≈ total vacuum)	1.0

The pre-conditioned samples were wrapped in polythene plastic bags in order to prevent moisture loss or moisture gain during the freeze-thaw cycle. They were then placed in a measuring frame consisting of two circular plates of stainless steel connected by three invar bars (see Figure 3.7.1). Invar has a low coefficient of heat expansion of about $0.8\ 10^{-6}$. The bottom measuring knobs of the test specimens were placed on invar bars with a length of 50 mm, which were mounted on the lower plate. The top measuring knob of each specimen was supported by an LVDT gauge which was mounted on the top plate. The LVDT gauge measured the length change during freezing and thawing. The length was measured to an accuracy of ±2 μm, which corresponds to a dilatation of about 0.01‰. The length was monitored every minute and sampled on a file in a PC. The measuring frame with the specimens was placed in a freezer and exposed to one freeze-thaw cycle of the shape shown in Figure 3.7.2. The temperature was measured by a thermocouple placed in a drilled hole in the centre of each specimen. The temperature was scanned every minute as well and sampled in a file on a PC.

Control tests were performed with pure water in the pore system. In one of these two tests, the temperature was not measured inside each individual specimen for the sandstones Botvide and Uddvide; therefore, the permanent dilatation could not be detected in these cases.

The results for each specimen were plotted as strain versus temperature. Examples of such plots are shown in Appendix K, in Figures K:9-K:55 and in Figures 3.7.3 and 3.7.4 below.

Damage can be defined either as a permanent dilatation after thawing (marked with arrow *a* in Figure 3.7.4) or as the dilatation caused by ice formation. This is calculated as the expansion occurring after freezing minus the extrapolated thermal contraction (arrow *b* in Figure 3.7.4). As line 2 is the extrapolation of the strain curve at degrees above zero, it is equivalent to the thermal contraction had no ice formation occurred. Because of the different coefficients of thermal expansion for the stone-water composite and the stone-ice composite, the direct linear correlation is not altogether correct. In principle, the calculated value of dilatation changes with changing temperature. In the following, it is defined as the expansion at -15 °C.

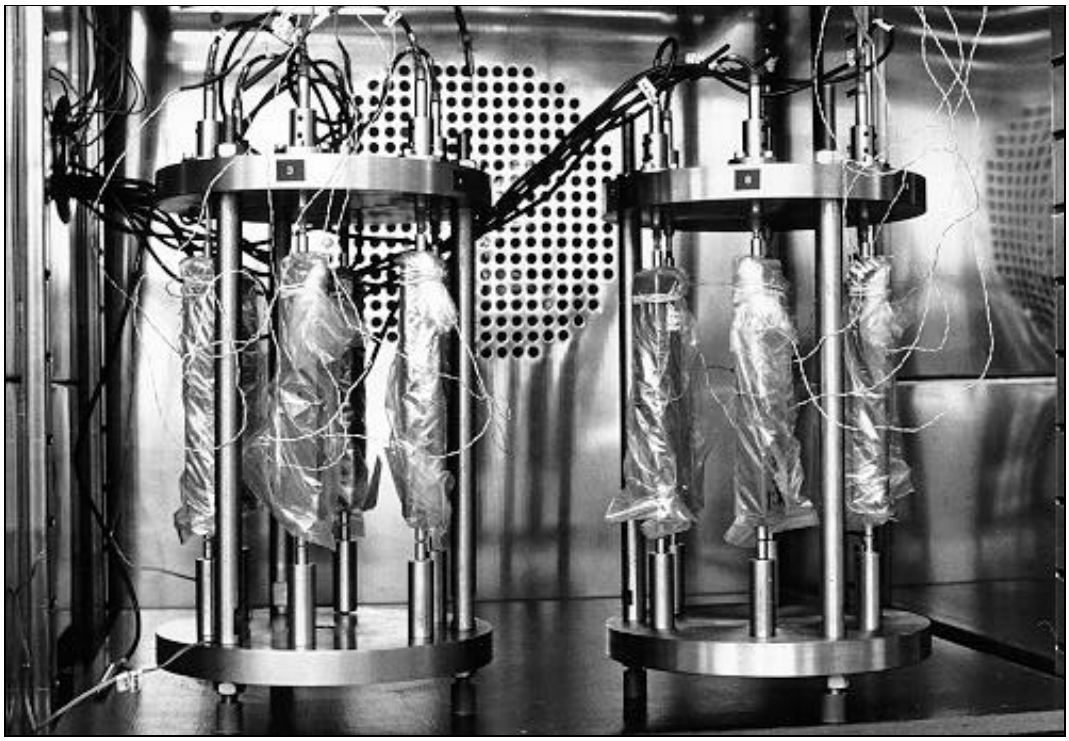

Figure 3.7.1. Measuring frame used in dilatation test with stone prisms wrapped in plastic bags.

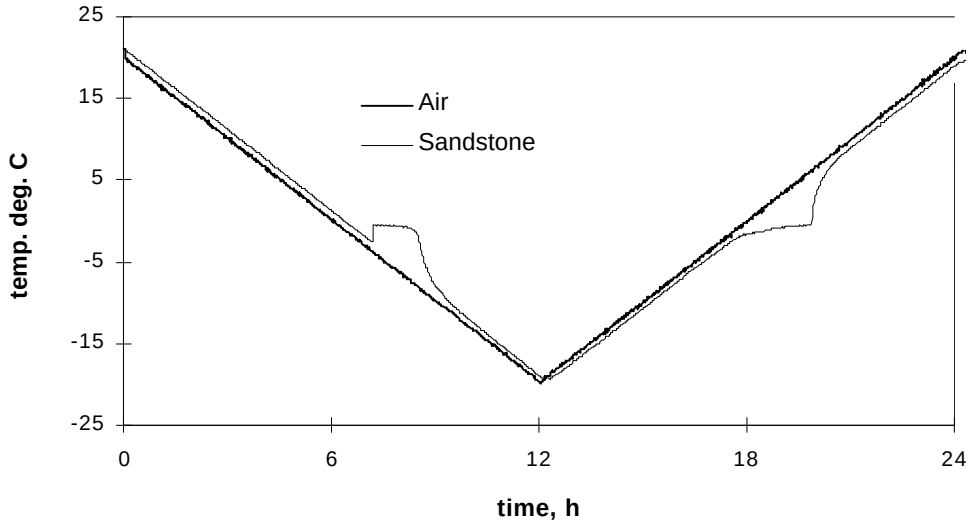

Figure 3.7.2. Freeze-thaw cycle used in the dilatation test.

As the final results used are calculated as a difference between two length values measured at the same specimen temperature, the length change of the measuring frame has a negligible influence, provided that the temperature of the frame is the same at both measuring times. As can be seen in Figure 3.7.2, the difference between the temperature of the surrounding air and the centre of a specimen is small at the measuring temperatures 20 °C and -15 °C, so the temperatures of the frame and the specimen are almost equal.

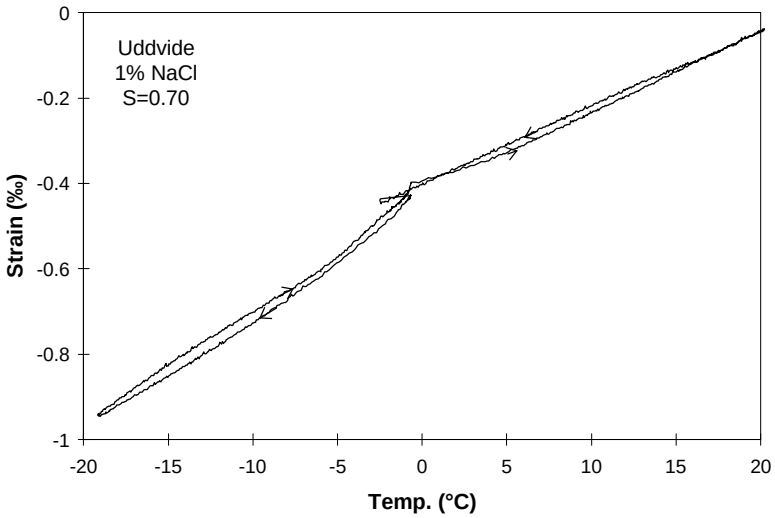

Figure 3.7.3. Strain versus temperature in a sandstone sample with a degree of saturation of 0.70.

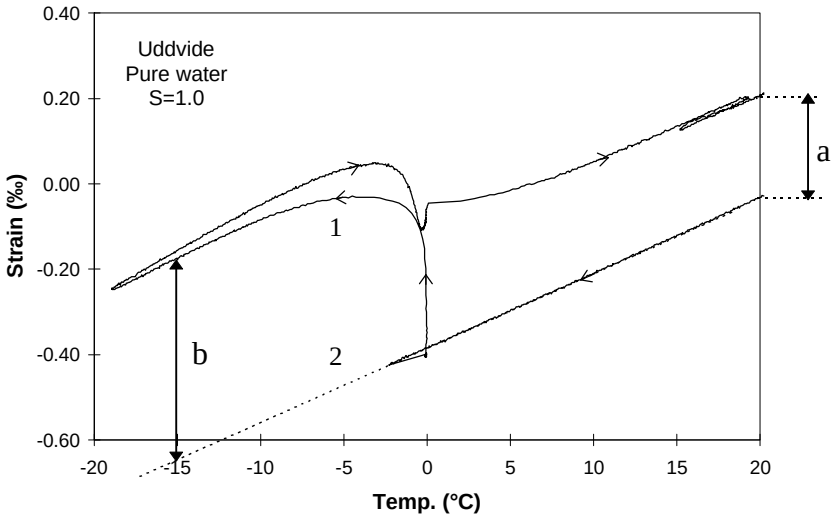

Figure 3.7.4. Strain versus temperature in a sandstone sample with a degree of saturation of 1.0.

3.7.3 Results of sandstone

Measured and calculated values of the sandstones are shown in Appendix P5. In Appendix K, Figures K:1-K:8, the results are shown as permanent and 'maximal' dilatation versus degree of saturation. Two examples of such graphs are shown in Figure 3.7.5 below. As mentioned above, the 'maximal' dilatation is defined as the dilatation caused by ice formation at -15 °C. From the results, the following can be stated:

Degree of saturation: At degrees of saturation lower than about 0.85, no permanent dilatation occurs, and the 'maximal' dilatation is often negative, that is, the specimens contract at freezing. At higher degrees of saturation, the dilatation increases with the degree of saturation. If a critical degree of saturation is to be found, it has to be defined as, for example, the degree of saturation at which the 'maximal' dilatation exceeds zero. This value is about 0.85 for all sandstones (except X:1), both with and without salt.

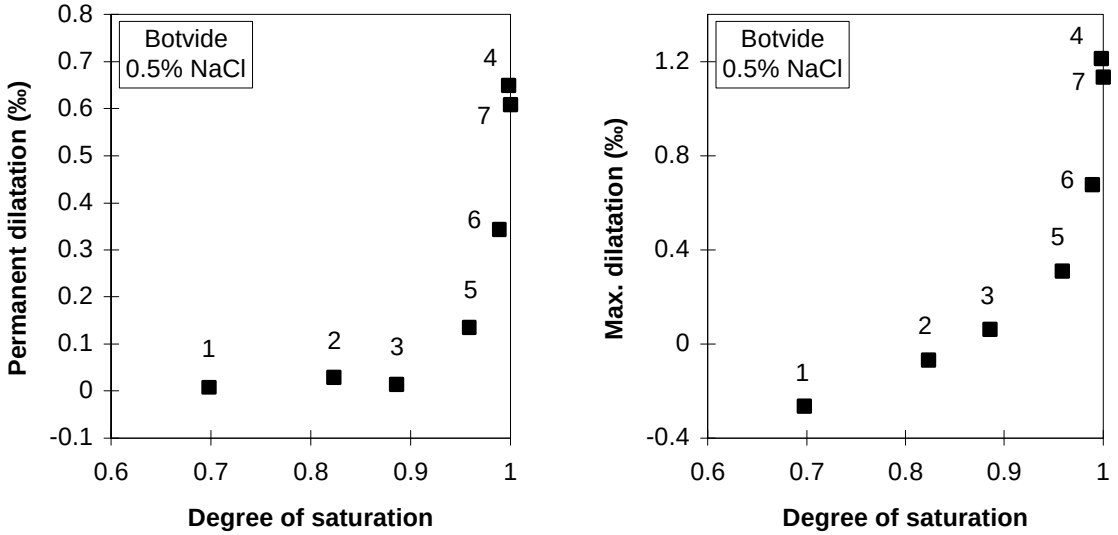

Figure 3.7.5. Permanent and maximal dilatation versus the degree of saturation of the sandstone Uddvide with a solution of 0.5% NaCl. Similar graphs for other sandstones and solutions are shown in Appendix K, Figures K:2-K:8.

A small weight loss occurred during the freeze-thaw test. This was the result of water loss since water was found in the plastic bags after the freeze-thaw test. The weight loss was about 0.2 g, which corresponds to a loss of about 2% of the initial water content in a saturated specimen or of about 0.02 to 0.03 in degree of saturation. The degree of saturation shown in Appendix K and in Figures 3.7.3-3.7.7 is a mean value of the values immediately before and immediately after the freezing and thawing, except for completely saturated specimens, for which the degree of saturation per definition is 1.0.

Stone types: The more porous the stone is, the more it dilates at high degrees of saturation. The stones Botvide and Uddvide, which have about the same porosity, dilate more than does the stone Valar, which in turn dilates more than the densest stone X:1. This is what one would expect as more porous stones contain more water at the same degree of saturation.

Salt: The samples containing salt in the pore water have a somewhat higher dilatation when the samples are completely saturated. At lower degrees of saturation, no effect of salt can be detected. There is no significant difference either between the salt types or the salt concentrations.

Permanent and 'maximal' dilatation: The relationship between the permanent and the 'maximal' dilatation is linear at high degrees of saturation (see Figure 3.7.7). The 'maximal' dilatation is about 1.7 times the permanent dilatation. At low degrees of saturation, the permanent dilatation is zero and the 'maximal' dilatation is negative.

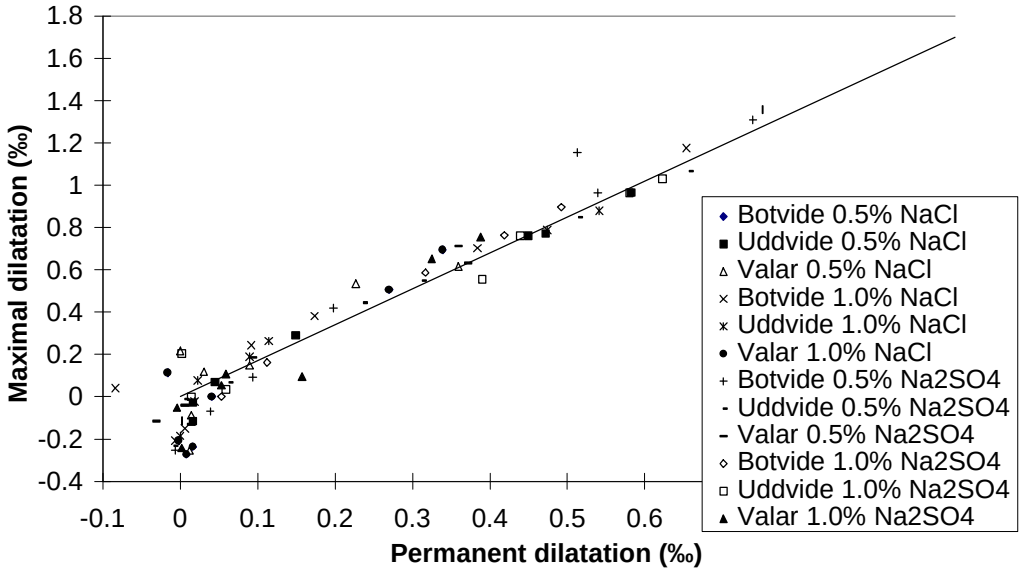

Figure 3.7.6. Maximal dilatation versus permanent dilatation.

Loss in dynamic modulus of elasticity: The relative loss in dynamic modulus of elasticity, E_1/E_0,, was also measured. E_1 is the value after one freeze-thaw cycle, and E_0 is the value before freezing. As can be seen in Figure 3.7.7 below, E_1/E_0, decreases with increasing degree of saturation, but no clear correlation between damage measured as loss in dynamic modulus of elasticity and damage measured as dilatation was found (see Figure 3.7.8). The internal damage measured as dilatation follows the degree of saturation more distinctly, as can be seen in Appendix K, Figures K:1-K:8.

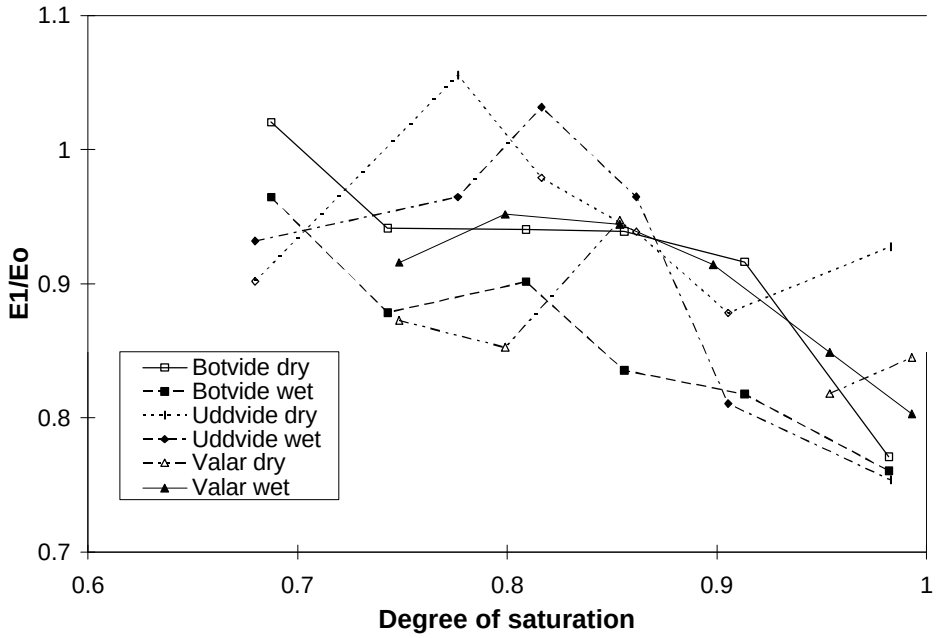

Figure 3.7.7. Relative dynamic modulus of elasticity after one freeze-thaw cycle of sandstone prisms with pure water in dilatation test. 'Dry' and 'wet' means that the resonant frequency was measured on dry and wet samples, respectively.

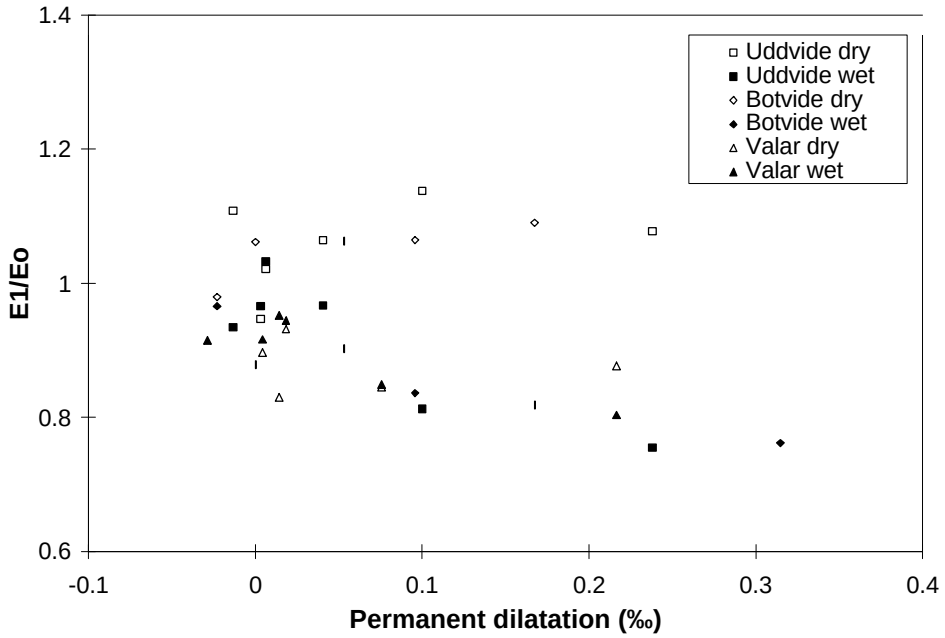

Figure 3.7.8. Relative dynamic modulus of elasticity versus permanent dilatation after one freeze-thaw cycle of sandstone prisms with pure water in dilatation test. 'Dry' and 'wet' means that the resonant frequency was measured on dry and wet samples, respectively.

Reproduced tests: The results from the control tests of the sandstones containing pure water show that the tests are reproducible (see Appendix K). However, as the temperature was not measured inside each individual specimen of the stone types Botvide and Uddvide in the control tests, only the maximal dilatation could be calculated for these stone types in this case. This was, however, the same in the two tests.

Movement during freezing and thawing: In Appendix K, Figures K:9-K:55, some examples of the movement of sandstone specimens during freezing and thawing are shown. The movement is shown as the strain versus the temperature of the specimen. The strain is the length change, measured with an LVDT gauge, divided by the total specimen length, which is 150 mm. The temperature is measured with a thermocouple in a drilled hole in the centre of each specimen.

The type of movement is almost equal for all stones of the same type having the same degree of saturation, irrespective of the type of solution in the pores. When the temperature lowers, the sample contracts because of the coefficient of heat expansion of the stone-water composite. The freezing occurs at a temperature some degrees below zero, because of supercooling. The temperature rise at freezing occurs because ice formation is an exothermic process. At the moment of the first ice formation, a small but measurable expansion takes place. Up until this point, the movement looks the same for specimens with both low and high degrees of saturation. The movement at lower temperatures, however, differs somewhat between specimens, depending on the degree of saturation.

At low degrees of saturation, the stone-ice composite contracts rather rapidly immediately after freezing. This might depend on a drying process; water from the pores is transported to the stress-free ice formed at the surface of the specimen. This ice does not contribute to the expansion. The size of this dilatation caused by drying, 0.1‰, seems reasonable (Schweda et al, 1996). The stone-ice composite contracts thermally, until the heating starts and a thermal expansion takes place. At some degrees below zero, when melting probably starts, the

specimen seems to expand more than the thermal coefficient of heat expansion should allow. This might be because moisture is being transported from the ice melting on the specimen surface into the pore system, that is, the reverse of what occurs during the drying at freezing described above. At some degrees above zero, a linear heat expansion of the stone-water composite takes place.

At high degrees of saturation, expansion at temperatures below 0 °C continues during cooling until all ice is formed. Then, the stone-ice composite contracts thermally, until the heating starts and a thermal expansion takes place. Ice melting probably starts at some degrees below zero, which can be explained by a freezing point depression of adsorbed water or water in small pores (Equation 2.4.1). The contraction at some degrees below 0 °C is caused by the melting ice. The expansion following the contraction can be explained as above; That is, water is transported into the pores from the surface of the specimen when enough ice has melted to create a suction. At some degrees above zero, a linear heat expansion of the stone-water composite takes place. The permanent dilatation depends on irreversible crack formation in the sample.

3.7.4 Results for granite and limestone

No dilatation occurred for the vacuum saturated granite. The most probable reason is that its porosity is too low. The dilatation of the limestone is presented in Table 3.7.2 below. The dilatation of the limestone is small compared to the dilatation of sandstone, as it is considerably more dense. There is no clear relationship between the permanent and the 'maximal' dilatation, probably because the dilatation is so small that various measurement errors obscure it.

Table 3.7.2. Dilatation (‰) for completely saturated samples of limestone.

	Pure water	0.5% NaCl	1.0% NaCl	0.5% Na_2SO_4	1.0% Na_2SO_4
Permanent	0	0	0.06	0.07	0.09
'Maximal'	0	0.13	0.11	0.17	0.15

3.7.5 Comparison between calculated and measured dilatations

The maximum possible dilatation caused by ice formation, ε, can be calculated by the formula below, assuming all freezable water actually freezes *in situ* in the specimen:

$$\varepsilon = \frac{1}{3} P \cdot (0.09 \cdot S \cdot (1 - \frac{x_0}{x(T)}) - (1 - S)) \qquad (3.7.1)$$

where

P porosity;
S degree of saturation;

$(1 - \frac{x_0}{x(T)})$ is a factor taking into account the fact that some part of the solution will remain liquid. This factor is described in more detail below. It should also be noted that even if there is no salt in the pores, all water is not always freezable because of surface effects (Equation 2.4.1). Such effects are, however, of interest only if the material is very fine-porous, that is, the surface area of the material is large enough.

If the degree of water saturation is less than 0.917, the sample will, theoretically, not expand as there is enough room for all the ice formed at freezing to fill the empty pore spaces. The calculated dilatations for pure water at various porosities versus the degree of saturation are shown in Figure 3.7.9. These values can be compared with the measured values of maximal dilatation shown in Appendix K. As can be seen, for saturated samples, the measured values are less than 1/10 of the calculated.

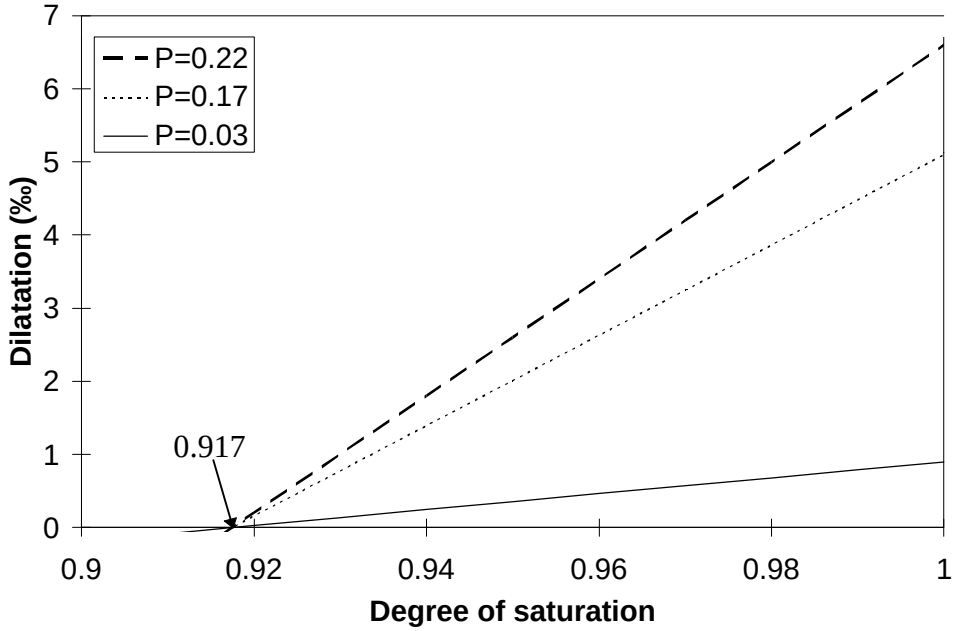

Figure 3.7.9. Calculated dilatation during the freezing phase versus degree of saturation.

If there is a salt solution in the pore system, only a part of the solution will form ice at a certain temperature. How large that part will be can be calculated by the following.

Notations:
m_{l0} amount of solution before freezing (kg);
m_s amount of salt dissolved in the pore water (kg);
m_i amount of ice at the temperature T (kg);
$m_l(T)$ amount of solution at the temperature T (kg);
x_0 salt concentration of the solution before freezing (kg/kg);
$x(T)$ salt concentration of the solution at the temperature T (kg/kg).

$$m_i + m_l(T) = m_{l0} \tag{3.7.2}$$

$$x(T) = \frac{m_s}{m_l(T)} \tag{3.7.3}$$

$$x_0 = \frac{m_s}{m_{l0}} \tag{3.7.4}$$

From the equations above is given

$$\frac{m_i}{m_{l0}} = 1 - \frac{x_0}{x(T)} \tag{3.7.5}$$

If T is known, $x(T)$ is found from a phase diagram for the salt-water system, according to Figure 3.7.10. The equations are only valid when freezing has started, that is, when the temperature is lower than the freezing temperature of the solution.

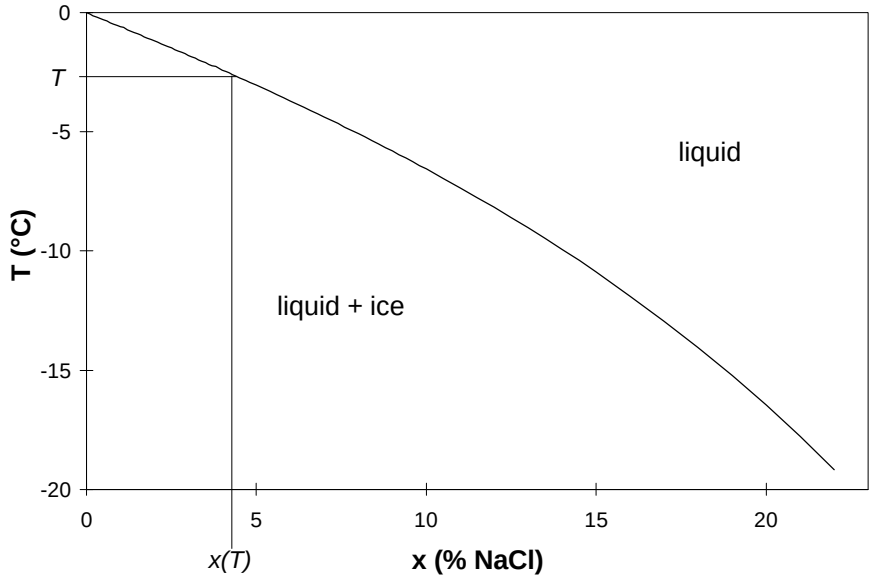

Figure 3.7.10. 2-phase diagram of NaCl in water.

The dilatation, ε, for a given solution can then be calculated:

$$\varepsilon = \frac{1}{3} P \cdot (0.09 \cdot S \cdot (\frac{m_m \cdot \rho_i}{m_{l0} \cdot \rho_{l0}}) - (1 - S)) \tag{3.7.7}$$

where ρ_w is the density of water and ρ_{l0} is the density of the solution before freezing. It is estimated that these two densities are about equal. This gives

$$\varepsilon = \frac{1}{3} P \cdot (0.09 \cdot S \cdot (1 - \frac{x_0}{x(T)}) - (1 - S)) \tag{3.7.8}$$

Such calculated dilatations for saturated samples with various porosities and NaCl concentrations are plotted versus the temperature in Appendix L. Corresponding experimental data from the dilatation tests described above are also shown.

Measured dilatations during the freezing phase from Fagerlund (1972) are presented in Table 3.7.3. Only pure water was used. The dilatations are on the same order of magnitude as the dilatations presented in Appendix K.

Table 3.7.3. Values of dilatations caused by freezing from Fagerlund, 1972.

Material	P (%)	S	measured ε (‰)
Underburnt brick	39.3	0.9	0.6
Hardburnt brick	31.3	0.77	0.75
Lime-silica brick	30.9	0.91	0.5
Aerated concrete type 1	81.2	0.5	0.05
Aerated concrete type 2	78	0.59	0.2
Aerated concrete type 3	80.7	0.58	0.55
Aerated concrete type 4	79.3	0.57	0.7

As can be seen in Appendix L, the measured dilatations are only a fraction of the theoretical dilatations. One explanation for this is that the specimens were actually not completely saturated at freezing as it is impossible to avoid some drying when handling the specimens. There are, then, empty spaces in the pore system that can be filled with the ice before dilatation occurs. Theoretically, if the degree of saturation is 0.917 or less, there is room for all ice to expand into empty spaces and no dilatation should occur, provided no hydraulic pressure occurs from the displacement of unfrozen water when ice is formed. Ice is also forced out from the pore system and formed at the surface of the specimens, which could be seen by visually inspecting the water-saturated, frozen stone prisms. The ice formed at the surface does not contribute to the expansion.

Another possible explanation is that the material is not necessarily totally elastic to the ice formation, which is an assumption made in the calculation. The forces from the formation of ice are considerable, about 10 MPa per °C below zero, but even so, as ice is formed from all sides of a pore wall, or in this case a mineral grain, it is exposed to a triaxial pressure. Pressures formed in this way can theoretically prevent a part of the solution from freezing, even though the pores of the sandstone are almost entirely too large to contain unfreezable water (see Chapter 2.4.2). However, it must be considered that the tensile strength of the actual stones is less than 2 Mpa. Therefore, the material cannot stop ice from being formed. Calorimetric studies (see Chapter 3.7.3) show that 85 to 95% of the water in the pore system of Gotland sandstone forms ice at freezing down to -20 °C.

3.8 Sealed multi-cycle freeze-thaw tests - S_{crit}-tests

3.8.1 Introduction

A measure of the critical degree of saturation was obtained in the dilatation tests described in Chapter 3.7. The test described here is another method of evaluating a critical degree of saturation. Sandstone specimens containing various amounts of water, that is, with various degrees of water saturation, were exposed to several freeze-thaw cycles. The specimens were wrapped in polythene plastic bags in order to prevent moisture transport during the freeze-thaw test. This method was originally published in Fagerlund (1977). The damage caused by freezing and thawing was measured as a relative decrease in dynamic modulus of elasticity, which is explained in more detail in Appendix G. The damage caused by freezing and thawing was also measured as a relative increase in volume. The volume was measured by the method described in Chapter 3.3.2.

$$V_0 = (Q_{a0} - Q_{w0}) \cdot \rho_w \tag{3.8.1}$$

$$V_n = (Q_{an} - Q_{wn}) \cdot \rho_w \tag{3.8.2}$$

where

V_0 specimen volume at the start of the test (m^3);
V_n specimen volume at the end of the test (m^3);
Q_{a0} weight of the vacuum-saturated specimen in air at the start of the test (kg);
Q_{w0} weight of the vacuum-saturated specimen in water at the start of the test (kg);
Q_{an} weight of the vacuum-saturated specimen in air at the end of the test (kg);
Q_{wn} weight of the vacuum-saturated specimen in water at the end of the test (kg);
ρ_w density of water (1000 kg/m^3).

3.8.2 Method

15 stone prisms with the dimensions 2 × 2 × 15 cm were sawed from blocks with the dimensions 15 × 15 × 30 cm from the sandstones Botvide, Uddvide and Valar. The sawing direction was unknown as the bedding direction of sandstone is not visible to the naked eye. Test data from the stones are presented in Appendix P6, Tables P6.1-P6.3. The prisms were dried at a temperature of 50 °C in an air-circulated oven until no more weight loss caused by moisture evaporation occurred (that is, for at least four days). The dried specimens were weighed and the resonant frequency was measured. The specimens were then vacuum saturated and weighed again in air and immersed in water in the same way as described in Chapter 3.2.2. The vacuum-saturated prisms were then conditioned by drying them to various required weights, Q, to give various required degrees of saturation, S_r, in the range of 0.6 to 1.0. The specimens were conditioned by drying them in an air-circulated oven at 50 °C, followed by drying with a blow-dryer.

$$Q = S_r (Q_a - Q_{d(50)}) + Q_{d(50)} \tag{3.8.3}$$

where

Q required weight (kg);
S_r required degree of saturation;
Q_a weight of vacuum-saturated specimen in air (kg);
$Q_{d(50)}$ weight of the specimen dried at 50 °C (kg).

After the final drying, the specimens were wrapped in polythene plastic bags and left overnight to make the moisture distribution more even. Immediately before the freezing and thawing, the specimens were temporarily taken out from the plastic bags and weighed, and the resonant frequency was measured. The moisture-conditioned specimens, wrapped in plastic bags, were then exposed to 15 freeze-thaw cycles of the type showed in Figure 3.8.1. A dummy, treated equally to the prisms but containing a thermocouple in a drilled hole in the centre, was also placed in the freezer.

Four prisms each of the limestone Öland B1 and the granite Bohus red Bratteby were treated in the same way as described above. Test data of the stones are presented in Appendix P6, Table P6.4. Only completely saturated prisms were tested for these stone types in order to see if these dense stone types were damaged at all. Two specimens of each stone were saturated with water and two with a solution of 2% $Na_2SO_4 \cdot 10H_2O$.

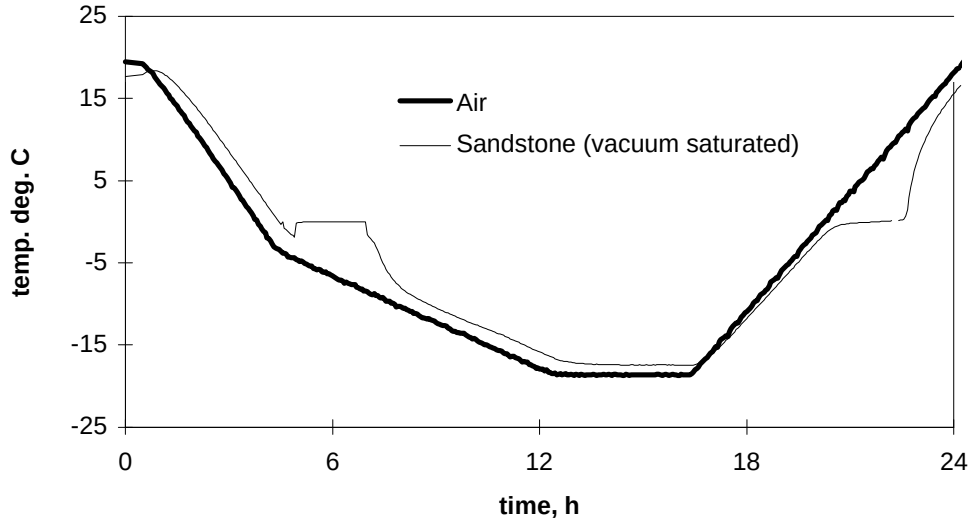

Figure 3.8.1. Freeze-thaw cycle of S_{crit}-test. There were 15 cycles.

After the freezing and thawing was finished, the specimens were again weighed, and the resonant frequency was determined.

A more accurate degree of saturation can be calculated when the test is finished and the specimens are dried at a temperature of 105 °C. As the specimens lost some water during the freeze-thaw test two values of S were calculated; S_0 is the degree of saturation at the start of the test and S_n is the degree of saturation at the end of the test. The lost water was found as condensed water inside the polythene plastic bags that were wrapped around the specimens during the freezing and thawing.

$$S_0 = \frac{Q_0 - Q_{d(105)}}{Q_a - Q_{d(105)}} \tag{3.8.4}$$

$$S_n = \frac{Q_n - Q_{d(105)}}{Q_a - Q_{d(105)}} \tag{3.8.5}$$

where

S_0 degree of saturation at start of the freeze-thaw test;
Q_0 specimen weight at start of the freeze-thaw test (kg);
S_n degree of saturation at end of the freeze-thaw test;
Q_n specimen weight at end of the freeze-thaw test (kg);
$Q_{d(105)}$ weight of the specimen dried at 105 °C (kg).

The resonant frequency was measured after the final drying as well.

3.8.3 Results of sandstone

In Appendix M, the results of the test are shown as relative loss in dynamic modulus of elasticity and relative increase in volume versus degree of saturation for the three sandstones Botvide, Uddvide and Valar. Two examples are shown in Figure 3.8.2. Two points are shown for each specimen as some weight loss occurred during the freeze-thaw test. Water was found in the plastic bags after the freeze-thaw test. Therefore, the degree of saturation changed from the higher value to the lower during the test. From the graphs, it is obvious that the two specimens with the highest degree of saturation are more damaged than the other specimens for the sandstones Botvide and Uddvide. The critical degree of saturation for these stone species is about 0.92 (Botvide 0.88 - 0.95 and Uddvide 0.89 - 0.96). For Valar only the specimen with the highest degree of saturation is more damaged than the other specimens, which gives a critical degree of saturation higher than 0.94. The values of the critical degree of water saturation in these tests were generally higher than the values obtained in the dilatation tests, which agrees with Fagerlund (1972). However, the values of the critical degree of water saturation obtained in the dilatation test is dependent on the definition, which in this case was the degree of saturation where the 'maximal' dilatation exceeds zero. If the definition instead would be for example the degree of saturation where the dilatation value exceeds the tensile strain capacity, which is perhaps a more relevant definition, the critical values determined with the two different methods might be almost equal.

The relative increase in volume versus the relative loss in dynamic modulus of elasticity is shown in Figure 3.8.3. The most saturated specimens that show a clear increase in volume also show a clear decrease in E-modulus, but the relationship between the two methods of measuring damage is far from linear.

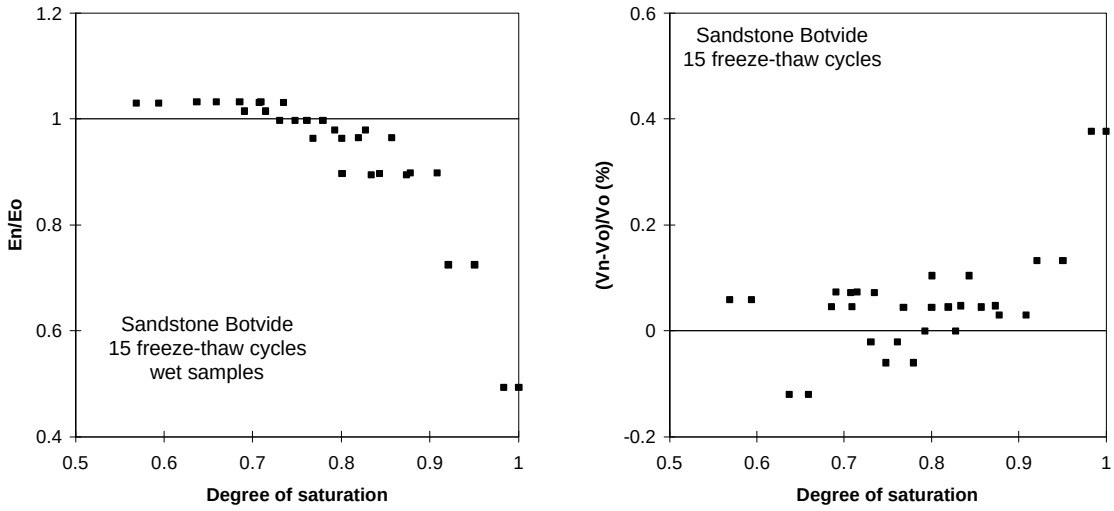

Figure 3.8.2. Loss in dynamic modulus of elasticity and relative increase in volume versus the degree of saturation of the sandstone Botvide. More results are shown in Appendix M.

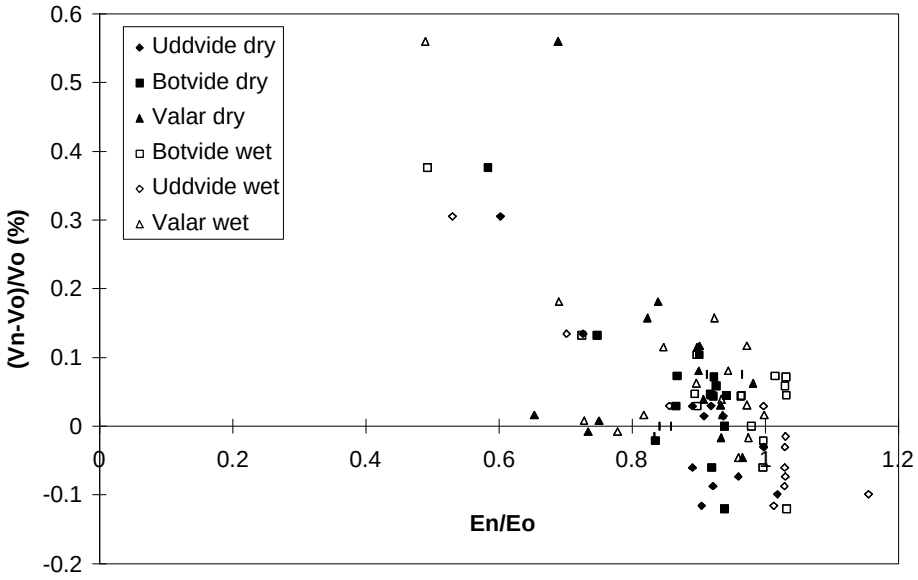

Figure 3.8.3. Relative increase in volume versus loss in dynamic modulus of elasticity.

3.8.4 Results of granite and limestone

The value of E_n/E_0 of the granite was 0.85 to 0.95 and of the limestone, 0.95 to 1.1. There was no significant difference between the stones saturated with water and those saturated with salt solution for neither of the stones. The fact that the spread of the values of granite was large makes it difficult to say whether it was damaged or not. No damage was detected for the limestone.

3.8.5 Visible damages

The damage in the S_{crit}-tests described above was normally not visible to the naked eye; however, visible damage in the form of cracking was found on some sandstone prisms with the dimensions 3 × 3 × 12 cm and with high degrees of saturation. Those prisms were freeze-thaw tested according to the freeze-thaw cycle shown in Figure 3.8.2, which has a higher freezing rate and a longer time at the minimum temperature (-20 °C) than in the test described above. A photograph of some of the damaged stone prisms is shown in Figure 3.8.4.

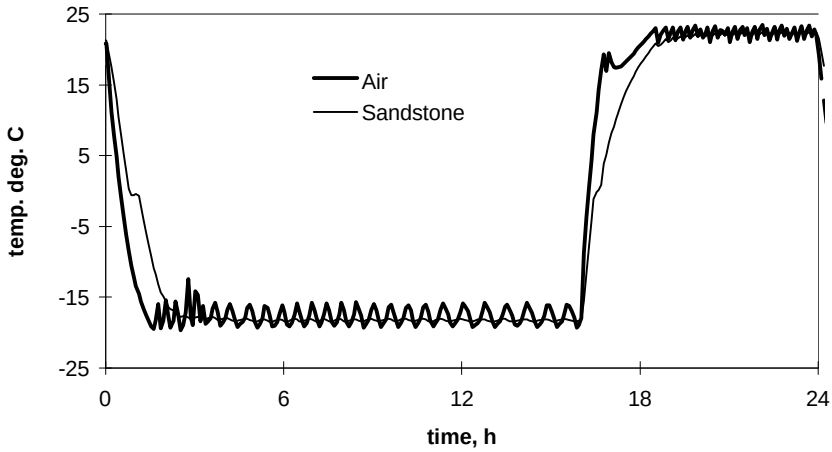

Figure 3.8.4. Freeze-thaw cycle in S_{crit}-test with visible damage. There were 9 cycles.

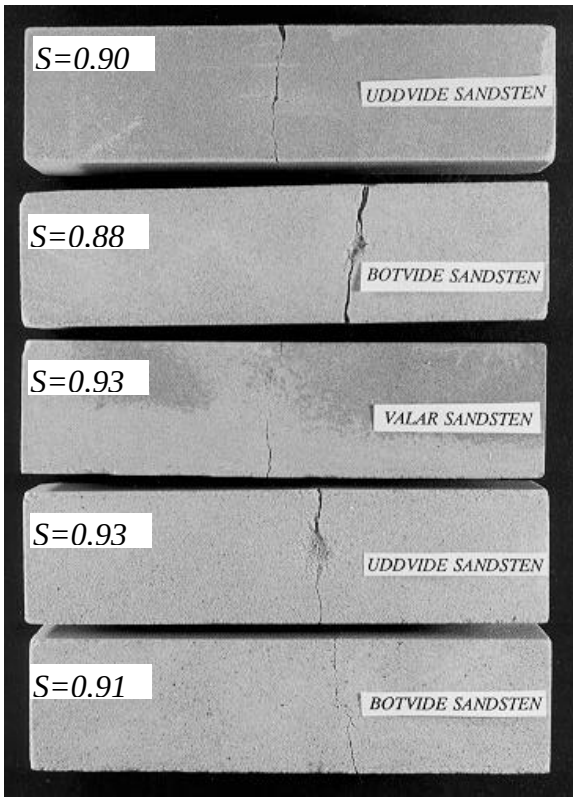

Figure 3.8.3. Damaged stone prisms (3 × 3 × 12 cm) after S_{crit}-test with high degrees of saturation according to the freeze-thaw cycle shown in Figure 3.8.2.

3.9 Calorimeter studies

3.9.1 Introduction

Some calorimeter studies were made on water-saturated stone to see at what temperature freezing actually occurred and to see if it was possible to make a quantitative analysis of how much of the pore water actually freezes.

3.9.2 Differential scanning calorimeter

A differential scanning calorimeter (DSC) records the difference between the enthalpy change that occurs in a sample and that which occurs in an inert reference material when they are both equally heated or cooled. Such an enthalpy change is caused by, for example, a phase transformation like ice formation or melting. For practical reasons only small pieces of material (a few cubic millimetres) can be tested in the apparatus because the temperature gradient in the sample has to be very small in order to give an adequate result.

Method

A PC-controlled DSC7 differential scanning calorimeter from Perkin Elmer with liquid nitrogen cooling equipment connected to it was used for the tests. A piece of the sandstone Botvide was crushed with a hammer into pieces small enough to be tested in the DSC. The pieces were dried in an air-circulated oven at 105 °C for one day and then capillary saturated in de-ionised water for one week. Samples of vacuum-saturated granite and limestone were tested in a similar way. Pure water and water mixed with an inert powder were also run. All tests were run with the tested material in closed, perforated aluminium sample holders specially designed for the instrument. A similar sample holder with Al_2O_3 as an inert material was placed in the reference cell.

Results
Results are shown in Appendix N as heat flow versus temperature. As can be seen in Figure N:1 the supercooling of the water in the pores of the sandstone is about 6 °C in this case. This can be compared with the results shown in Figures 3.7.3 and 3.7.4 in which the freezing of the pore water occurs at a somewhat higher temperature — at about three degrees below zero. Supercooling for pure water is 17 °C (Figure N:3). The same supercooling temperature was obtained on several runs. For water mixed with an inert material (Al_2O_3 or sand, Figure N:5), the supercooling is about the same as for water in the pores of sandstone (6 °C), which implies that it is actually a supercooling phenomenon and not a freezing point depression caused by small pores (Equation 2.4.1, Chapter 2.4). The relatively high supercooling can perhaps be explained by the relatively fast scanning rate and by the fact that the heat flow between the instrument and the sample was not as good as it ought to have been. The most plausible explanation, however, is that the instrument records another temperature than that of the specimen. The heat flow, on the other hand, is governed by the temperature of the specimen. Therefore, there is no direct correlation between the measurement of ice formation or melting (the heat flow) and the temperature. During the cooling phase the recorded temperature is too low and during the heating phase it is too high. Compensations can be made for this, but that was not done here, because the objective was to determine the amount of water frozen and not at what temperature it freezes or melts.

Figures N:2, N:4 and N:6 show the melting. For the wet sandstone and the water mixed with an inert material (Figures N:2 and N:6), the melting starts at one or two degrees above zero. For the pure water (Figure N:4), the melting temperature recorded starts at 0 °C.

The amount of freezing water was not large enough to make a quantitative analysis. A quantitative analysis is only possible when a sample holder contains water only. An example of such a calculation made using the PC connected to the instrument, is shown in Figure N:4. The heat of fusion calculated using the DSC and the PC connected to the instrument was correct compared to the values found in the literature (333 J/g - 334 J/g).

In samples of granite and limestone, the amount of water was too small to give any result for freezing and thawing in the DSC.

3.9.3 Setaram micro-calorimeter

In a differential low temperature Calvet Setaram Microcalorimeter, considerably larger samples can be used than can be used in the DSC described previously. The principle of measuring heat formation during heating and cooling caused by, for example, a phase transition, is equal for both of these calorimetric instruments. The tests described below were performed partly at Technical University of Denmark, Department of Structural Engineering and Materials, under the supervision of Dr Kurt Kielsgard Hansen, and partly at The Lund Institute of Technology, Department of Building Materials under the supervision of Sture Lindmark.

Method
The test specimens were in the form of circular cylinders with a diameter of 14 mm and a length of 65 mm. During a run, the specimens were enclosed in an air-tight stainless steel sample holder, slightly larger than the specimens. An empty reference cell was used in the Setaram instrument. The samples tested were vacuum saturated and surface dry.

The limestone Öland B1 and granite Bohus Red Bratteby were tested in the instrument in Denmark. A small amount (a few milligrams) of AgI powder was applied to the top of the sample. The crystal structure of AgI is similar to that of ice so it helps ice nucleation and thus prevents supercooling. The rate of cooling was constant at 3.3 °C/min, and the rate of heating was constant at 4.1 °C/min. These rates are high compared to the rates of temperature lowering in nature, which are 0.1 °C/min at the most.

The Gotland sandstones Botvide and Valar and the Borghamn limestone were tested at Lund. No AgI powder was used in this case. The rate of cooling and heating was constant 3.6 °C/min.

Results and discussion

The weights of the samples under saturated and dry condition are shown in Table 3.9.1.

Table 3.9.1. Weight of samples (g) in a test run in a Setaram Microcalorimeter.

	Weight of dry sample (105 °C)	Weight of vacuum-saturated, surface dry sample	Weight of water	% of water frozen
Limestone Öland B1	22.53	22.84	0.31	1)
Granite	25.19	25.22	0.03	1)
Sandstone Botvide	19.69	21.76	2.07	95
Sandstone Valar	21.17	22.79	1.62	85
Borghamn Limestone	25.68	25.80	0.12	40

1) Too small amount of water to be quantified.

All results are shown in Appendix O. The results from cooling and heating of the limestone Öland B1 and granite Bohus Red Bratteby are shown as heat capacity versus temperature. Unfortunately the amount of ice was too small to make a quantification possible in this case. As can be seen from these results, some supercooling occurred at freezing in spite of the AgI. The melting occurs at a higher temperature than the freezing does, and the freezing also occurs during a shorter time interval than does the melting, which was also the case with the DSC. The fact that melting starts at some degrees below zero can depend on a freezing point depression because of small pores (Equation 2.4.1). The results from the Setaram calorimeter in Denmark show that ice is formed even in dense and very dense stones like limestone and granite, which implies that damage can be caused by ice formation even in dense stones, provided the amount of ice is great enough. The porosity of the surface of exposed, dense stone might be increased by, for example, selective dissolution if certain minerals (Sjöberg et al, 1992). Then the possibility of frost damage to occur might be even higher.

The results from cooling and heating of the sandstones and the Borghamn limestone are shown as heat flow versus temperature and time. Supercooling occurred in this case as well. The fact that the melting seems to start at some degrees above zero is a result of the construction of the instrument, as was described above; the temperature is measured in the calorimeter block and not in the sample itself. Quantification of the ice formed is possible. The results show that about 95% of the water in the Botvide sandstone was frozen, about 85% of the water in the Valar sandstone was frozen and about 40% of the water in the Borghamn limestone was frozen.

The fact that melting starts below zero degrees in all runs with the instrument in Denmark but above zero in all runs with the instrument in Sweden can also depend on some uninvestigated difference between the two instruments.

4 Conclusions and some comments on the frost resistance of the tested natural stones in practice

The hypothesis initiating this study was that freezing in some cases might have a considerable effect on deterioration of ancient stone in exposed buildings and monuments, or even being the major cause of destruction in the Nordic climate. This hypothesis has not been contradicted by this study. Two of the stone types tested here, namely, Gotland sandstone and the limestone Öland B1, have a low, or very low, frost resistance compared to other modern building materials.

In so-called scaling tests, in which the specimens are submerged in a salt solution during freezing and thawing, it was also shown that very weak solutions are much more harmful than is pure water. In these tests, the damage primarily occurs as scaling. The stone type most sensitive to surface scaling in weak solutions is the limestone Öland B1. The stones are almost unharmed when freezing occurs in pure water, but as little as 0.25% of NaCl in the surrounding solution is enough to cause severe scaling of a type similar to what is seen in nature. Therefore, it is not unreasonable to assume that much damage observed on exposed limestone or sandstone in buildings and monuments is caused by surface scaling induced by frost.

When sandstone specimens are freeze-thaw tested in a moisture-isolated state, that is, with no surrounding solution, only internal damage occurs. In such tests, it was shown that damage occurs when the degree of saturation exceeds a critical value, which confirms findings made in other studies with different types of materials. Damage becomes more severe the more the degree of saturation exceeds the critical value. For the more dense materials limestone and granite, the damage is low also when the materials are completely saturated.

A relevant question is whether it is possible for the stones to reach a degree of saturation high enough to cause damage under natural conditions. For sandstone, the degree of saturation reaches a value of about 0.8 after capillary suction for one week. This degree of saturation is not, according to the freeze-thaw tests, enough to cause severe damage at freezing. As water, because of its quick transport through sandstone, is relatively homogeneously re-distributed after short periods of water suction, such as during a rain, the degree of saturation under normal conditions probably does not exceed the critical levels in any part of the stone, as long as this is not surface treated. However, if the material sucks in water for a long time, for example, by capillary suction from the soil, it is highly probable that the sandstone will actually be damaged by frost as the water content in the stone continues to increase for a long time and will sooner or later exceed the critical level. The sandstone reaches complete saturation (equivalent to vacuum saturation) before three months of suction.

The granite and limestones are completely saturated after capillary suction for one week, but the damage stated for these stones when freeze-thaw tested in pure water was not extensive.

5 References

Amoroso, G. G., Fassina, V., ‘Stone decay and conservation’, Materials Science Monographs, 11, Elsevier Science Publishers B. V., Amsterdam, 1983.

Arfvidsson, J., ‘Isoterma fuktförlopp i porösa material, Beräkning och utvärdering av mätdata’, ‘Isothermal moisture transport in porous materials, Calculation and evaluation of material data’, Lund Institute of Technology, Division of Building Physics, Report TVBH-1007, Lund, 1994.

Arnfelt, H., ‘Skador på betongvägar uppkomna genom saltbehandling vintertid’, ‘Damage to concrete pavements by wintertime salt treatment’, Meddelande 66, Statens Väginstitut, Stockholm, 1943, pp 4-28.

Asp, M., Conservator, Conservation Institute of National Antiquities, personal communication, 1996.

ASTM C 215-85 ‘Standard test method for fundamental transverse, longitudinal and torsional frequencies of concrete specimens’, 1985.

‘Betonghandboken, Material’, ‘Concrete Handbook, Materials’, Second edition, Svensk Byggtjänst, Stockholm, 1994.

Bro 94, ‘Allmän teknisk beskrivning för broar’, ‘General technical description for bridges’, Vägverket, 1994.

Central Board of National Antiquities, ‘Degradation of materials and the Swedish heritage’, 1992-1995.

Collins, A. R., ‘The destruction of concrete by frost’, Journal of Institute of Civil Engineers, 23, 1944, pp 29-41.

Conservation Institute of National Antiquities, ‘Air pollution and the cultural heritage, action plan 90’, Stockholm, 1990.

Conservation Institute of National Antiquities, ‘Stone weathering, Air pollution effects evidenced by chemical analysis’, Stockholm, 1991.

Conservation Institute of National Antiquities, ‘Air pollution and the Swedish heritage, progress 1988-1991’, Stockholm, 1992.

Chatterji, S., Christensen, P., ‘A mechanism of breakdown of limestone nodules in a freeze/thaw environment’, Cement and Concrete Research, 9, 1979, pp 741-746.

Defay, R., Prigogine, I., Everett, D. H., ‘Surface tension and absorption’, Longmans, London, 1966, pp 217-285.

Fagerlund, G., ‘Kritiska vattenmättnadsgrader i samband med frysnig av porösa och spröda material’, ‘Critical degrees of saturation at freezing of porous and brittle materials’, Lund Institute of Technology, Division of Building Technology, Report 34, Lund, 1972.

Fagerlund, G., ‘The critical degree of saturation method of assessing the freeze/thaw resistance of concrete’, Matériaux et Constructions, vol. 10, no 58, 1977.

Fagerlund, G., ‘Principer för betongs frostbeständighet’, ‘Principles of frost durability of concrete’, Nordisk betong, 2, 1981, pp 5-13.

Fagerlund, G., ‘Frost resistance of high performance concrete - Some theoretical considerations’, Lund Institute of Technology, Division of Building Materials, Report TVBM-3056, Lund, 1993, a.

Fagerlund, G., ‘Frostagrepp - beskrivning av verkande mekanismer, Föredrag vid seminariet ‘Beständig betong’ i Stockholm den 24 augusti och i Köpenhamn den 2 september 1993’,’Frost action - description of active mechanisms, lecture at the seminar ‘Durable concrete’ in Stockholm August 24 and in Copenhagen September 2 1993’, Lund Institute of Technology, Division of Building Materials, Report TVBM-7056, Lund, 1993, b.

Fagerlund, G., ‘Kapillaritet som orak till nedbrytning av kalcitbunden sandsten - en hypotes’, ‘Capillarity as a cause of the deterioration of calcite-bound sandstone – a hypothesis’, Lund Institute of Technology, Division of Building Materials, Report TVBM-3058, Lund, 1994, a.

Fagerlund, G., ‘Predicting the service life of concrete exposed to frost action through a modelling of water absorption process in the air-pore system’, RILEM/NATO workshop ‘The modelling of microstructure and its potential for studying transport properties and durability’, St. Rémy-les-Chevreuse, July 10-13, 1994, b.

Fagerlund, G., ‘Fukt och porer, Bidrag till kursen byggnadsmaterial FK’, ‘Moisture and pores, Contribution to the building materials continuation course’, Lund, March 1995.

‘Handbook of chemistry and physics’, 70th edition, CRC Press, Florida, 1989-1990.

Hedenblad, G., ‘Materialdata för fukttransportberäkningar, En katalog’, ‘Material data for moisture transport calculations’ Fuktsäkerhet i byggnader, Byggforskningsrådet - BFR, Svenska byggbranschens utvecklingsfond - SBUF, 1996.

Hedenblad, G., Nilsson, L. O., ‘Kapillär mättnadsgrad - ett verktyg för noggrann bestämning av fuktinnehåll i betong’, ‘Degree of capillary saturation - a tool for accurate determination of the moisture content in concrete’, Report TVBM-3022, Lund, 1985.

Hobbs, P. V., ‘Ice physics’, Clarendon Press, Oxford, 1974.

Holmes, A., ‘Principles of physical geology’, Thomas Nelson & Sons Ltd, London, 1965.

Hägg, G., ‘Allmän och oorganisk kemi’, ‘General and inorganic chemistry’, eighth edition, Almqvist & Wiksell, Uppsala, 1984.

Janz, M., ‘Methods of measuring the moisture diffusivity at high moisture levels’, Lund Institute of Technology, Division of Building Materials, Report TVBM-3076, Lund, 1997.

Johansson, L.-G., Lindqvist, O., Mangio, R. E., ‘Corrosion of calcareous stones in humid air containing SO_2 and NO_2’, Durability of Building Materials, 5, 1988, pp 439-449.

Knutsson, S., ‘Tjäle – är det något att intressera sig för?’, ‘Frost heave, is that something to take interest in?’, Bygg & Teknik, 8, 1995, pp 65-70.

Lala, D., Kucera, V., Sjöström, C., ‘Luftföroreningar, Korrosion och andra effekter på byggnadsmaterial’, ‘Air pollution, corrosion and other effects on building materials’, R114:1989, Statens råd för byggnadsforskning, Stockholm, 1989.

Larsen, E. S., Nielsen, C. B., ‘Decay of bricks due to salt’, Materials and Structures, 23, 1990, pp 16-25.

Lautridou, J. P., Ozouf, J. C., ‘Progress in physical geography, Experimental frost shattering, 15 years of research at the Centre de Géomorphologie du Centre National de la Recherche Scientifique’, Caen.

Lewin, S. Z., ‘The mechanism of masonry Decay through crystallisation’, Report to the Committee on Conservation of Historic Stone Buildings and Monuments, National Academy Press, Washington D. C, 1982, pp 120-144.

Lindmark, S., ‘Inverkan på testresultatet av variationer i saltkoncentrationer, saltfördelningar och fryscykelutformning vid saltfrostprovning enligt SS 13 72 44, presenterad vid XV:e Nordiska Betongforskningsmötet, Göteborg 1993’, ‘Influence on test results of variations in salt concentration, salt distribution and freeze-thaw cycle at salt-freeze testing according to (Swedish Standard) SS 13 72 44, presented at the XV Meeting of Nordic Concrete Research, Gothenburg 1993’, Lund Institute of Technology, Division of Building Materials, Report TVBM-7055, Lund, 1993.

Lindmark, S., ‘A hypothesis on the mechanism of surface scaling due to combined salt- and frost attack’, Lund Institute of Technology, Division of Building Materials, Report TVBM-7104, Lund, 1996.

Löfvendahl, R., Asp, M. ‘Uppskattning av saltinnehåll i gotländsk sandsten med cellstofflakning’, ‘Estimation of salt content in Gotland sandstone by leaching with cellulose cotton’, Report 950404, RAÄ, RIKs 1606-2051, Stockholm, 1995.

Micromeritics, Instruction manual, Poresizer 9310, V1.04, U.S.A., February 1987.

Mikhail, R. Sh., Abo-El-Enein, S. A., ‘Studies on water and nitrogen adsorption on hardened cement pastes, development of surface in low porosity pastes’, Cement and Concrete Research, vol. 2, 1972, pp 401-414.

Nevander, L. E., Elmarsson, B., ‘Fukthandbok, Praktik och teori’, ‘Handbook of moisture, Practice and theory’, Second edition, AB Svensk Byggtjänst, Stockholm, 1994.

Powers, T. C., ‘A working hypothesis for further studies of frost resistance of concrete’, Journal of American Concrete Institute, Feb. 1945, pp 245-272.

Powers, T. C., Brownyard, T. L., ‘Studies of the physical properties of hardened Portland cement paste’, Proceedings of American Concrete Institute, 41, 1946-1947, pp 496-498.

Powers, T. C., ‘The air requirement of frost-resistant concrete’, Proceedings Highway Research Board, 29, PCA Bulletin 33, 1949, pp 184-211.

Powers, T. C., Helmuth, R. A., ‘Theory of volume changes in hardened Portland-cement paste during freezing’, Proceedings Highway Research Board, 32, 1953, pp 285-297.

Powers, T. C., ‘Physical properties of cement paste’, Proceedings of the 4th international symposium on the chemistry of cement, Session V, Properties of cement paste and concrete, Washington 1960, National Bureau of Standards Monograph 43, vol. 2, 1962, pp 577-613.

Schweda, P., Wessman, L., Wirje, A., ‘Längdändring hos kalksten och sandsten, varierande luftfuktighet och saltlösningar’, ‘Length change of limestone and sandstone, varying humidity and salt solutions’, Division of Building Materials , Report TVBM-7103, Lund, September 1996.

Sjöberg, L., Mörth, M., Schweda, P., Lindblom, S., Frogner, P., Estmark, B., ‘Experimentella studier av silikatmineralvittring’, ‘Experimental studies of weathering of silicate minerals’, Department of Geology and Geochemistry, Stockholm University, 1992.

SS 13 72 44 ‘Betongprovning - Hårdnad betong - Avflagning vid frysning’, ‘Concrete testing - hardened concrete - Scaling at freezing’, Third edition, 1995.

‘Stenhandboken’, ‘Handbook of stone’, Sveriges Stenindustriförbund, Johanneshov, 1986.

Taber, S., ‘The mechanics of frost heaving’ Journal of Geology, 38, 1930, pp 303-317.

Verbeck, G. J., Klieger, P., ‘Studies of ‘salt’ scaling of concrete’, Highway Research Board, Bulletin 150, 1957.

Wadsö, L. ‘Microcalorimetric investigations of building materials’, Report TVBM-3063, Lund, 1994.

Wessman L., Carlsson T., ‘Karaktärisering av några svenska naturstenar med tunnslipsmikroskopi’, ‘Characterisation of some Swedish natural stones with thin section microscopy’, Lund Institute of Technology, Division of Building Materials, Report TVBM - 7095, Lund, 1995.

Widhalm, C., Tschegg, E., Eppensteiner, W., ‘Anisothropic thermal expansion causes deformation of marble claddings’, Eurocare - Euromarble EU 496, Proceedings of the fifth workshop, Innsbruck, October 10 -15, 1994.

Appendix A
Porosity and density

P	is the porosity (%);
s_p	is the standard deviation of the porosity (%);
ρ_b	is the bulk density (kg/m^3);
s_ρ	is the standard deviation of the bulk density (kg/m^3);
ρ_s	is the solid density (kg/m^3);
n	is the number of samples used in the test.

Table A:1. Porosity and density of stones obtained by the 'weighing method' described in Chapter 3.3.2.

Stone	Origin	Name	P (%)	s_p	ρ_b (kg/m^3)	s_ρ	ρ_s (kg/m^3)	n
Sandstone (calcite-bound)	Gotland	Botvide (Burgsvik)	22.2	0.3	2080	11	2674	88
Sandstone (calcite-bound)	Gotland	Uddvide (Qviberg)	22.7	0.8	2069	25	2675	90
Sandstone (calcite-bound)	Gotland	Valar	17.4	0.7	2220	35	2687	79
Sandstone (calcite-bound)	Gotland	Valar* extra dense	9*	3*	2474*	75*	2706*	12*
Sandstone (calcite-bound)	Gotland	X:1	16.8	0.1	2236	4	2689	12
Limestone	Horns Udde Öland	Öland B1	3.6	0.4	2639	14	2731	10
Limestone	Gillberga Öland	Öland G1	3.40	0.04	2628	0.9	2720	4
Limestone	Gillberga Öland	Öland G2	1.8	0.2	2666	4	2714	4
Limestone	Gillberga Öland	Öland Flammig	1.7	0.1	2709	5	2757	10
Limestone	Borghamn	Light grey	1.8	0.6	2678	13	2726	92
Granite	Hunnebostrand Bohuslän	Bohus red Bratteby	0.61	0.05	2637	8	2654	13

* It was found that for some Valar blocks with the size 15 × 15 × 30 cm that some of the stone prisms were considerably more dense than the majority of the Valar prisms. These prisms are therefore treated separately. The porosity of these prisms was in the range of 6-13%, i.e. the variation is very large.

Appendix B
Thin sections

Thin section microscopy is a method used to study the structure of pores larger than about 20 μm. A very thin (about 25 μm) slice of the porous material is mounted between two microscope glass slides. The porous material is normally impregnated with epoxy coloured with a fluorescent dye. This makes the sample more coherent and stable, and it also makes it easier to study and analyse the image under the microscope. Automatic image analysis normally makes it possible to quantitatively evaluate porosity, pore-size distribution, pore shape and continuity, but unfortunately, this was not possible with the materials studied here. The curvature of the grains gave rise to various shades of yellow between the epoxy-filled pores and the somewhat transparent grains, which meant that the colour contrast between the grains and the pores was not sharp enough. For this reason, only a qualitative evaluation could be made.

Thin section microscopy is treated in Chapter 3.3.1.

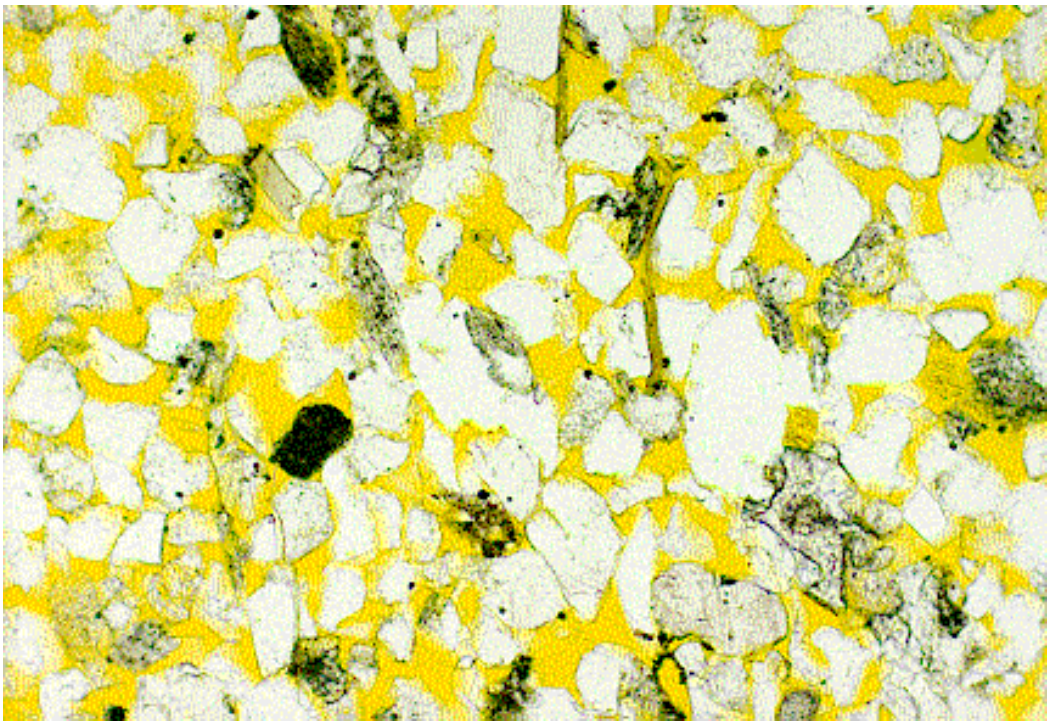

Figure B:1. Thin sections of the calcite-bound sandstone Botvide from Gotland. The picture is 1.2 × 0.8 mm in reality. The white grains are quartz, the dark rods are clay minerals, the dark grains are other minerals and the yellow parts are 'empty spaces' filled with epoxy.

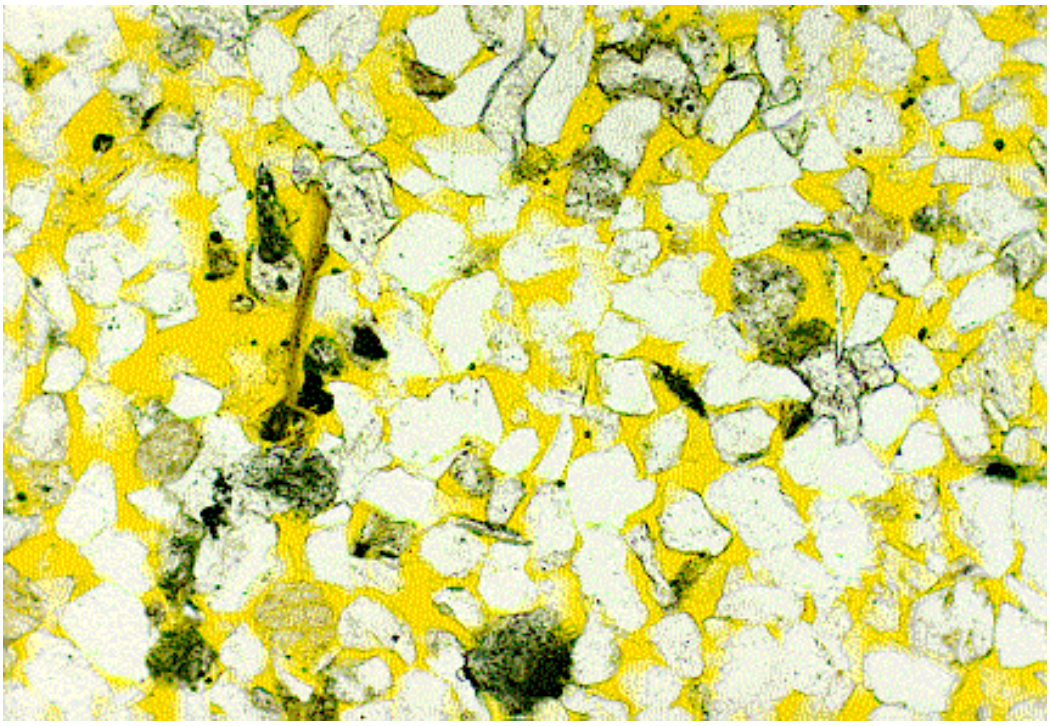

Figure B:2. Thin sections of the calcite-bound sandstone Uddvide from Gotland. The picture is 1.2 × 0.8 mm in reality. The white grains are quartz, the dark rods are clay minerals, the dark grains are other minerals and the yellow parts are 'empty spaces' filled with epoxy.

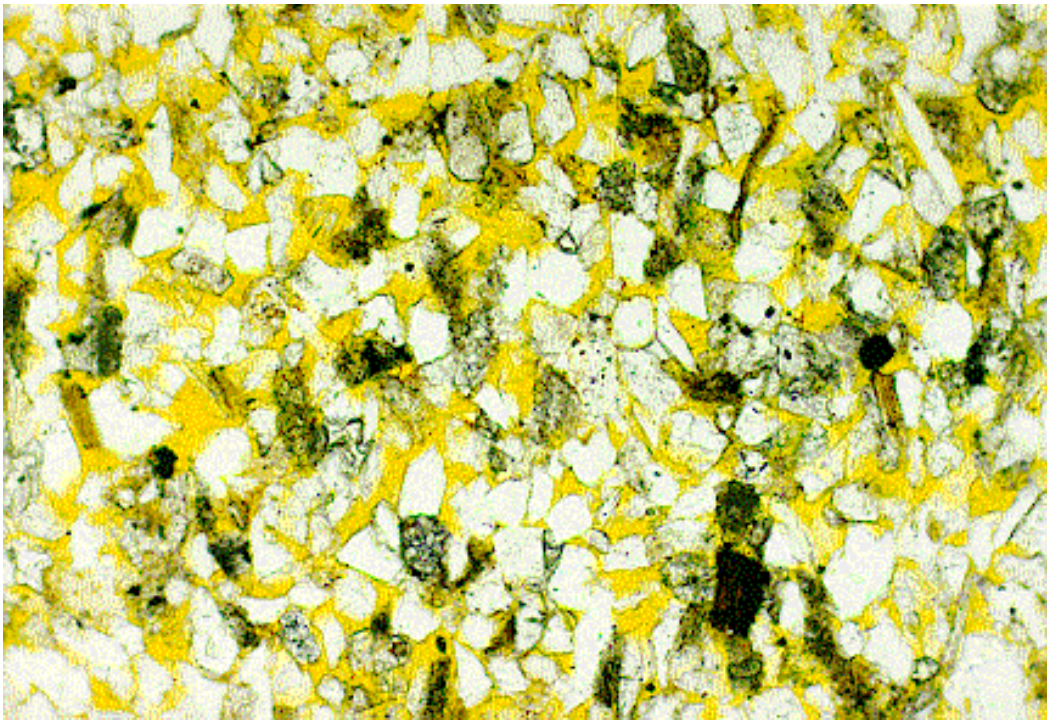

Figure B:3. Thin sections of the calcite-bound sandstone Valar from Gotland. The picture is 1.2 × 0.8 mm in reality. The white grains are quartz, the dark rods are clay minerals, the dark grains are other minerals and the yellow parts are 'empty spaces' filled with epoxy.

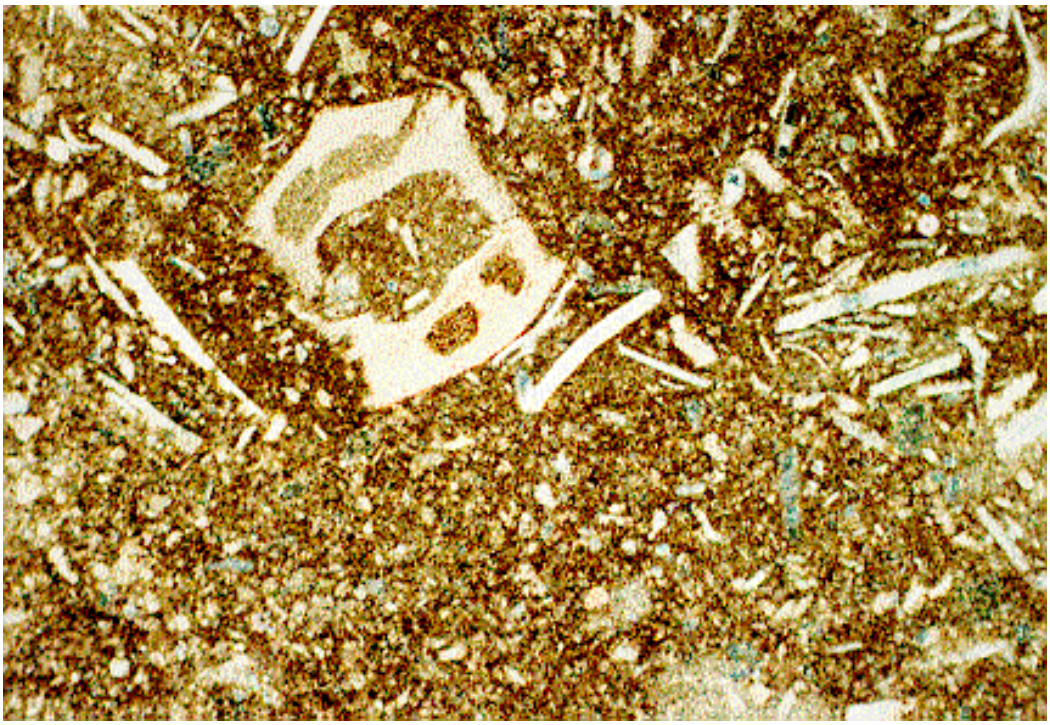

Figure B:4. Limestone Öland B1 from Horns Udde, Öland. The picture is 3 × 2 mm in reality. Light fossils are seen in a darker matrix.

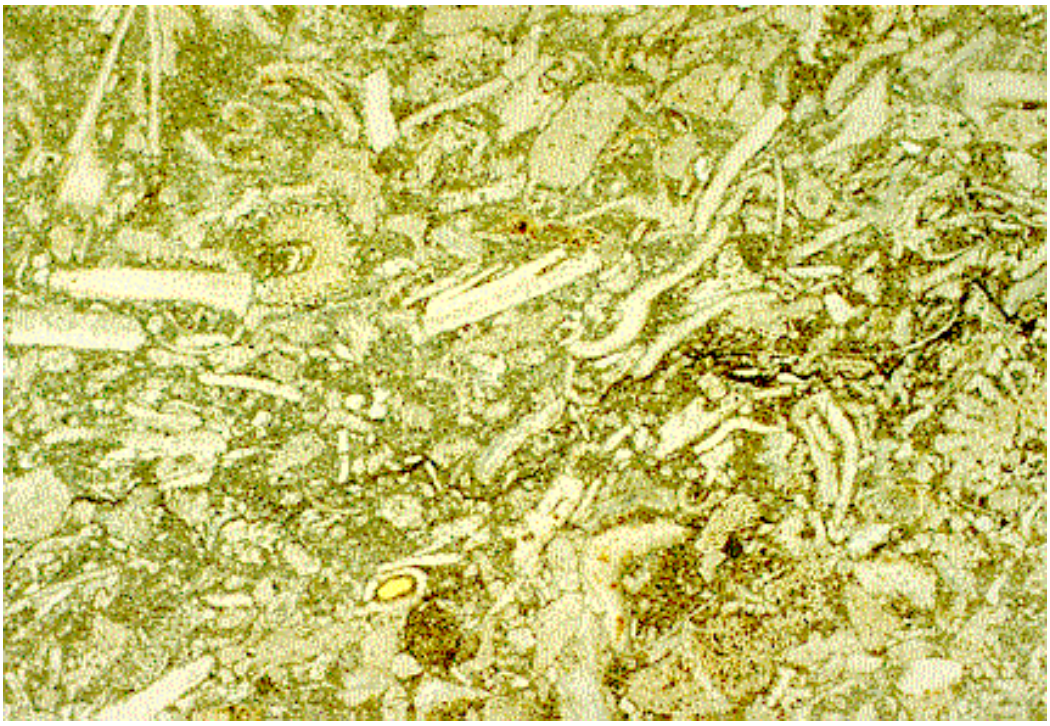

Figure B:5. Limestone Öland Flammig from Gillberga, Öland. The picture is 3 × 2 mm in reality. Light fossils are seen in a darker matrix.

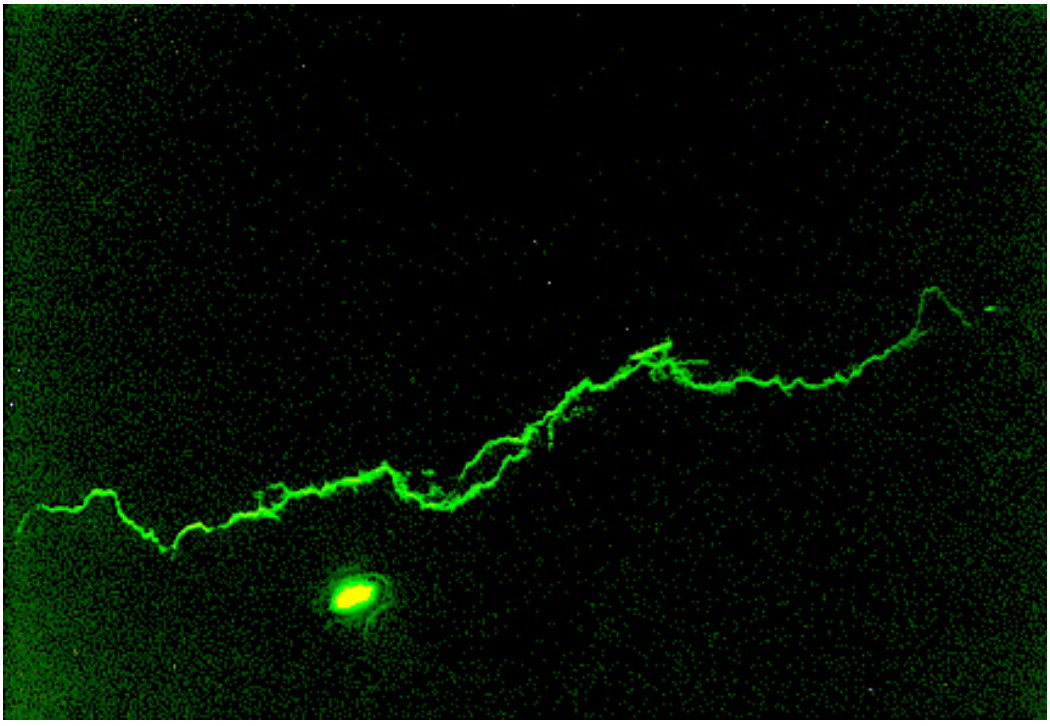

Figure B:6. The same picture as above taken in fluorescent light, which makes a crack and a big pore, possibly emanating from a loosened fossil, visible.

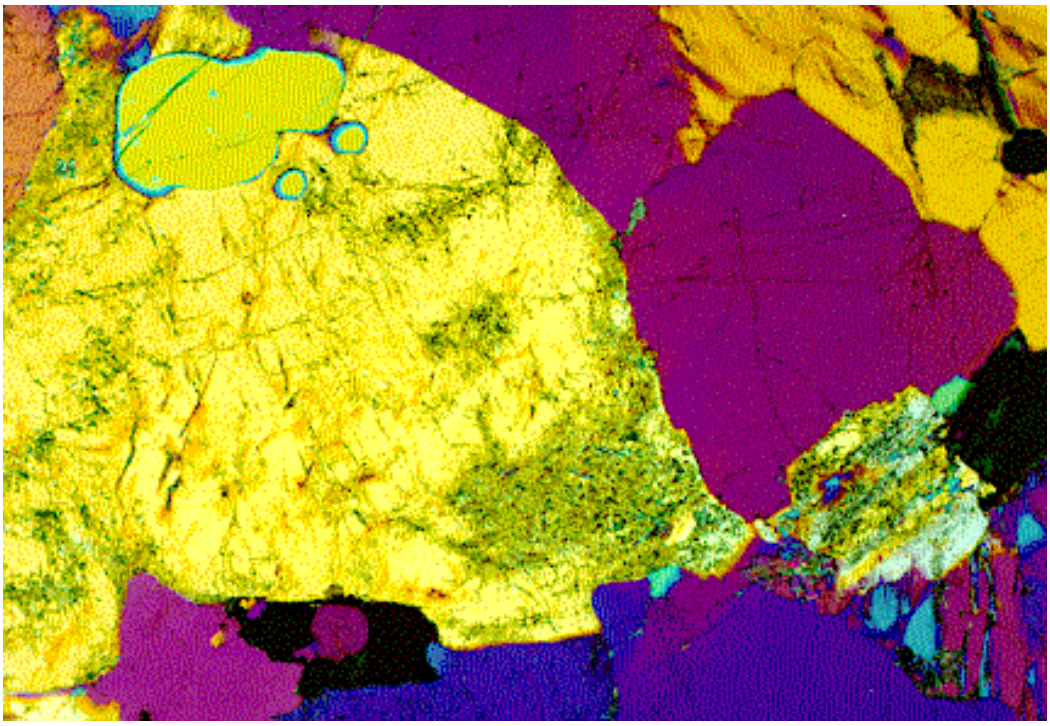

Figure B:7. Granite from Hunnebostrand, Bohuslän. The picture is 3 × 2 mm in reality. The picture is taken in polarised light with I *-filter, to make the different grains visible.*

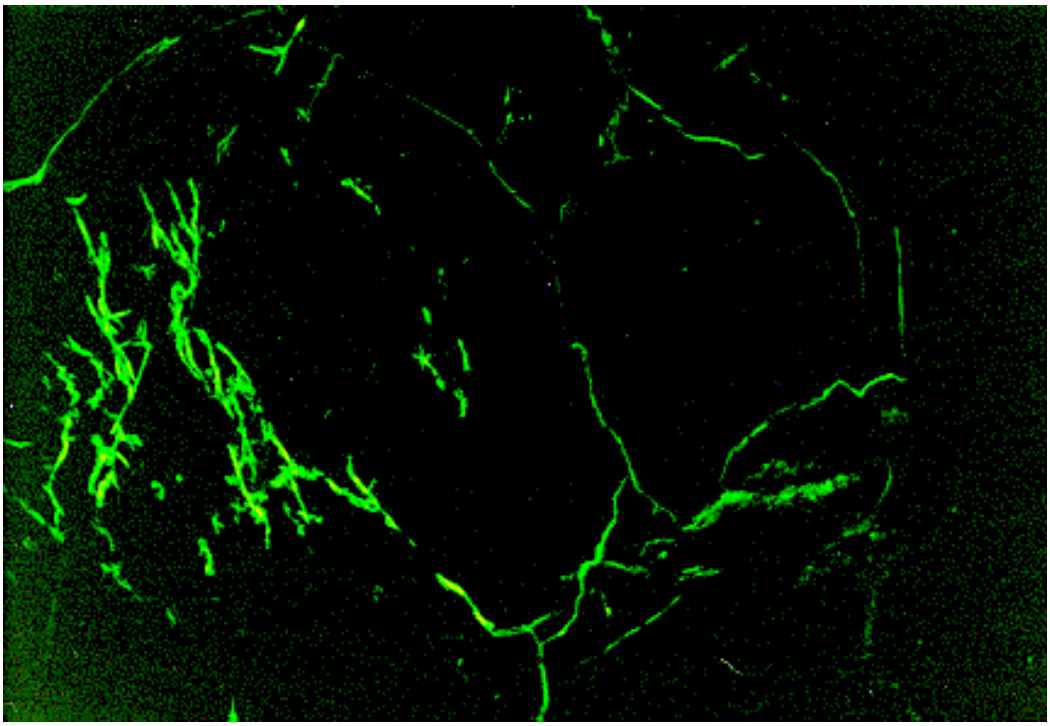

Figure B:8. The same picture as above taken in fluorescent light, which makes cracks between individual grains visible.

Appendix C
Sorption isotherms

When an equilibrium state is reached between a porous material and the surrounding air of a certain relative humidity, the material will contain a certain amount of moisture. The graph describing the equilibrium moisture content as a function of the relative humidity is called the *sorption isotherm* or *moisture equilibrium curve*. In this appendix sorption isotherms are shown for the Gotland sandstones Botvide and Valar, the limestone Öland B1 and the granite Bohus Red Bratteby. The sorption isotherm of the sandstone Uddvide is shown in Chapter 3.3.4. No hysteresis, that is, difference between absorption and desorption, was found for either of the stones.

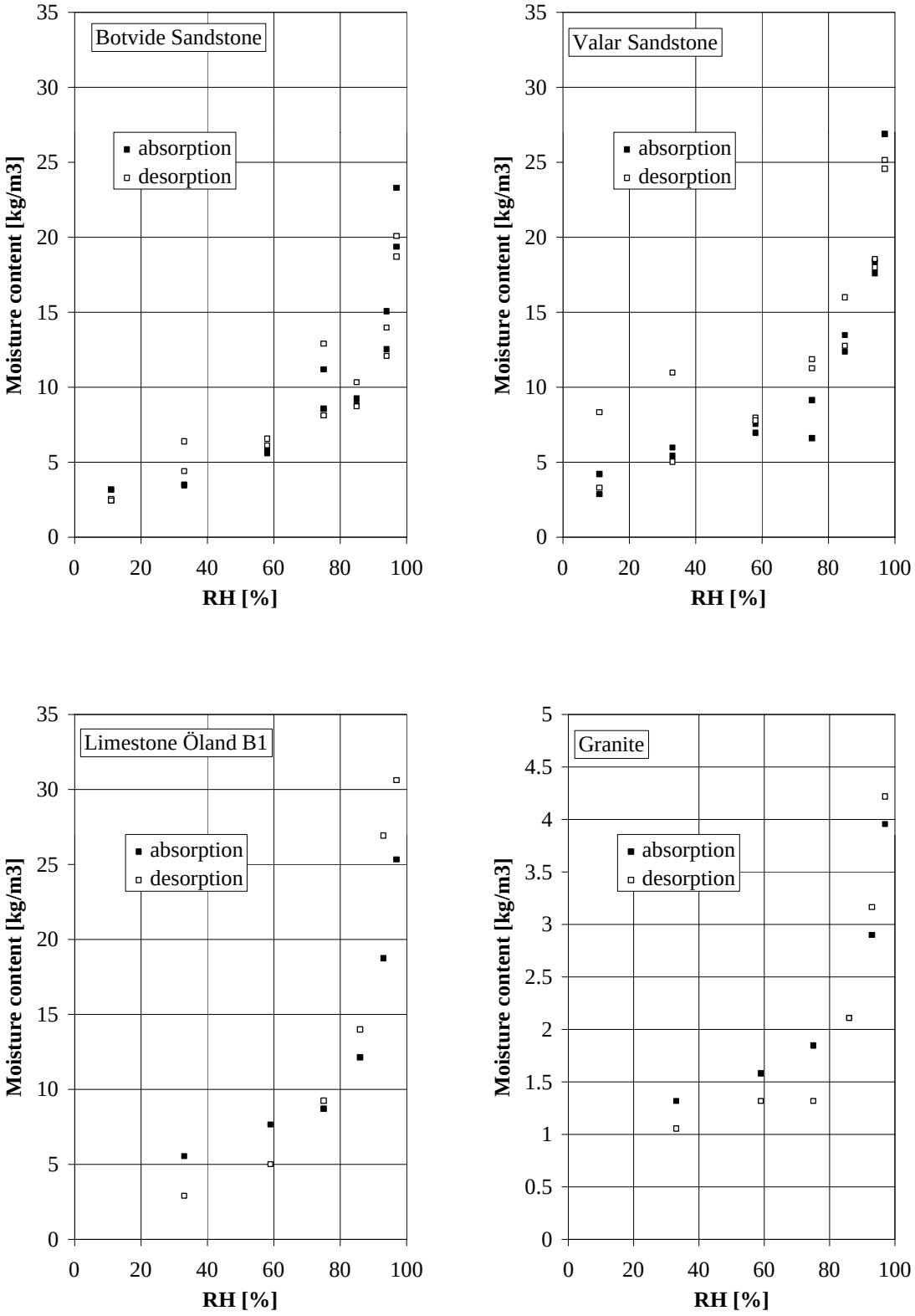

Figure C:1. Sorption isotherms for the Gotland sandstones Botvide and Valar, the limestone Öland B1 and the granite Bohus Red Bratteby. Note that the scale of the y-axis of the granite differs from the others.

Appendix D
Sorption enthalpies for a natural sandstone

by Lars Wadsö and Lubica Wessman

Extract from Wadsö, 1994

Introduction

Water vapour may be absorbed in materials by several different processes:

- Surface adsorption proportional to the internal surface area
- Capillary condensation in micropores
- 'Chemisorption' on hygroscopic binding sites.

These different processes are together responsible for the total sorption. A rock is composed of different minerals. Sorption of water vapour in a rock can take place on both the pure mineral grains (crystals) and in the boundaries between the grains. In this experiment the thermal power of the water vapour absorption on a rock sample was measured. Chemical action on rock (for example, by acid rain) would probably increase the internal surfaces and the number of micropores. In some rocks this would be the result of attack on the minerals, in other rocks it would be the grain boundaries that would be attacked.

Method

A sample of crushed rock was placed in the measuring cell of the sorption calorimeter. First dry nitrogen gas was passed through the calorimeter for a day or so, until a good baseline was established. Then the relative humidity (RH) of the gas was increased to 90%, and the heat of absorption was measured. Only one measurement was made.

Material

The sample used was 0.259 g of a calcite bound quartz sandstone (Valar, Gotland, Sweden). It had been crushed to pieces less than 1 mm in diameter. It has a high porosity (17.4% measured with a vacuum and water technique).

Result

Figure D:1 gives the heat of sorption curve for the sandstone.

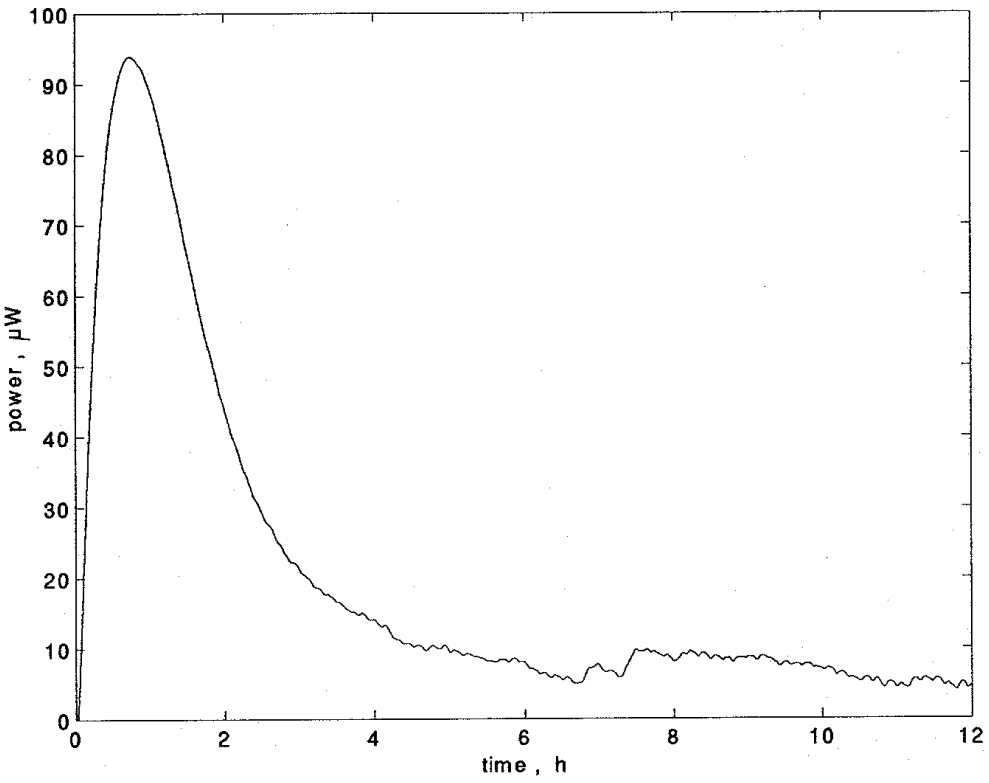

Figure D:1. The heat production of the water vapour sorption on a natural rock from 0% to 90% relative humidity. The measurement continued for another 65 h, but for unknown reasons it then became very 'noisy'. Only the part shown was used in the calculations.

Discussion

The experiment discussed was from a preliminary study with the aim of testing the method. Therefore, the accuracy of the result is not known. The heat released from the sandstone sample was 1.2 J. This corresponds to 4.6 J/g rock (the empty calorimeter gave a heat of 0.017 J for the same RH-interval). Assuming that the heat of sorption is equal to the heat of condensation (2440 kJ/kg water at 25 °C), the moisture content increase was 0.2% for the Valar sandstone (between 0 and 90% RH). We can see two practical applications of microcalorimetry in the study of deterioration of natural rocks. Firstly, sorption microcalorimetry may be a useful method for studying deterioration of rocks as the internal surface and the microporosity then probably will increase. Secondly, chemical reactions between minerals and pollutants can also be conveniently studied by microcalorimetry.

Appendix E
Results of capillary suction tests

When a slice with limited height of a porous material is placed with one surface in contact with water (Figure E:1.a), capillary transport of water will take place. When the mass of water per area of suction surface, m_s (kg/m^3), in the porous material is plotted against the square-root of time, the result in principle looks as in Figure E:1.b. The reason why m_s increases also after the knick-point is reached, is that the pores are further filled with water when air in enclosed bubbles, contained in pores bigger than about 1 μm, is dissolved (Fagerlund, 1994b).

The results from the capillary suction tests are expressed as degree of saturation, *S*, versus the square root of time. This makes it possible to compare the moisture content directly with the dilatation tests (Chapter 3.7) and the 'S_{crit}-tests' (Chapter 3.8). Note, however, that *S*-values for suction times lower than t_k are fictitious since *S* is based on the total pore volume in the specimen and only a fraction of the specimen is penetrated by moisture. Therefore, for the wet part of the specimen, *S* is just as high as S_k or even higher because of the dissolution of air in the pores.

Capillary suction is treated in more detail in Chapter 3.5.1.

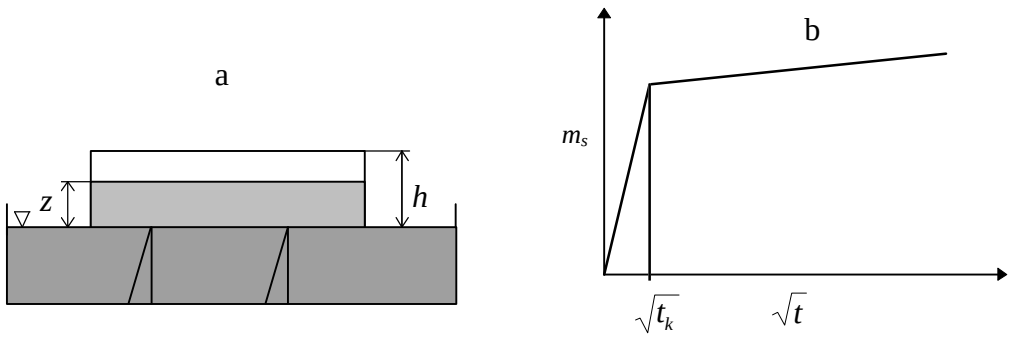

Figure E:1. a) Principle of capillary suction test. b) The result is presented as water sorption as a function of the square-root of time.

Some of the values of *S* exceed 1, which must either mean that the weighing of the specimens was not accurate, or that there is actually more water in the pore system after capillary suction than after vacuum saturation. For the granite this is at least partly explained by the approximate calculation of the degree of saturation, see Chapter 3.5.1.

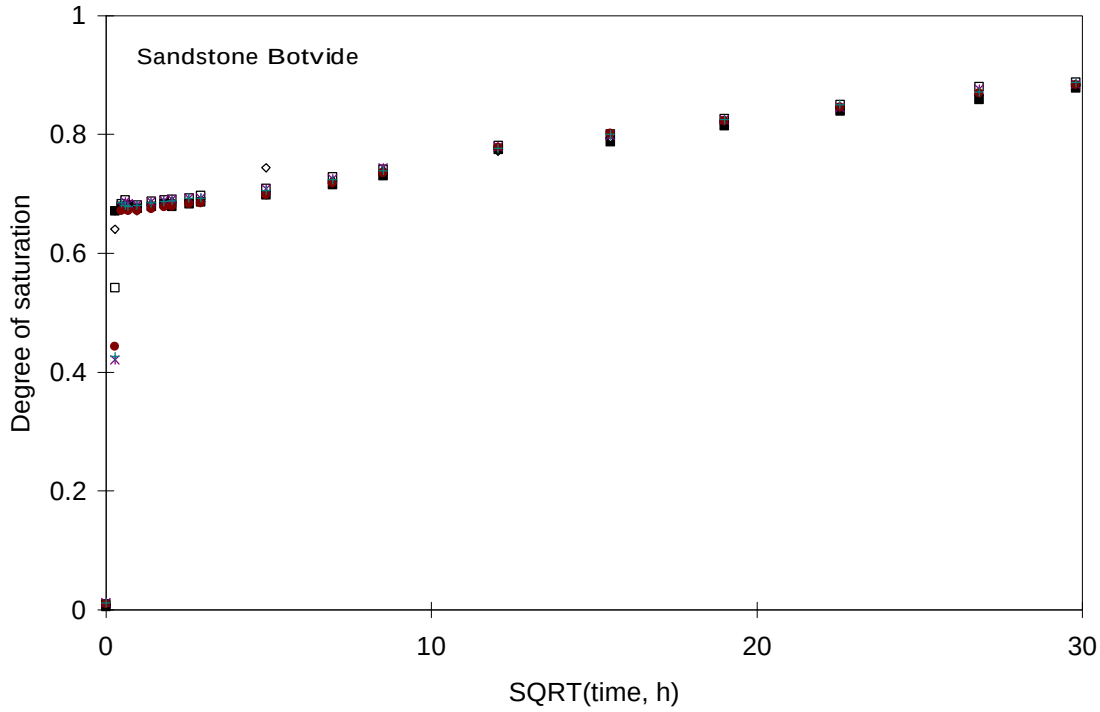

Figure E:2. Result from capillary suction test of the sandstone Botvide.

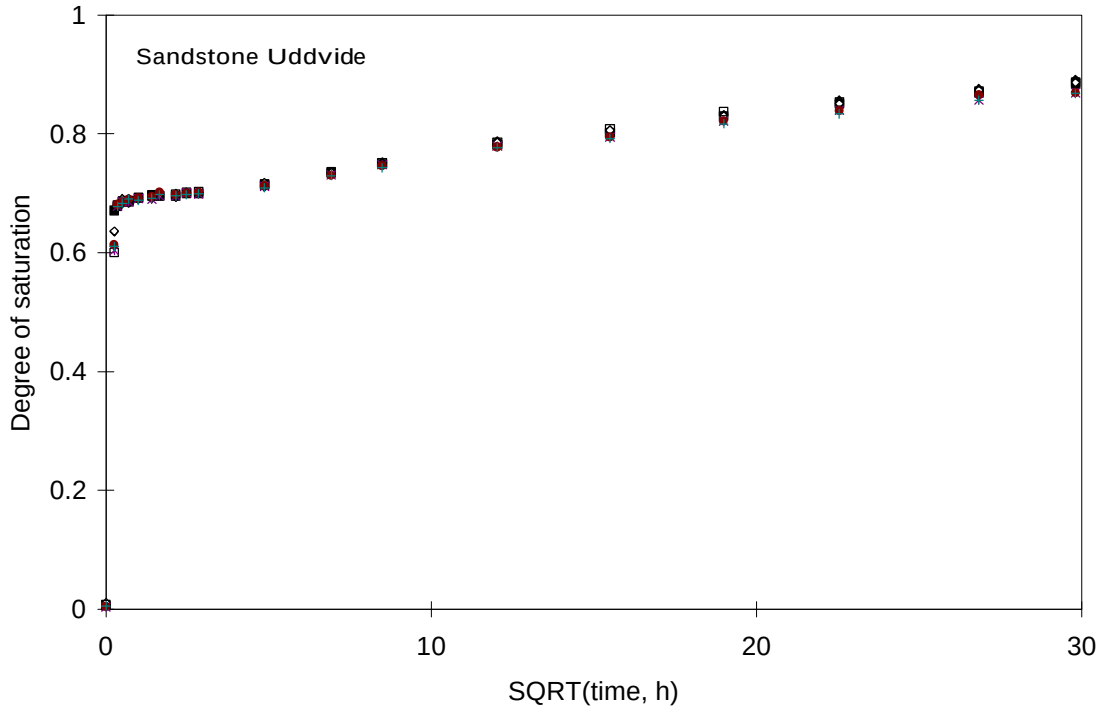

Figure E:3. Result from capillary suction test of the sandstone Uddvide.

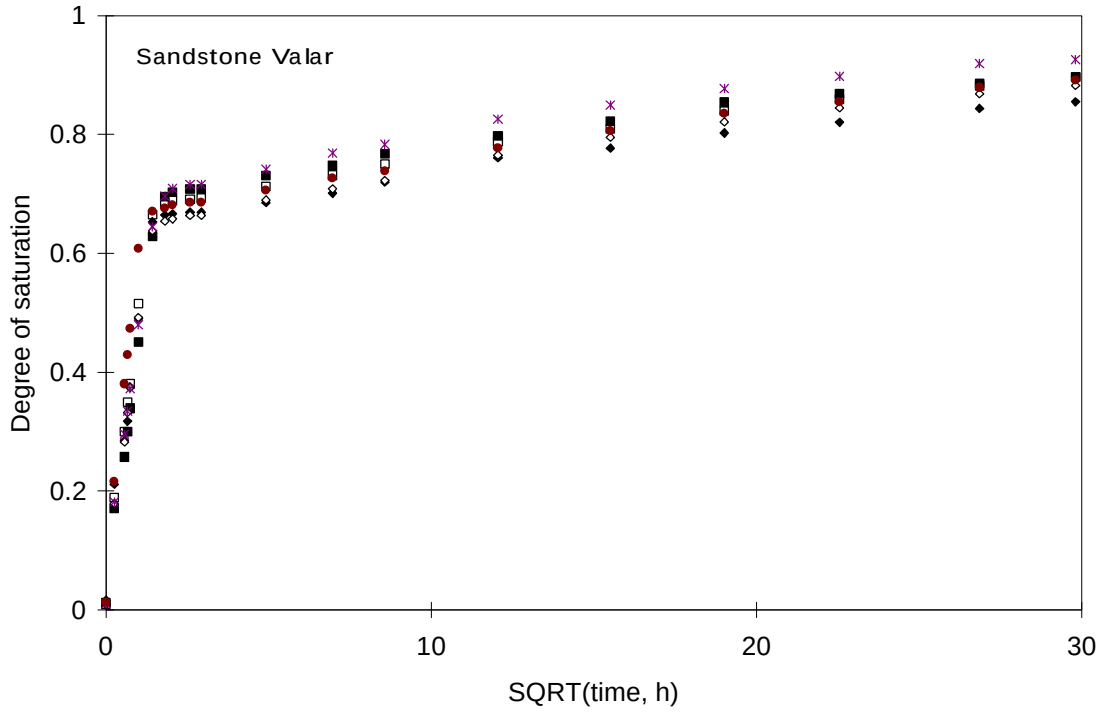

Figure E:4. Result from capillary suction test of the sandstone Valar.

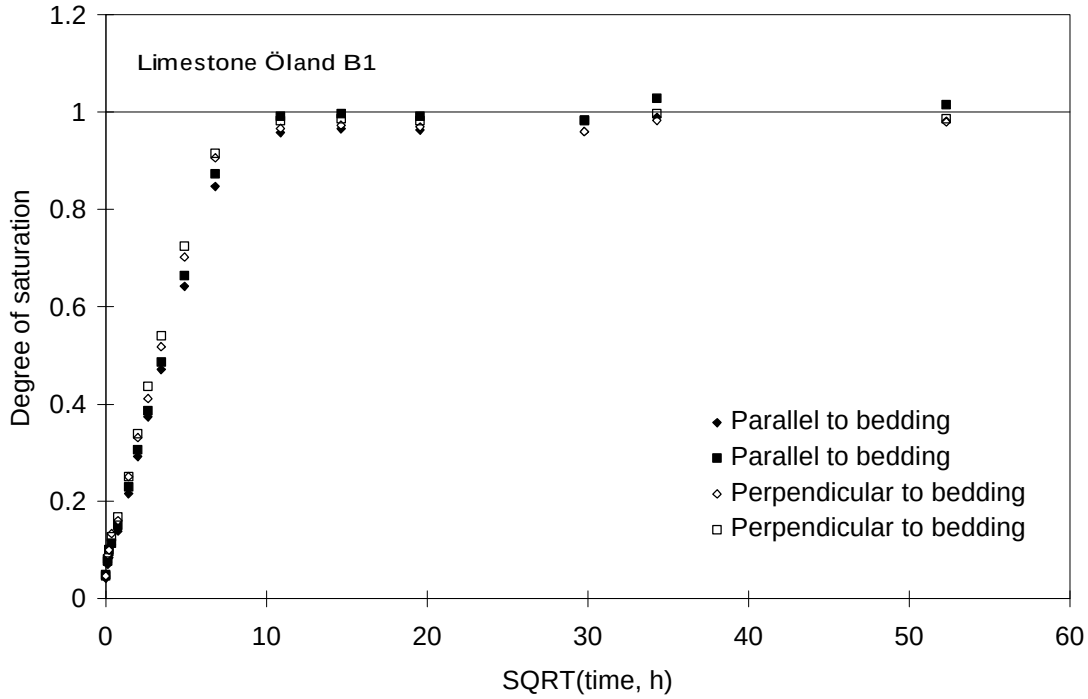

Figure E:5. Result from capillary suction test of the limestone Öland B1.

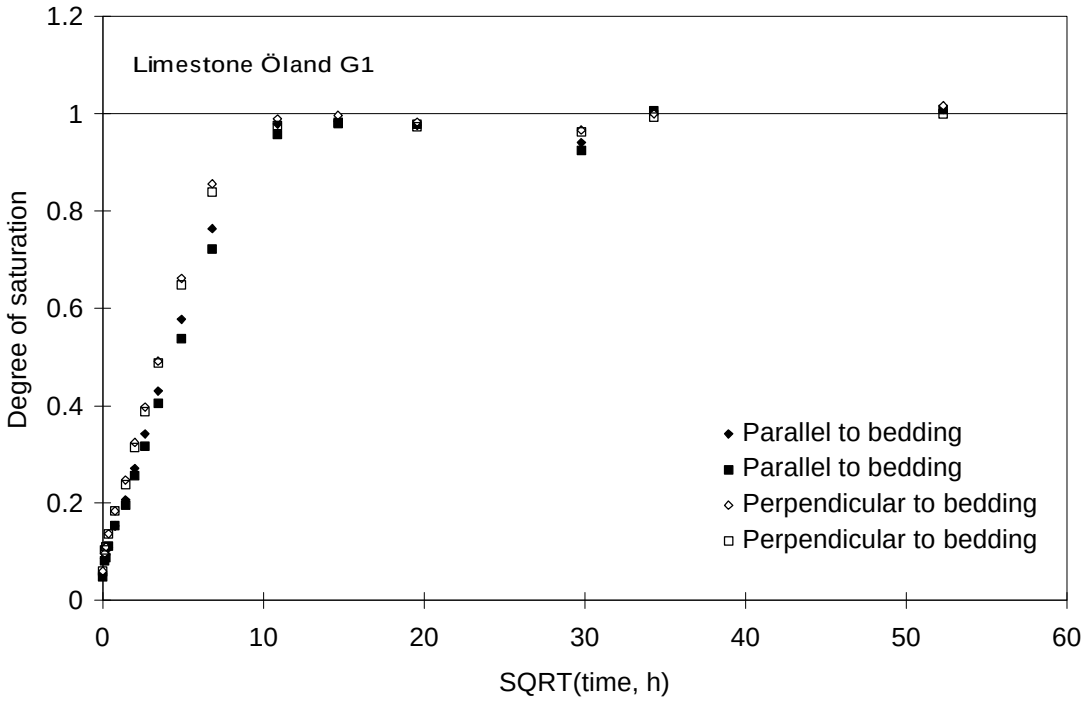

Figure E:6. Result from capillary suction test of the limestone Öland G1.

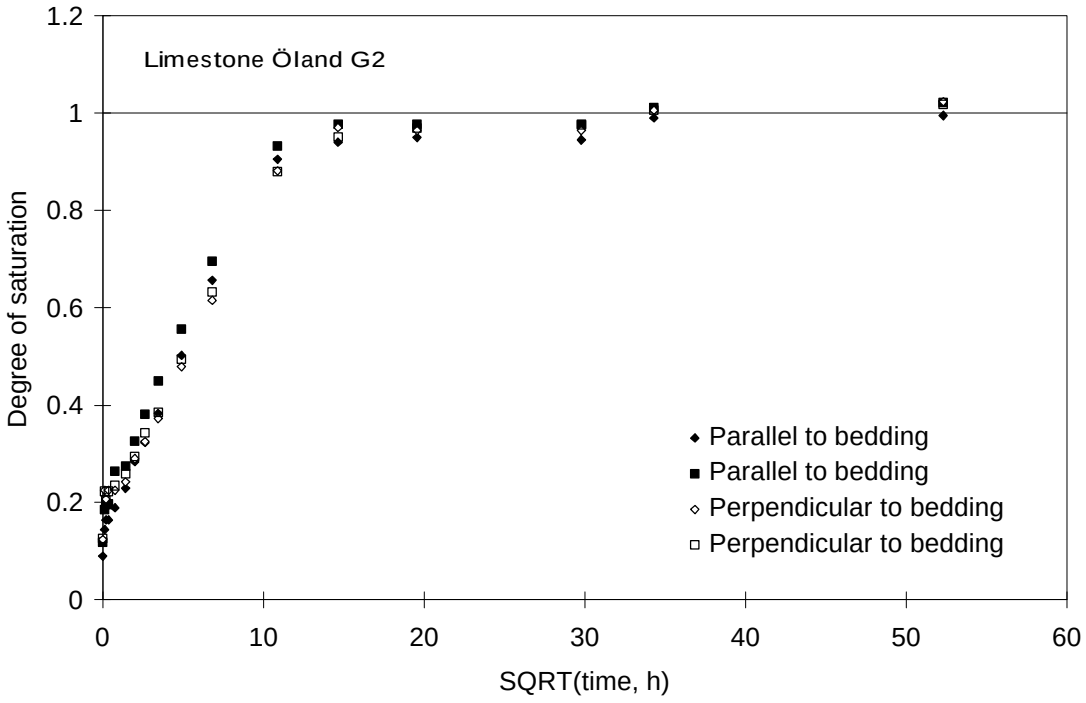

Figure E:7. Result from capillary suction test of the limestone Öland G1.

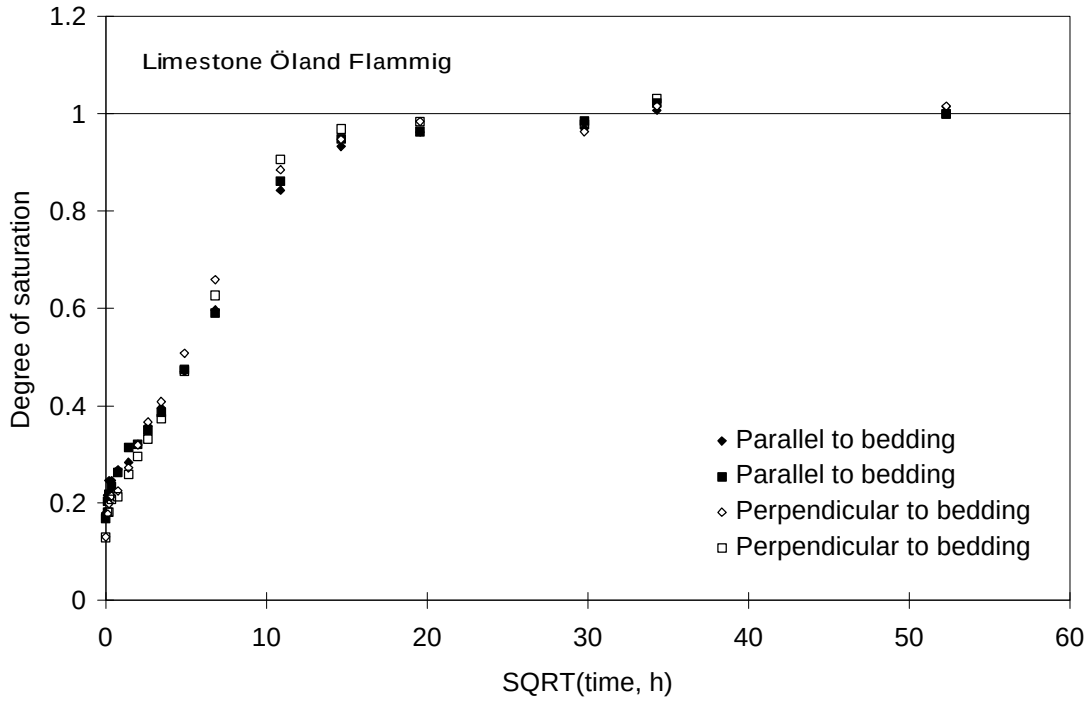

Figure E:8. Result from capillary suction test of the limestone Öland Flammig.

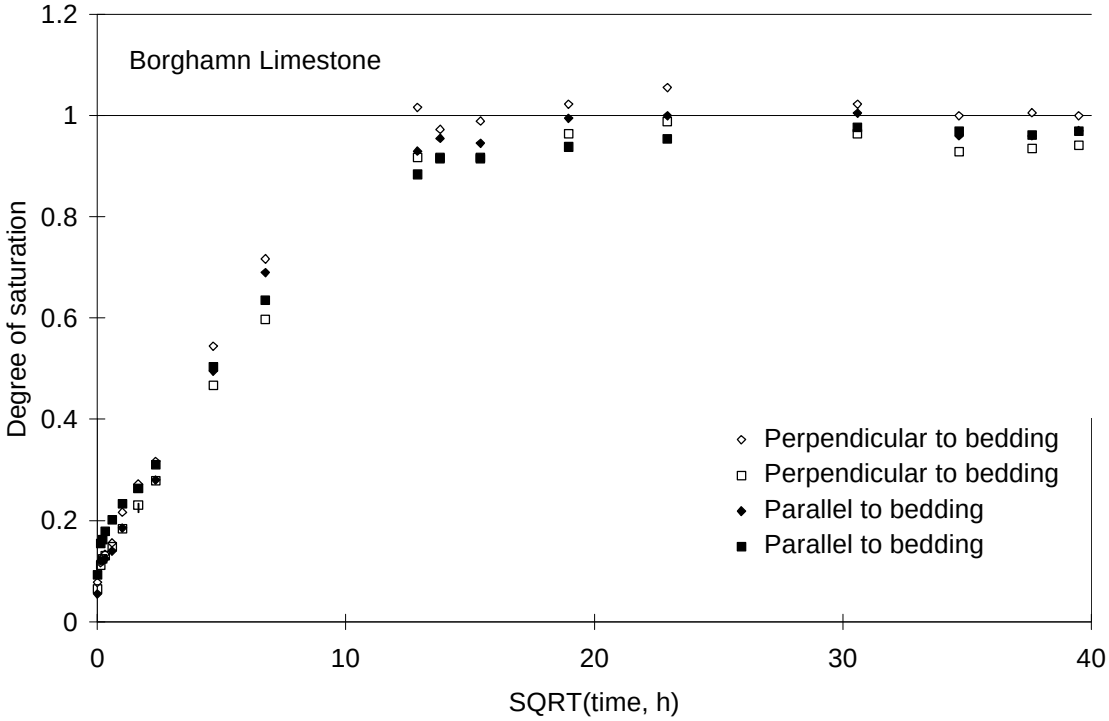

Figure E:9. Result from capillary suction test of the Borghamn limestone.

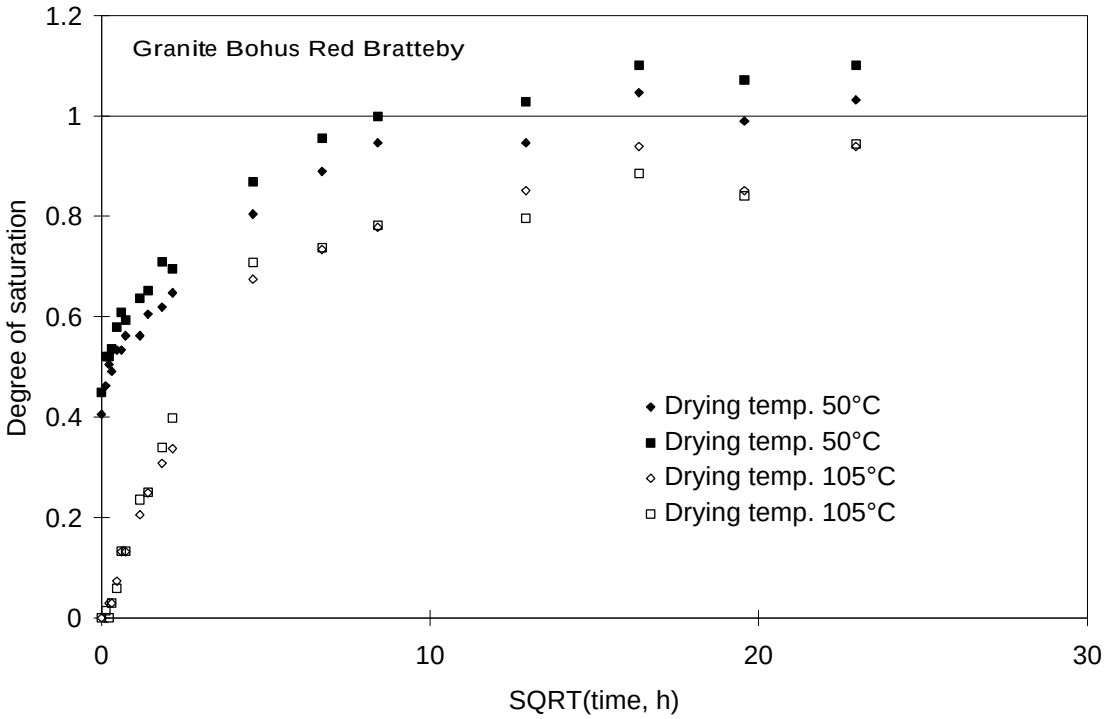

Figure E:10. Result from capillary suction test of the granite Bohus Red Bratteby.

Appendix F
Kirchhoff potential and moisture permeability

The moisture flow through a porous material can be described by:

$$q = -D_\varphi \frac{\partial \varphi}{\partial x} \qquad \text{(F:1)}$$

where

q is the moisture flow (kg/m^{2}s);

D_φ is the coefficient of moisture transport (various units, depending on φ);

φ is the moisture state. When the conditions are isothermal, φ can be the mass of water per volume of material (w [kg/m^3]), the mass of water per mass of material (u [kg/kg]), the relative humidity (φ [%]), the partial pressure (p [Pa]) or the humidity by volume of air (v [kg/m^3]) (Arfvidsson, J. 1994).

x is the distance of flow (m).

When φ is the humidity by volume of air, D_φ is the moisture permeability, written δ_v.

The moisture flow can also be expressed in terms of the Kirchhoff potential, ψ.

$$\psi = \int D_\varphi \, \partial \varphi \qquad \text{(F:2)}$$

$$q = -\frac{\partial \psi}{\partial x} \qquad \text{(F:3)}$$

The graphs here show the results from the cup method in terms of the Kirchhoff-potential ψ and the moisture permeability δ_v versus the relative humidity (RH) inside the cup. Results are given for the sandstones Uddvide and Valar, for the granite and the limestone Öland B1. The outer RH was 35% and the temperature was 20°C. The graph showing δ_v versus RH is the derivative of the graph showing ψ versus RH (Hedenblad, 1996).

The experimental method is described in more detail in Chapter 3.5.2.

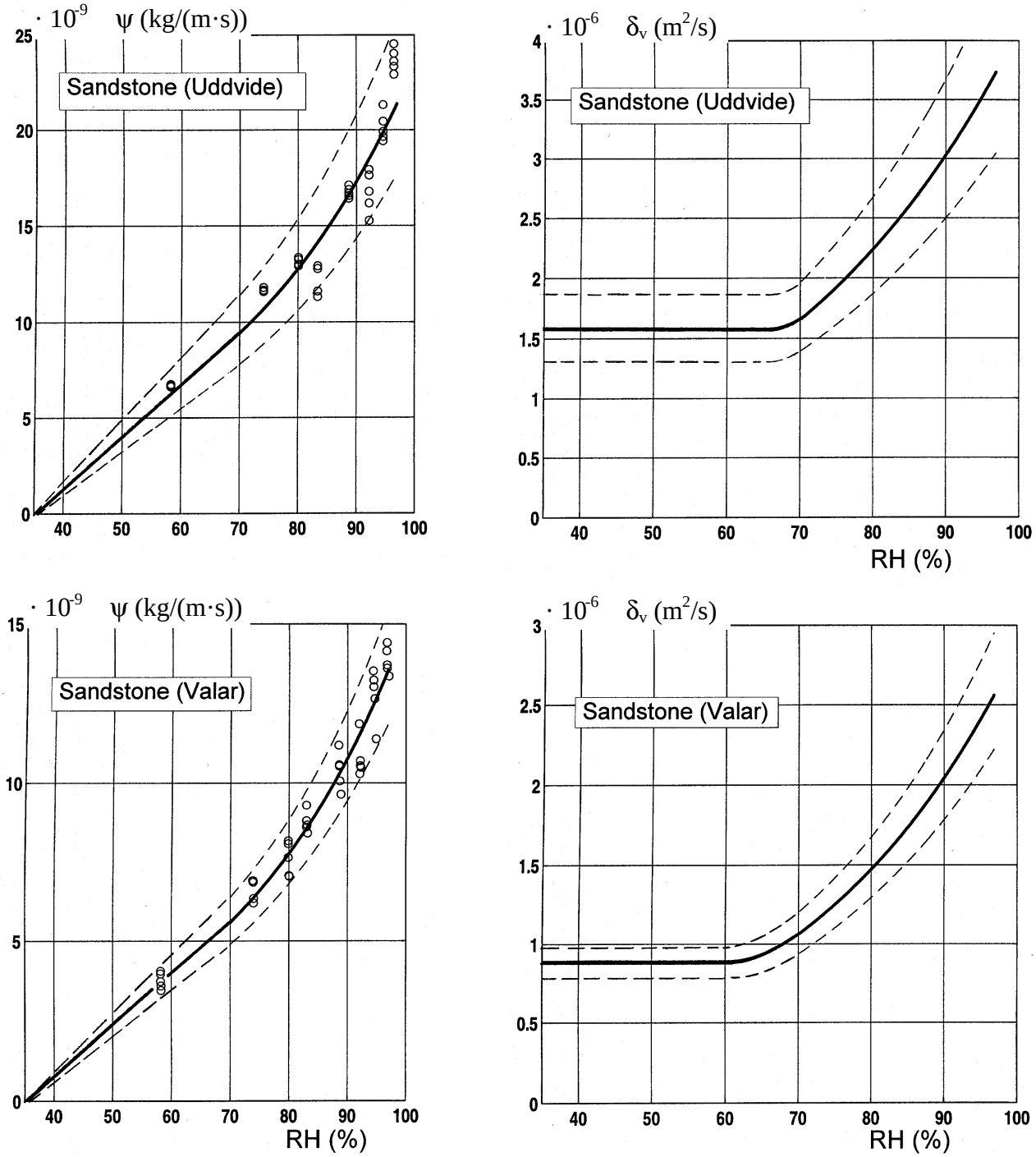

Figure F:1. The Kirchhoff potential ψ *and the moisture diffusivity* δ_v *versus the relative humidity* RH *for the sandstones Uddvide and Valar.*

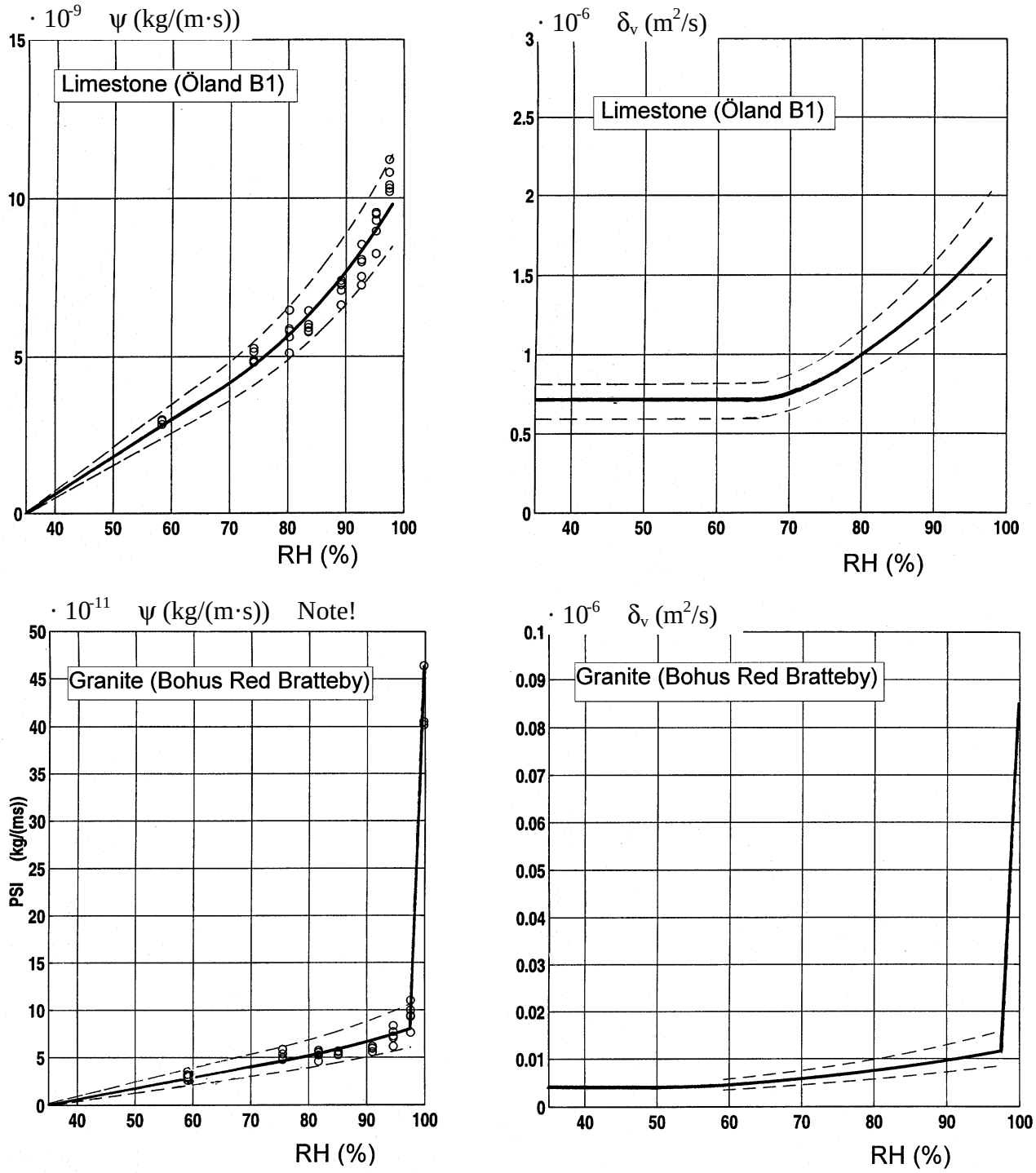

Figure F:2. The Kirchhoff potential ψ *and the moisture diffusivity* δ_v *versus the relative humidity* RH *for the Limestone Öland B1 and the granite Bohus Red Bratteby.*

Appendix G
Dynamic modulus of elasticity

Measuring the dynamic modulus of elasticity is a non-destructive method which indicates the loss of cohesion of the specimen, for example, because of formation of microcracks. The dynamic modulus of elasticity *E* can be calculated from the fundamental frequency of transverse vibration and the dimensions of the specimen:

$$E = \frac{f^2 \cdot m \cdot l^3 \cdot T}{I \cdot C^2} \qquad \text{(G:1)}$$

where

E is the dynamic modulus of elasticity (Pa);

f is the fundamental frequency of transverse vibration (Hz);

m is the mass (kg);

l is the length (m);

T is a correction factor, depending on the dimensions of the specimen and Poisson's ratio of the material. When Poisson's ratio is 0.17, which is a plausible value for stone, and the dimensions are 30 × 30 × 120 mm, T is 1.38. When the dimensions are 20 × 20 × 150, T is 1.13 (ASTM C 215 - 85).

C is a constant, which depends on the mode of vibration. At the fundamental tone *C* is 3.56.

I is the moment of inertia (m^4), calculated by

$$I = \frac{bh^3}{12} \qquad \text{(G:2)}$$

where *b* is the width of the rectangular specimen and *h* is its height. In this case *b* = *h* = 30 mm.

The fundamental frequency of transverse vibration was measured with the equipment shown on the photograph in Figure G:1. The specimen is brought to oscillate by an oscillator applied to the centre of the specimen. The vibrations of the specimen are recorded by an accelerometer, which is applied to the specimen with a rubber band. The signal from the accelerometer is analysed in the spectrum analyser and the frequency of the fundamental tone can thus be detected.

E_n is the dynamic E-modulus after the freeze-thaw test and E_0 is the dynamic E-modulus before the freeze-thaw test. In this report E_n / E_0 is calculated as f_n^2 / f_0^2 multiplied by a correction factor *CF*, which takes care of the change of the mass and of the geometry of the specimen caused by surface scaling.

$$CF = \frac{(l-2y)^3 \cdot b^4 \cdot Q_n}{(b-2y)^4 \cdot l^3 \cdot Q_0} \qquad \text{(G:3)}$$

where Q_n and Q_0 are the specimen weights after and before the freeze-thaw test respectively. y is the corrosion depth provided the scaling is evenly distributed all over the specimen prism.

$$y = \frac{Q_{ds}}{\rho_b \cdot 0.0162} \qquad \text{(G:4)}$$

where

Q_{ds} is the dry weight of scaled-off material (kg);
ρ_b is the bulk density (kg/m^3);

0.0162 is the external surface area of a prism with the dimensions 30 × 30 × 120 mm.

CF is mostly close to 1, unless the scaling is very severe.

T in equation G:1 above is supposed to be constant, that is, it is not supposed to be changed by scaling. This is an oversimplification, since Poisson's ration is probably changed when the material is changed internally.

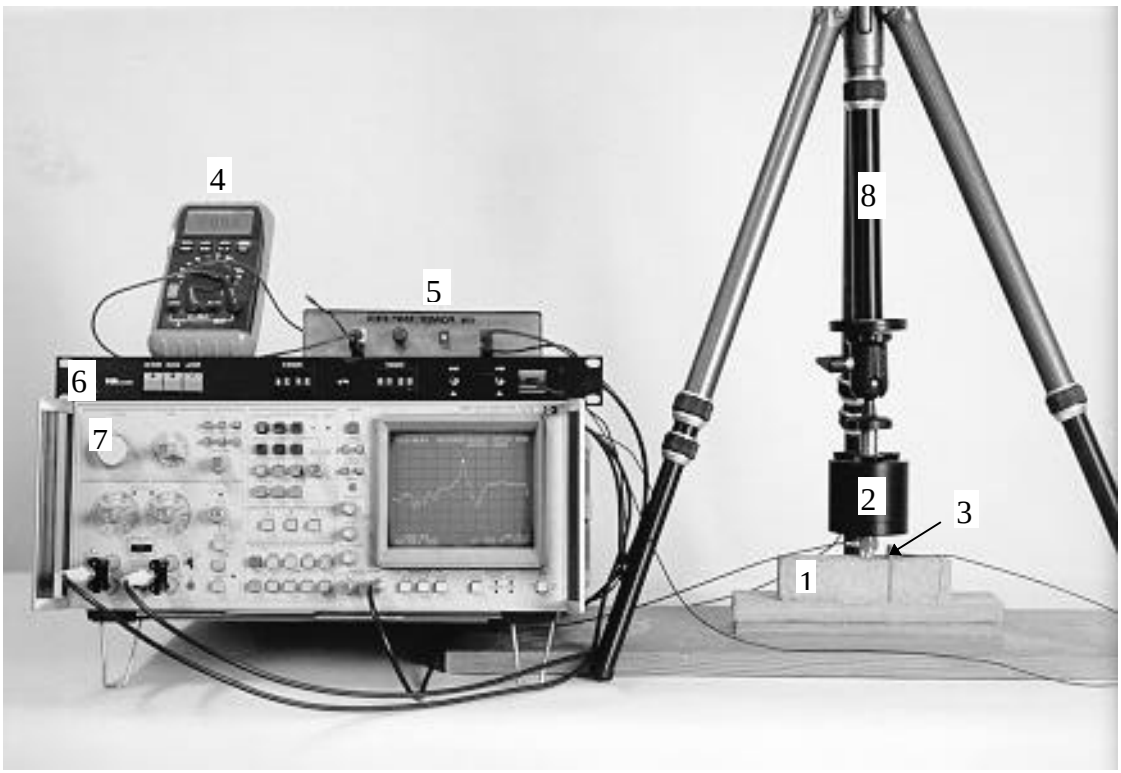

Figure G:1. Equipment to measure the fundamental frequency of transverse vibration.
1) Specimen. 2) Vibrator 3) Accelerometer. 4) Ammeter to avoid overloading of the vibrator. 5) Amplifier to adjust the signal to the vibrator. 6) Amplifier for amplification of the signal from the accelerometer. 7) Spectrum analyser. 8) Adjustable stand.

Appendix H
Freeze-thaw cycles in the scaling tests

In this appendix the freeze-thaw cycles for the scaling tests presented in Chapter 3.6 are shown. Thermocouples were placed in drilled holes in the centre of dummy specimens. The cycle was changed a couple of times in test series 1 with sandstone tested in NaCl. This was a mistake due to initial problems with the temperature control function. The cycles in test series 3 with sandstone tested in NaCl, in the test with granite, and in the test with different internal and external concentrations are practically the same.

The fact that thermocouples in different stones do not record exactly the same temperature cycle can be because the stones do not have the same thermal properties, such as heat conductivity and heat capacity. A difference in the amount of the surrounding solution and the placing of the thermocouple also might affect the temperature curve.

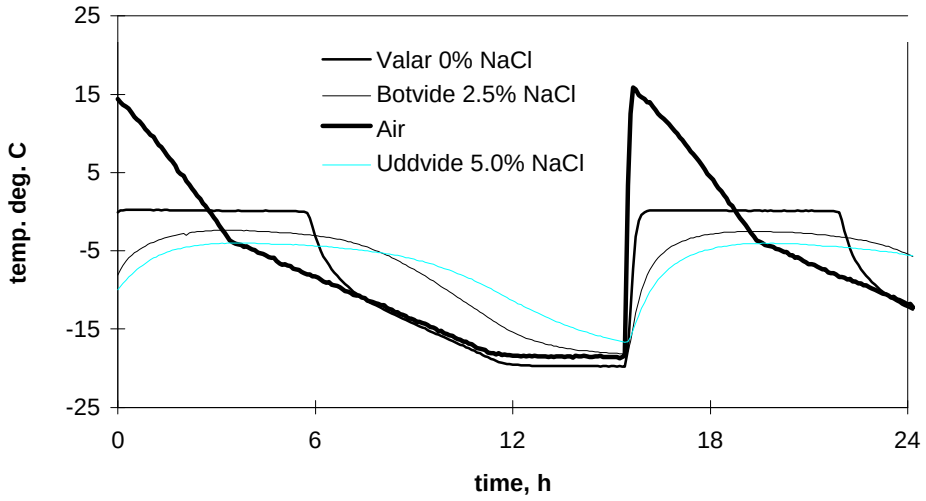

Figure H:1. Freeze-thaw cycles 1-3 in scaling test 1.

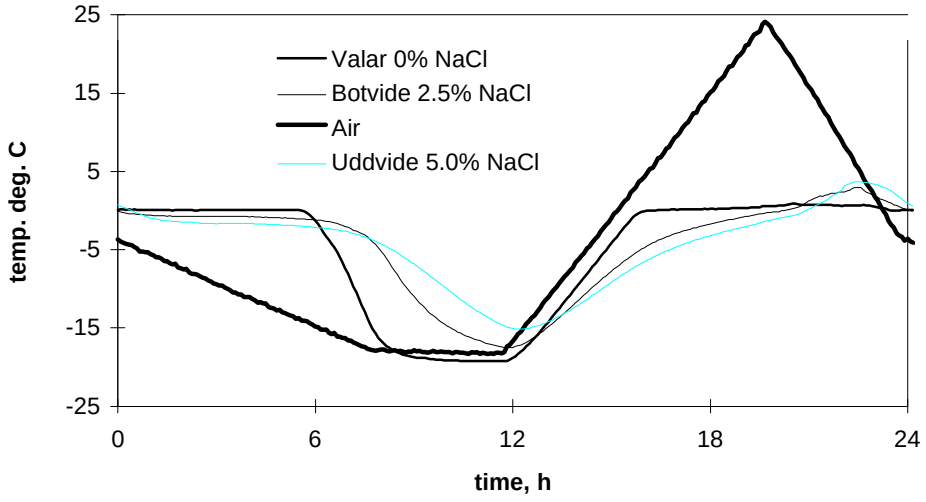

Figure H:2. Freeze-thaw cycles 4-10 in scaling test 1.

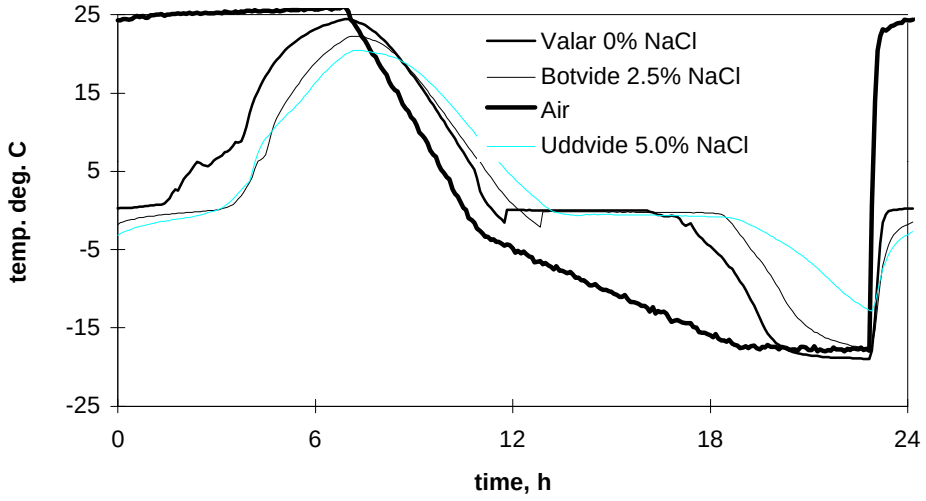

Figure H:3. Freeze-thaw cycles 11-20 in scaling test 1.

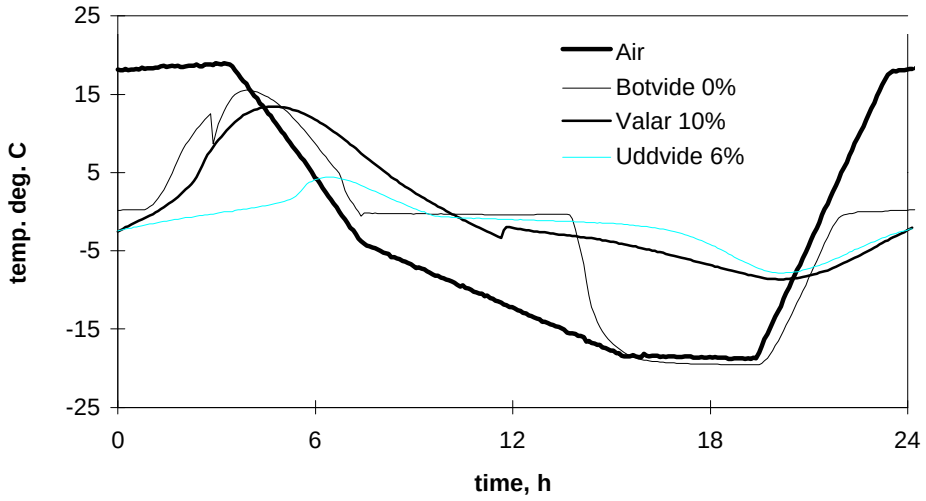

Figure H:4. Freeze-thaw cycle in scaling test 2. The total number of cycles was 7.

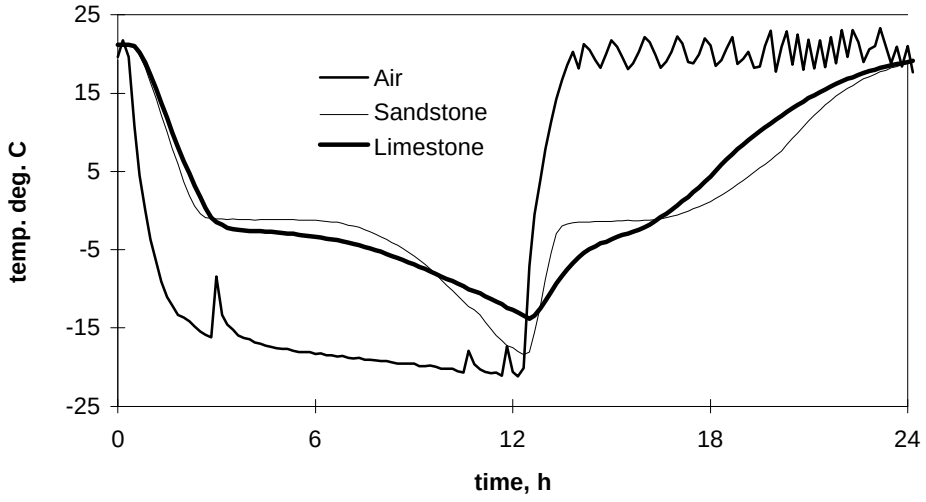

Figure H:5. Freeze-thaw cycle in scaling test 3. The total number of cycles was 20.

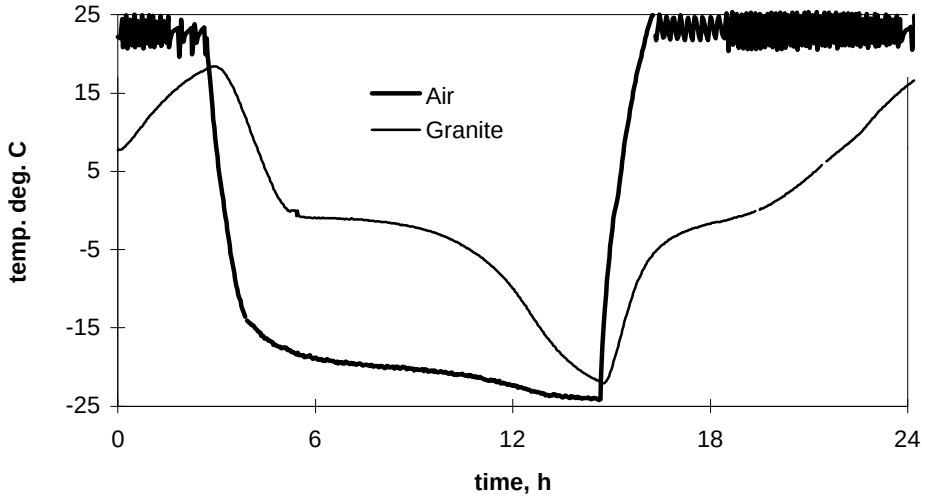

Figure H:6. Freeze-thaw cycle in freeze-thaw test of granite.
The total number of cycles was 35.

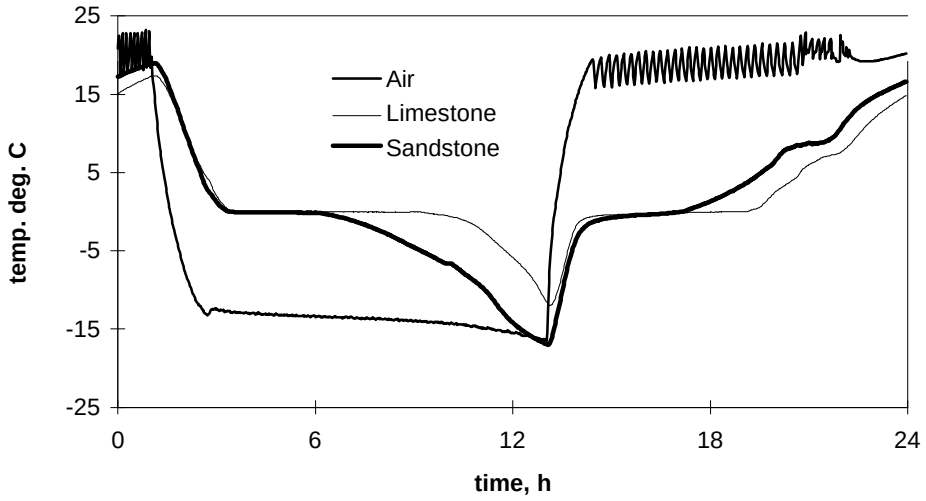

Figure H:7. Freeze-thaw cycle in freeze-thaw test with different initial internal and external salt concentrations.

Appendix I
Photographs of specimens exposed to scaling test

The photographs show damaged stone prisms after terminated scaling test. During the test all prisms were placed in standing position as in the photograph. They were completely submerged in salt solutions of various concentrations. Note that the scalings are unevenly distributed and that for the sandstones the most severe scalings occur on the upper part while on the limestones they occur on the lower part. The reason behind this is not clarified. Possibly it is due to a gradual separation of the solution so that a higher concentration occurs at the bottom. It might be that the limestone, like concrete, is most sensitive to a somewhat stronger solution and sandstone to a weaker solution.

The tests are described in more detail in Chapter 3.6.

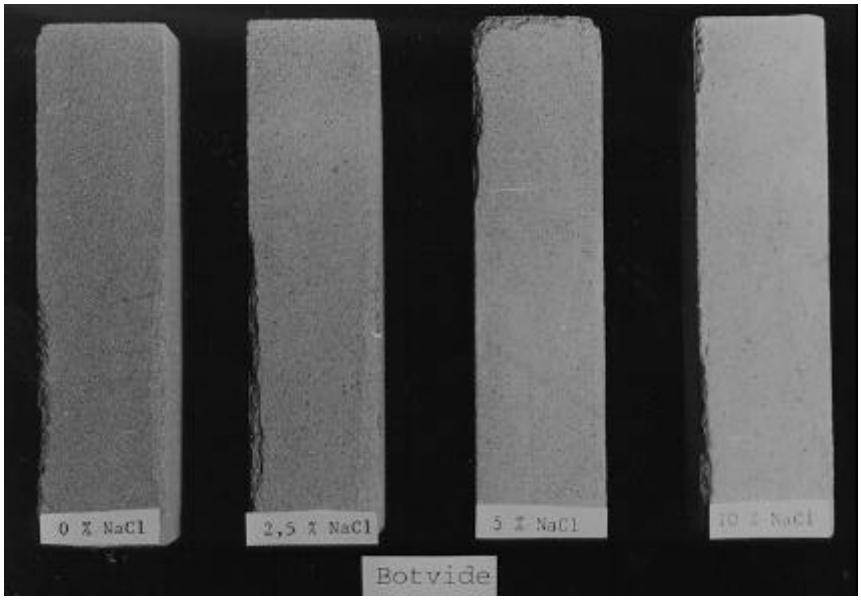

Figure I:1. Prisms of the sandstone Botvide after freeze-thaw test 1 (20 cycles). The solutions used were, from left to right, 0%, 2.5%, 5% and 10% NaCl.

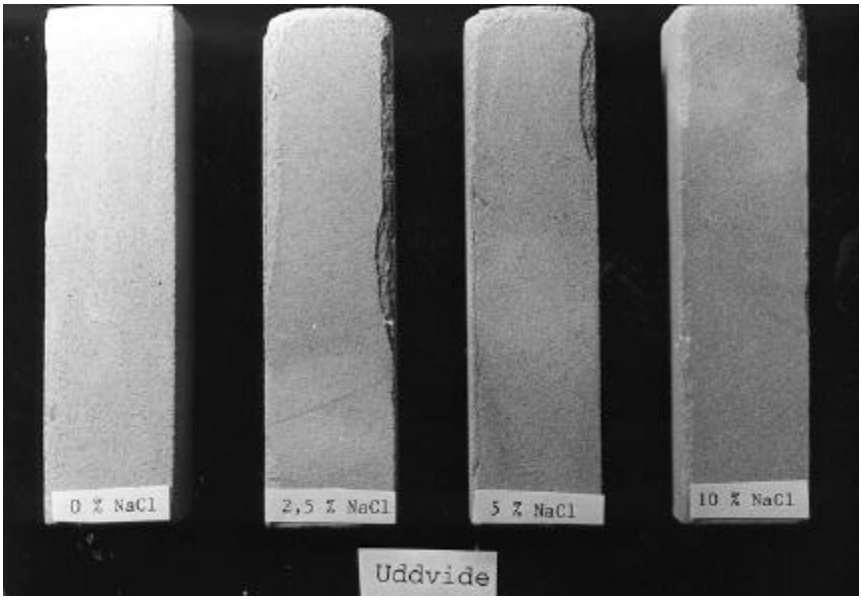

Figure I:2. Prisms of the sandstone Uddvide after freeze-thaw test 1 (20 cycles). The solutions used were, from left to right, 0%, 2.5%, 5% and 10% NaCl.

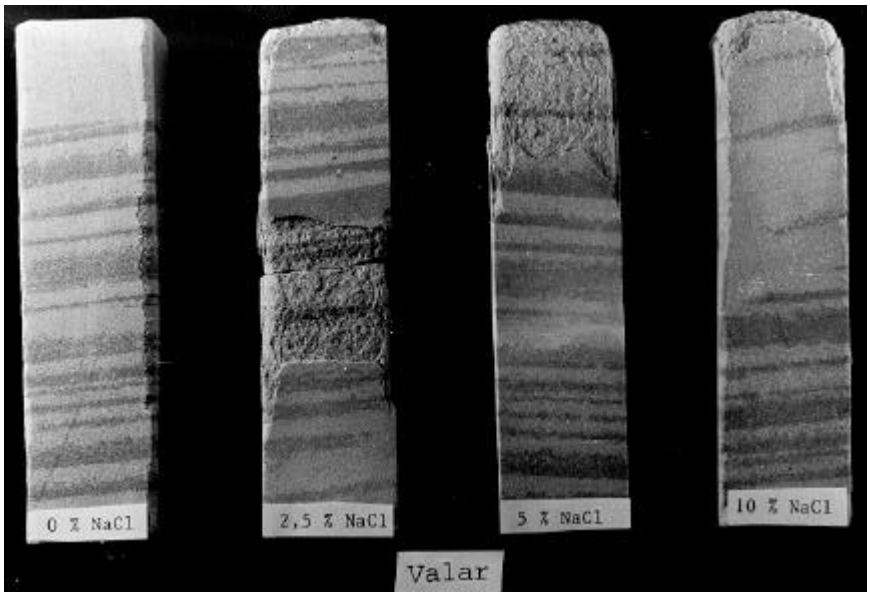

Figure I:3. Prisms of the sandstone Valar after freeze-thaw test 1 (20 cycles). The solutions used were, from left to right, 0%, 2.5%, 5% and 10% NaCl. Darker, clay-mineral-rich lines parallel to the bedding are visible. Scalings are visible on the stones freeze-thaw-tested in salt solution. (The stone in 2.5% NaCl was broken into two pieces when handled after the test.)

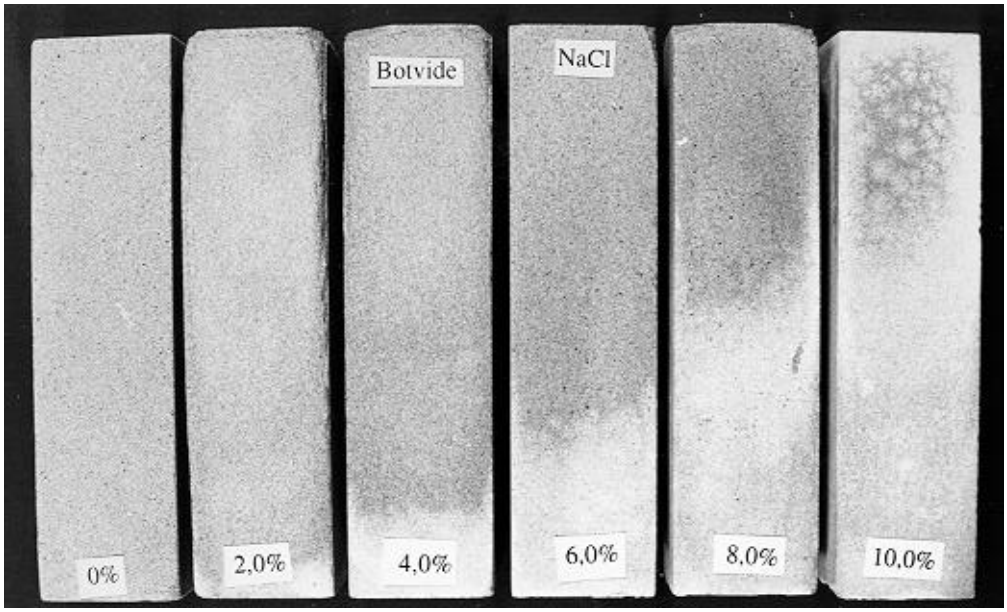

Figure I:4. Prisms of the sandstone Botvide after freeze-thaw test 2 (7 cycles). The solutions used were, from left to right, 0%, 2%, 4%, 6%, 8% and 10% NaCl. The white salt efflorescences occurred during final drying in standing position.

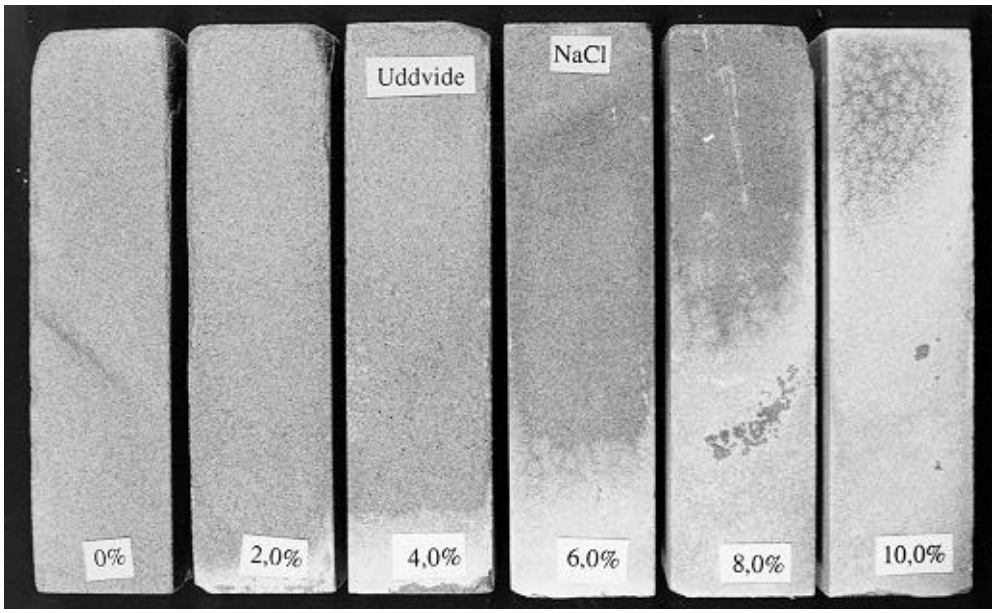

Figure I:5. Prisms of the sandstone Uddvide after freeze-thaw test 2 (7 cycles). The solutions used were, from left to right, 0%, 2%, 4%, 6%, 8% and 10% NaCl. The white salt efflorescences occurred during final drying in standing position.

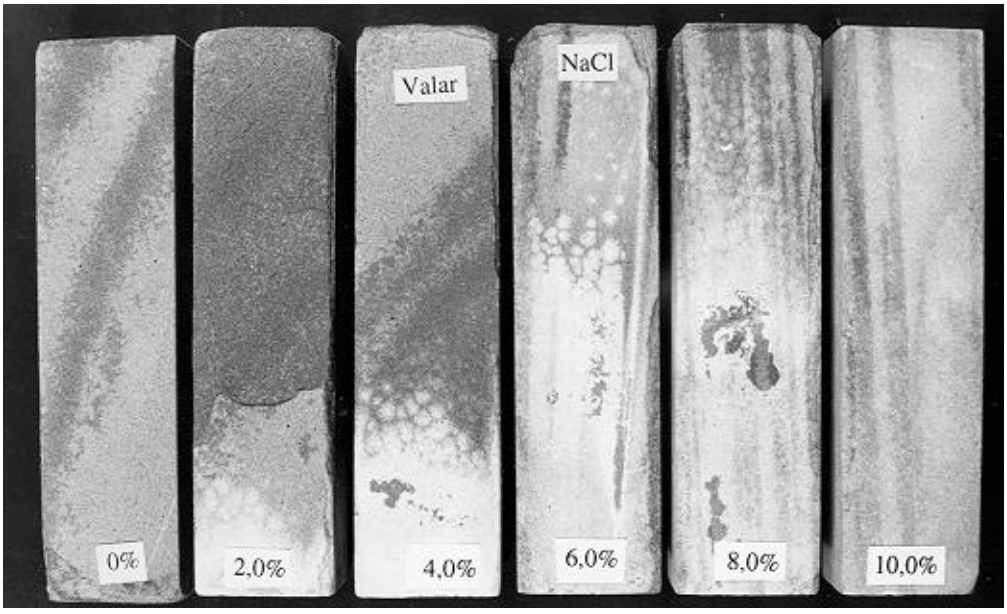

Figure I:6. Prisms of the sandstone Valar after freeze-thaw test 2 (7 cycles). The solutions used were, from left to right, 0%, 2%, 4%, 6%, 8% and 10% NaCl. The white salt efflorescences occurred during final drying in standing position. Darker, clay-mineral-rich lines parallel to the bedding are visible. Scaling is visible mainly on the stone freeze-thaw-tested in 2% salt solution.

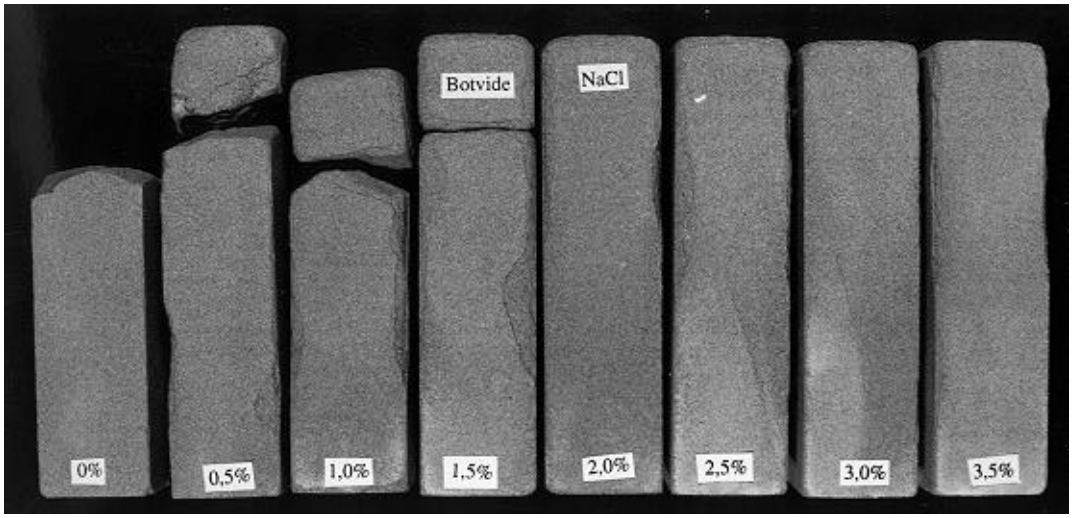

Figure I:7. Prisms of the sandstone Botvide after freeze-thaw test 3 (20 cycles). The solutions used were, from left to right, 0%, 0.5%, 1%, 1.5%, 2%, 2.5%, 3% and 3.5% NaCl. The piece that fell off the specimen freeze-thaw-tested in pure water was completely crumbled.

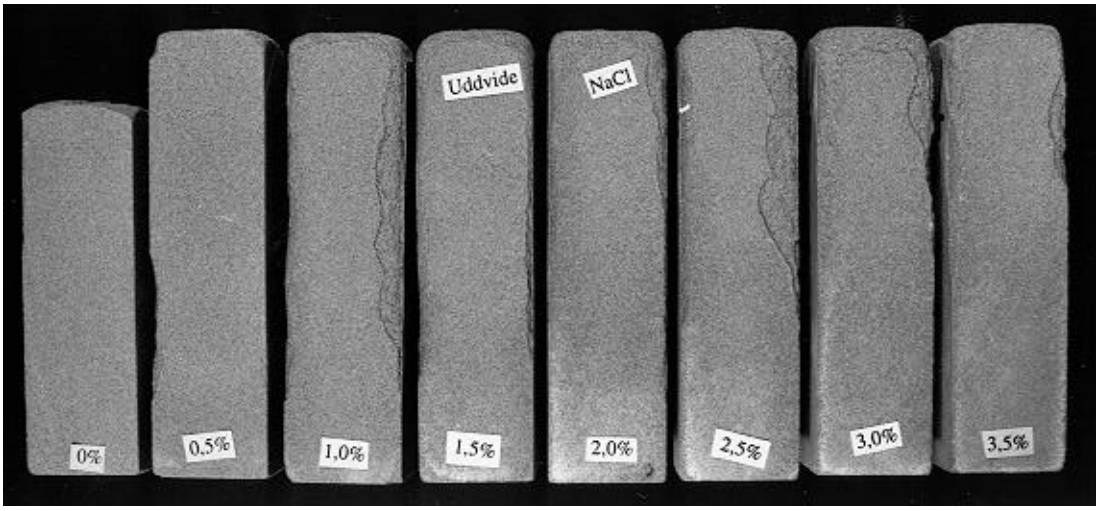

Figure I:8. Prisms of the sandstone Uddvide after freeze-thaw test 3 (20 cycles). The solutions used were, from left to right, 0%, 0.5%, 1%, 1.5%, 2%, 2.5%, 3% and 3.5% NaCl. The piece that fell from the specimen freeze-thaw-tested in pure water was completely crumbled.

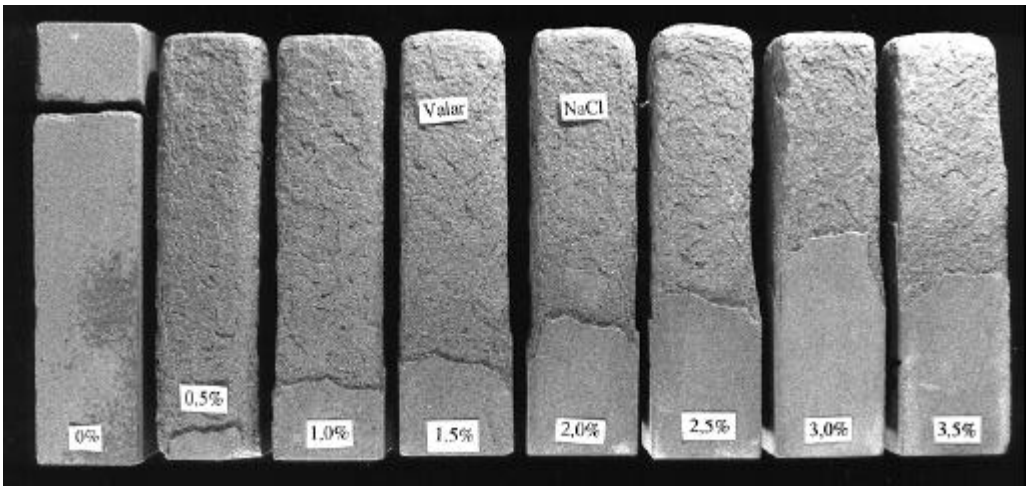

Figure I:9. Prisms of the sandstone Valar after freeze-thaw test 3 (20 cycles). The solutions used were, from left to right, 0%, 0.5%, 1%, 1.5%, 2%, 2.5%, 3% and 3.5% NaCl.

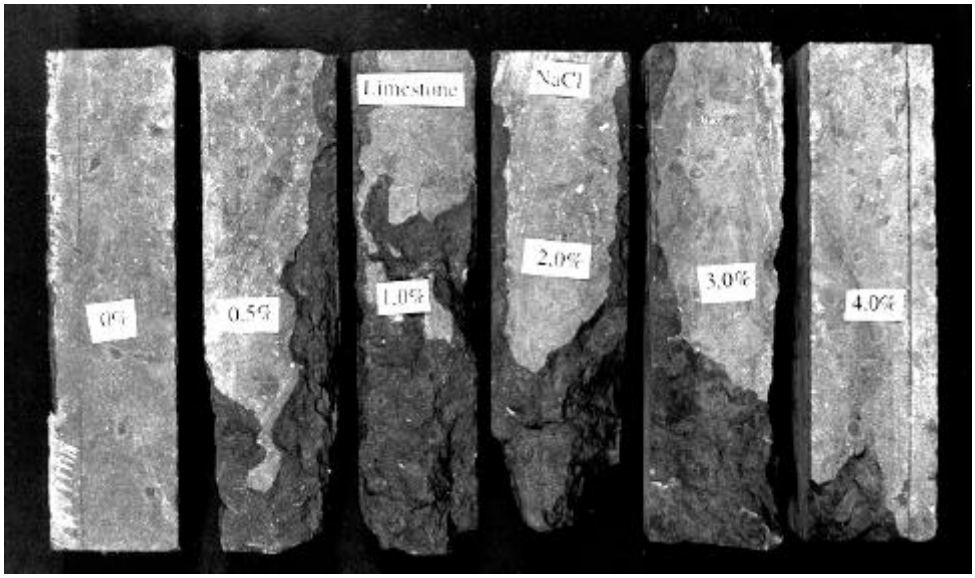

Figure I:10. Prisms of Limestone Öland B1 after freeze-thaw test (4 cycles). The solutions used were, from left to right, 0%, 0.5%, 1%, 2%, 3% and 4% NaCl.

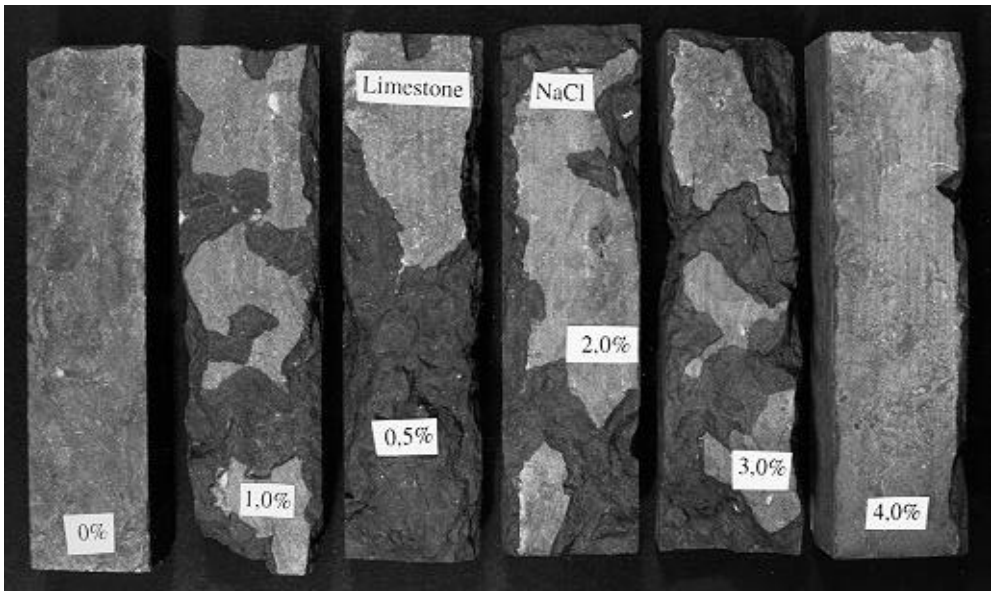

Figure I:11. Prisms of Limestone Öland B1 after freeze-thaw test (4 cycles). The solutions used were, from left to right, 0%, 0.5%, 1%, 2%, 3% and 4% NaCl.

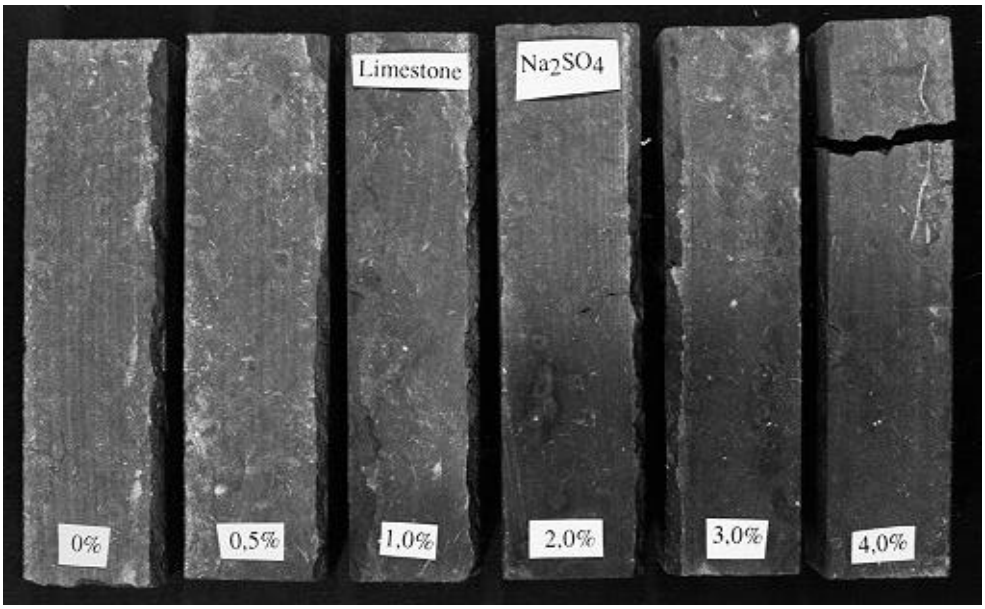

Figure I:12. Prisms of Limestone Öland B1 after freeze-thaw test (20 cycles). The solutions used were, from left to right, 0%, 0.5%, 1%, 2%, 3% and 4% Na_2SO_4×10 H_2O.

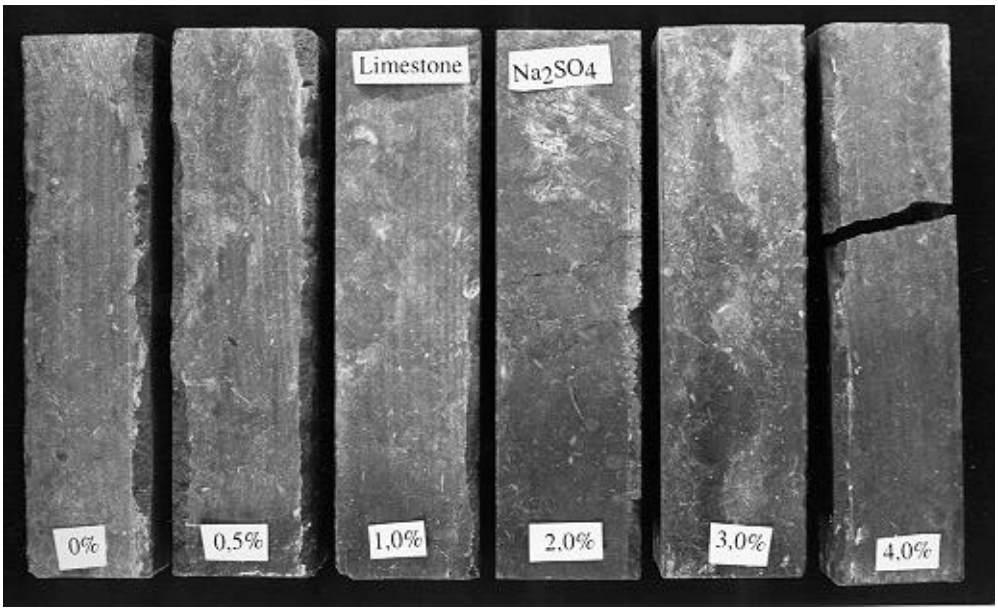

Figure I:13. Prisms of Limestone Öland B1 after freeze-thaw test (20 cycles). The solutions used were, from left to right, 0%, 0.5%, 1%, 2%, 3% and 4% Na_2SO_4×10 H_2O.

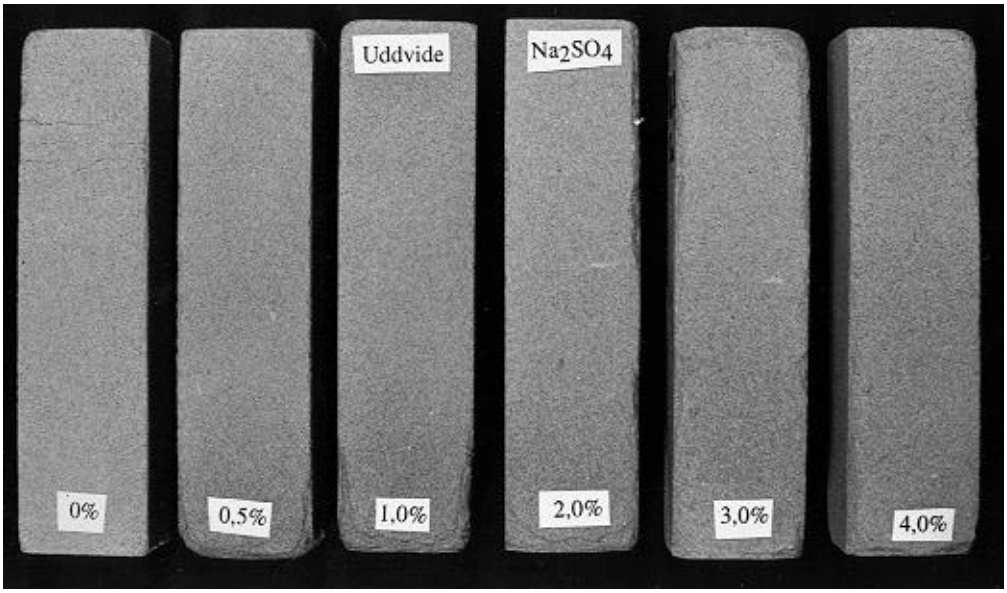

Figure I:14. Prisms of the sandstone Uddvide after freeze-thaw test (20 cycles). The solutions used were, from left to right, 0%, 0.5%, 1%, 2%, 3% and 4% Na_2SO_4×10 H_2O.

Appendix J
Results of scaling test with different initial internal and external concentrations

The scaling test with different initial internal and external salt concentrations is described in Chapter 3.6.6. Some stone prisms were so badly damaged in this test that the resonant frequency was either impossible to measure or the result of the measurement was very uncertain. In addition, the correction factor used for transforming the fundamental frequency of transverse vibration to dynamic modulus of elasticity is based on even scaling on all sides. The real scaling is uneven.

Comments on the results:

Sandstone tested in NaCl - Internal damage (Figures J:1-J:4.)
When the external solution is pure water less damage occurs than when the external solution contains salt. There seem to be no significant difference between the different external concentrations 0.25%, 0.5% and 1.0%.

Sandstone tested in NaCl - Weight loss (Figures J:5-J:8)
When the external solution is pure water (Figure J:5) the damage increases when the concentration of the internal solution is increasing. When the external solution contains salt the concentration of the internal solution seems to have no effect. The external solution however has considerable effect. The mean values in Figure 3.6.9, Chapter 3.6.6, show that the damage at external concentration 0%<<0.5%<0.25%<1.0%.

Sandstone tested in Na_2SO_4 - Internal Damage (Figures J:9-J:12)
Neither the internal nor the external concentration have any significant effect on the internal damage.

Sandstone tested in Na_2SO_4 - Weight loss (Figures J:13-J:16)
The internal concentration has no significant effect on the external damage. The mean values in Figure 3.6.10, Chapter 3.6.6, show that when the external solution is pure water less damage occurs than when the external solution contains salt. There is no significant difference between the external concentrations 0.25%, 0.5% and 1.0%.

Limestone tested in NaCl - Internal Damage (Figures J:17-J:20)
No internal damage could be detected. The resonant frequency was difficult to measure, because of changes of the dimensions of the prisms, caused by huge weight loss.

Limestone tested in NaCl - Weight loss (Figures J:21-J:24)
A small tendency can be seen of more damage occurring when the internal solution is pure water. The mean values in Figure 3.6.11, Chapter 3.6.6, show that when the external solution is pure water less damage occurs than when the external solution contains salt. There is no significant difference between the external concentrations 0.25%, 0.5% and 1.0%.

Limestone tested in Na_2SO_4 - Internal Damage (Figures J:25-J:28)
The internal damage of limestone in Na_2SO_4 is detectable, but relatively small. Neither the internal nor the external concentration have any significant effect on the internal damage.

Limestone tested in Na_2SO_4 - Weight loss (Figures J:29-J:32)
The external damage of limestone in Na_2SO_4 is detectable, but relatively small. There is no significant difference between the various internal concentrations. Few, rather large pieces fall off. The mean values in Figure 3.6.12, Chapter 3.6.6, show that when the external solution is pure water less damage occurs than when the external solution contains salt. There is no significant difference between the external concentrations 0.25%, 0.5% and 1.0%.

Note: A sudden ‘break’ in the graph indicates a broken sample — a large piece has fell off the main prism or it broke into two pieces.

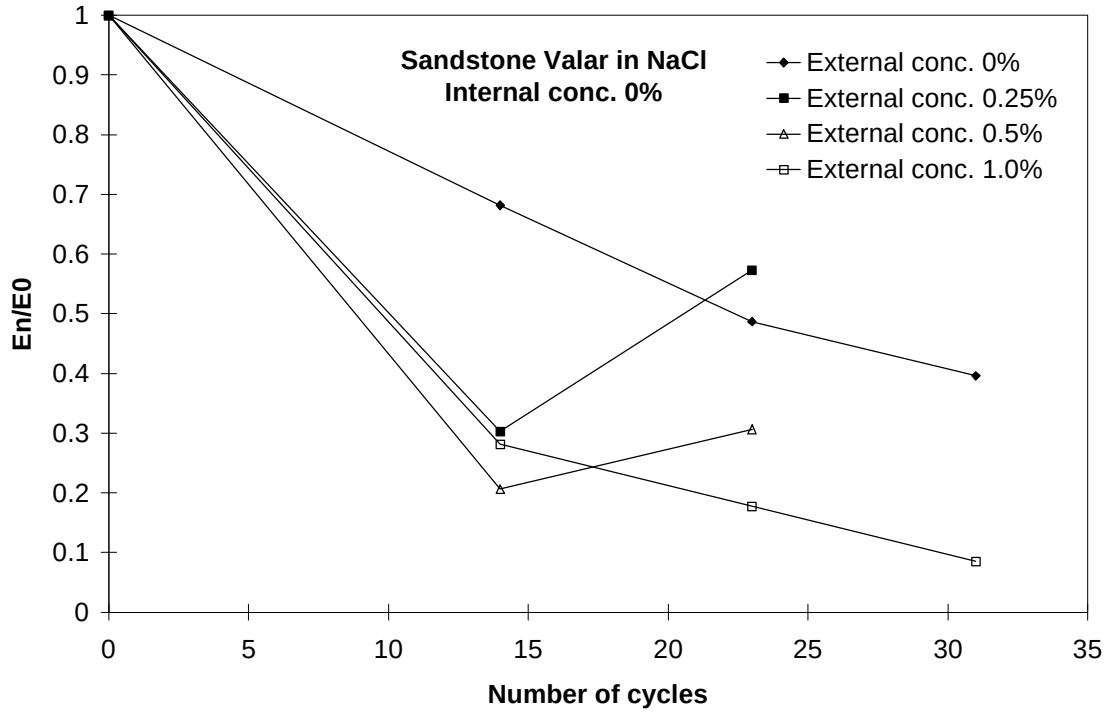

Figure J:1. The relative loss in dynamic modulus of elasticity versus number of freeze-thaw cycles of sandstone with various external NaCl concentrations, and pure water internally. In the specimens with external concentration of 0.25% and 0.5% the fundamental frequency could not be measured at 32 cycles.

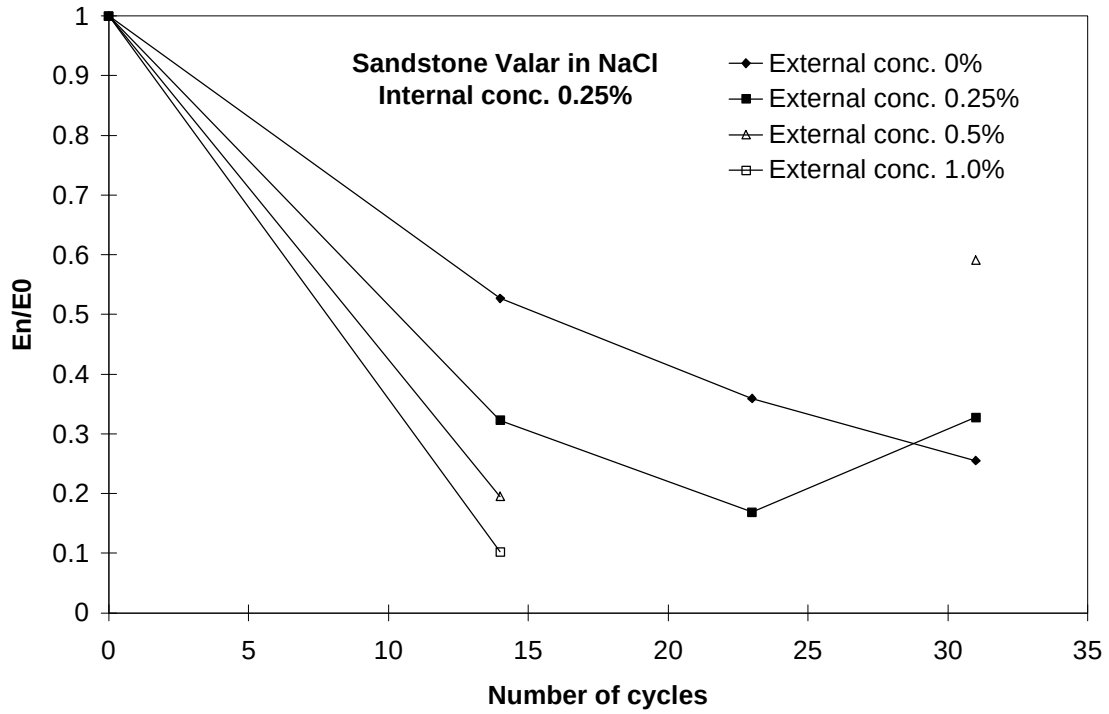

Figure J:2. The relative loss in dynamic modulus of elasticity versus number of freeze-thaw cycles of sandstone with various external NaCl concentrations, and internal concentration of 0.25% NaCl. In the specimens with external concentration of 0.5% and 1.0% the fundamental frequency could not be measured at 23 and 32 cycles.

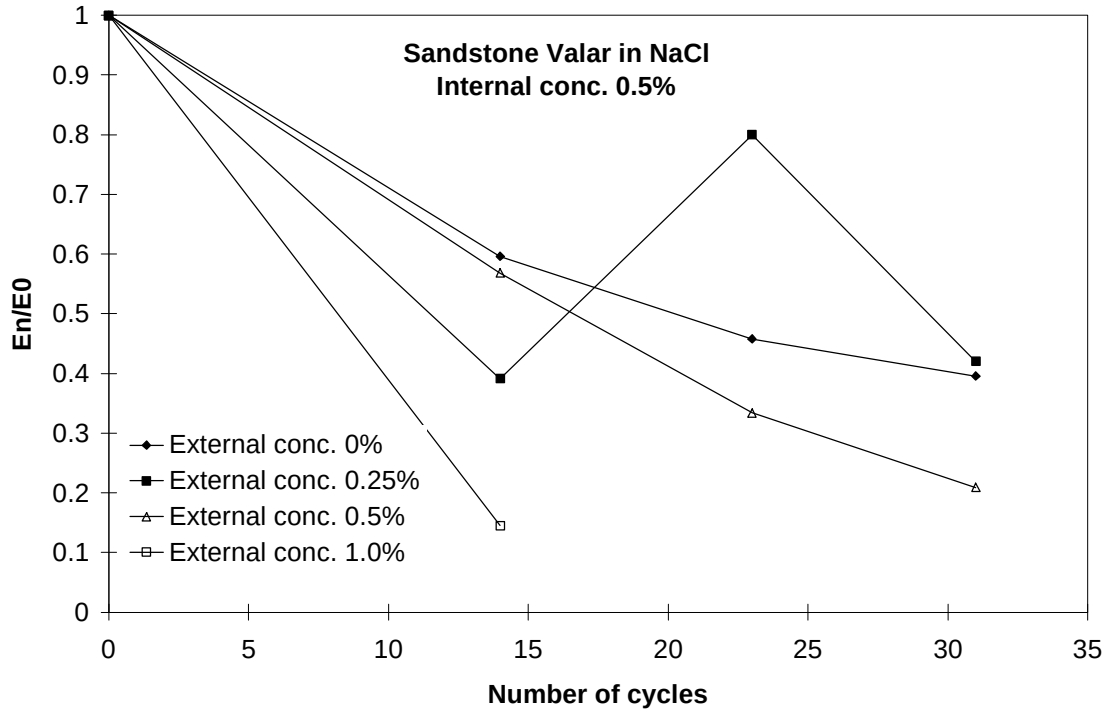

Figure J:3. Loss in dynamic modulus of elasticity versus number of freeze-thaw cycles of sandstone with various external NaCl concentrations, and internal concentration of 0.5% NaCl. In the specimen with external concentration of 1.0% the fundamental frequency could not be measured at 23 and 32 cycles.

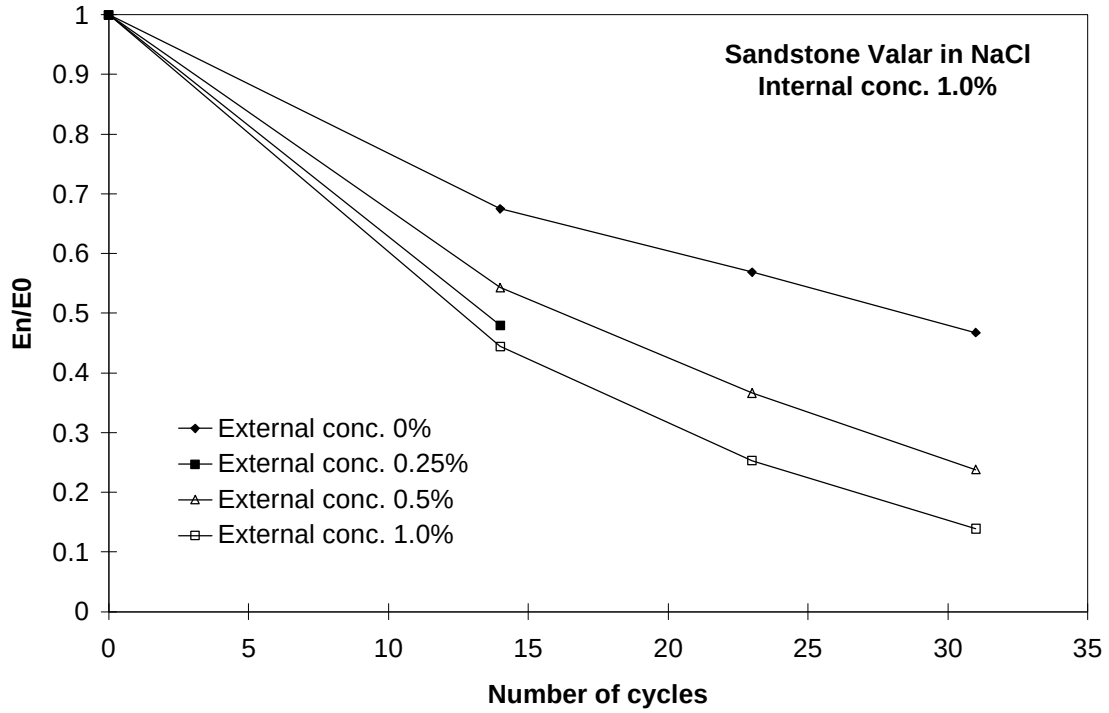

Figure J:4. The relative loss in dynamic modulus of elasticity versus number of freeze-thaw cycles of sandstone with various external NaCl concentrations and internal concentration of 1.0% NaCl. In the specimen with external concentration of 0.25% the fundamental frequency could not be measured at 23 and 32 cycles.

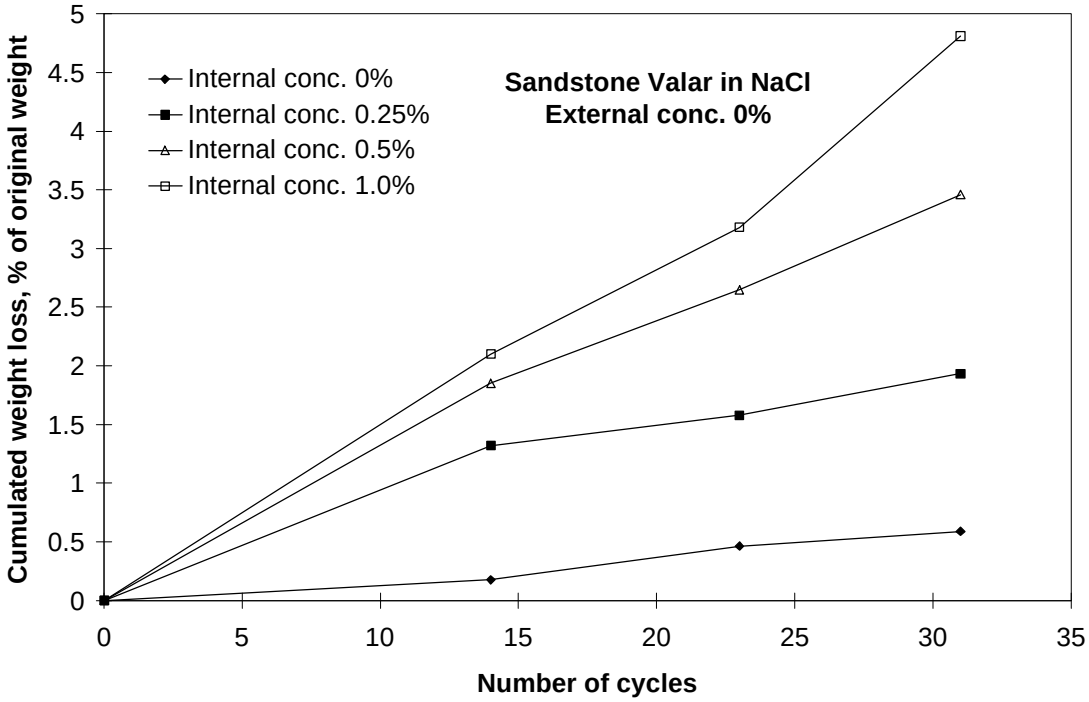

Figure J:5. Cumulated weight loss versus number of freeze-thaw cycles of sandstone with various internal NaCl concentrations and pure water externally.

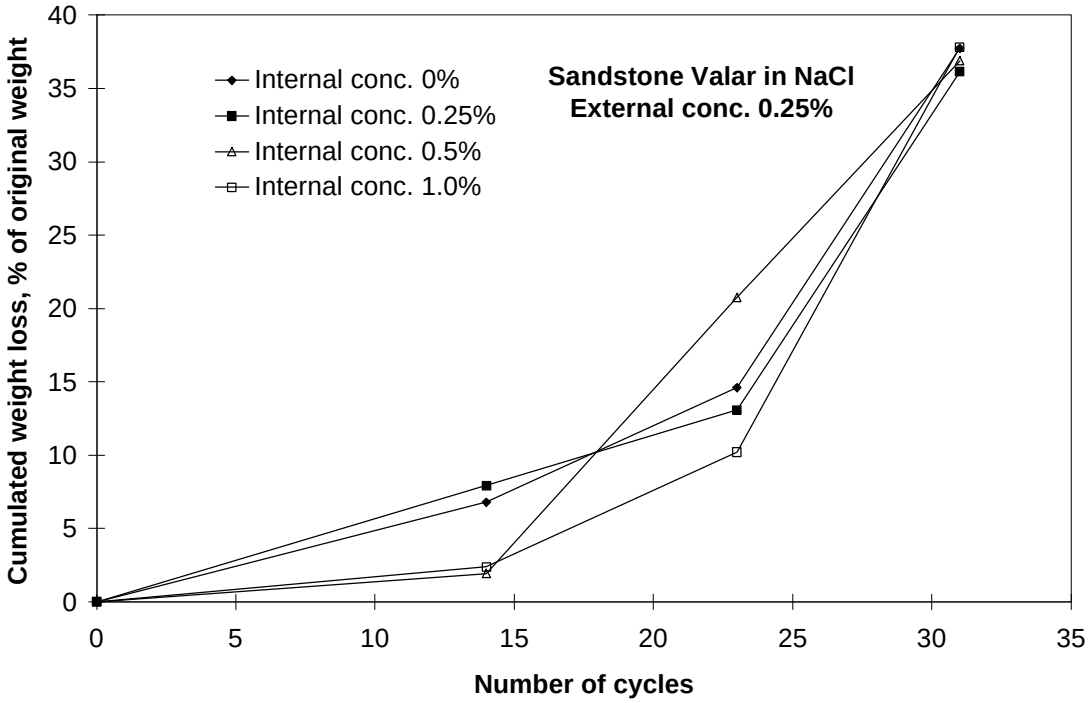

Figure. J:6. Cumulated weight loss versus number of freeze-thaw cycles of sandstone with various internal NaCl concentrations and external concentration of 0.25% NaCl.

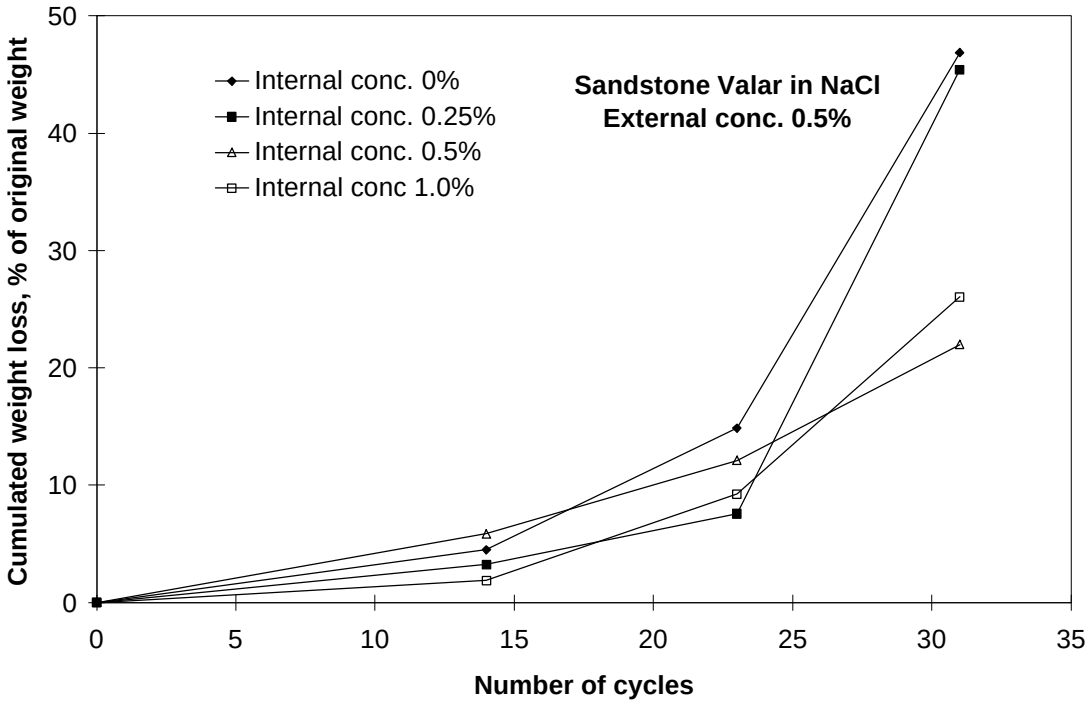

Figure J:7. Cumulated weight loss versus number of freeze-thaw cycles of sandstone with various internal NaCl concentrations and external concentration of 0.5% NaCl.

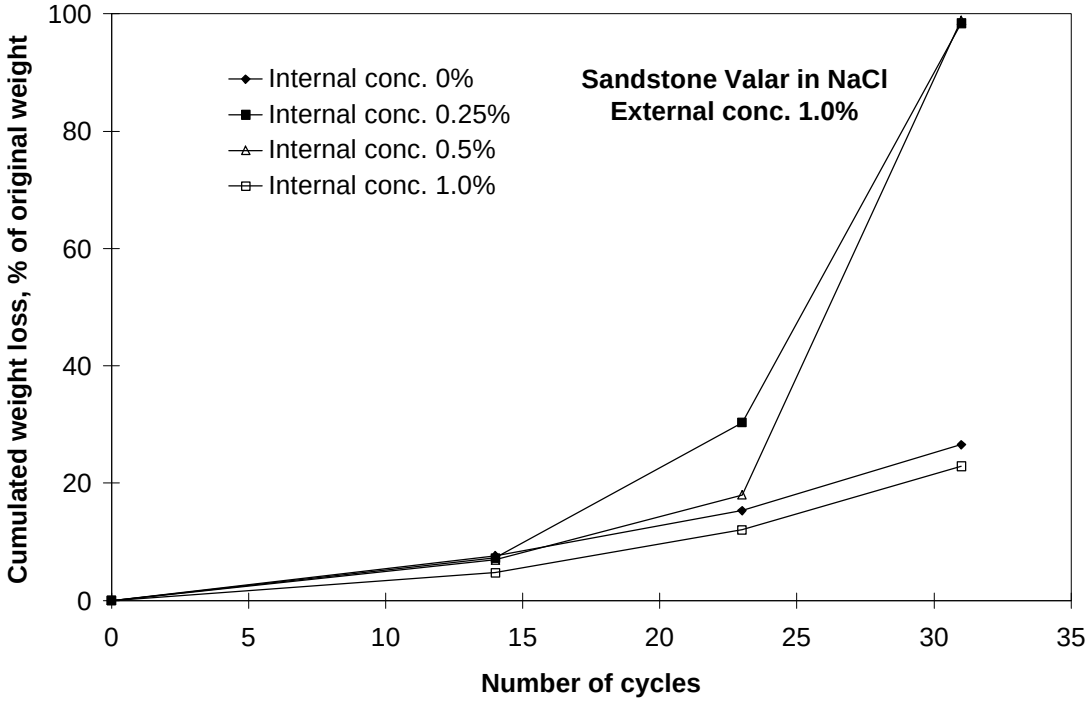

Figure J:8. Cumulated weight loss versus number of freeze-thaw cycles of sandstone with various internal NaCl concentrations and external concentration of 1.0% NaCl.

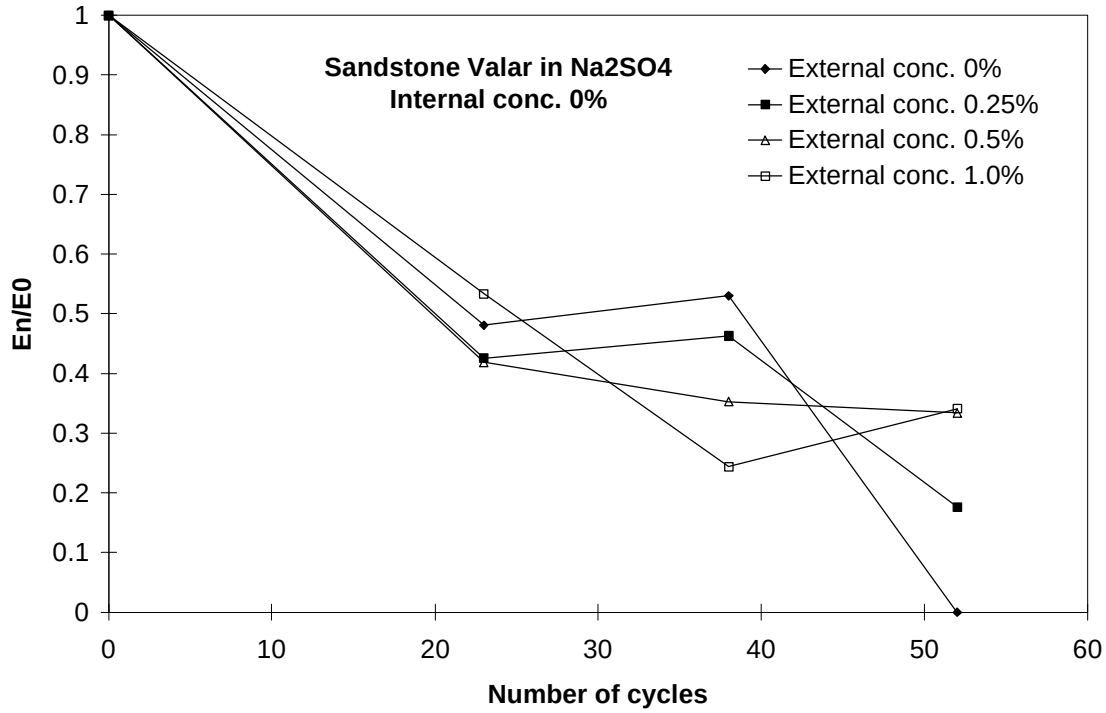

Figure J:9. The relative loss in dynamic modulus of elasticity versus number of freeze-thaw cycles of sandstone with various external concentrations of $Na_2SO_4 \cdot 10H_2O$ and pure water internally. E = 0 indicates that the specimen is broken.

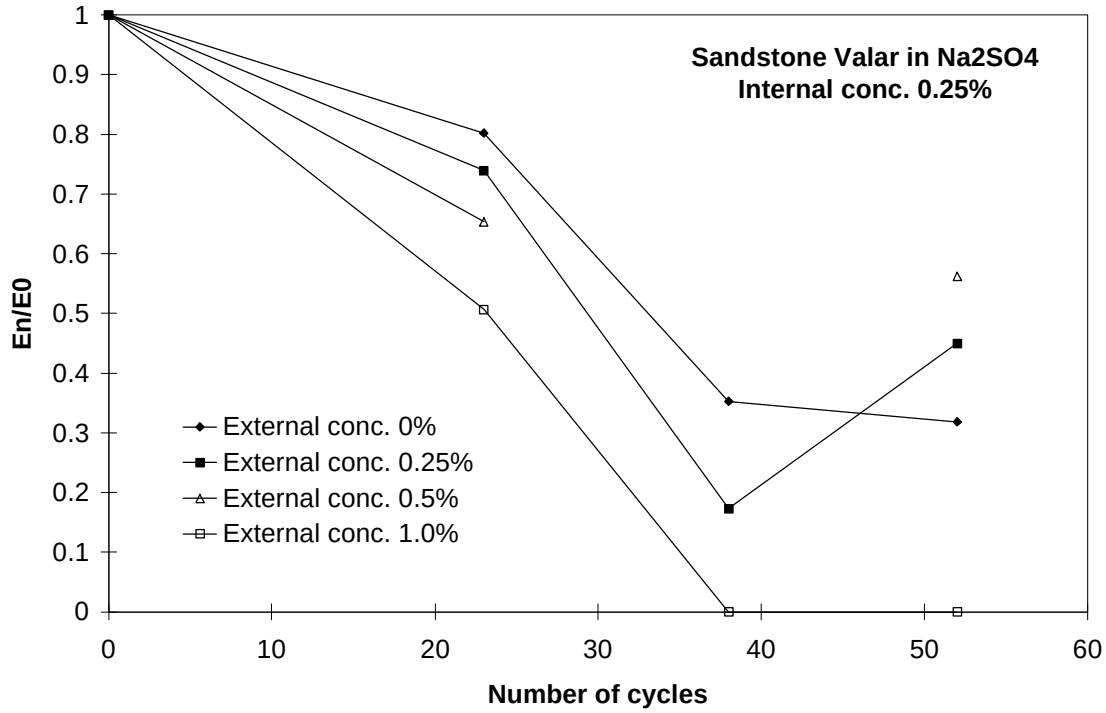

Figure J:10. The relative loss in dynamic modulus of elasticity versus number of freeze-thaw cycles of sandstone with various external concentrations of $Na_2SO_4 \cdot 10H_2O$ and internal concentration of 0.25% $Na_2SO_4 \cdot 10\ H_2O$. In the specimen with external concentration of 0.5% the fundamental frequency could not be measured at 38 cycles. E = 0 indicates that the specimen is broken.

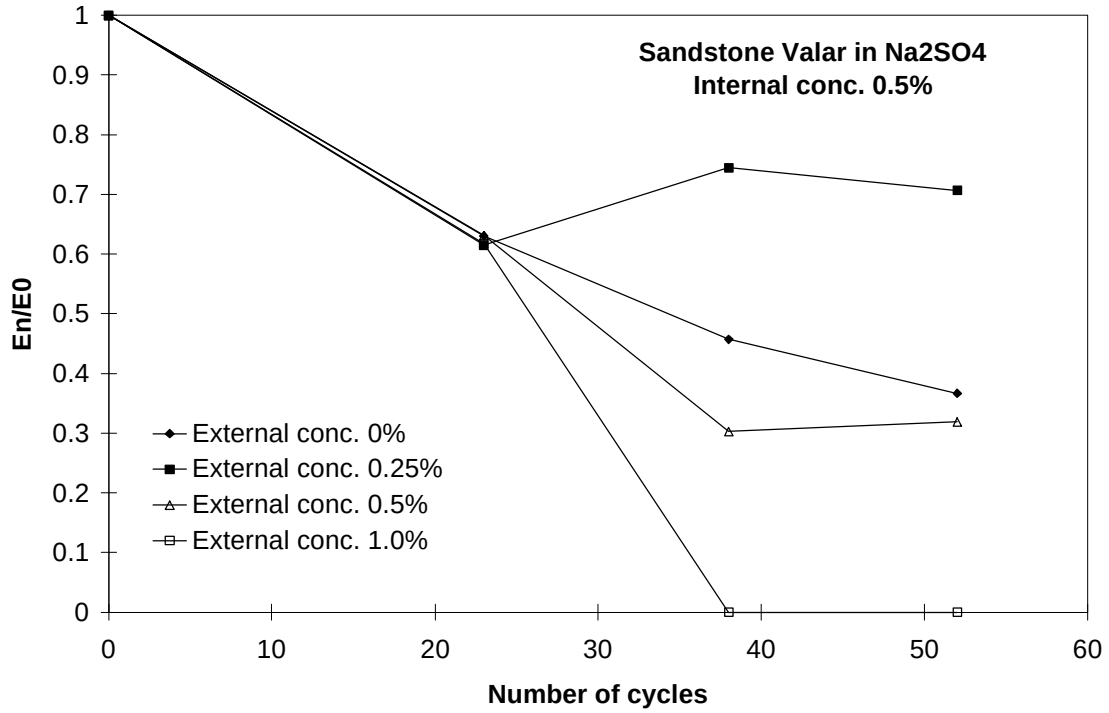

Figure J:11. The relative loss in dynamic modulus of elasticity versus number of freeze-thaw cycles of sandstone with various external concentrations of $Na_2SO_4 \cdot 10H_2O$ and internal concentration of 0.5% $Na_2SO_4 \cdot 10\ H_2O$. E = 0 indicates that the specimen is broken.

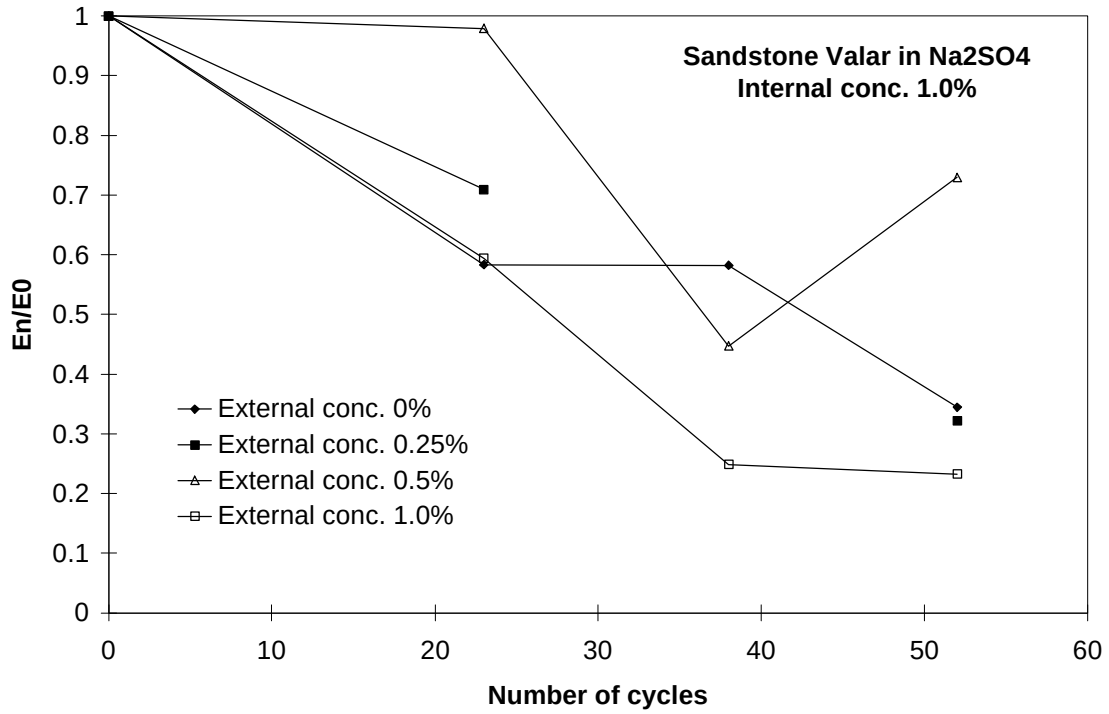

Figure J:12. The relative loss in dynamic modulus of elasticity versus number of freeze-thaw cycles of sandstone with various external concentrations of $Na_2SO_4 \cdot 10\ H_2O$ and internal concentration of 1.0% $Na_2SO_4 \cdot 10\ H_2O$. In the specimens with external concentration of 0.25% the fundamental frequency could not be measured at 38 cycles.

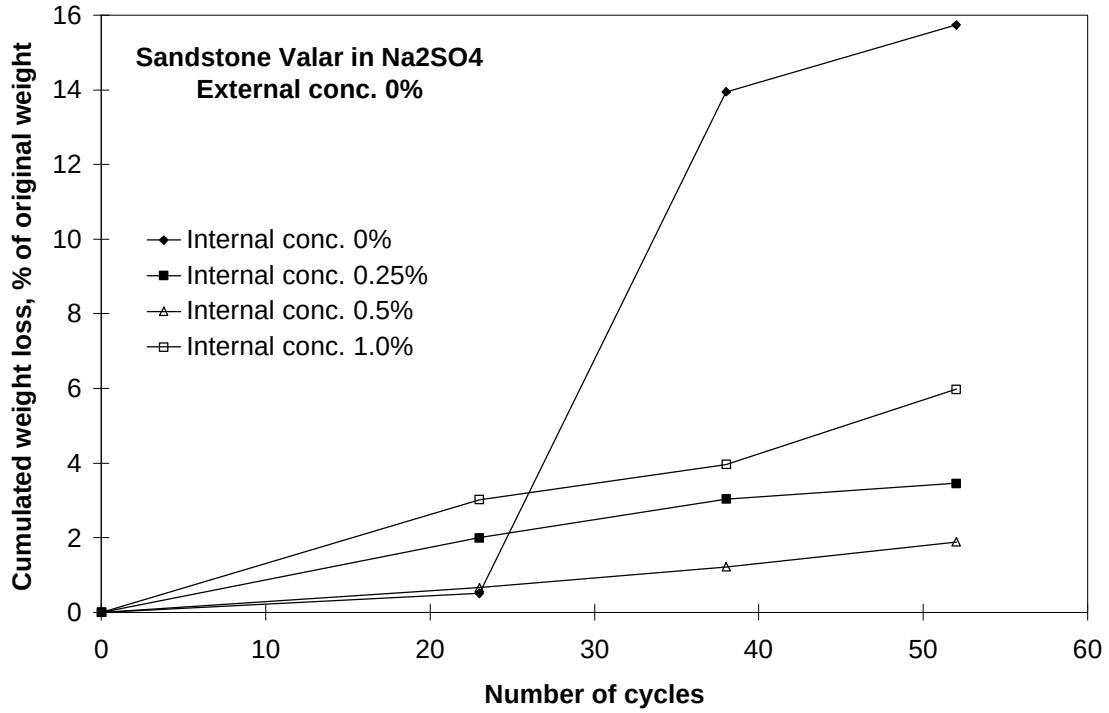

Figure J:13. Cumulated weight loss versus number of freeze-thaw cycles of sandstone with various internal concentrations of $Na_2SO_4 \cdot 10\ H_2O$, and pure water externally.

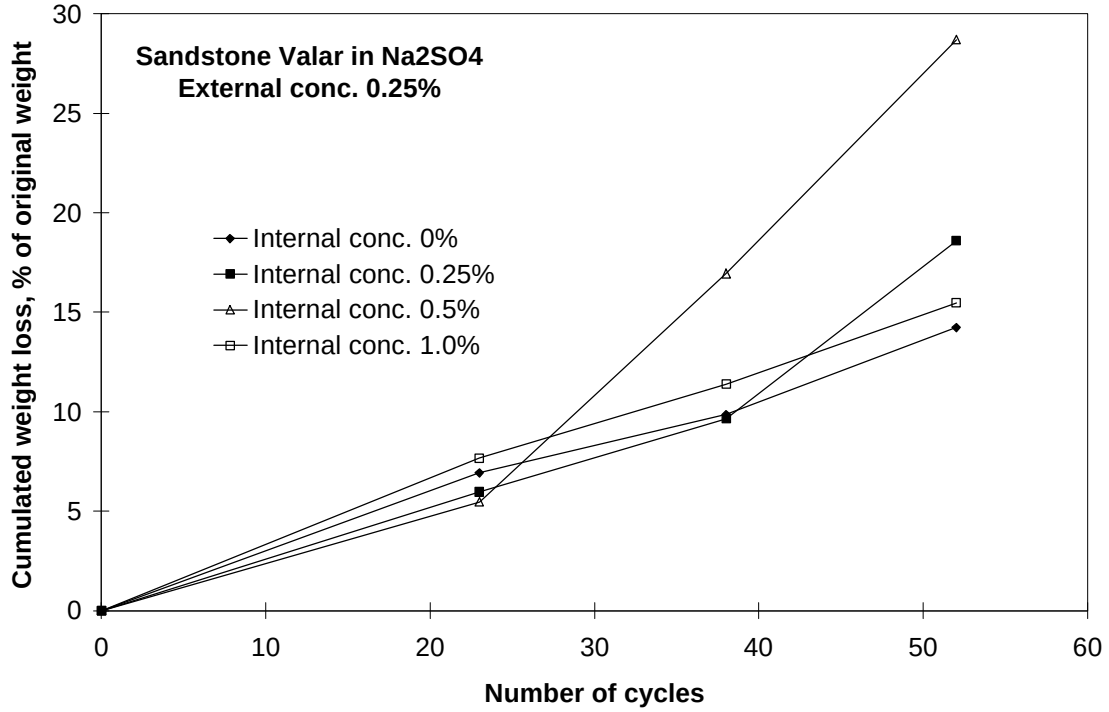

Figure J:14. Cumulated weight loss versus number of freeze-thaw cycles of sandstone with various internal concentrations of $Na_2SO_4 \cdot 10\ H_2O$, and external concentration of 0.25% $Na_2SO_4 \cdot 10\ H_2O$.

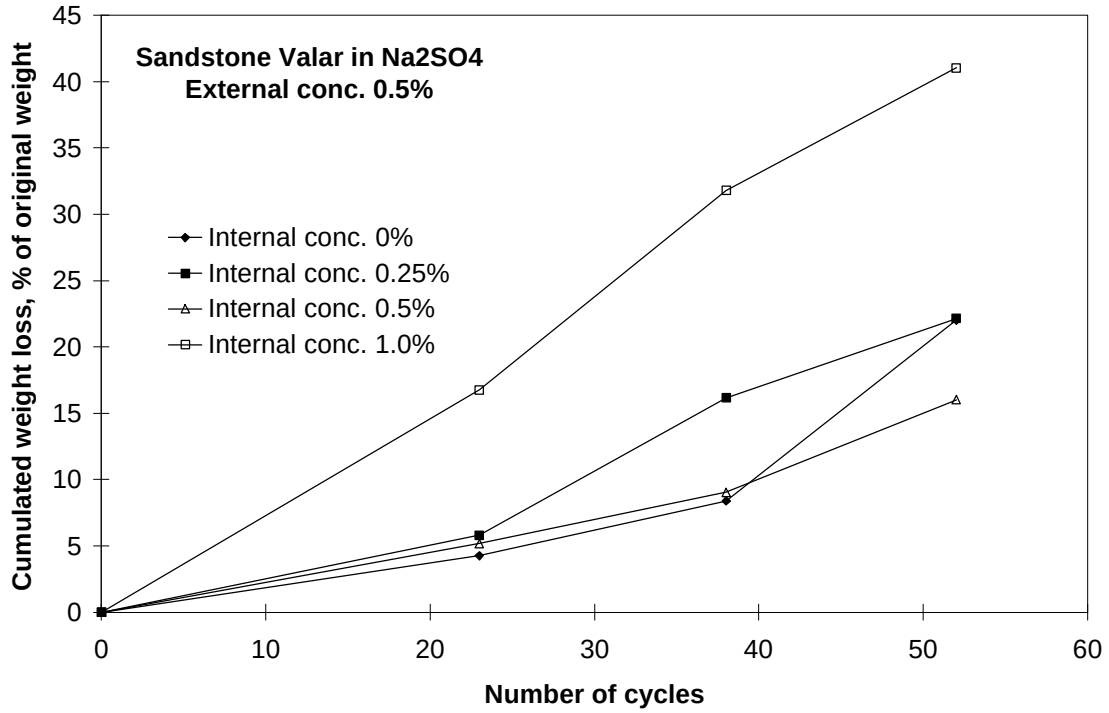

Figure J:15. Cumulated weight loss versus number of freeze-thaw cycles of sandstone with various internal concentrations of $Na_2SO_4 \cdot 10\ H_2O$, and external concentration of 0.5% $Na_2SO_4 \cdot 10\ H_2O$.

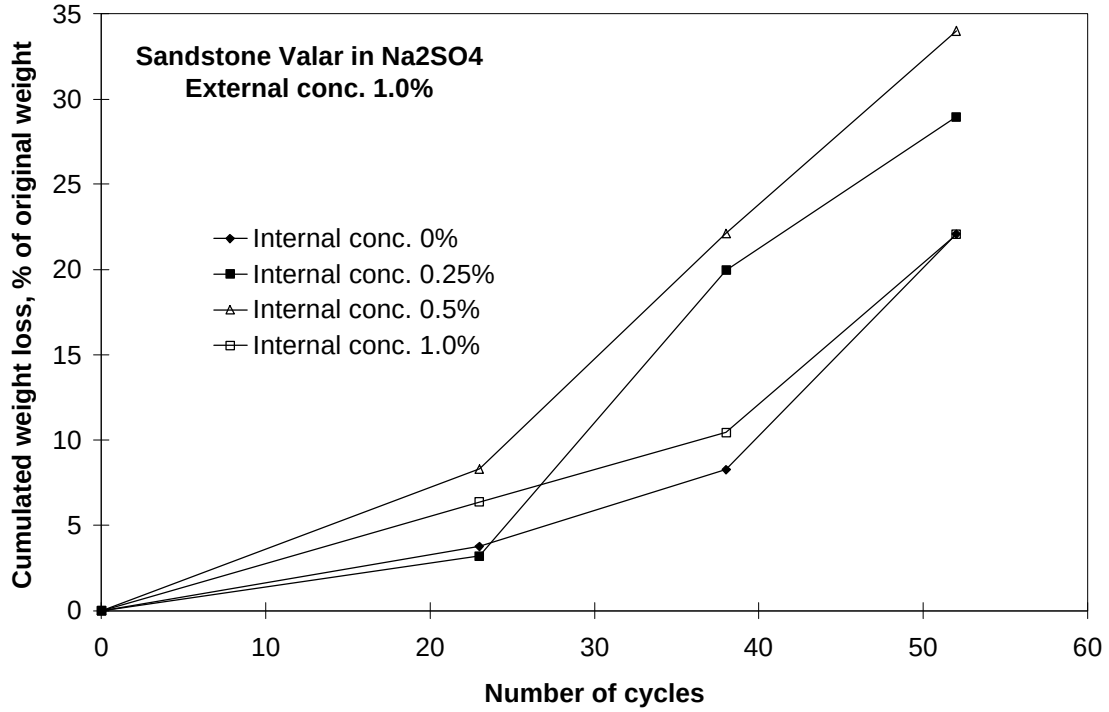

Figure J:16. Cumulated weight loss versus number of freeze-thaw cycles of sandstone with various internal concentrations of $Na_2SO_4 \cdot 10\ H_2O$, and external concentration of 1.0% $Na_2SO_4 \cdot 10\ H_2O$.

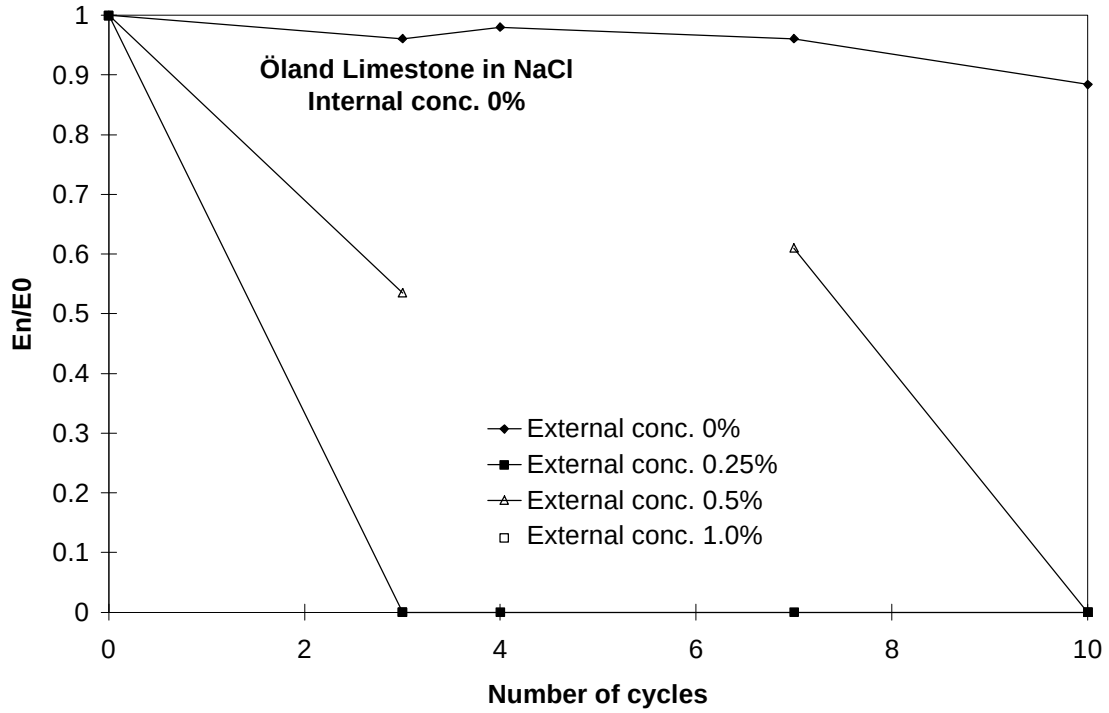

Figure J:17. The relative loss in dynamic modulus of elasticity versus number of freeze-thaw cycles of limestone with various external NaCl concentrations, and pure water internally. In some of the specimens the fundamental frequency could not be measured, as they were badly damaged by scaling. E = 0 indicates that the specimen is broken.

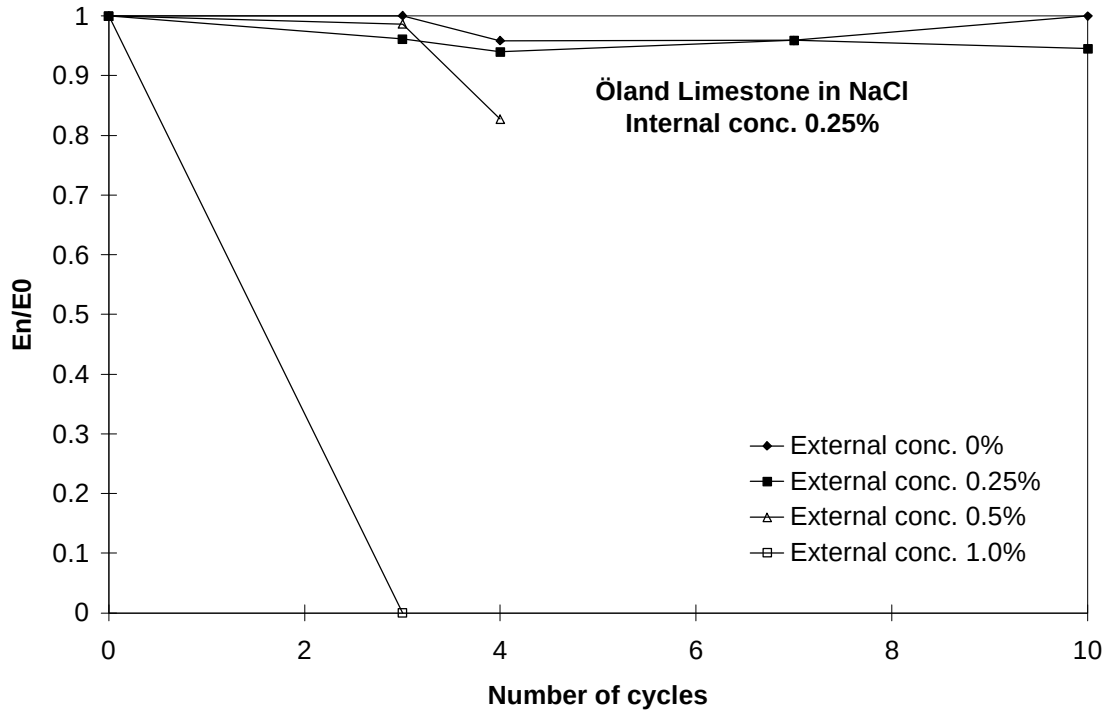

Figure J:18. The relative loss in dynamic modulus of elasticity versus number of freeze-thaw cycles of limestone with various external NaCl concentrations, and internal concentration of 0.25% NaCl. In some of the specimens the fundamental frequency could not be measured, as they were badly damaged by scaling. E = 0 indicates that the specimen is broken.

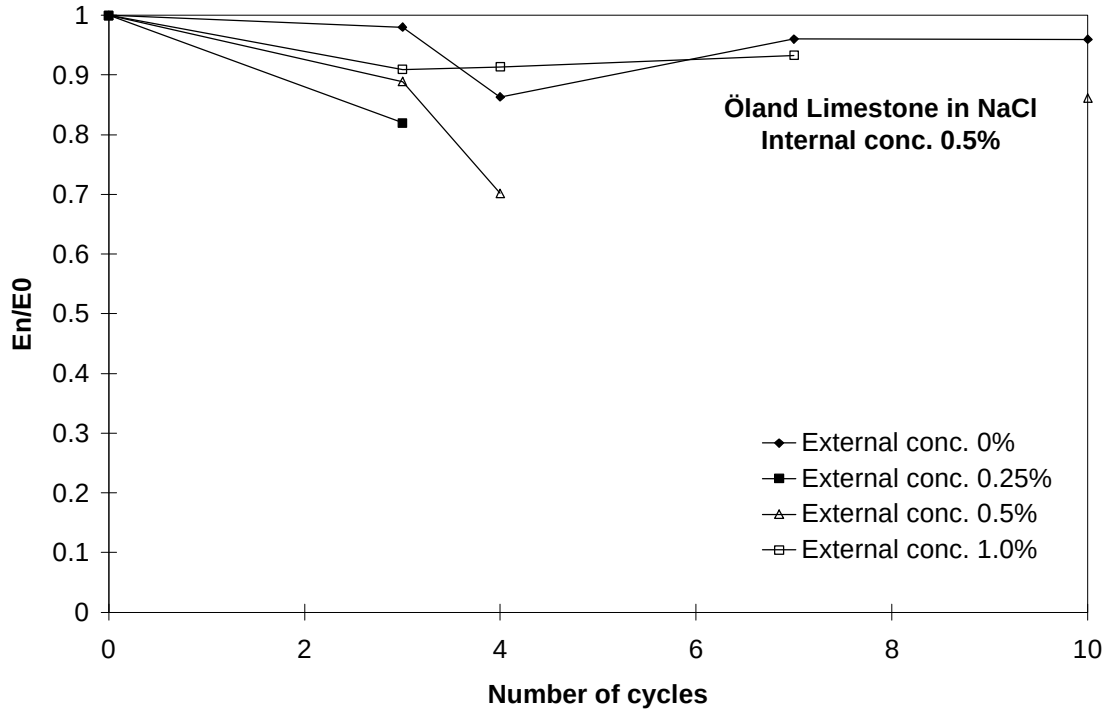

Figure J:19. The relative loss in dynamic modulus of elasticity versus number of freeze-thaw cycles of limestone with various external NaCl concentrations, and internal concentration of 0.5% NaCl. In some of the specimens the fundamental frequency could not be measured, as they were badly damaged by scaling.

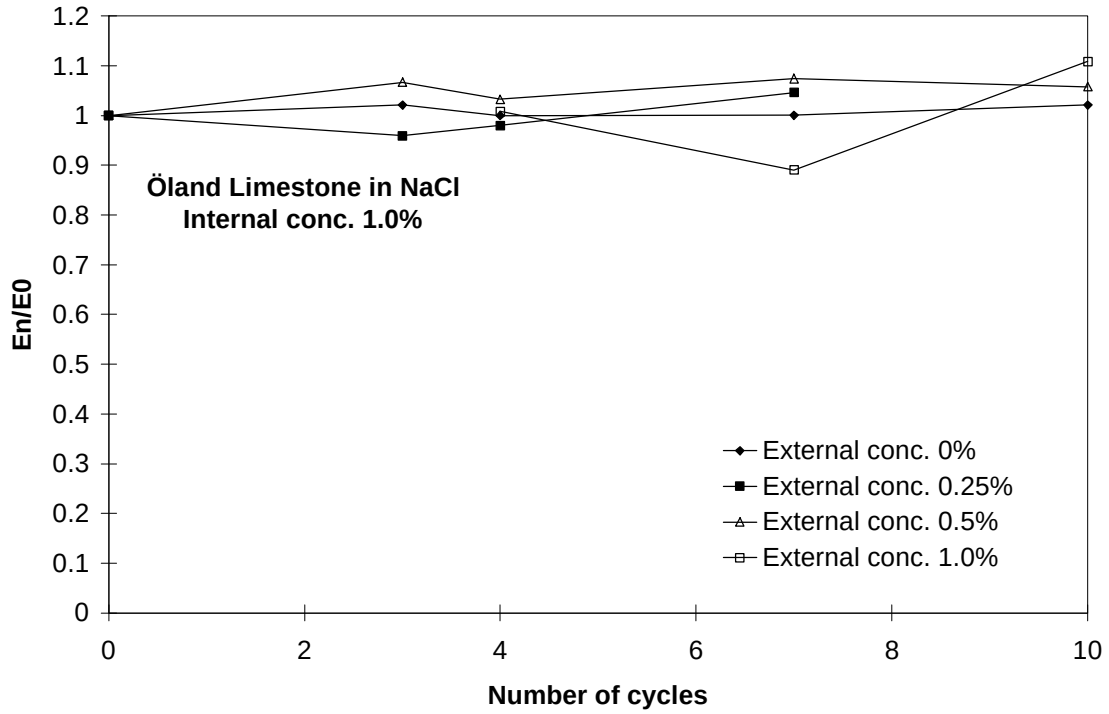

Figure J:20. The relative loss in dynamic modulus of elasticity versus number of freeze-thaw cycles of limestone with various external NaCl concentrations, and internal concentration of 1.0% NaCl. In some of the specimens the fundamental frequency could not be measured, as they were badly damaged by scaling.

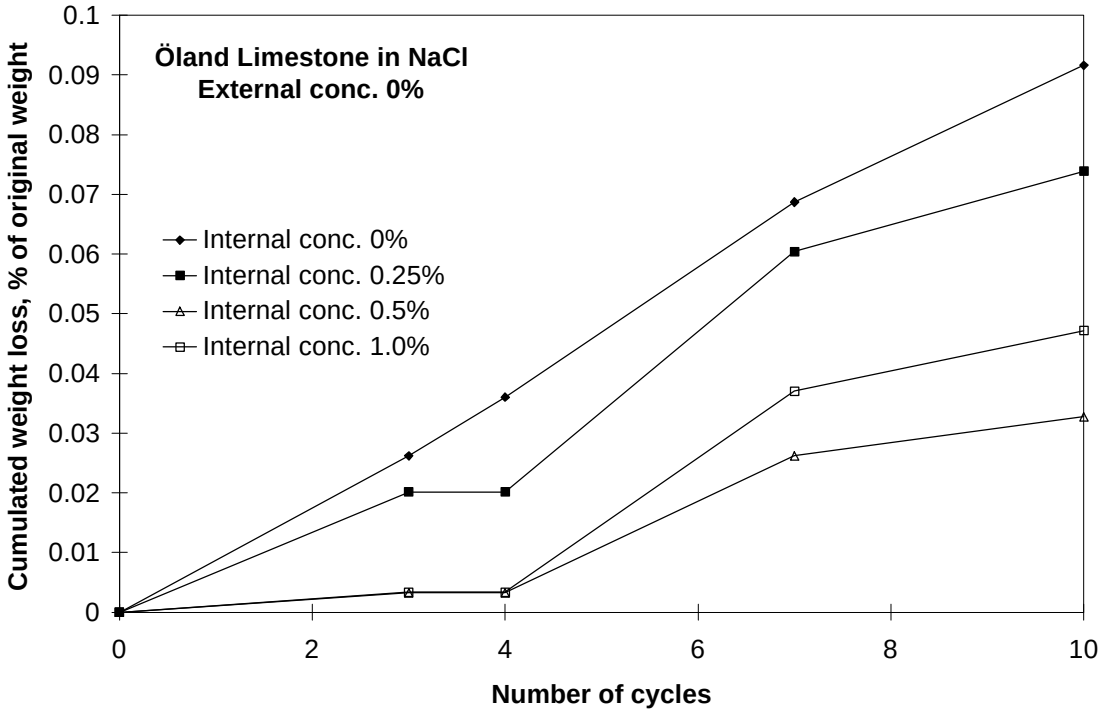

Figure J:21. Cumulated weight loss versus number of freeze-thaw cycles of limestone with various internal NaCl concentrations, and external pure water.

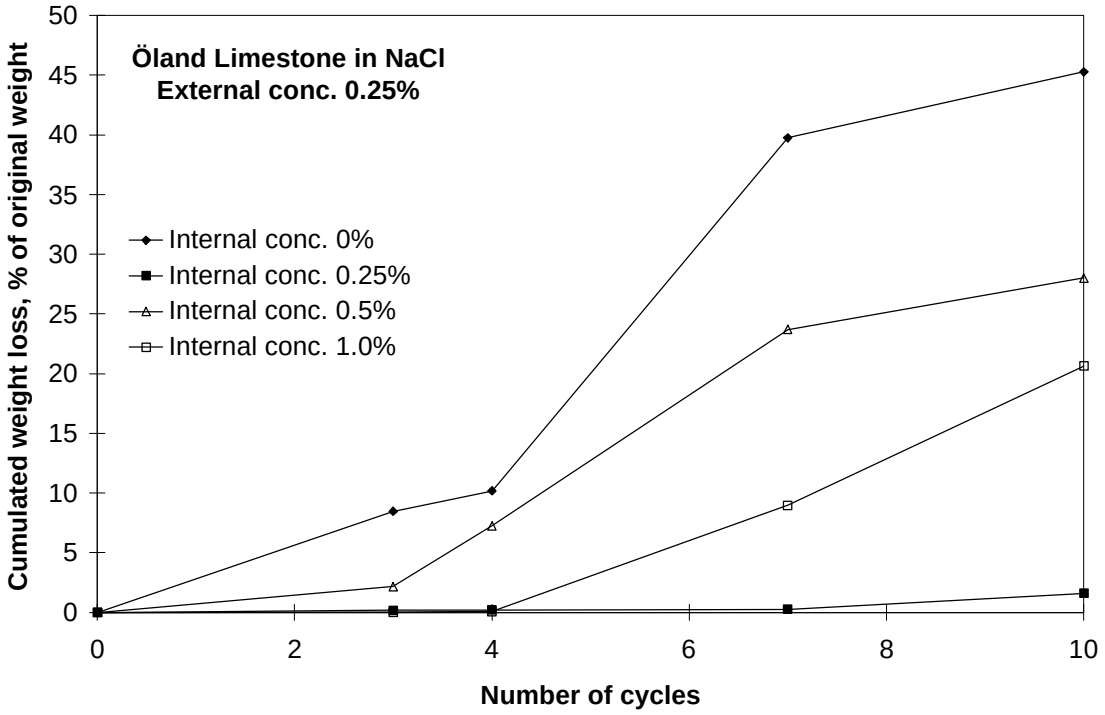

Figure J:22. Cumulated weight loss versus number of freeze-thaw cycles of limestone with various internal NaCl concentrations, and external concentration of 0.25% NaCl.

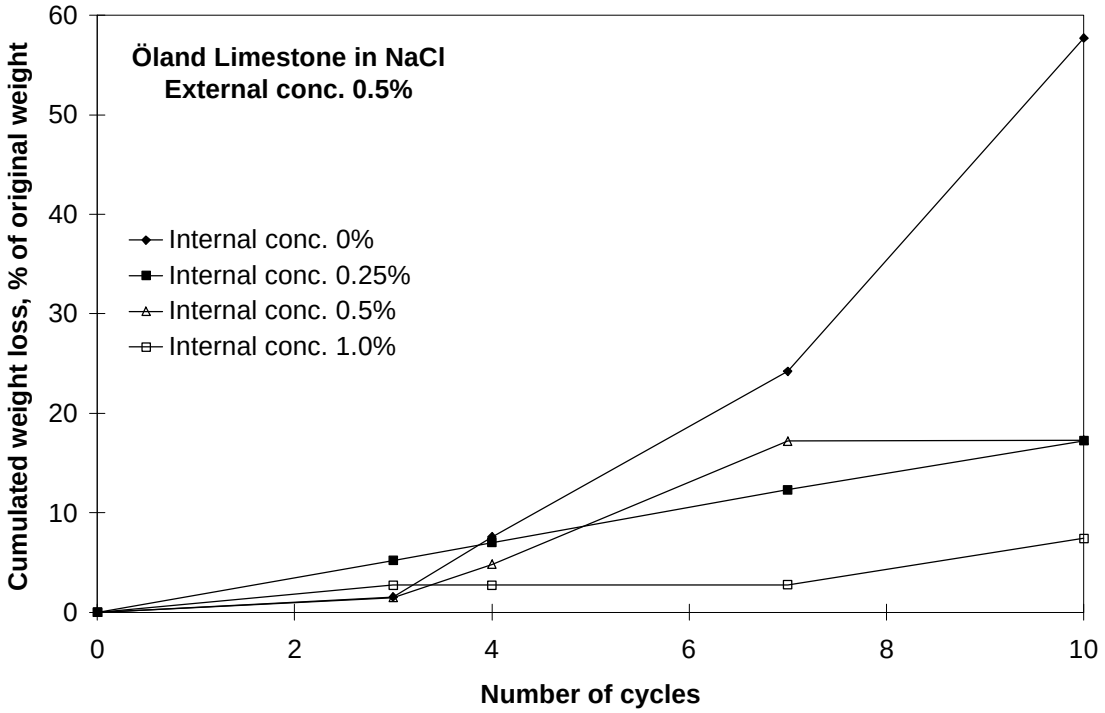

Figure J:23. Cumulated weight loss versus number of freeze-thaw cycles of limestone with various internal NaCl concentrations, and external concentration of 0.5% NaCl.

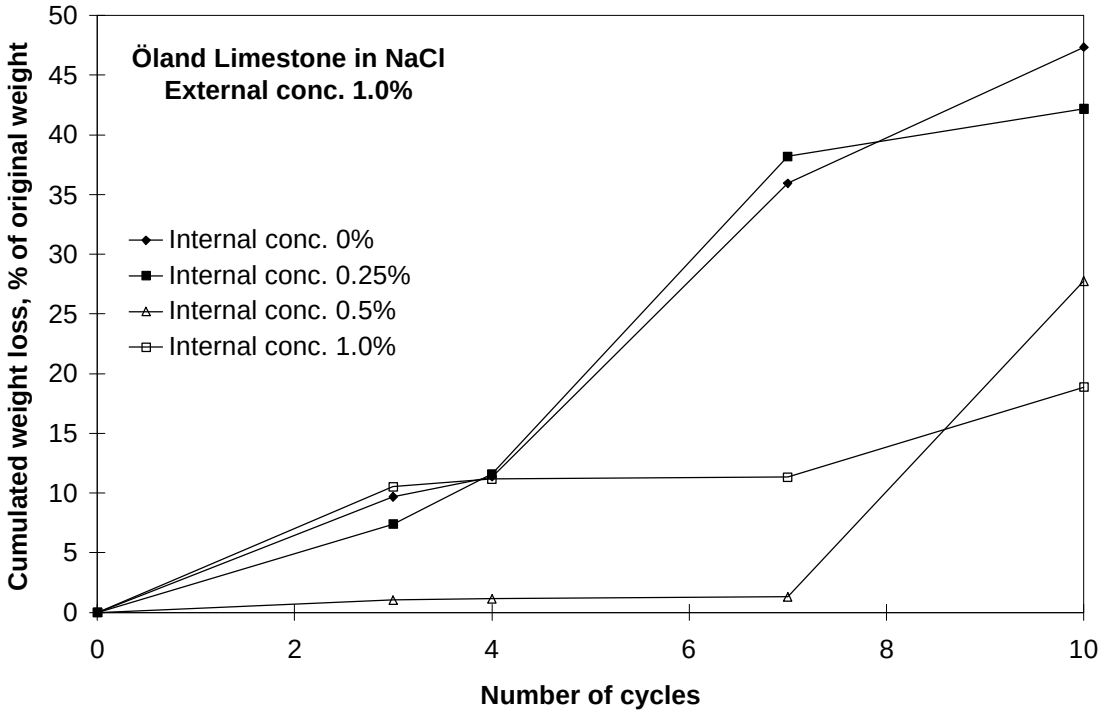

Figure J:24. Cumulated weight loss versus number of freeze-thaw cycles of limestone with various internal NaCl concentrations, and external concentration of 1.0% NaCl.

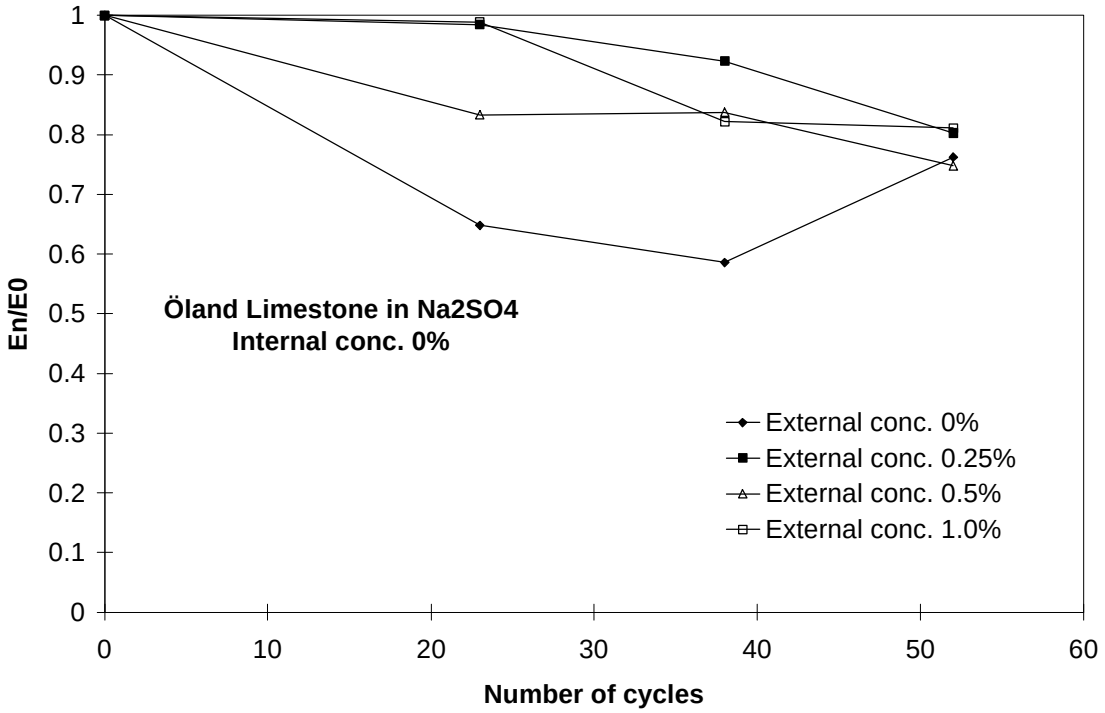

Figure J:25. The relative loss in dynamic modulus of elasticity versus number of freeze-thaw cycles of limestone with various external concentrations of $Na_2SO_4 \cdot 10\ H_2O$, and internal pure water.

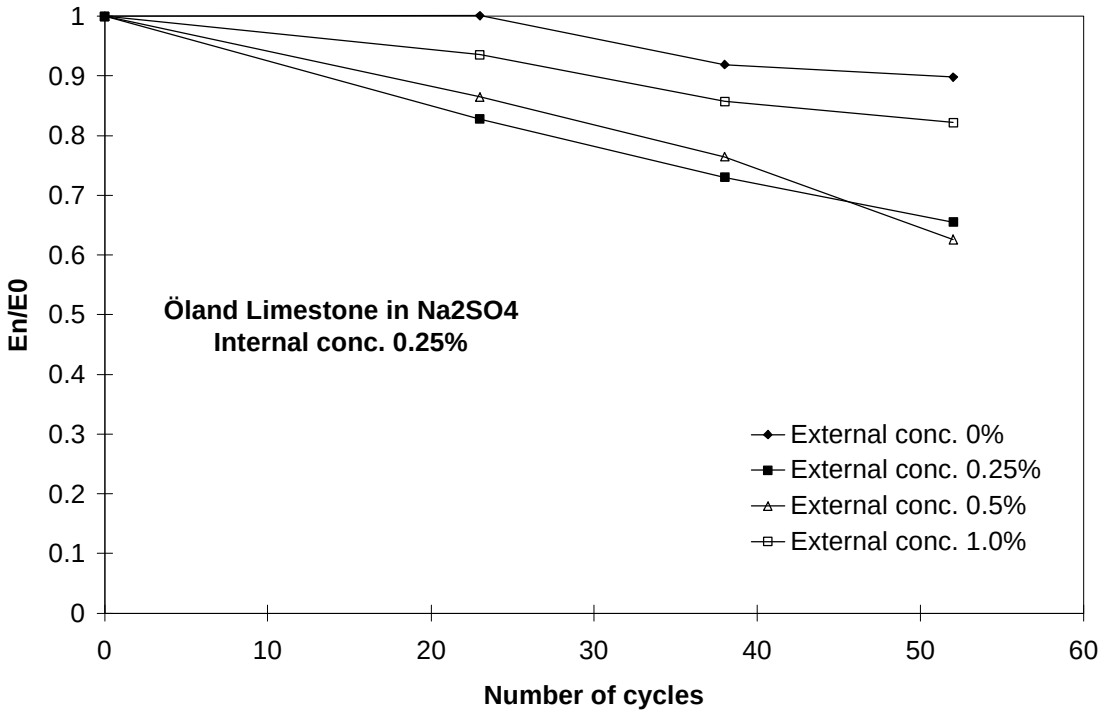

Figure J:26. The relative loss in dynamic modulus of elasticity versus number of freeze-thaw cycles of limestone with various external concentrations of $Na_2SO_4 \cdot 10\ H_2O$, and internal concentration of 0.25% $Na_2SO_4 \cdot 10\ H_2O$.

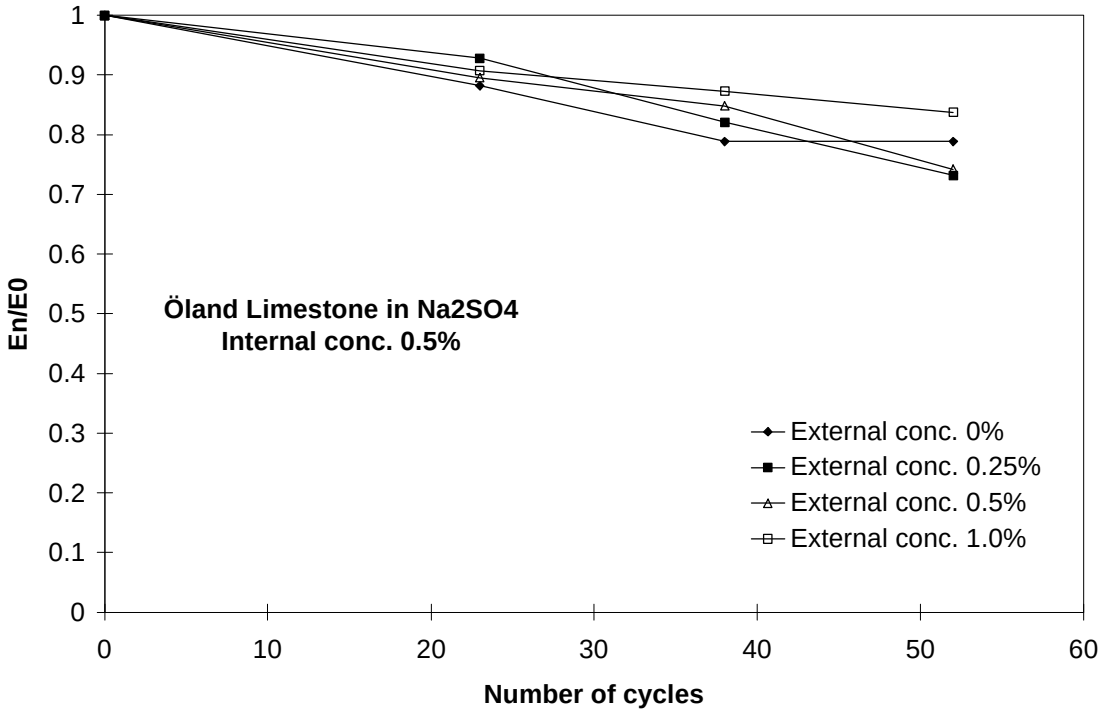

Figure J:27. The relative loss in dynamic modulus of elasticity versus number of freeze-thaw cycles of limestone with various external concentrations of $Na_2SO_4 \cdot 10\ H_2O$, and internal concentration of 0.5% $Na_2SO_4 \cdot 10\ H_2O$.

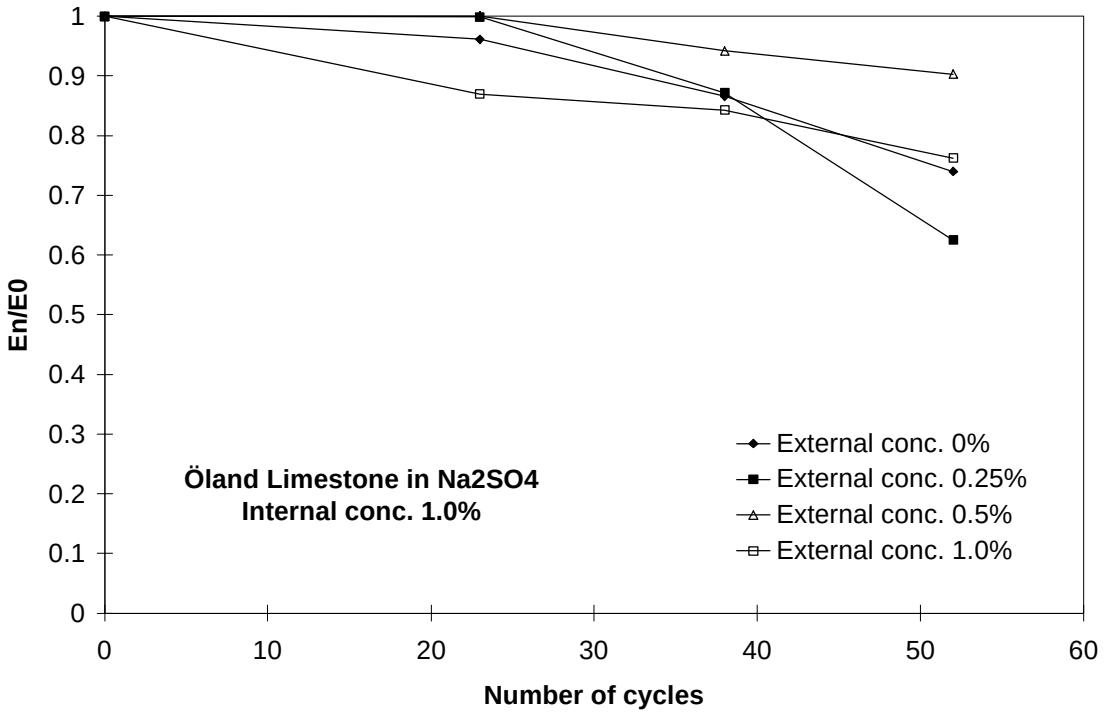

Figure J:28. The relative loss in dynamic modulus of elasticity versus number of freeze-thaw cycles of limestone with various external concentrations of $Na_2SO_4 \cdot 10\ H_2O$, and internal concentration of $Na_2SO_4 \cdot 10\ H_2O$.

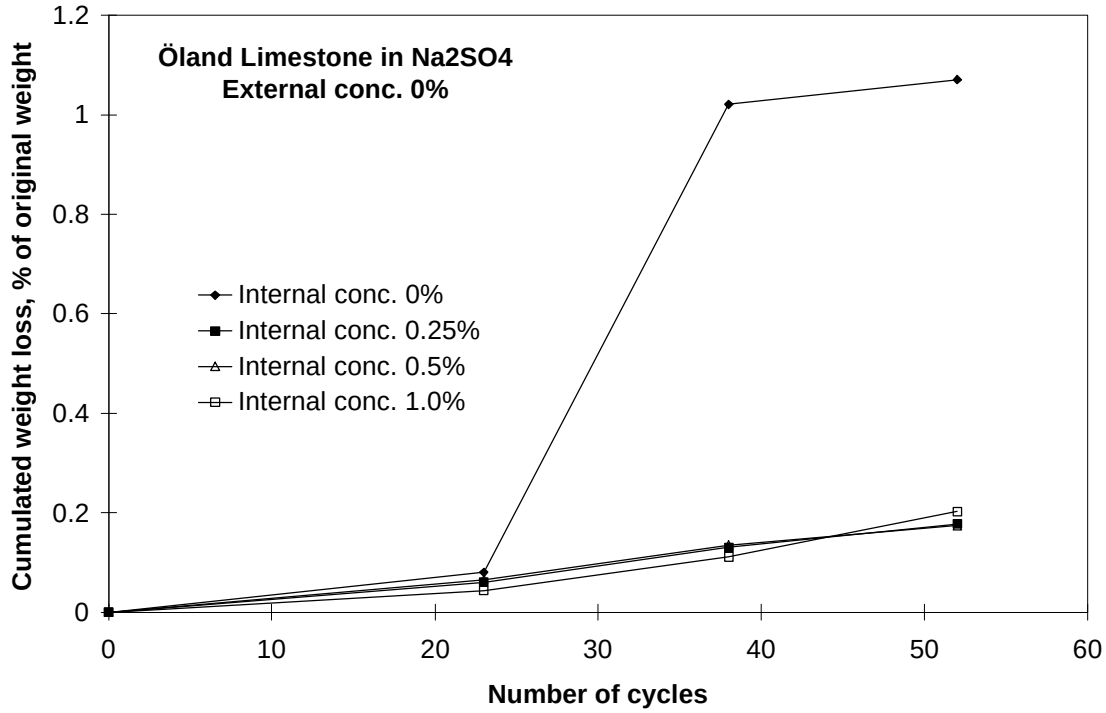

Figure J:29. Cumulated weight loss versus number of freeze-thaw cycles of limestone with various internal concentrations of $Na_2SO_4 \cdot 10\ H_2O$, and external pure water.

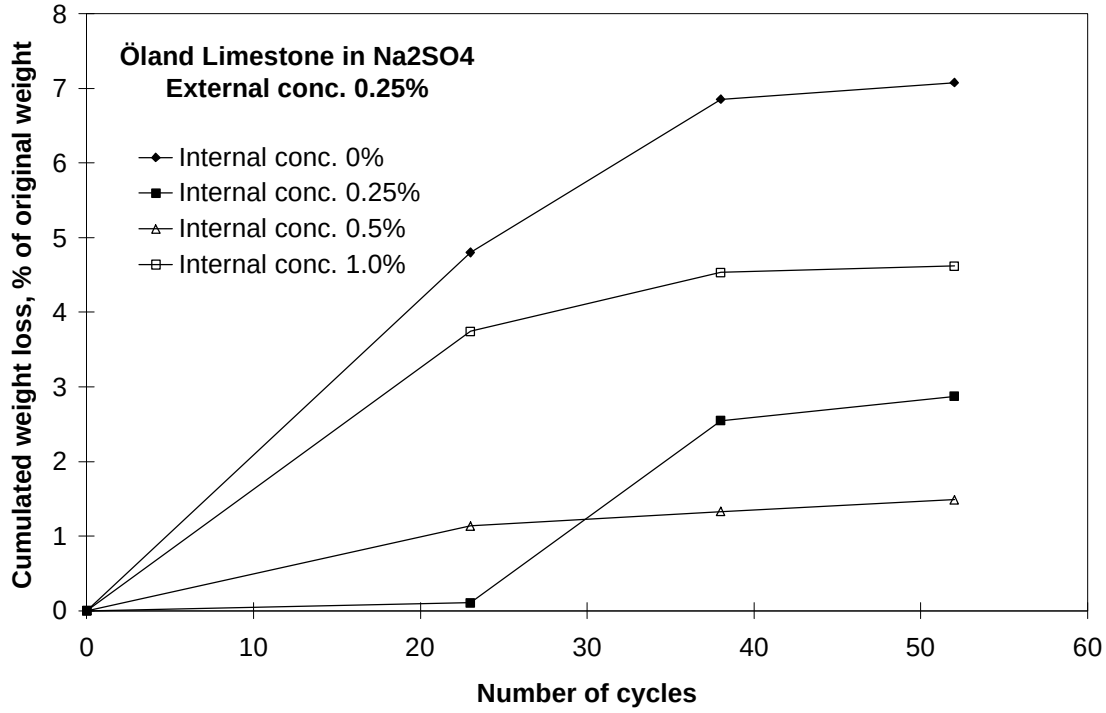

Figure J:30. Cumulated weight loss versus number of freeze-thaw cycles of limestone with various internal concentrations of $Na_2SO_4 \cdot 10\ H_2O$, and external concentration of 0.25% $Na_2SO_4 \cdot 10\ H_2O$.

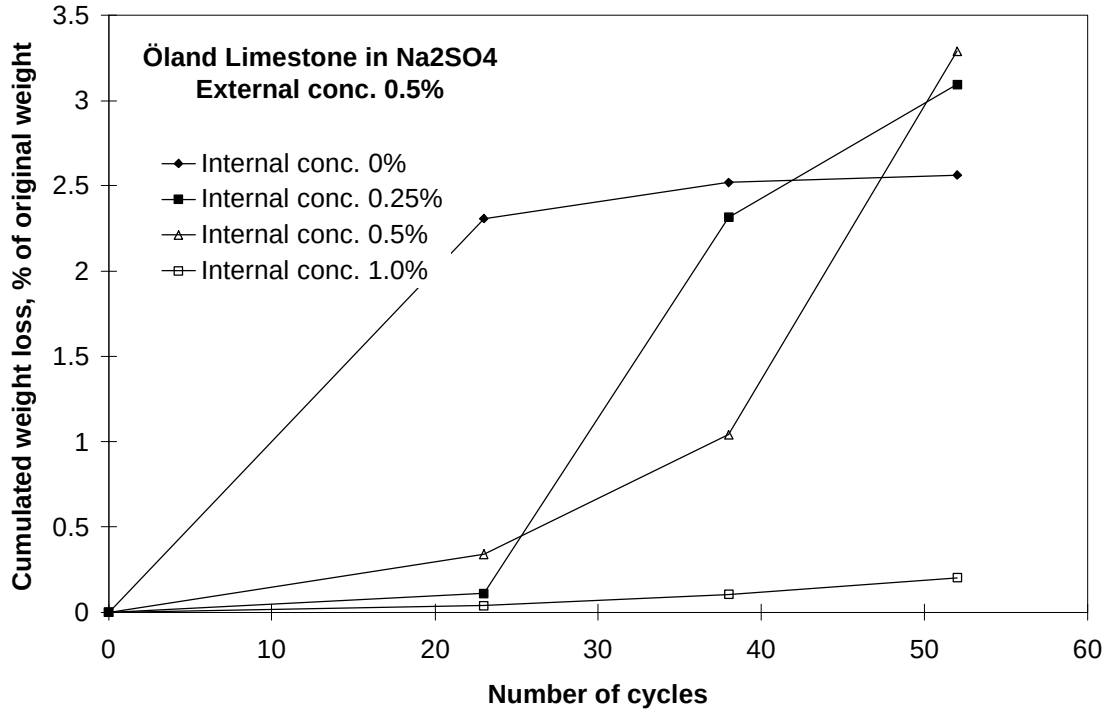

Figure J:31. Cumulated weight loss versus number of freeze-thaw cycles of limestone with various internal concentrations of $Na_2SO_4 \cdot 10\ H_2O$, and external concentration of 0.5% $Na_2SO_4 \cdot 10\ H_2O$.

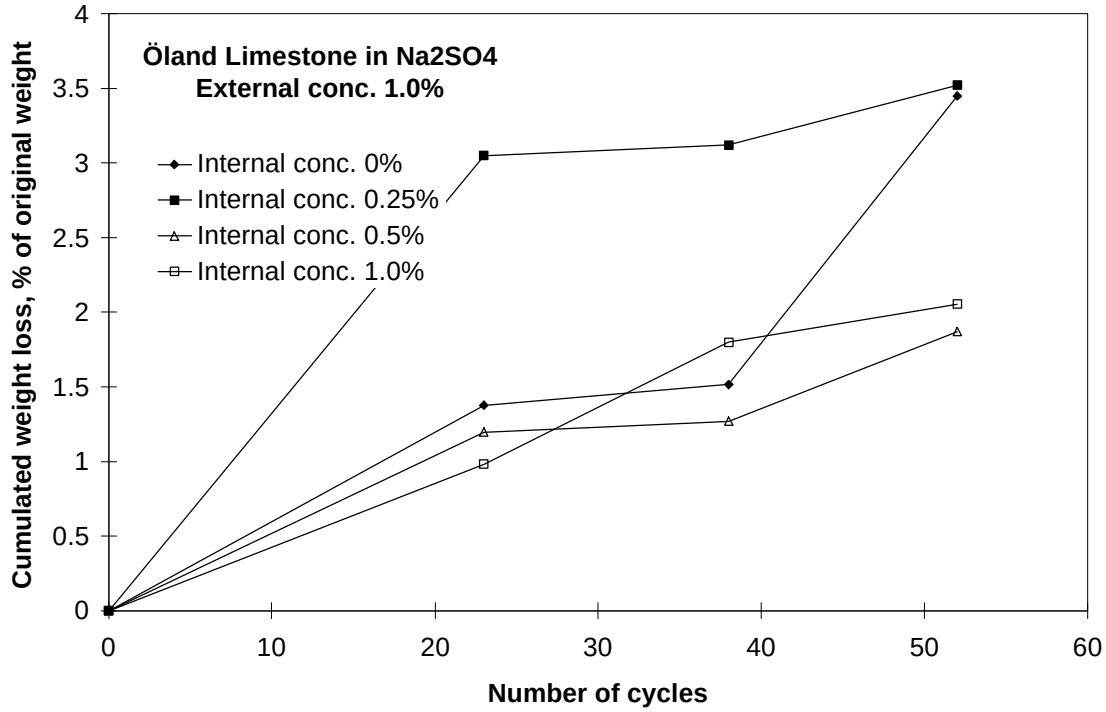

Figure J:32. Cumulated weight loss versus number of freeze-thaw cycles of limestone with various internal concentrations of $Na_2SO_4 \cdot 10\ H_2O$, and external concentration of 1.0% $Na_2SO_4 \cdot 10\ H_2O$.

Appendix K
Results of dilatation tests

The dilatation test is described in Chapter 3.7. The numbers in the graphs describe the method of moisture conditioning of the samples before freezing. The meaning of the numbers is described in table K.1 (below).

Table K.1. Moisture conditioning of dilatation samples

Number	Treatment	Approximate degree of saturation
1	Submerged in solution for 1 day	0.69
2	Submerged in solution for 7 days	0.82
3	Submerged in solution for 21 days	0.88
4	Submerged in solution for 3 months	S~1.0
5	Absorption following evacuation to about 280 mbar	0.94
6	Absorption following evacuation to about 250 mbar	0.97
7	Absorption following evacuation about 1 mbar (≈ total vacuum)	1.0

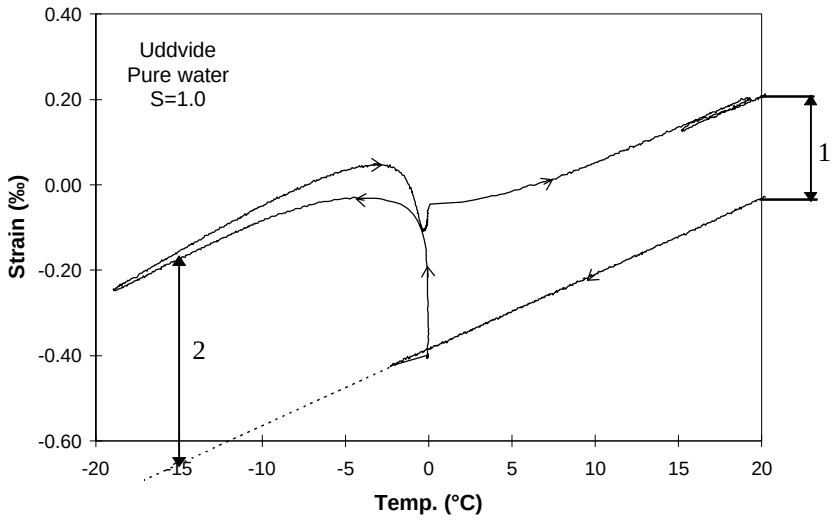

Figure K:1. Definition of permanent (1) and 'maximal' (2) dilatation. The 'maximal' dilatation is defined as the dilatation caused by ice formation at -15°C.

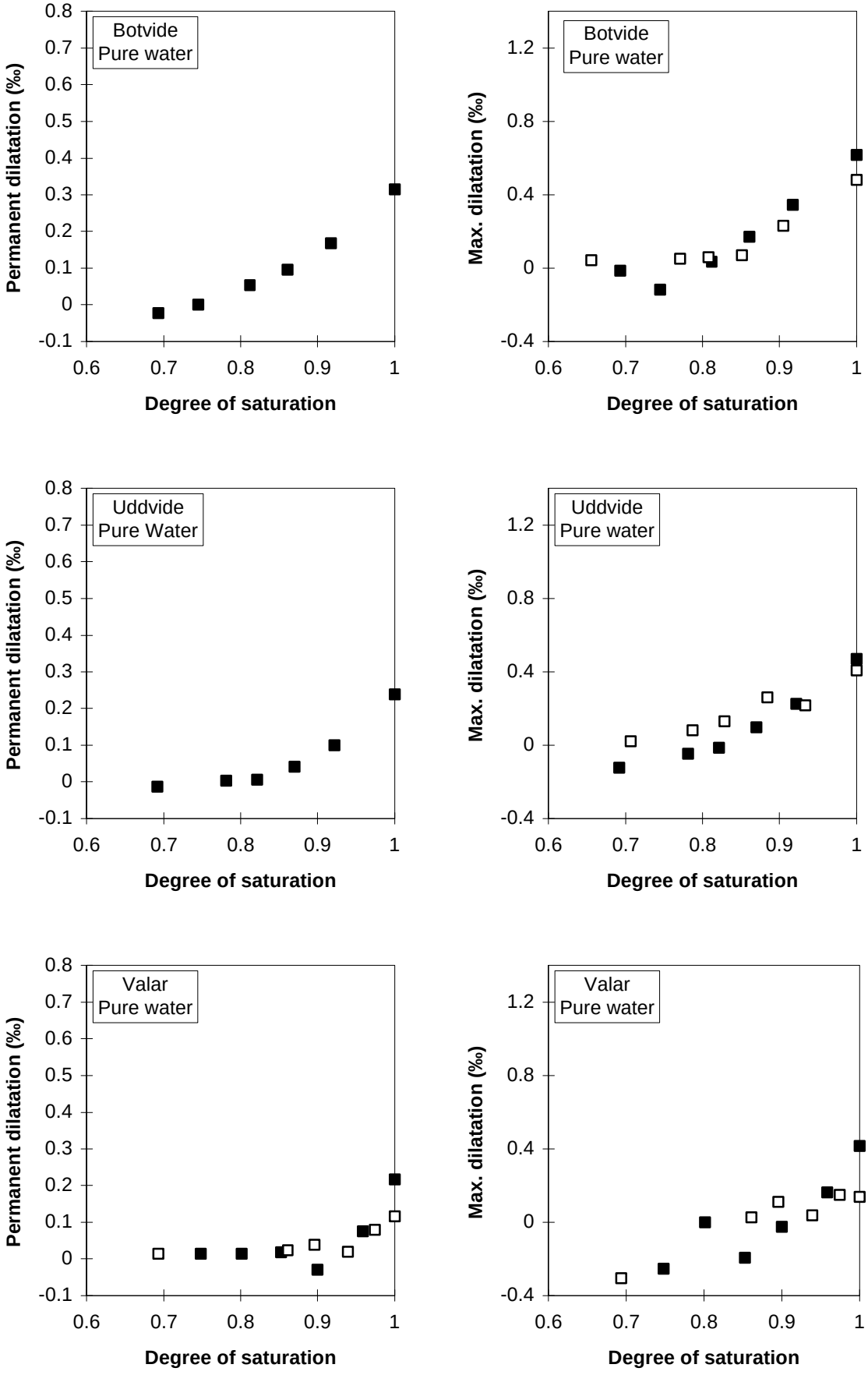

Figure K:2. The permanent and the 'maximal' dilatation versus the degree of saturation for sandstones frozen with pure water in the pore system.

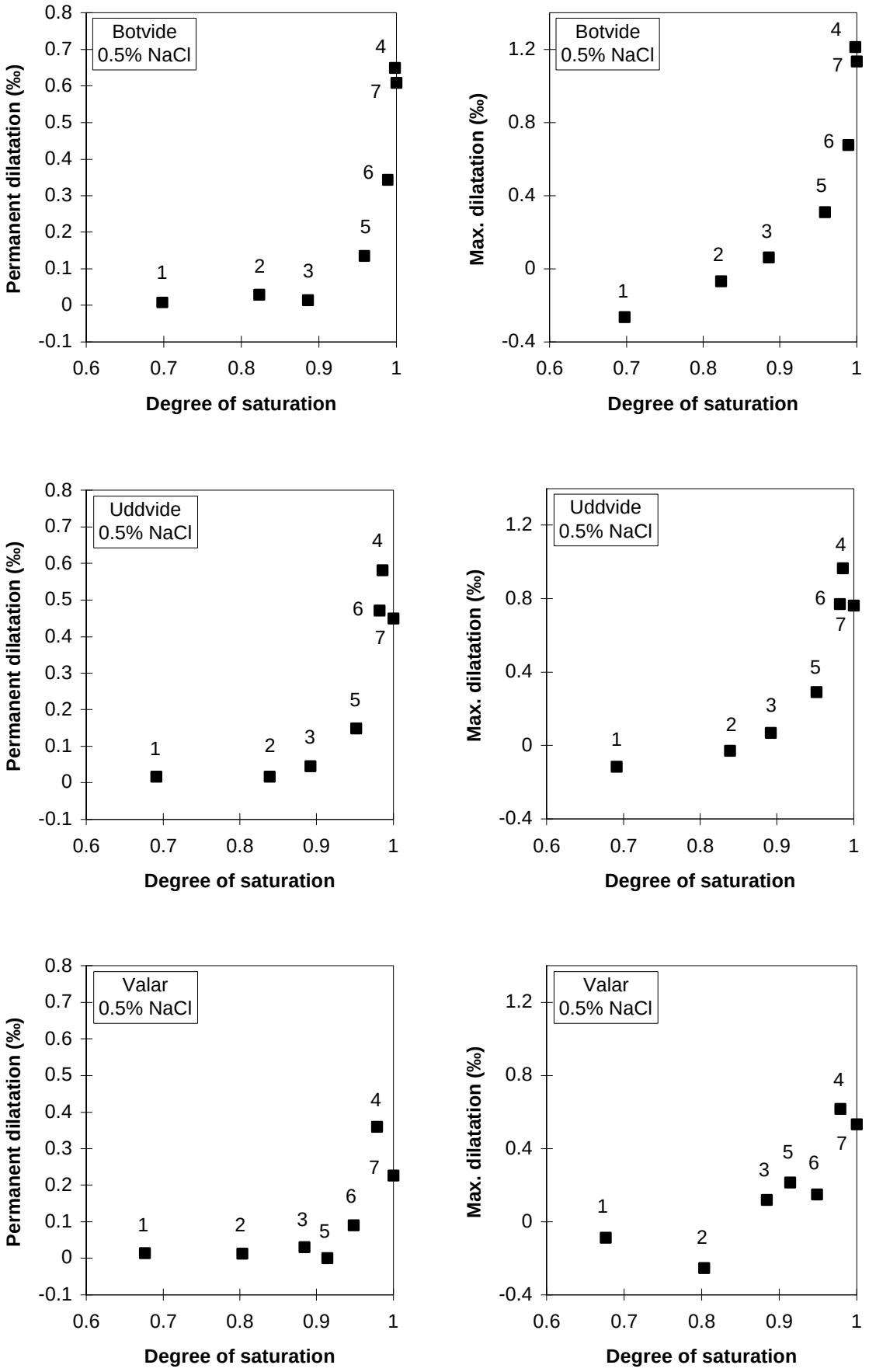

Figure K:3. The permanent and the 'maximal' dilatation versus the degree of saturation for sandstones frozen with a solution of 0.5% NaCl in the pore system.

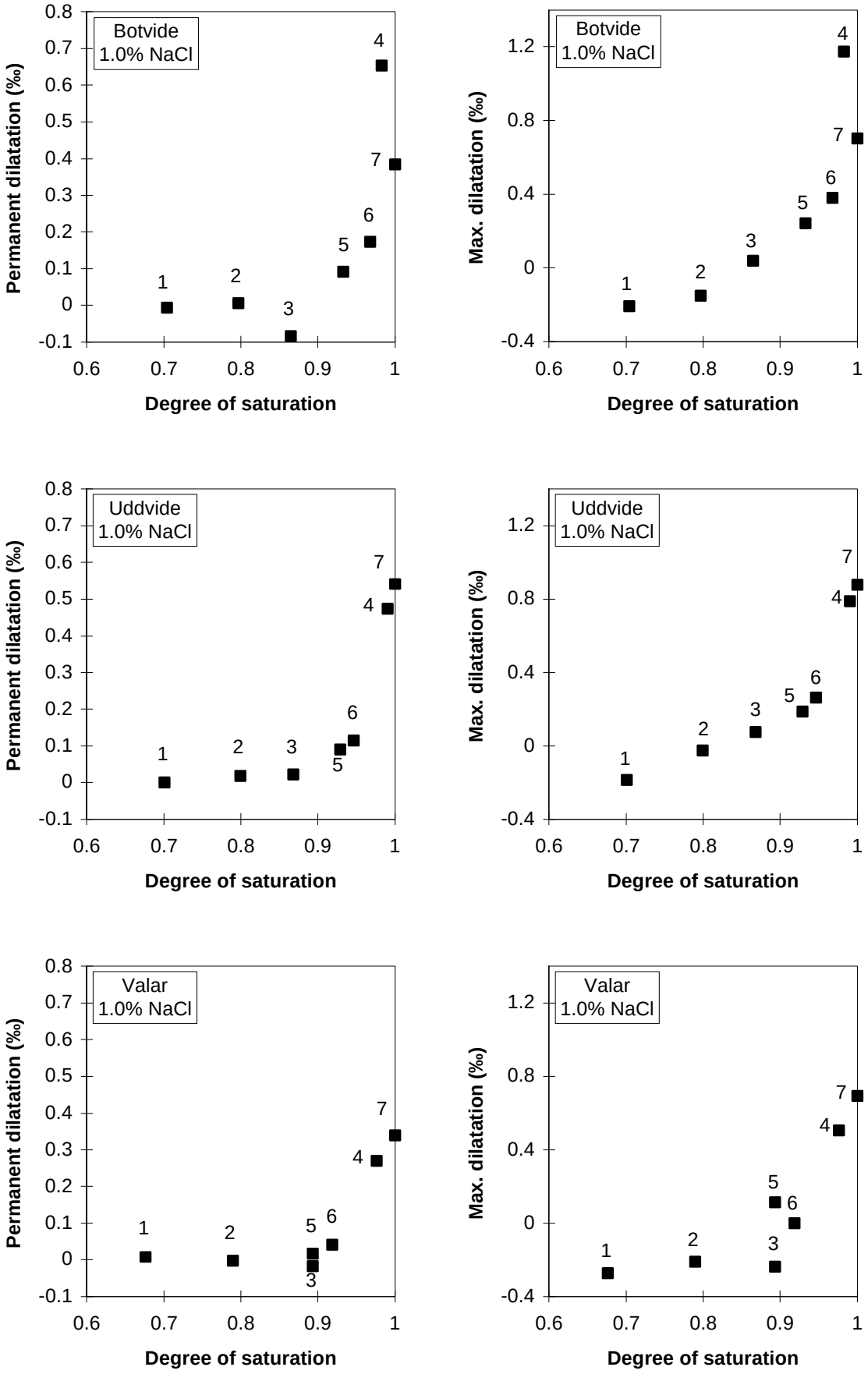

Figure K:4. The permanent and the 'maximal' dilatation versus the degree of saturation for sandstones frozen with a solution of 1.0% NaCl in the pore system.

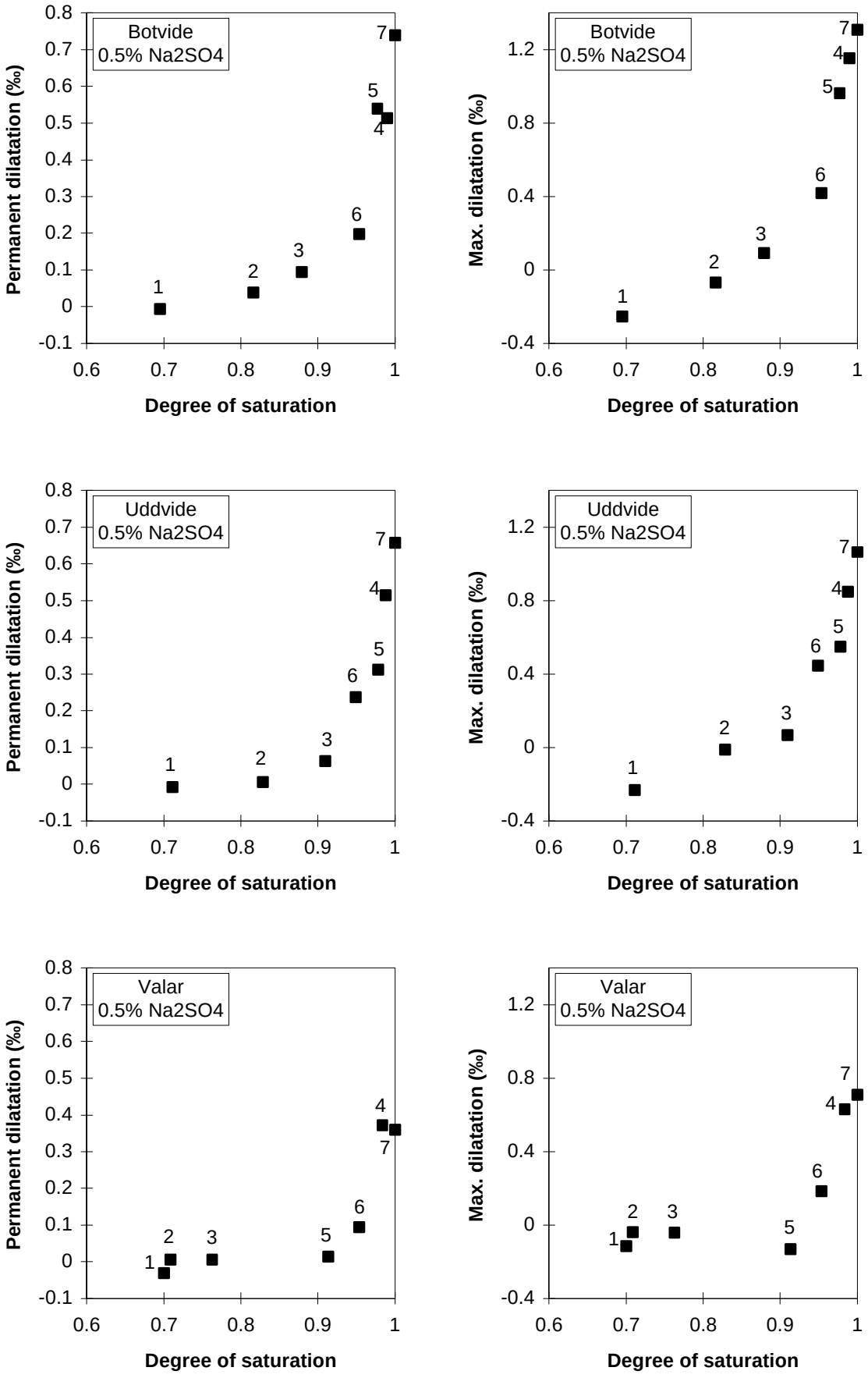

Figure K:5. The permanent and the 'maximal' dilatation versus the degree of saturation for sandstones frozen with 0.5% $Na_2SO_4 \cdot 10H_2O$ in the pore system.

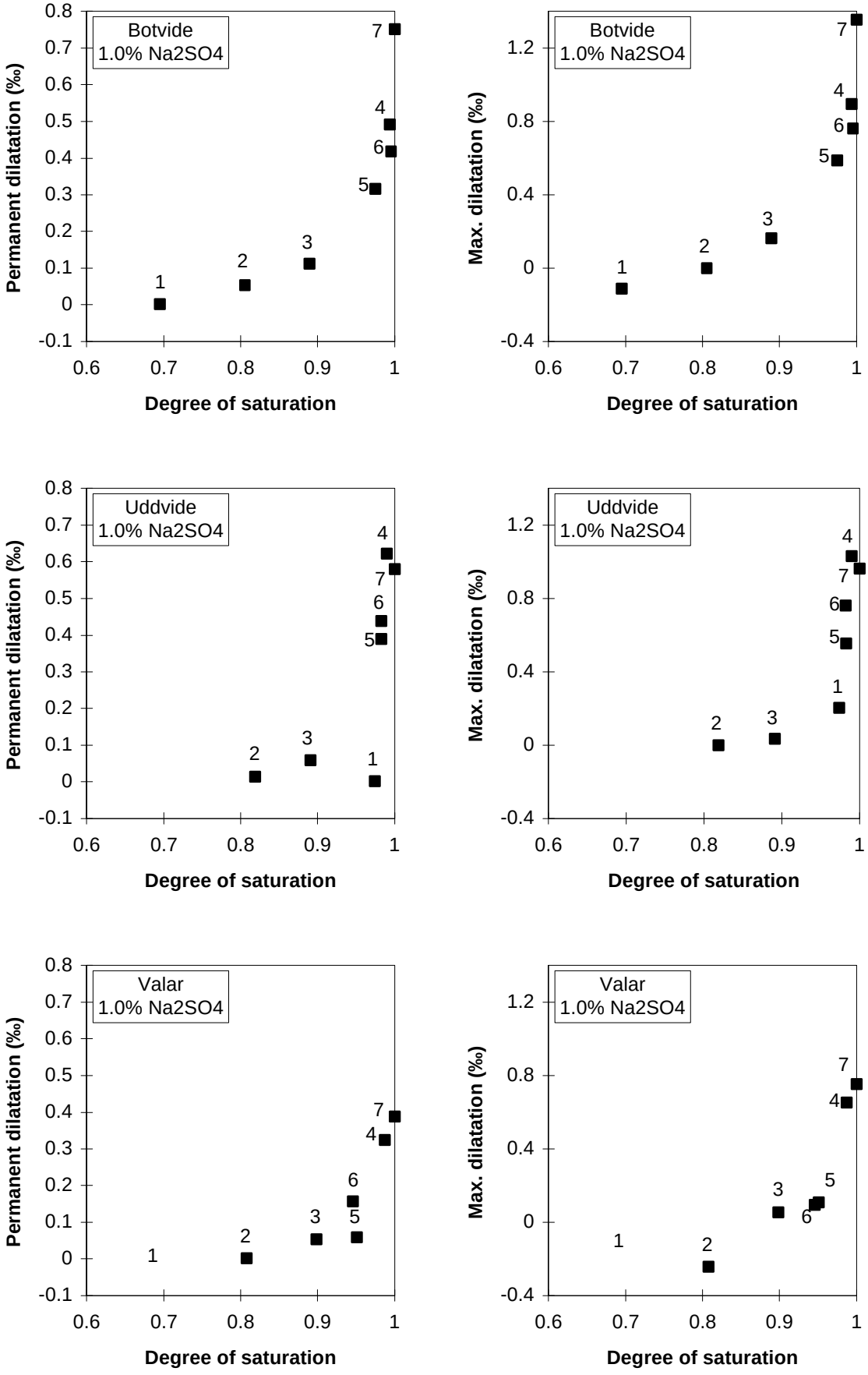

Figure K:6. The permanent and the 'maximal' dilatation versus the degree of saturation for sandstones frozen with 1.0% $Na_2SO_4 \cdot 10H_2O$ in the pore system.

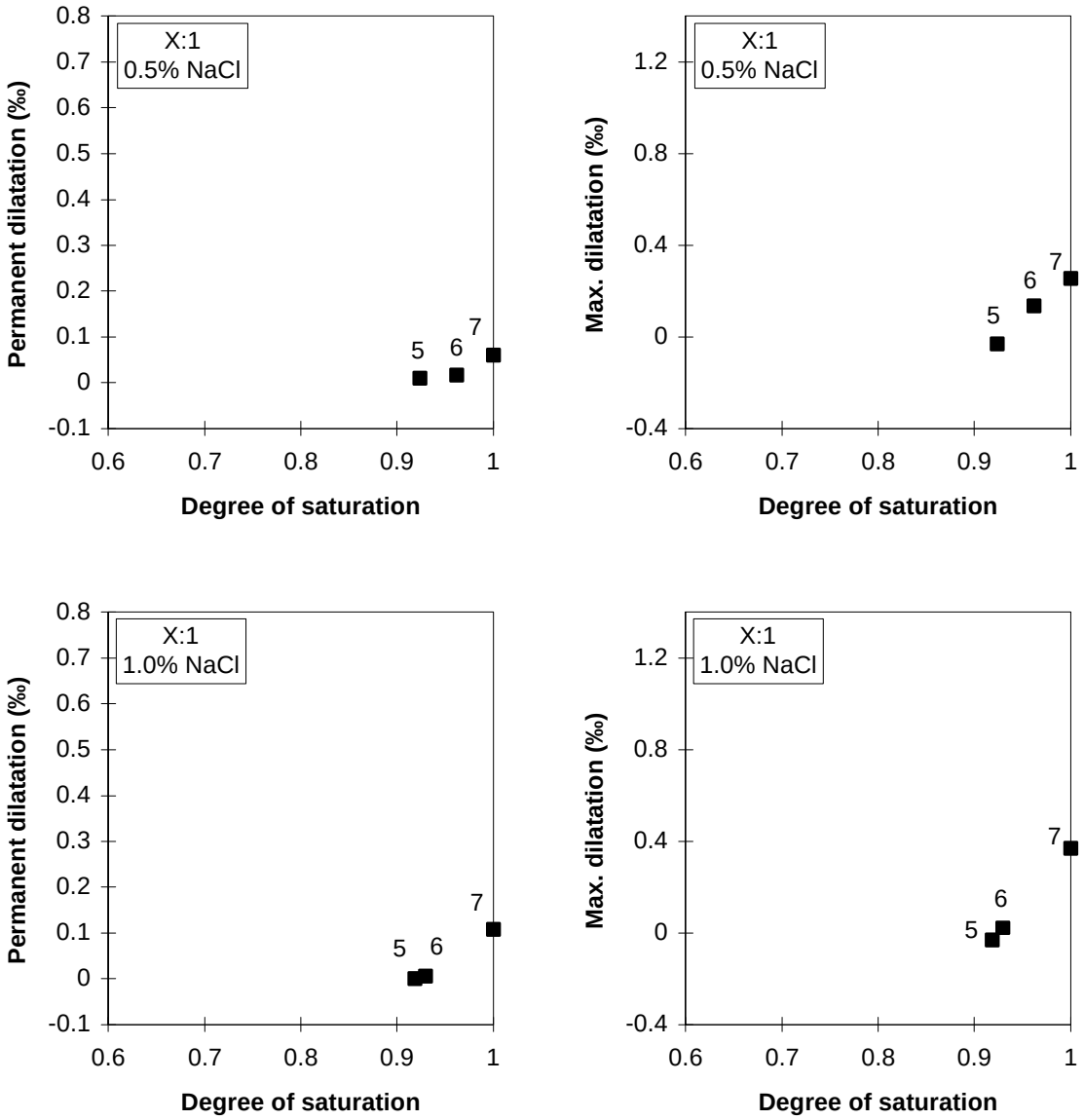

Figure K:7. The permanent and the 'maximal' dilatation versus the degree of saturation for the sandstone X:1 frozen with 0.5% and 1.0% NaCl in the pore system.

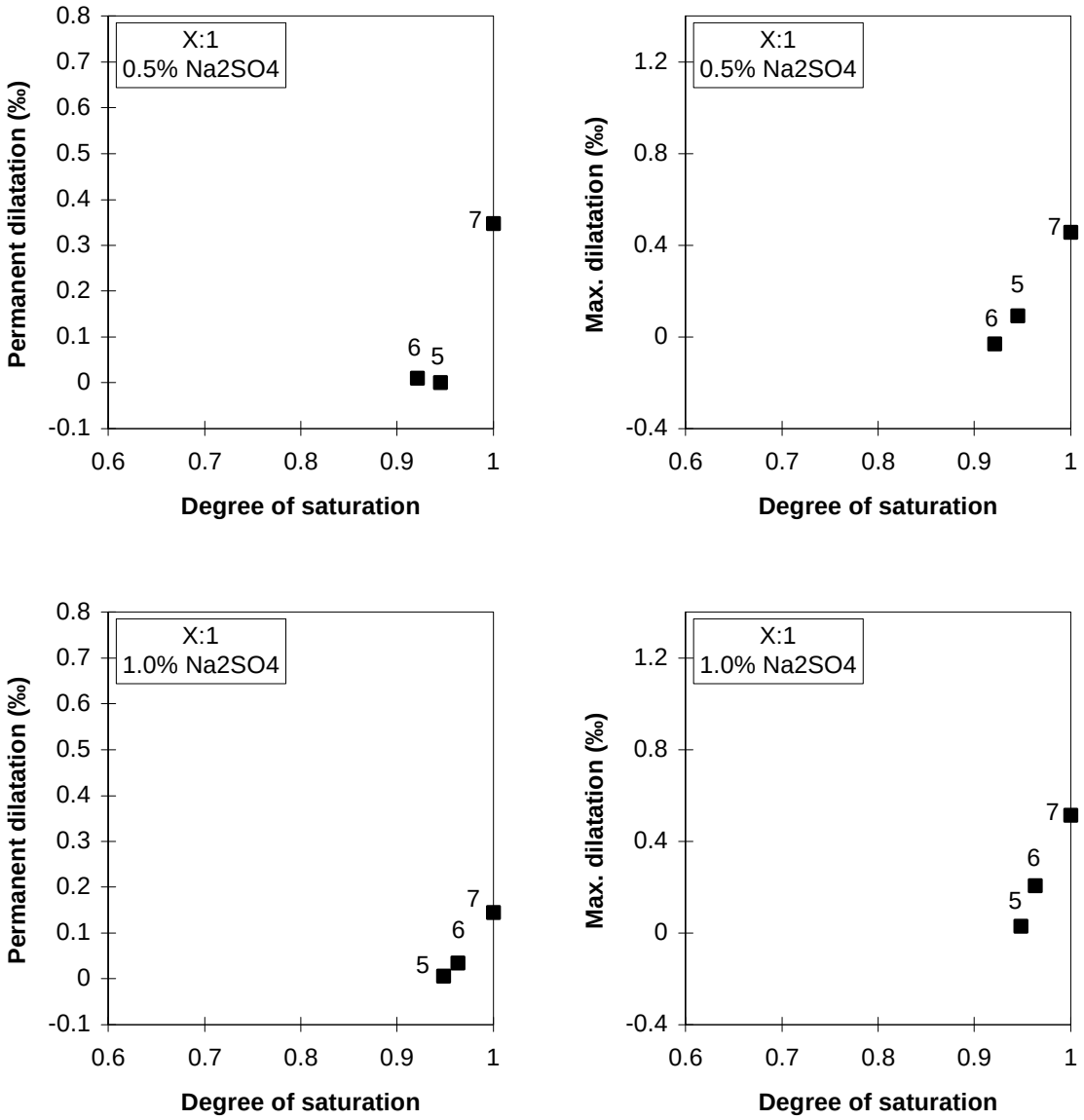

Figure K:8. The permanent and the 'maximal' dilatation versus the degree of saturation for the sandstone X:1 frozen with 0.5% and 1.0% $Na_2SO_4 \cdot 10H_2O$ in the pore system.

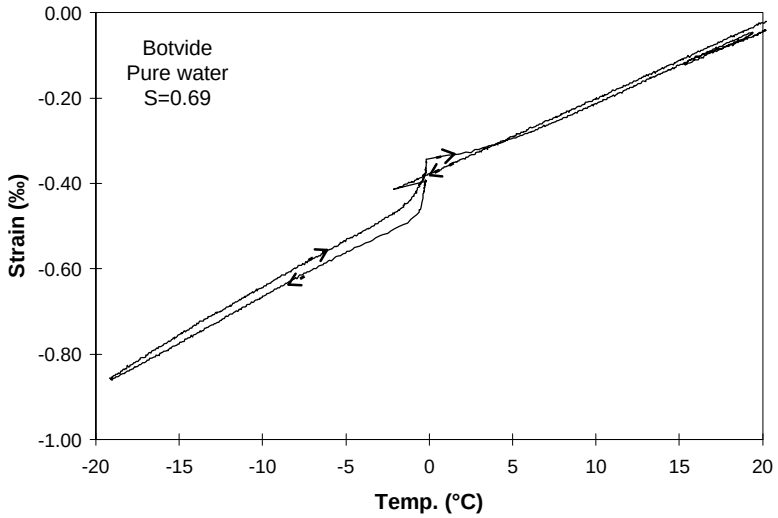

Figure K:9. Strain versus temperature of a Botvide sandstone with a degree of saturation of 0.69.

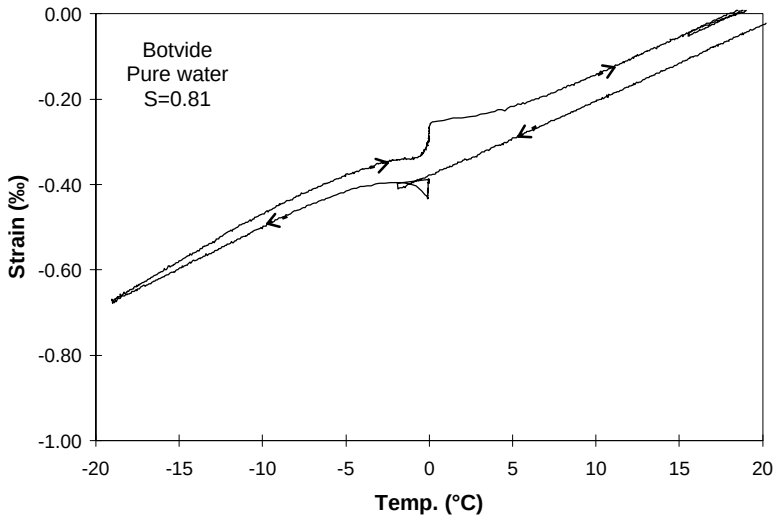

Figure K:10. Strain versus temperature of a Botvide sandstone with a degree of saturation of 0.81.

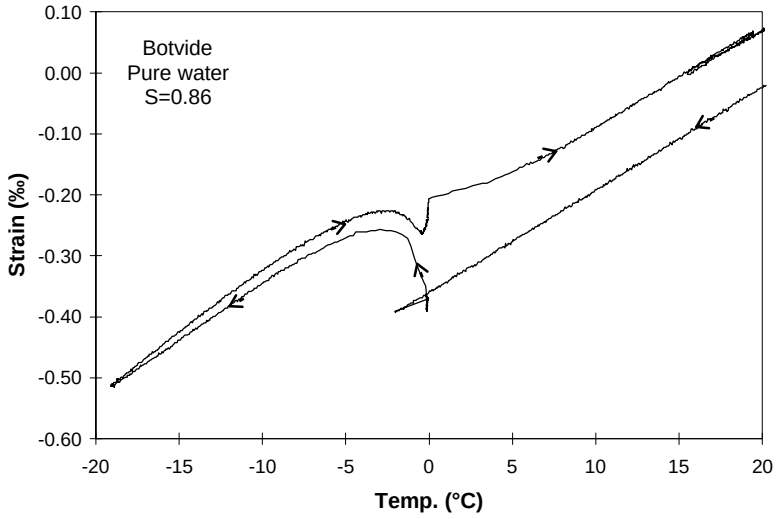

Figure K:11. Strain versus temperature of a Botvide sandstone with a degree of saturation of 0.86.

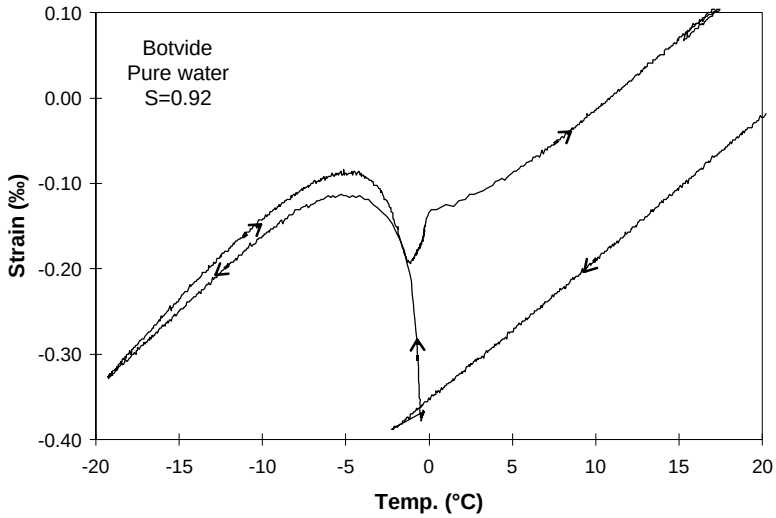

Figure K:12. Strain versus temperature of a Botvide sandstone with a degree of saturation of 0.92.

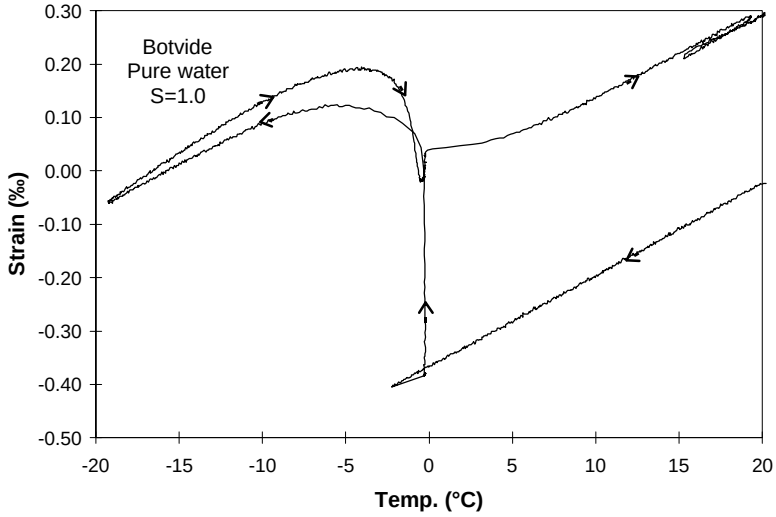

Figure K:13. Strain versus temperature of a Botvide sandstone with a degree of saturation of 1.0.

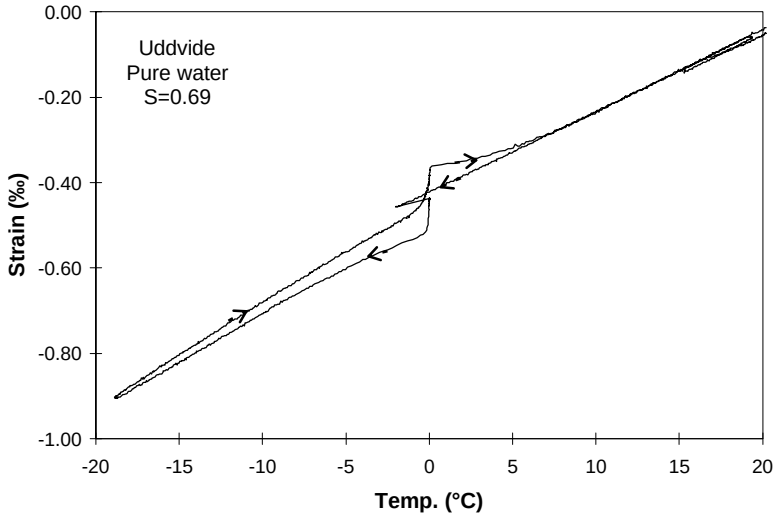

Figure K:14. Strain versus temperature of an Uddvide sandstone with a degree of saturation of 0.69.

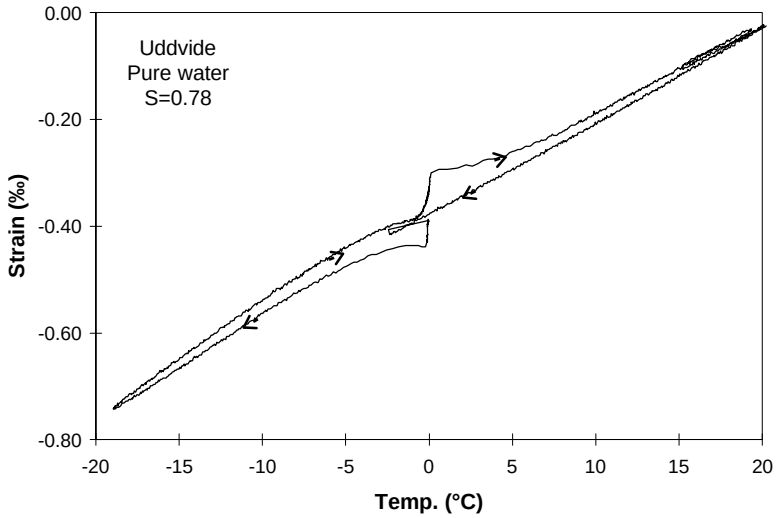

Figure K:15. Strain versus temperature of an Uddvide sandstone with a degree of saturation of 0.78.

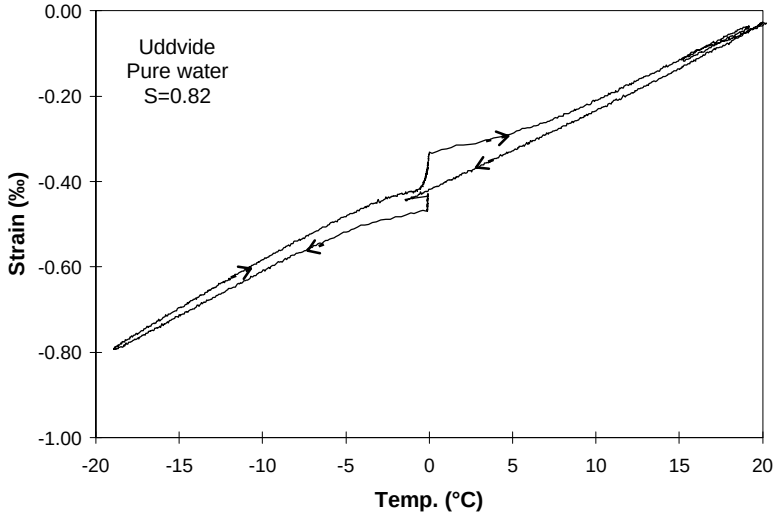

Figure K:16. Strain versus temperature of an Uddvide sandstone with a degree of saturation of 0.82.

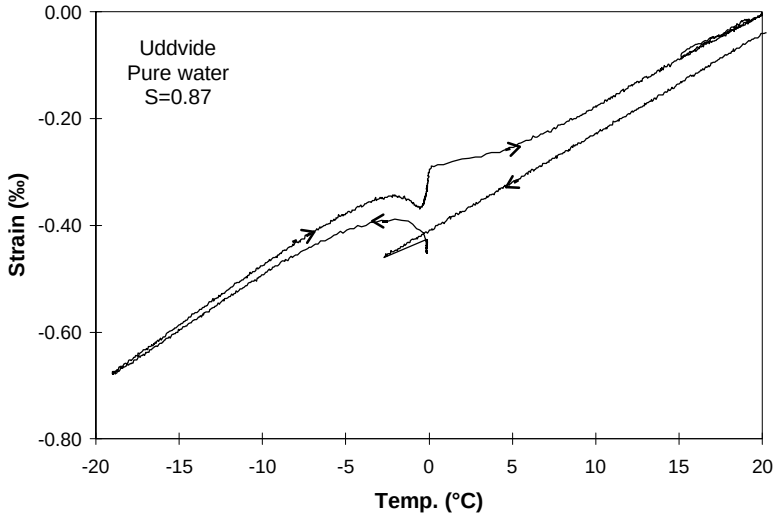

Figure K:17. Strain versus temperature of an Uddvide sandstone with a degree of saturation of 0.87.

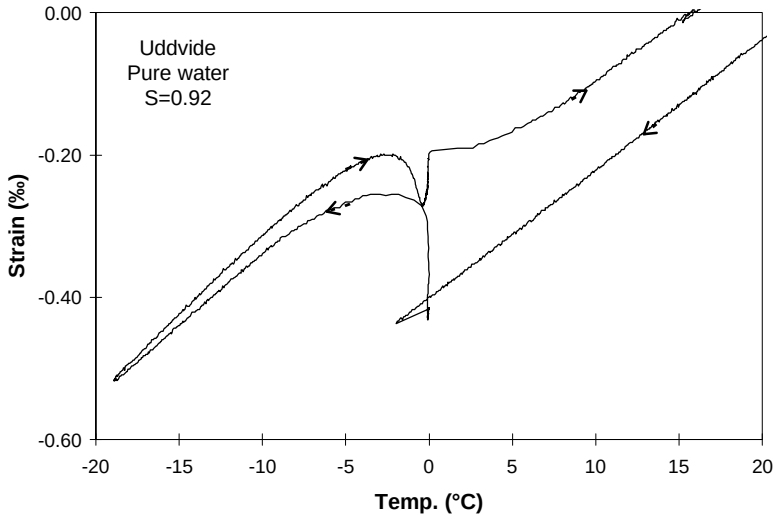

Figure K:18. Strain versus temperature of a Botvide sandstone with a degree of saturation of 0.92.

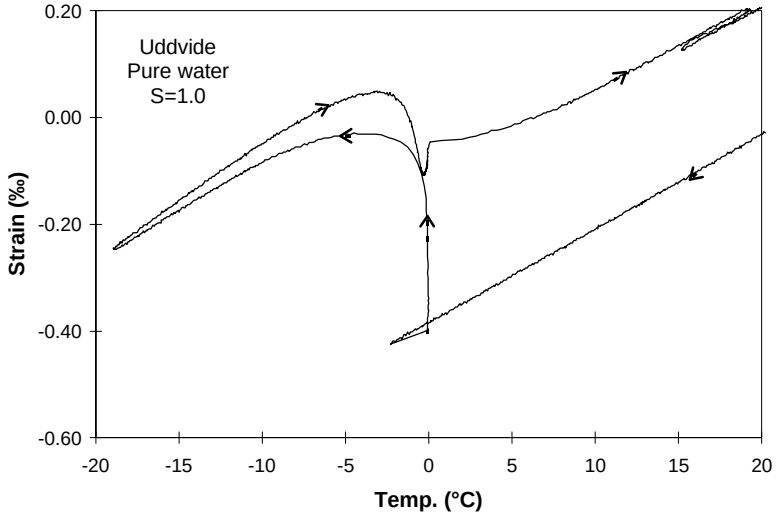

Figure K:19. Strain versus temperature of an Uddvide sandstone with a degree of saturation of 1.0.

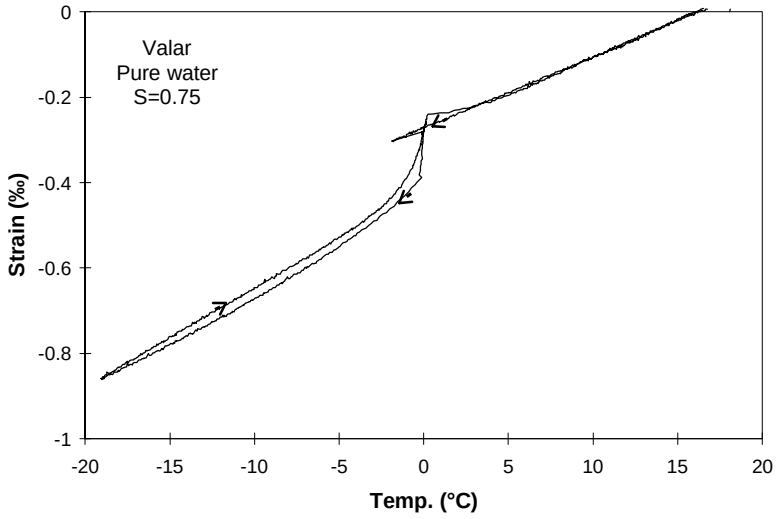

Figure K:20. Strain versus temperature of a Valar sandstone with a degree of saturation of 0.75.

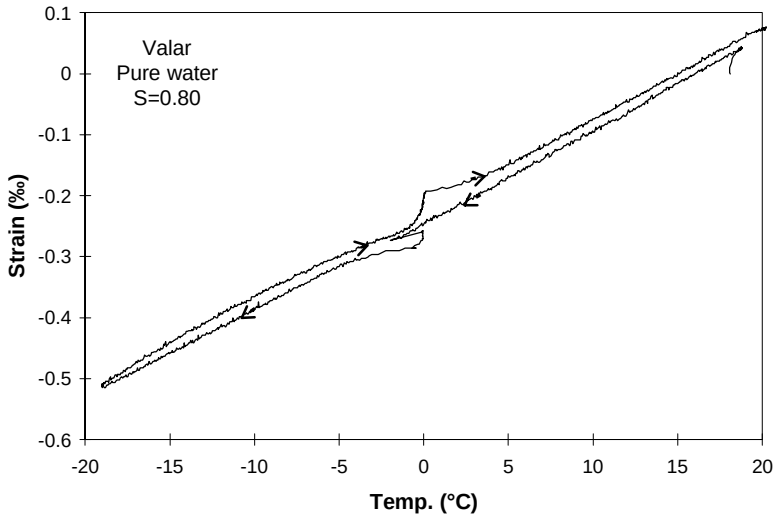

Figure K:21. Strain versus temperature of a Valar sandstone with a degree of saturation of 0.80.

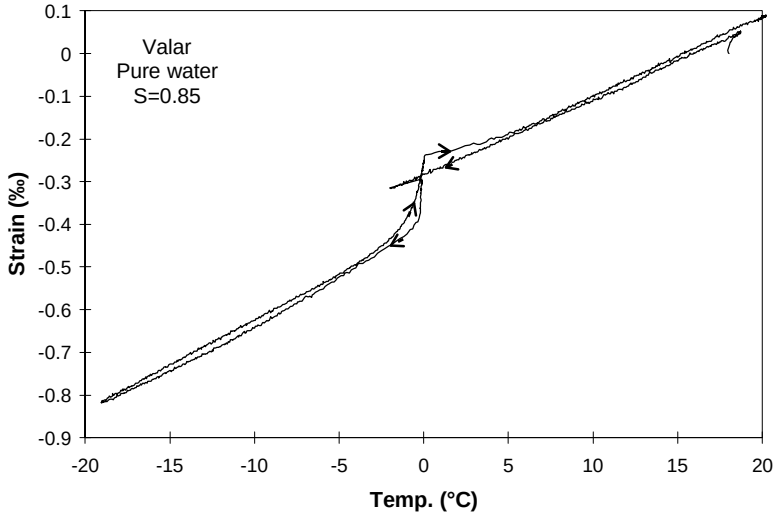

Figure K:22. Strain versus temperature of a Valar sandstone with a degree of saturation of 0.85.

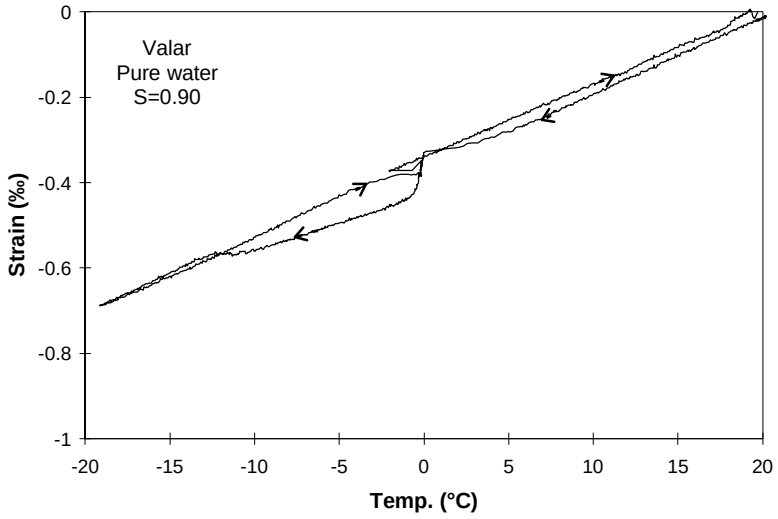

Figure K:23. Strain versus temperature of a Valar sandstone with a degree of saturation of 0.90.

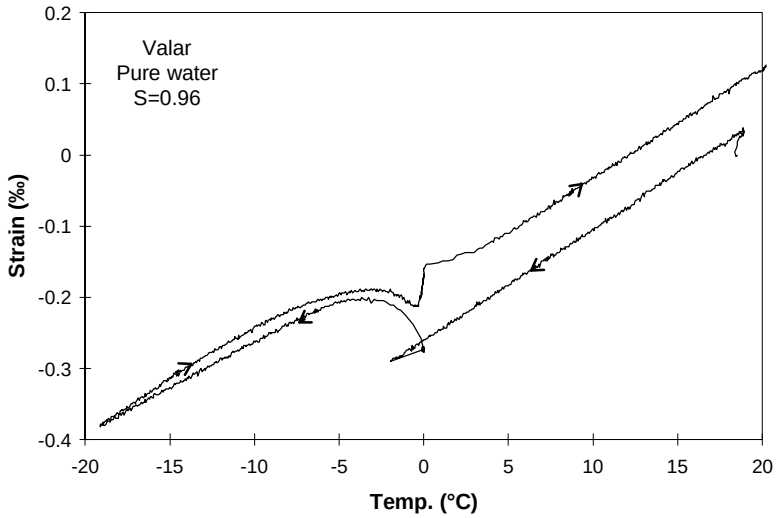

Figure K:24. Strain versus temperature of a Valar sandstone with a degree of saturation of 0.96.

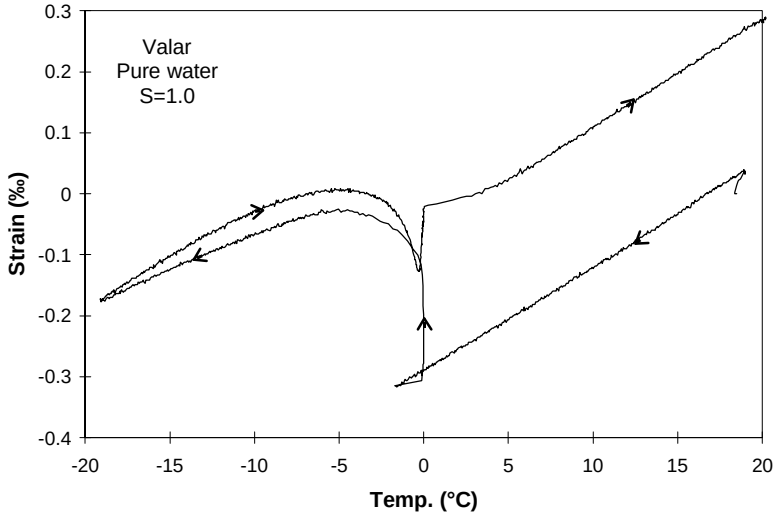

Figure K:25. Strain versus temperature of a Valar sandstone with a degree of saturation of 1.0.

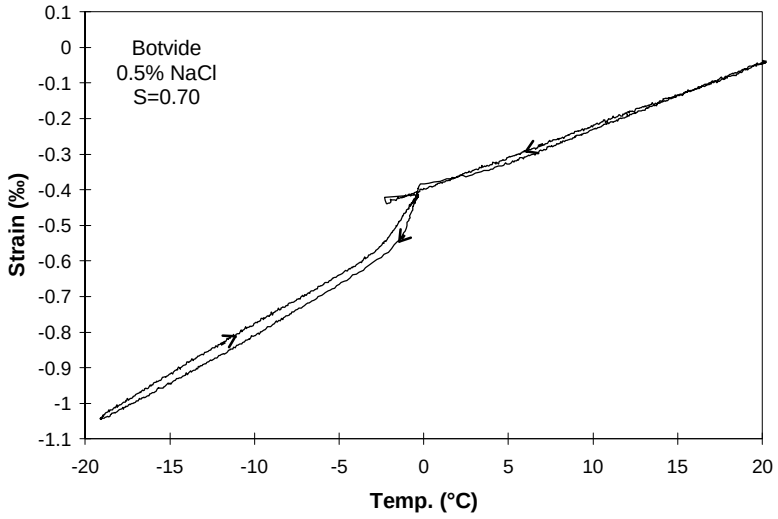

Figure K:26. Strain versus temperature of a Botvide sandstone with a degree of saturation of 0.70, conditioned by sucking a solution of 0.5% NaCl for one day.

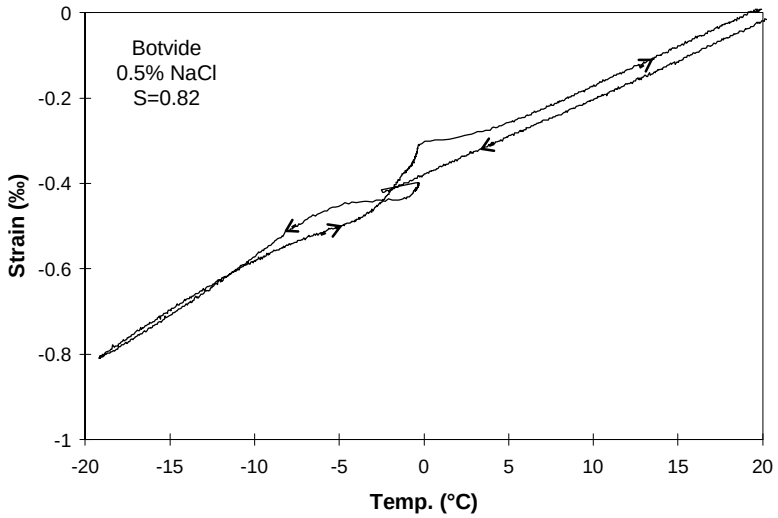

Figure K:27. Strain versus temperature of a Botvide sandstone with a degree of saturation of 0.82, conditioned by sucking a solution of 0.5% NaCl for 7 days

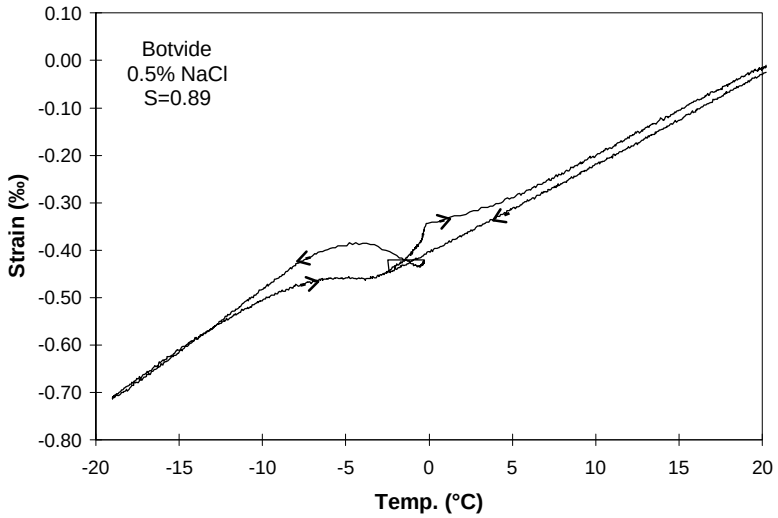

Figure K:28. Strain versus temperature of a Botvide sandstone with a degree of saturation of 0.89, conditioned by sucking a solution of 0.5% NaCl for 21 days.

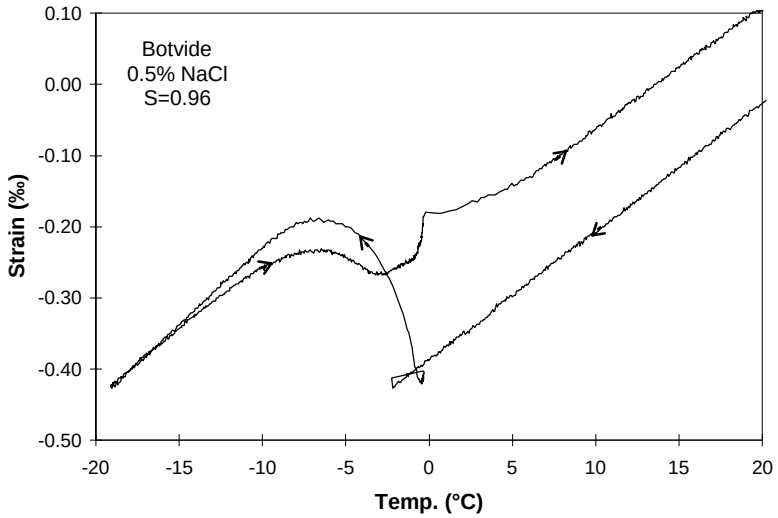

Figure K:29. Strain versus temperature of a Botvide sandstone with a degree of saturation of 0.96, conditioned by absorption of a 0.5% NaCl solution, following evacuation to about 280 mbar.

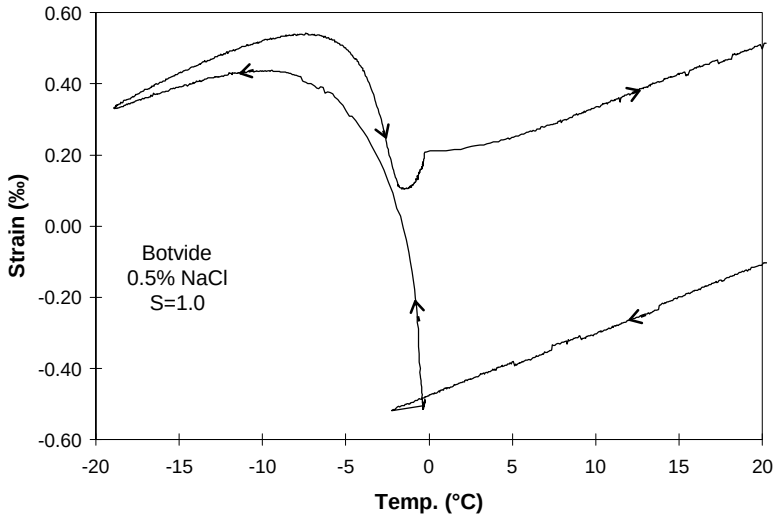

Figure K:30. Strain versus temperature of a Botvide sandstone with a degree of saturation of 1.0, conditioned by absorption of a 0.5% NaCl solution, following evacuation to about 1 mbar (vacuum).

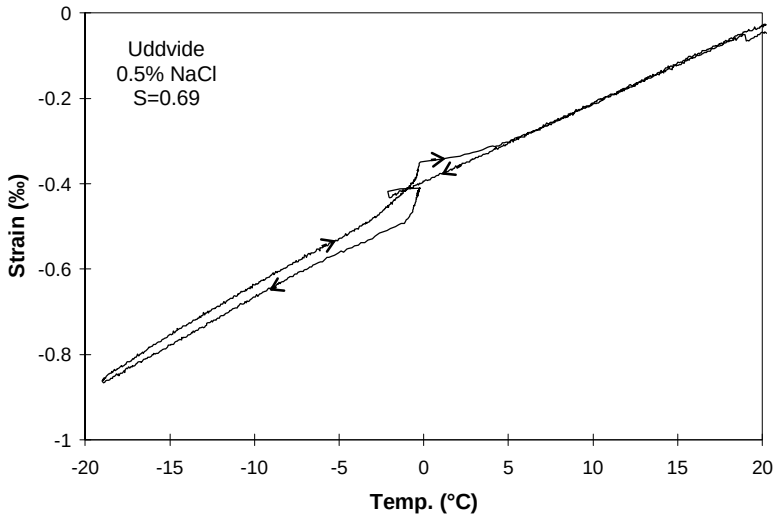

Figure K:31. Strain versus temperature of an Uddvide sandstone with a degree of saturation of 0.69, conditioned by sucking a solution of 0.5% NaCl for one day.

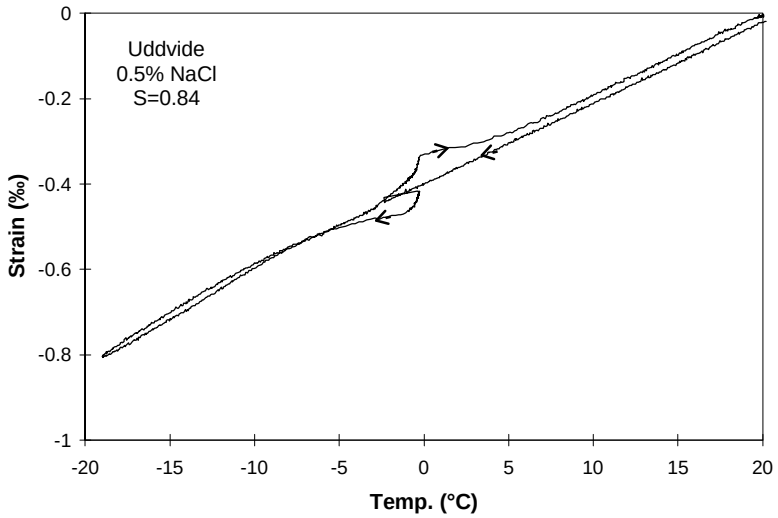

Figure K:32. Strain versus temperature of an Uddvide sandstone with a degree of saturation of 0.84, conditioned by sucking a solution of 0.5% NaCl for 7 days.

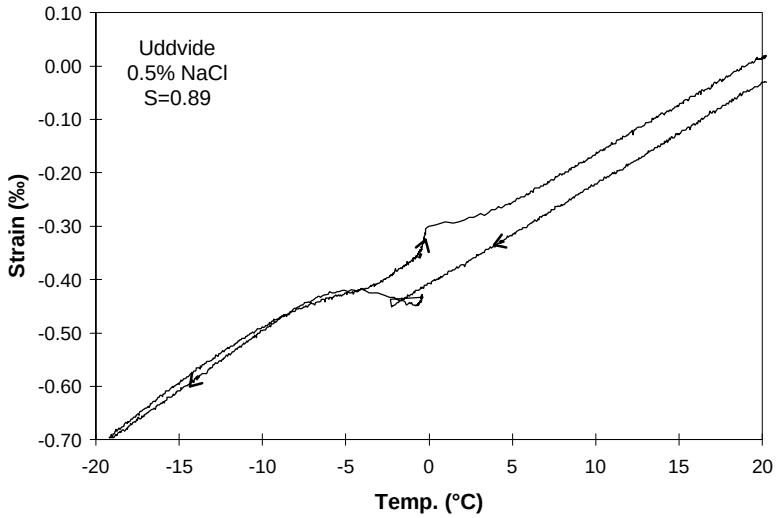

Figure K:33. Strain versus temperature of an Uddvide sandstone with a degree of saturation of 0.89, conditioned by sucking a solution of 0.5% NaCl for 21 days.

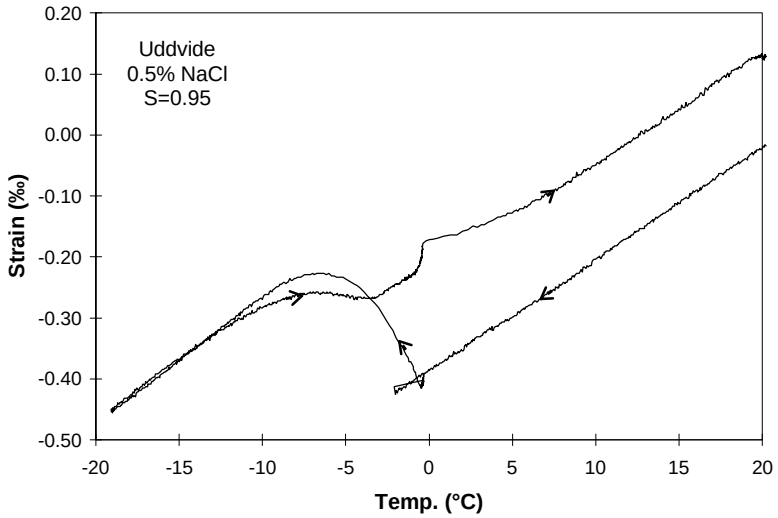

Figure K:34. Strain versus temperature of an Uddvide sandstone with a degree of saturation of 0.95, conditioned by absorption of a 0.5% NaCl solution, following evacuation to about 280 mbar.

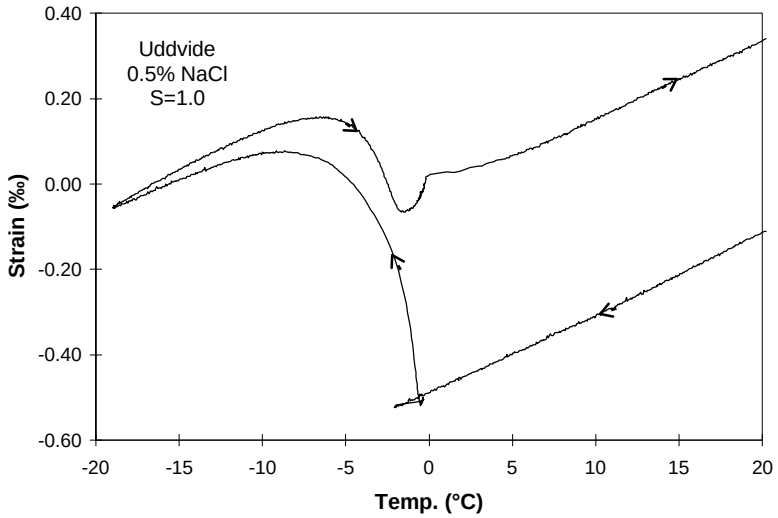

Figure K:35. Strain versus temperature of an Uddvide sandstone with a degree of saturation of 1.0, conditioned by absorption of a 0.5% NaCl solution, following evacuation to about 1 mbar (vacuum).

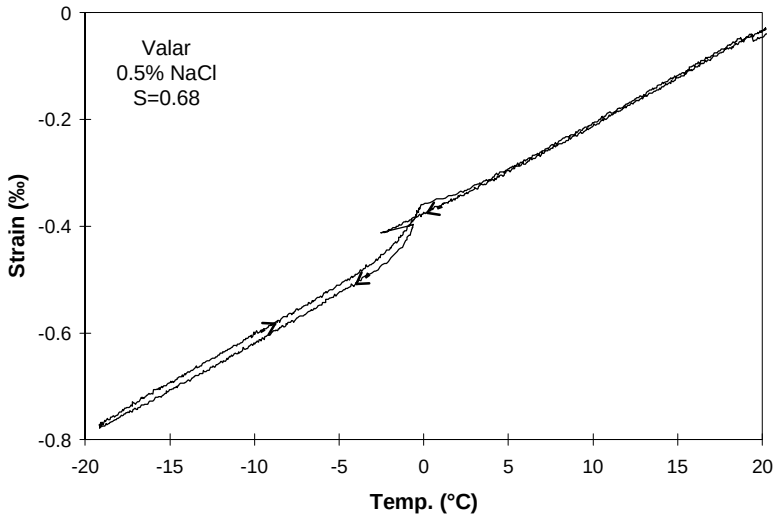

Figure K:36. Strain versus temperature of a Valar sandstone with a degree of saturation of 0.68, conditioned by sucking a solution of 0.5% NaCl for one day.

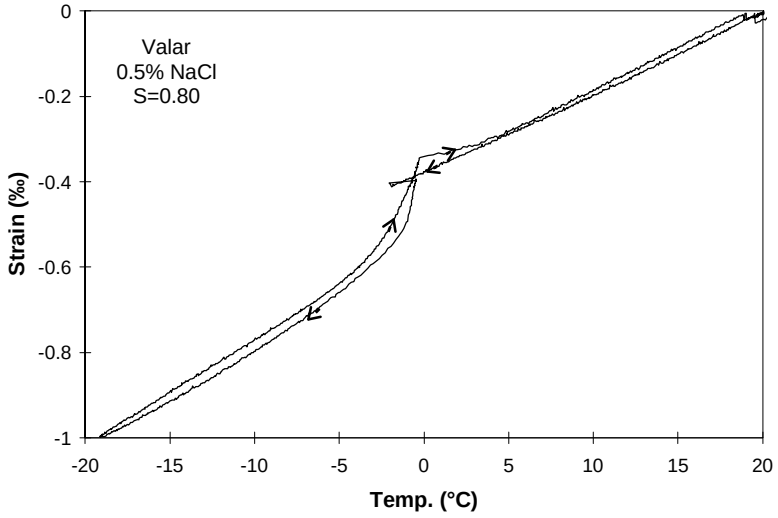

Figure K:37. Strain versus temperature of a Valar sandstone with a degree of saturation of 0.80, conditioned by sucking a solution of 0.5% NaCl for 7 days.

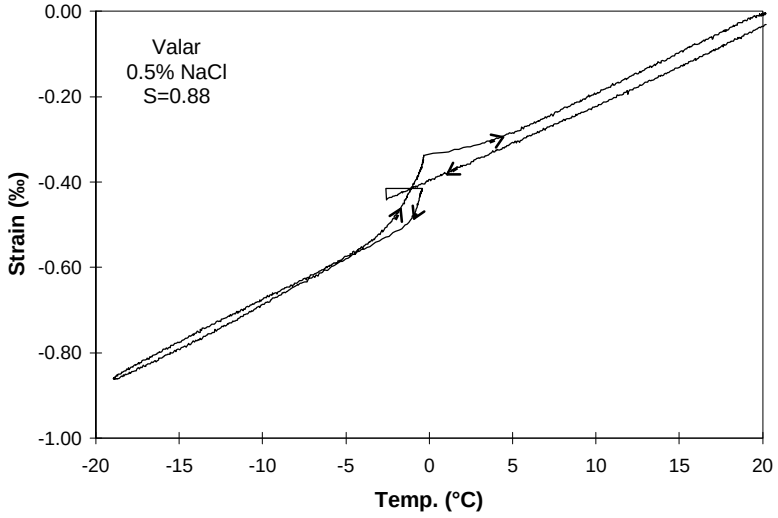

Figure K:38. Strain versus temperature of a Valar sandstone with a degree of saturation of 0.88, conditioned by sucking a solution of 0.5% NaCl for 21 days.

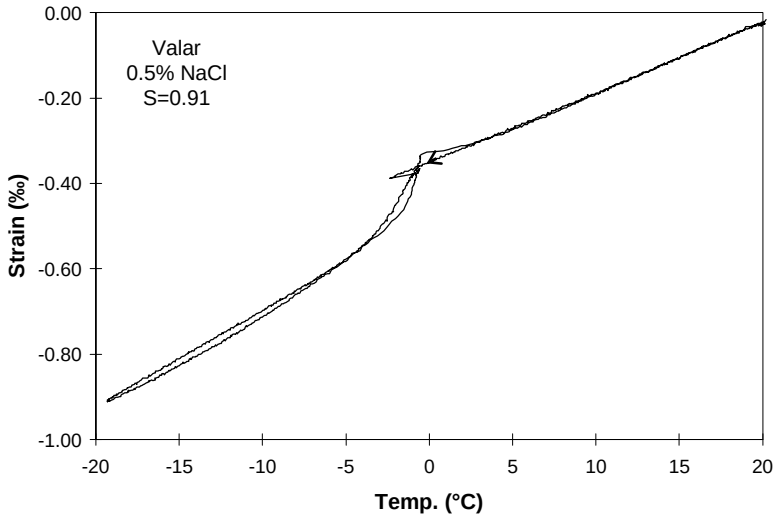

Figure K:39. Strain versus temperature of a Valar sandstone with a degree of saturation of 0.91, conditioned by absorption of a 0.5% NaCl solution, following evacuation to about 280 mbar.

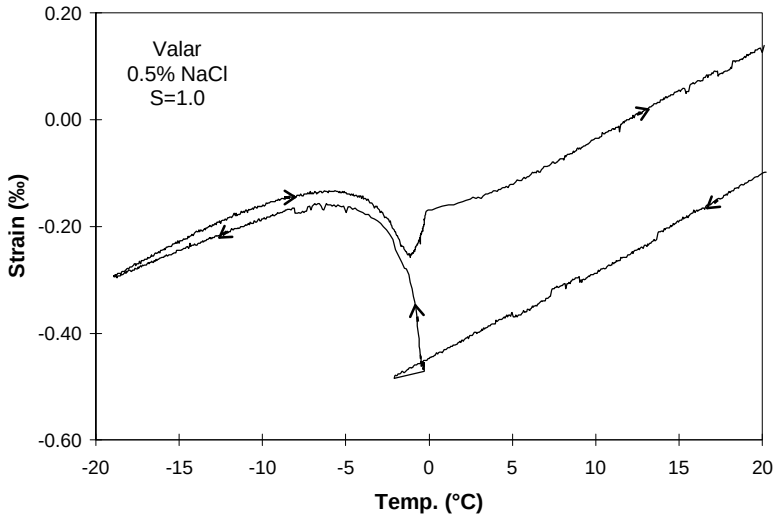

Figure K:40. Strain versus temperature of a Valar sandstone with a degree of saturation of 1.0, conditioned by absorption of a 0.5% NaCl solution, following evacuation to about 1 mbar (vacuum).

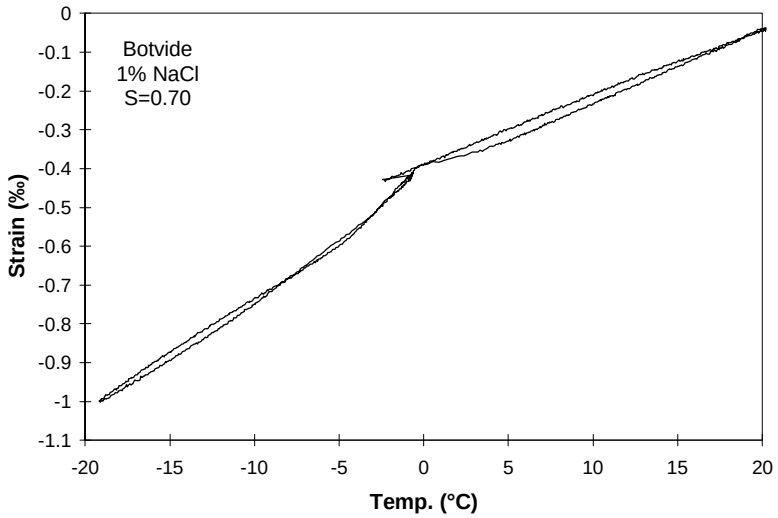

Figure K:41. Strain versus temperature of a Botvide sandstone with a degree of saturation of 0.70, conditioned by sucking a solution of 1.0% NaCl for one day.

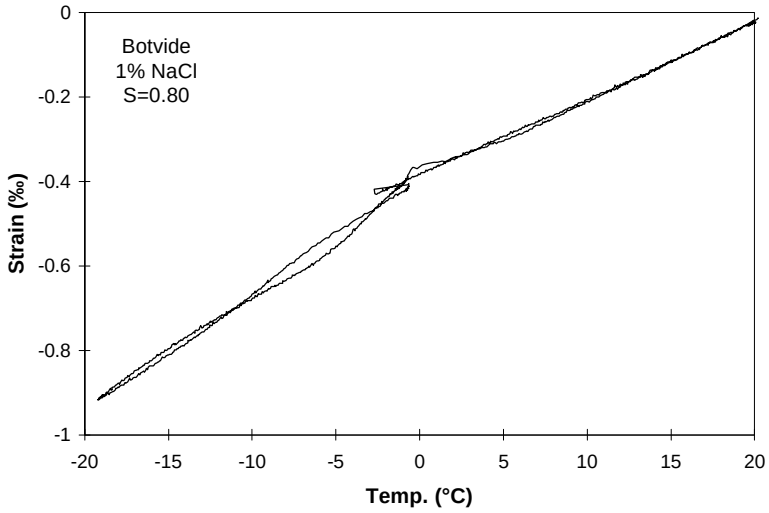

Figure K:42. Strain versus temperature of a Botvide sandstone with a degree of saturation of 0.80, conditioned by sucking a solution of 1.0% NaCl for 7 days.

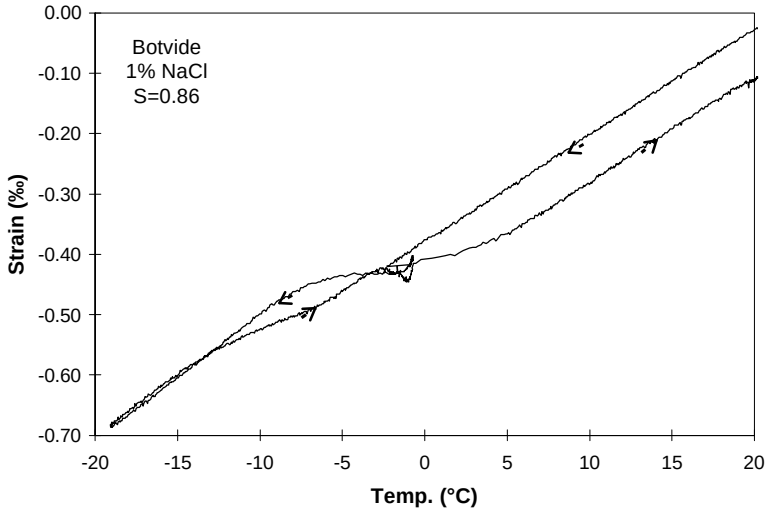

Figure K:43. Strain versus temperature of a Botvide sandstone with a degree of saturation of 0.86, conditioned by sucking a solution of 1.0% NaCl for 21

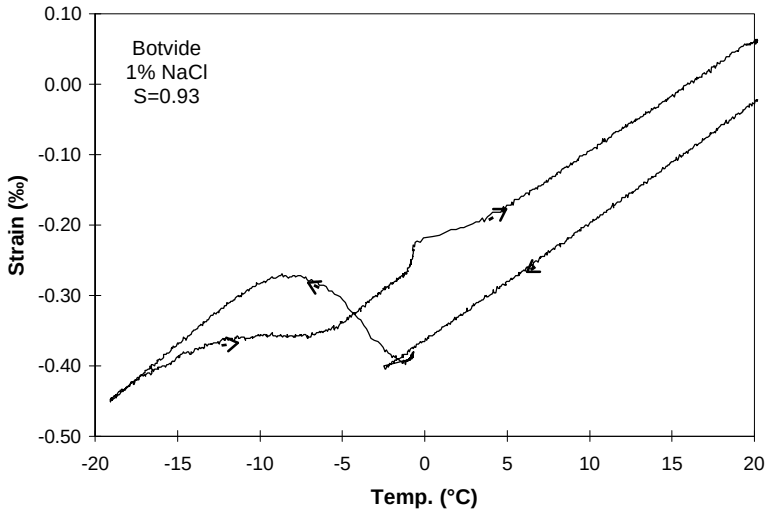

Figure K:44. Strain versus temperature of a Botvide sandstone with a degree of saturation of 0.93, conditioned by absorption of a 1.0% NaCl solution, following evacuation to about 280 mbar.

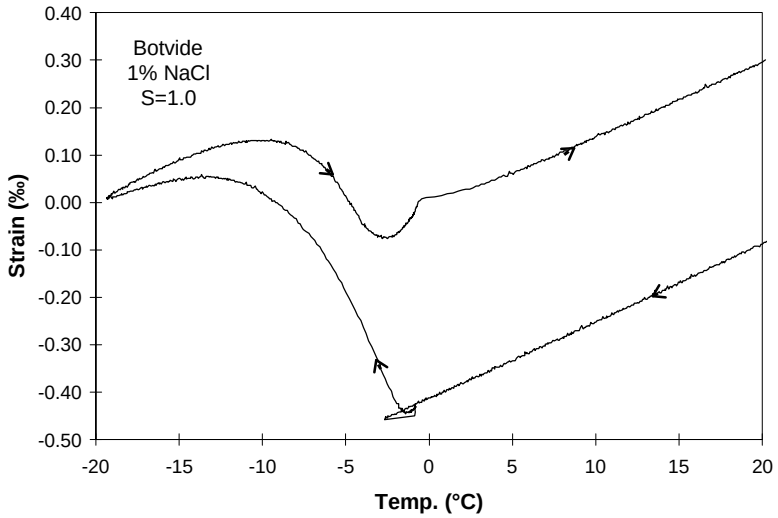

Figure K:45. Strain versus temperature of a Botvide sandstone with a degree of saturation of 1.0, conditioned by absorption of a 1.0% NaCl solution, following evacuation to about 1 mbar (vacuum).

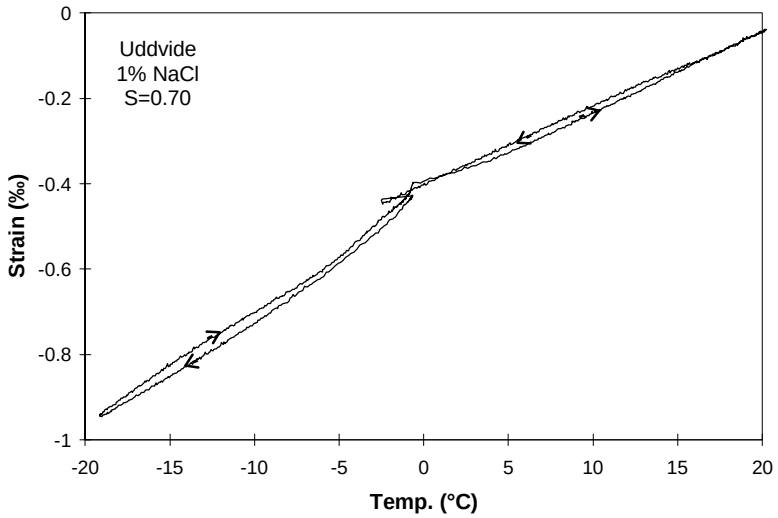

Figure K:46. Strain versus temperature of an Uddvide sandstone with a degree of saturation of 0.70, conditioned by sucking a solution of 1.0% NaCl for one day.

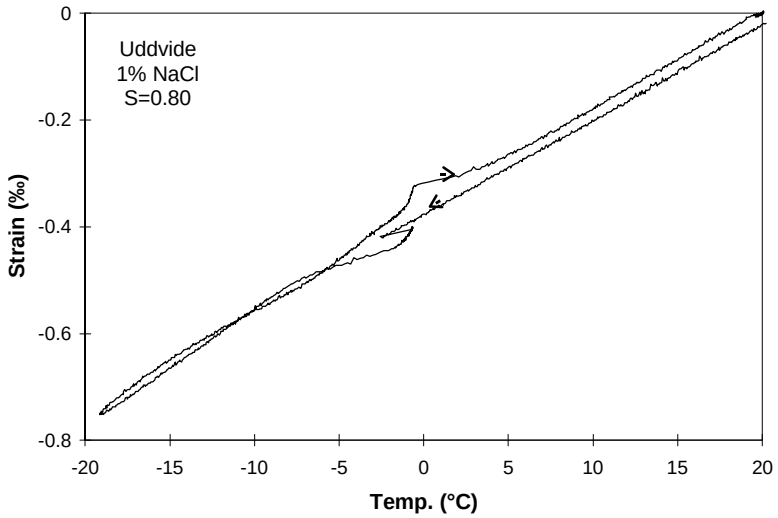

Figure K:47. Strain versus temperature of an Uddvide sandstone with a degree of saturation of 0.80, conditioned by sucking a solution of 1.0% NaCl for 7 days.

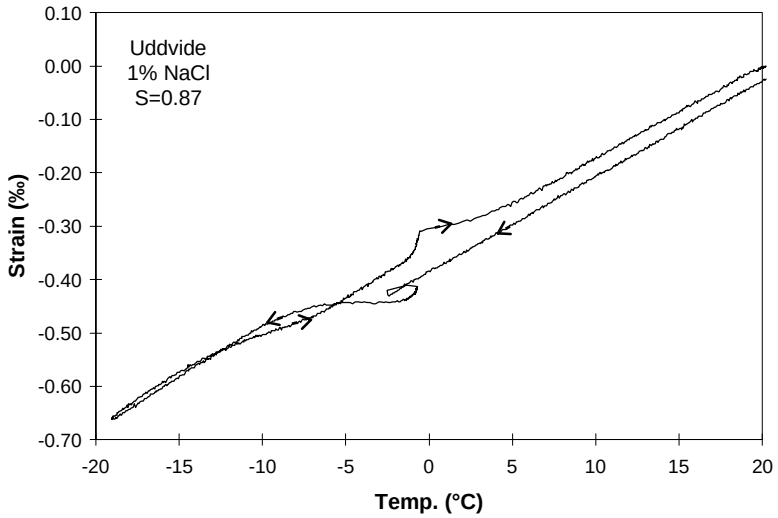

Figure K:48. Strain versus temperature of an Uddvide sandstone with a degree of saturation of 0.87, conditioned by sucking a solution of 1.0% NaCl for 21 days.

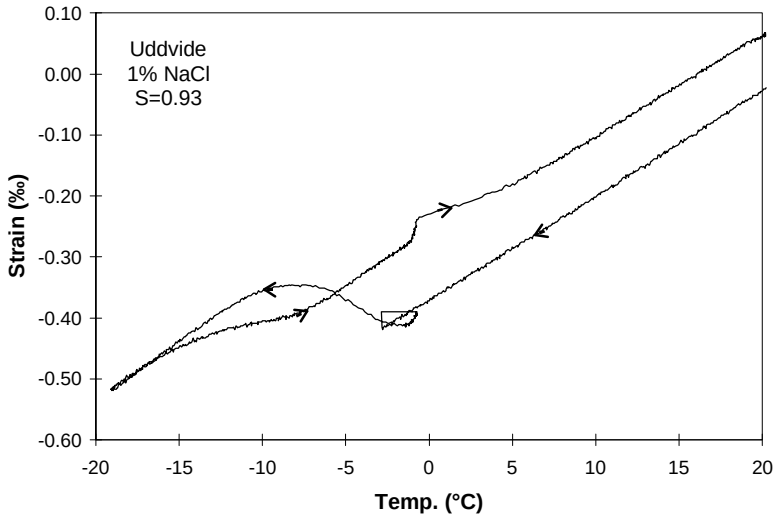

Figure K:49. Strain versus temperature of an Uddvide sandstone with a degree of saturation of 0.93, conditioned by absorption of a 1.0% NaCl solution, following evacuation to about 280 mbar.

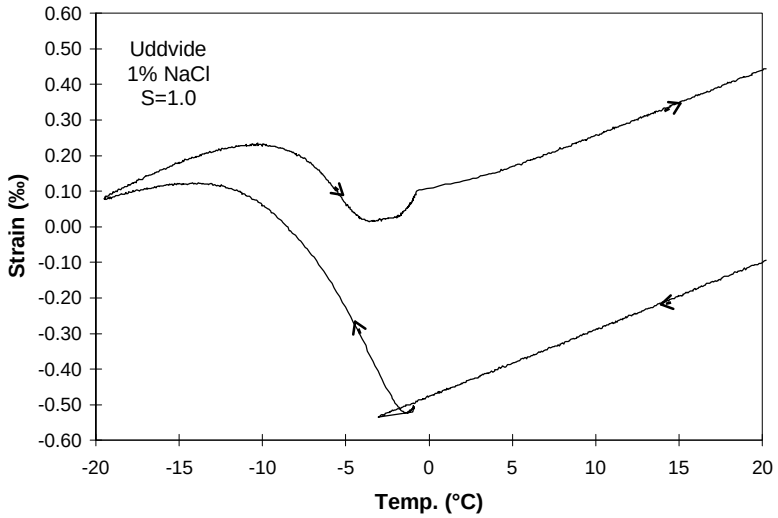

Figure K:50. Strain versus temperature of an Uddvide sandstone with a degree of saturation of 1.0, conditioned by absorption of a 1.0% NaCl solution, following evacuation to about 1 mbar (vacuum).

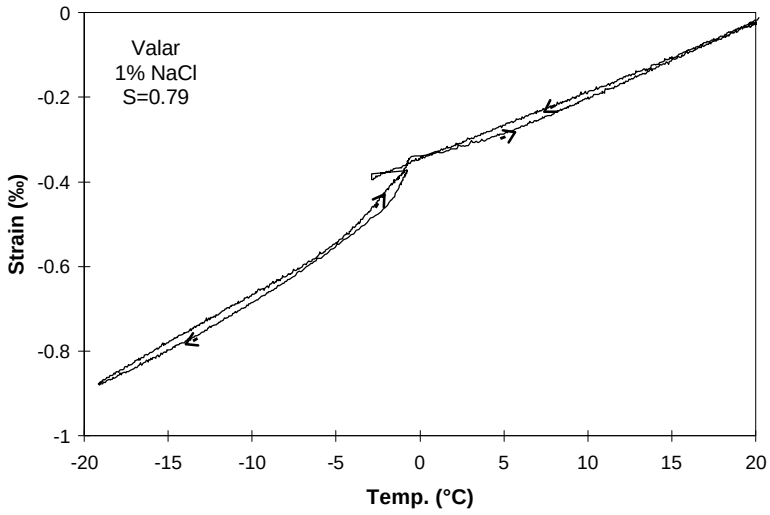

Figure K:51. Strain versus temperature of a Valar sandstone with a degree of saturation of 0.79, conditioned by sucking a solution of 1.0% NaCl for 7 days.

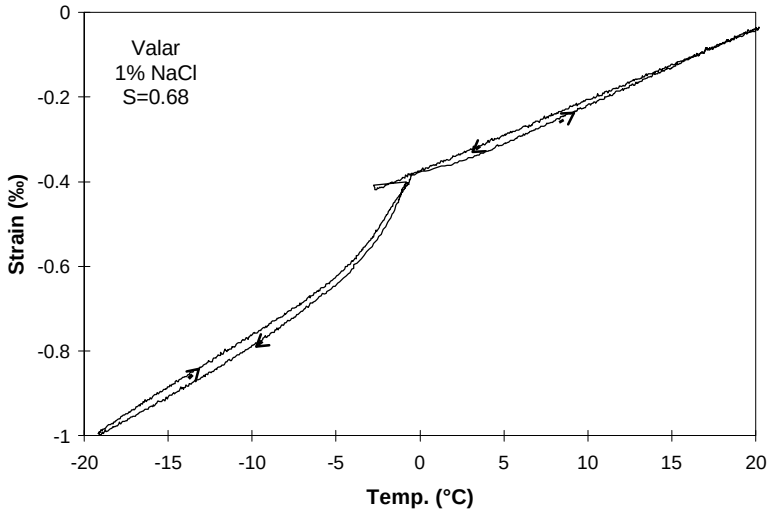

Figure K:52. Strain versus temperature of a Valar sandstone with a degree of saturation of 0.68, conditioned by sucking a solution of 1.0% NaCl for one day.

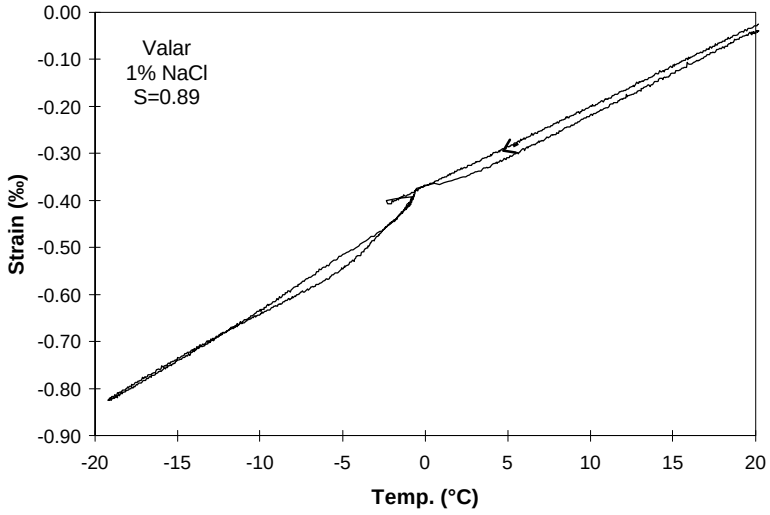

Figure K:53. Strain versus temperature of a Valar sandstone with a degree of saturation of 0.89, conditioned by sucking a solution of 1.0% NaCl for 21 days.

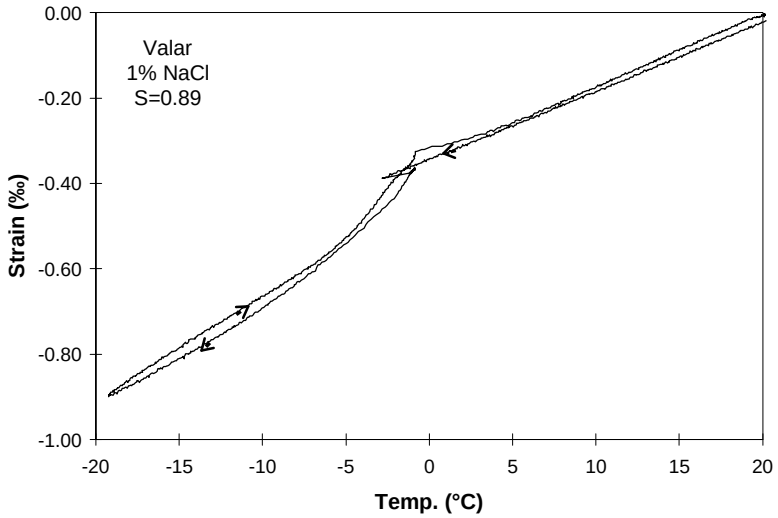

Figure K:54. Strain versus temperature of a Valar sandstone with a degree of saturation of 0.89, conditioned by absorption of a 1.0% NaCl solution, following evacuation to about 280 mbar.

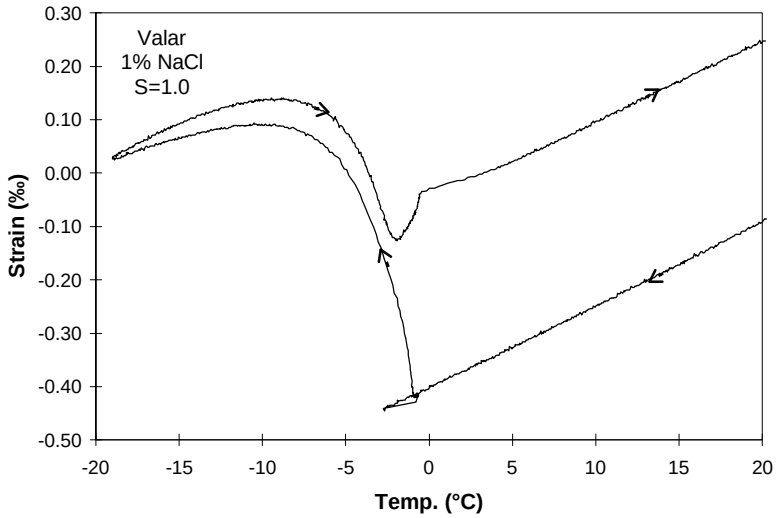

Figure K:55. Strain versus temperature of a Valar sandstone with a degree of saturation of 1.0, conditioned by absorption of a 1.0% NaCl solution, following evacuation to about 1 mbar (vacuum).

Appendix L
Comparison between calculated and measured dilatations

Below in Figure L:1 the calculated dilatations of completely saturated samples with various porosities (P) and various NaCl concentrations are plotted versus the temperature. Corresponding experimental data from the tests described in Chapter 3.7 are shown in Figures L:2-L:5 below. The dilatations in Figure L:1 have been calculated according to the description in Chapter 3.7.5. A comparison between the calculated dilatations in Figure L:1 and the measured dilatations in Figures L:2-L:5 shows that the calculated values are about 10 times as large as the measured values. The most plausible reason for this discrepancy is that the specimens are actually not completely saturated at freezing, as it is impossible to avoid some drying when handling the specimens. There are then empty spaces in the pore system, which can be filled with the ice before dilatation occurs. Theoretically, if the degree of saturation is 0.917 or less, there is room for all ice to expand into empty spaces and no dilatation should occur, provided no hydraulic pressure occurs due to displacement of unfrozen water when ice is formed. Ice is also forced out from the pore system and formed at the surface of the specimens, which has been seen at ocular inspection of water saturated, frozen stone prisms. The ice formed at the surface does not contribute to the expansion.

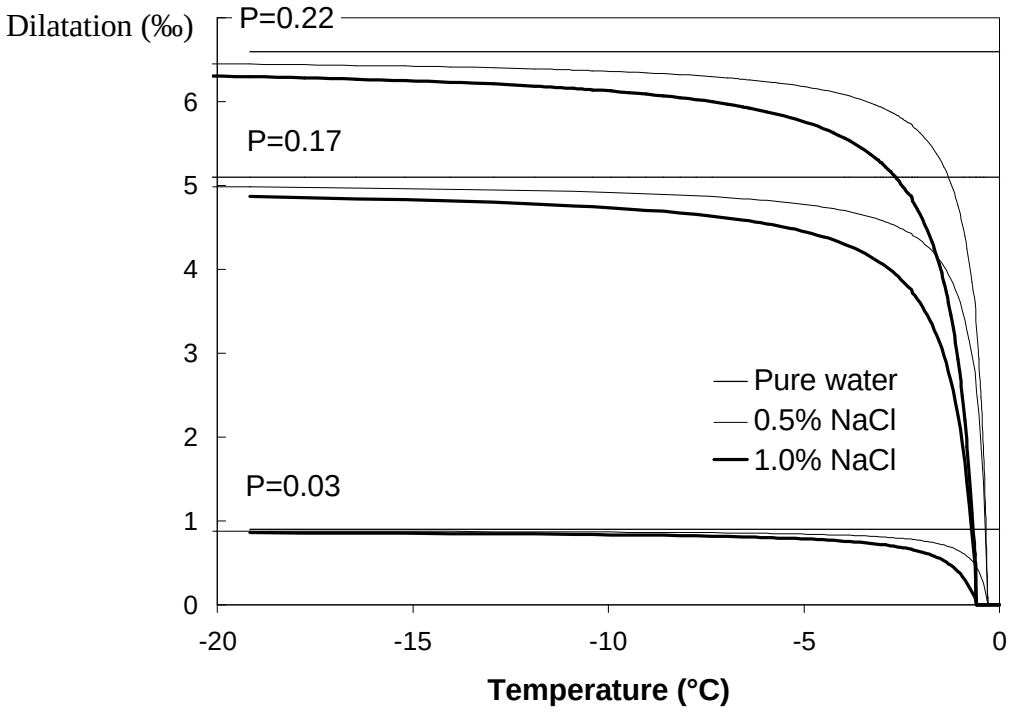

Figure L:1. The calculated dilatation of completely saturated samples with various porosities (P) and various NaCl concentrations versus the temperature.

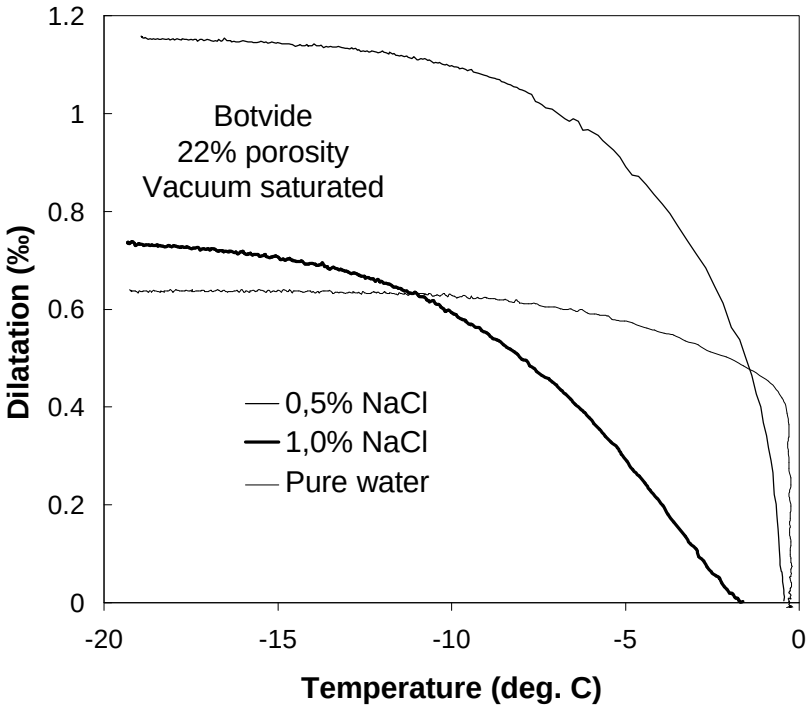

Figure L:2. The measured dilatation of completely saturated samples of the sandstone Botvide with various NaCl concentrations versus the temperature.

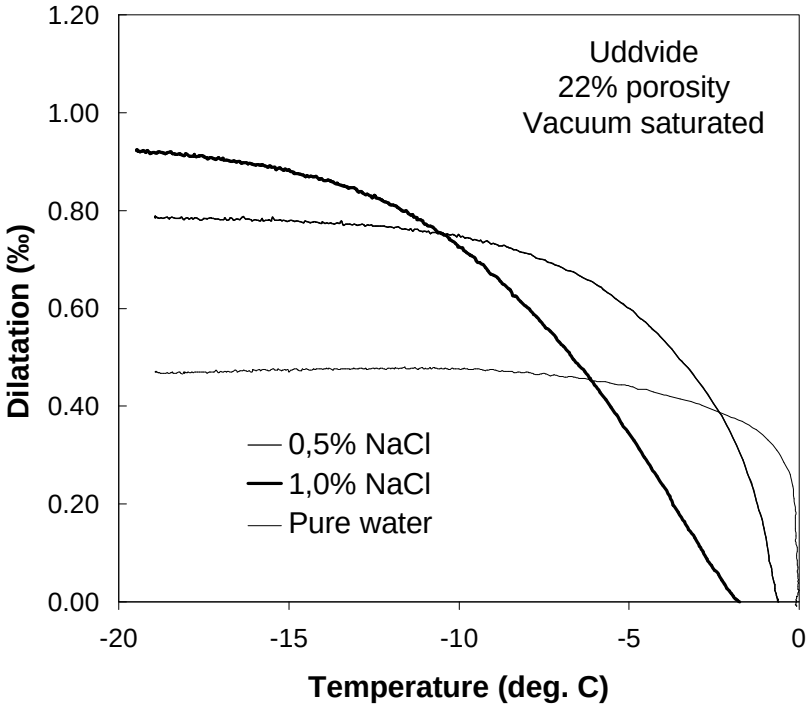

Figure L:3. The measured dilatation of completely saturated samples of the sandstone Uddvide with various NaCl concentrations versus the temperature.

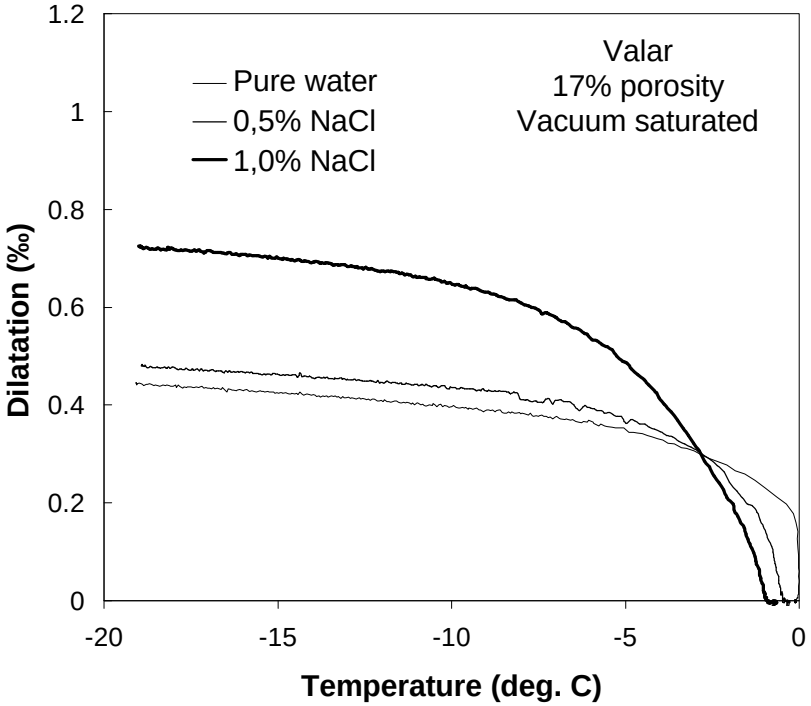

Figure L:4. The measured dilatation of completely saturated samples of the sandstone Valar with various NaCl concentrations versus the temperature.

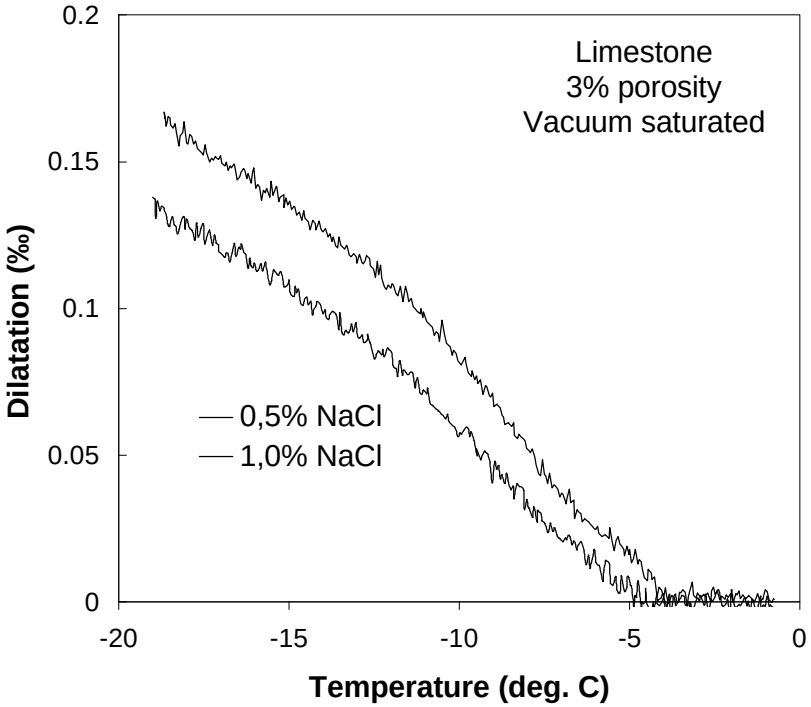

Figure L:5. The measured dilatation of completely saturated samples of the limestone Öland B1 with various NaCl concentrations versus the temperature.

Appendix M
Results of the S_{crit}-tests

The results from the sealed multi-cycle freeze-thaw test, or S_{crit}-test described in Chapter 3.8 are presented either as a decrease in the dynamic modulus of elasticity or as a relative increase in the volume versus the degree of saturation. The dynamic modulus of elasticity is described in more detail in Appendix G. The specimen volume at the end of the test, V_n, and the specimen volume at the start of the test, V_0, are calculated according to Equations 3.8.1 and 3.8.2.

$$V_0 = (Q_{a0} - Q_{w0}) \cdot \rho_w \quad (3.8.1)$$

$$V_n = (Q_{an} - Q_{wn}) \cdot \rho_w \quad (3.8.2)$$

where

V_0	specimen volume at the start of the test (m^3);
V_n	specimen volume at the end of the test (m^3);
Q_{a0}	weight of vacuum saturated specimen in air at the start of the test (kg);
Q_{w0}	weight of vacuum saturated specimen in water at the start of the test(kg);
Q_{an}	weight of vacuum saturated specimen in air at the end of the test(kg);
Q_{wn}	weight of vacuum saturated specimen in water at the end of the test(kg);
ρ_w	density of water (1000 kg/m^3).

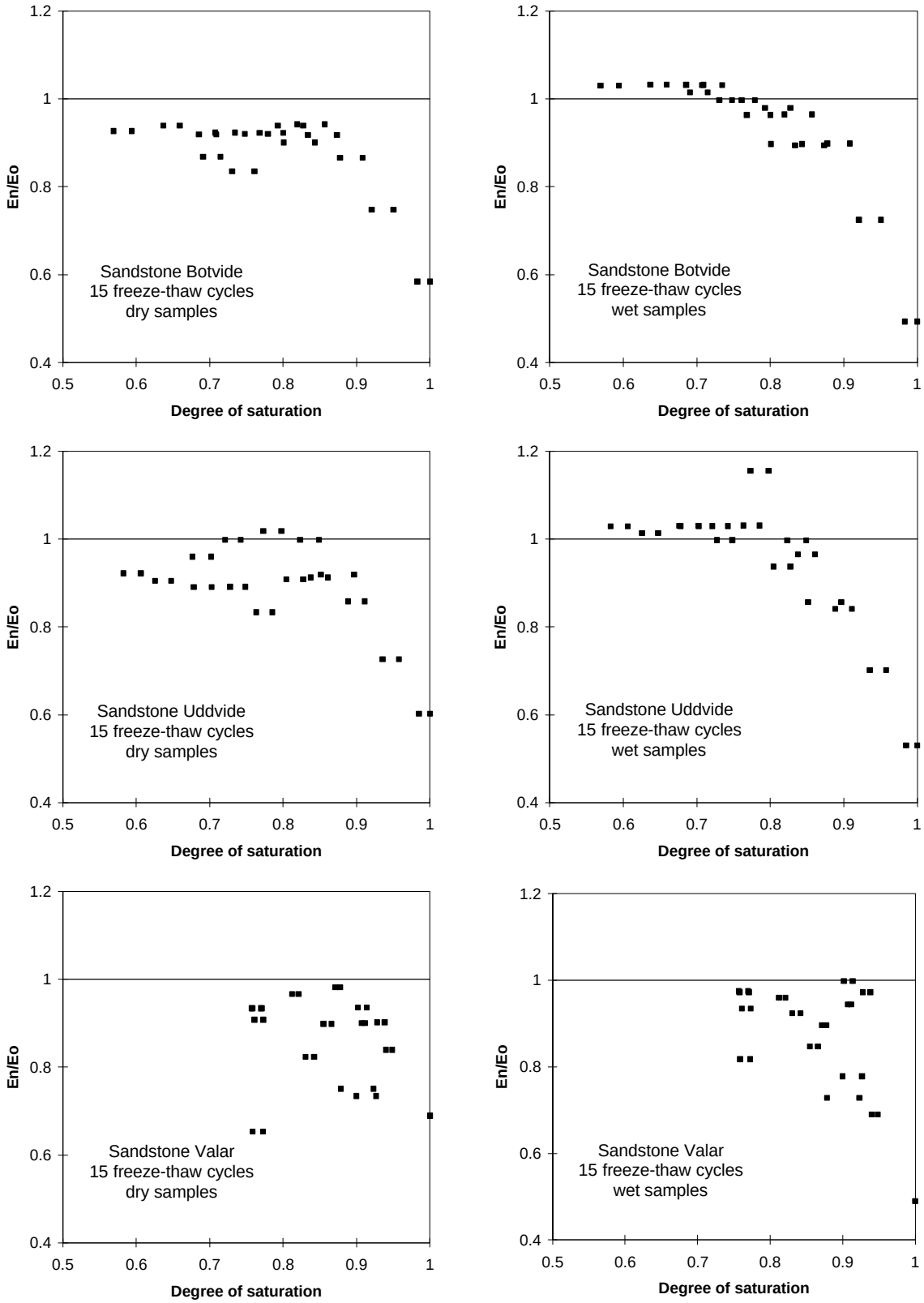

Figure M:1. Decrease in dynamic modulus of elasticity.

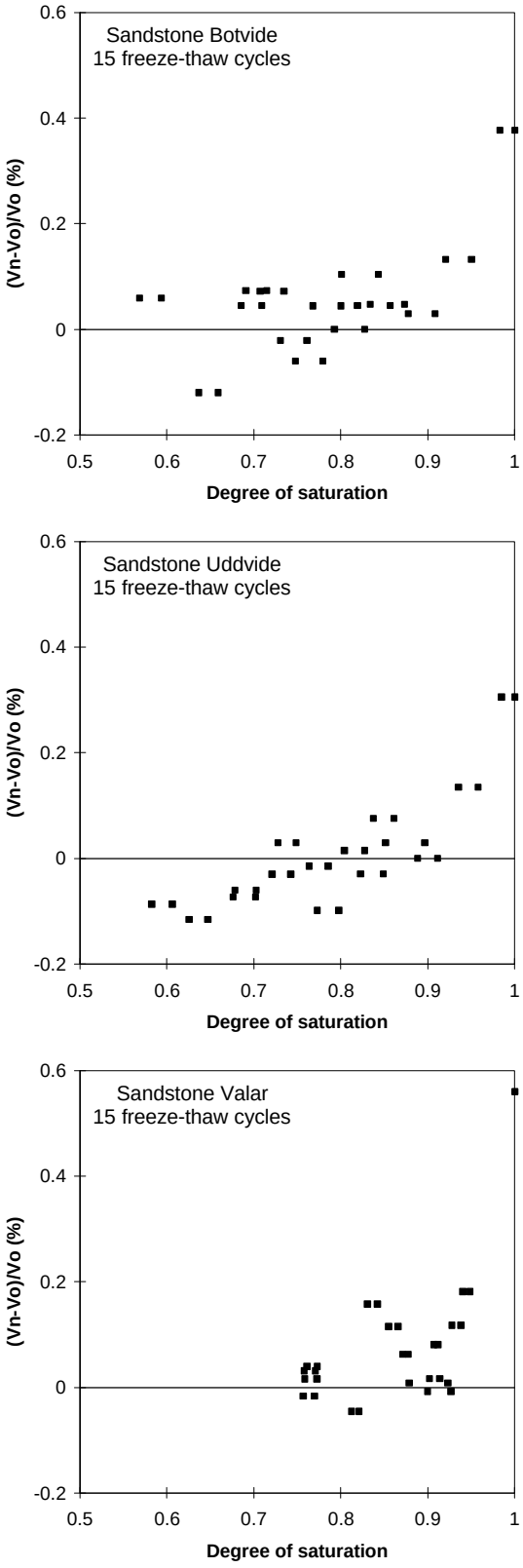

Figure M:2. Relative increase in volume.

Appendix N
Results of Differential Scanning Calorimetry

A differential scanning calorimeter (DSC) records the difference between the enthalpy change which occurs in a sample and that in an inert reference material, when they are both equally heated or cooled. Such an enthalpy change is caused by, for example, a phase transformation such as ice formation or melting. The calorimeter was of the type DSC7 from Perkin Elmer.

The results are further commented in Chapter 3.9.2.

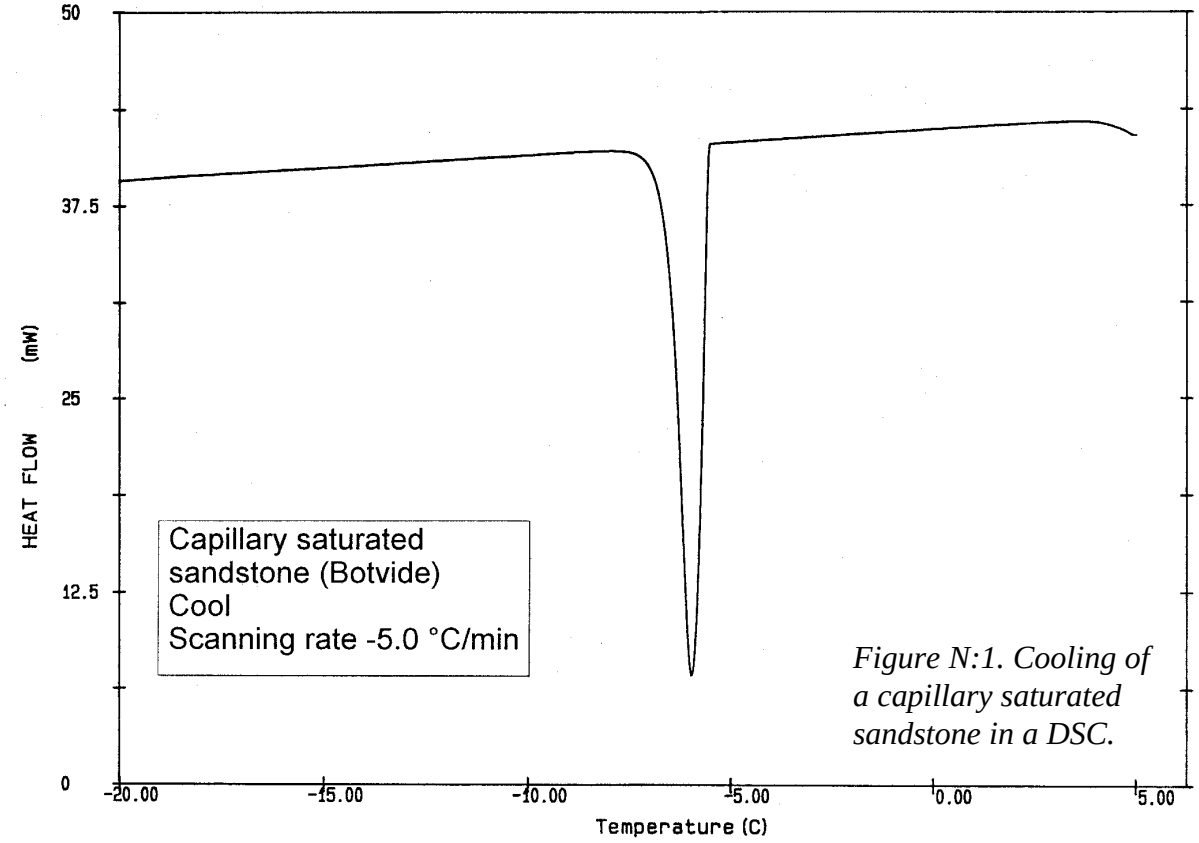

Figure N:1. Cooling of a capillary saturated sandstone in a DSC.

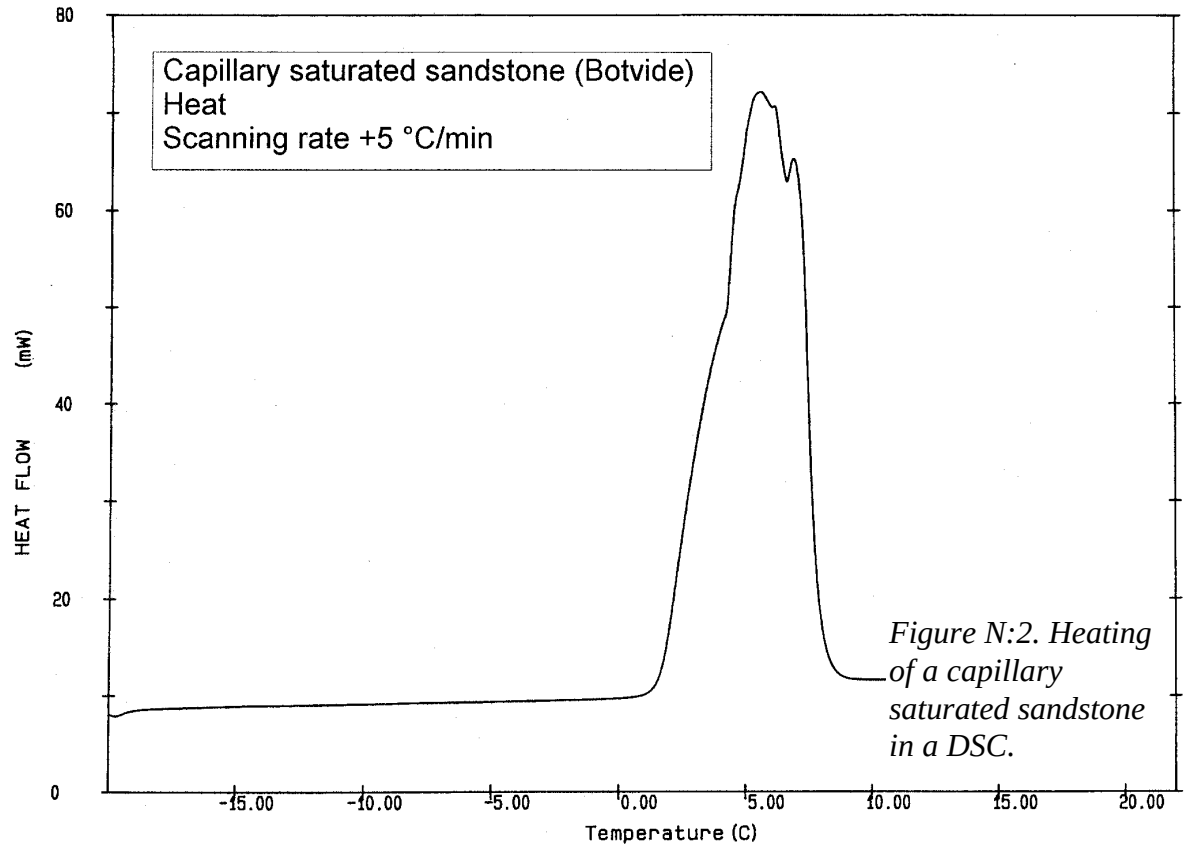

Figure N:2. Heating of a capillary saturated sandstone in a DSC.

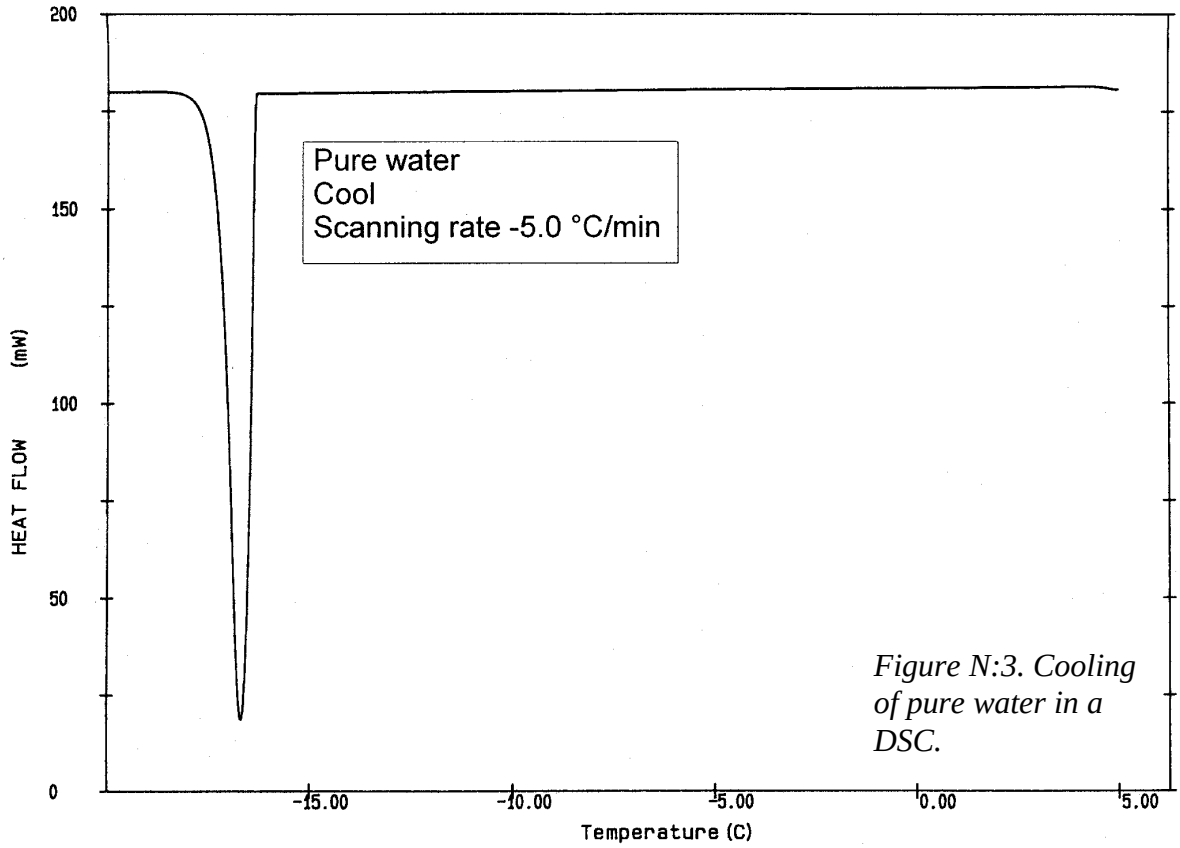

Figure N:3. Cooling of pure water in a DSC.

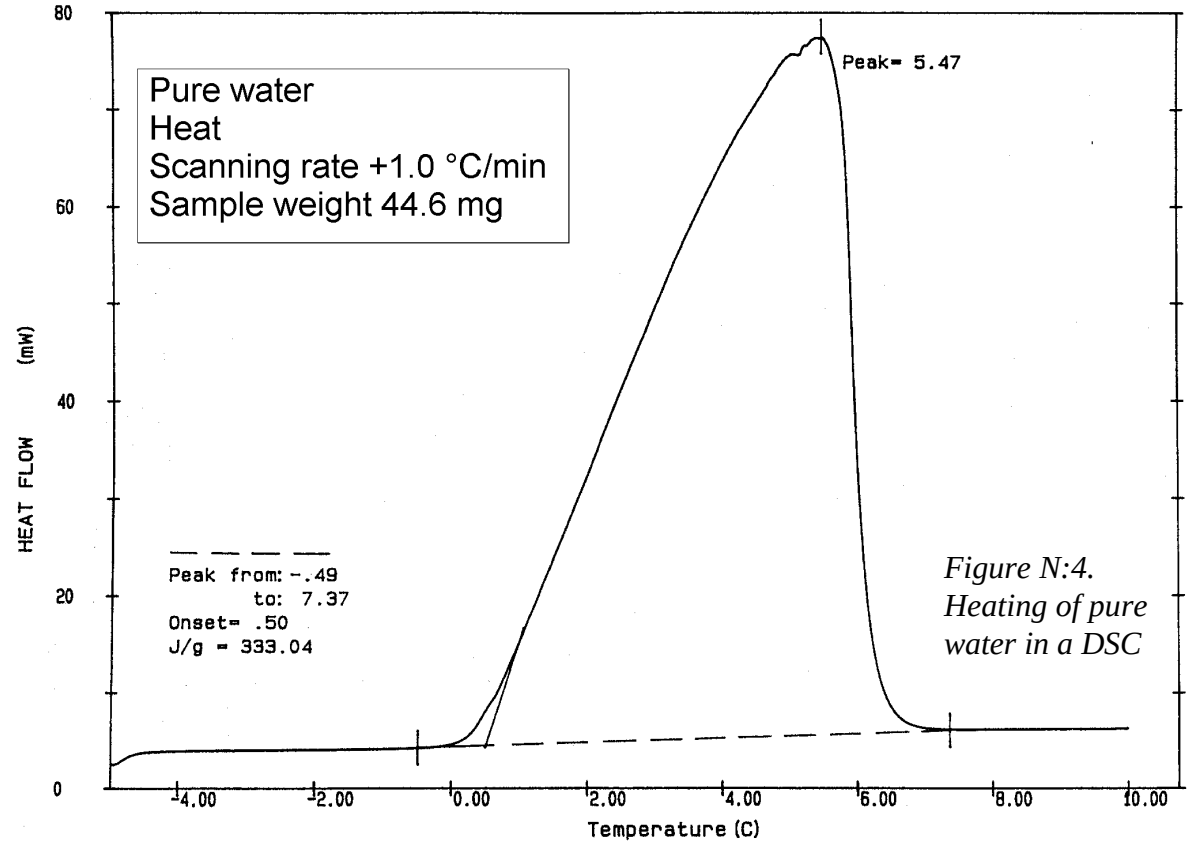

Figure N:4. Heating of pure water in a DSC

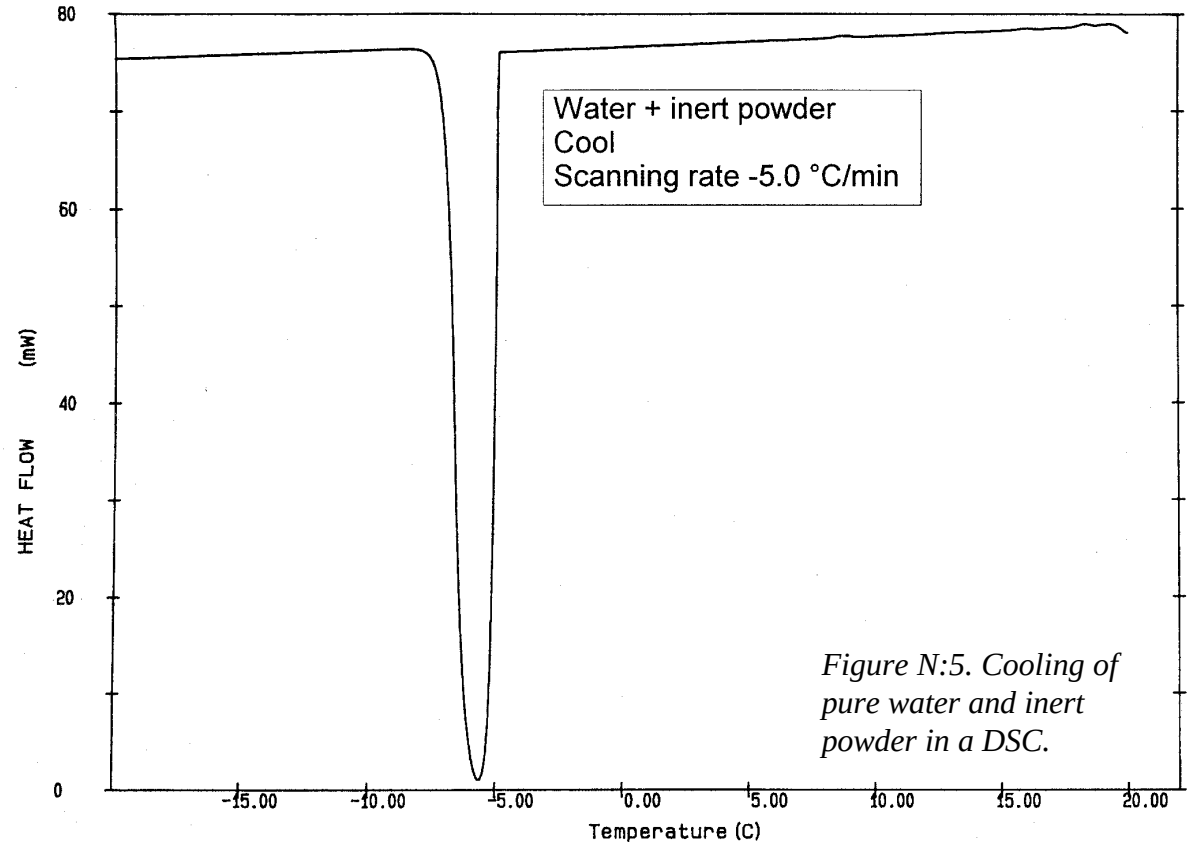

Figure N:5. Cooling of pure water and inert powder in a DSC.

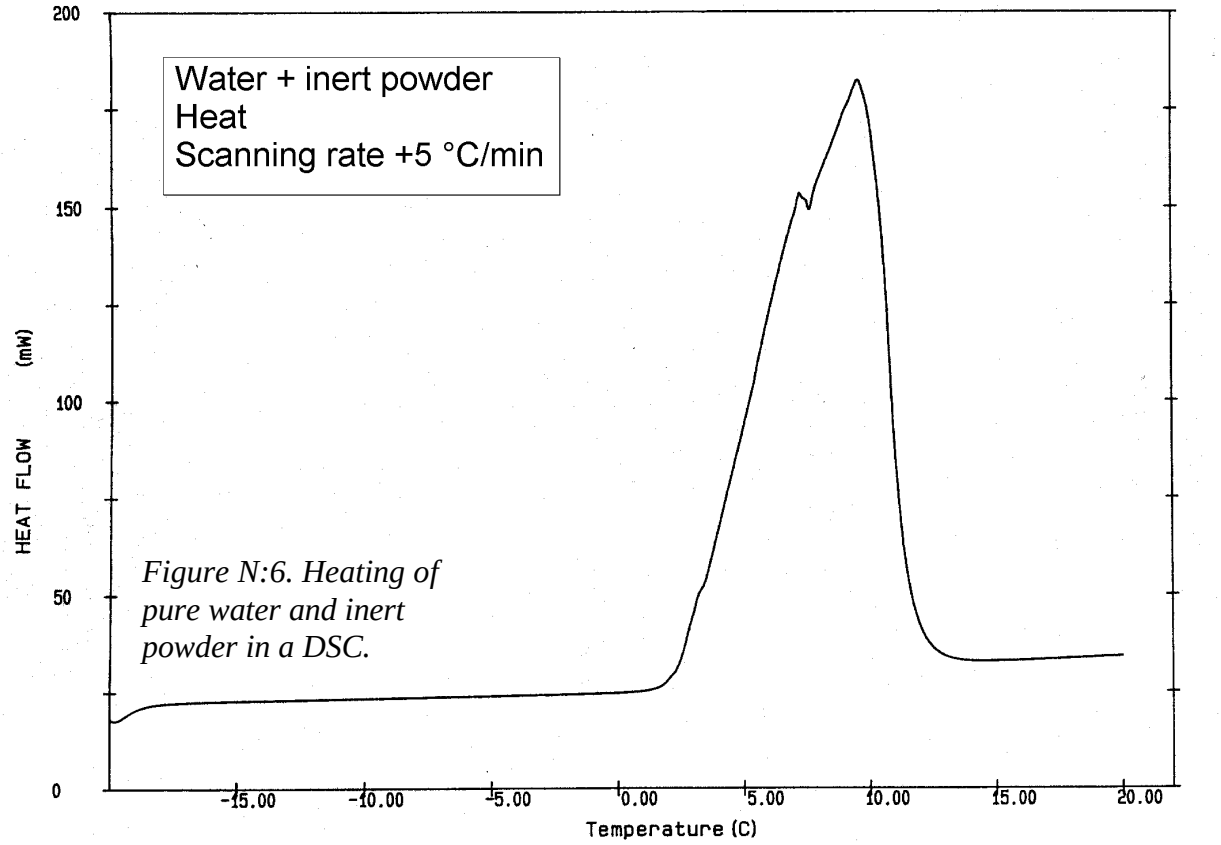

Figure N:6. Heating of pure water and inert powder in a DSC.

Appendix O
Results of Setaram micro-calorimetry

In a differential low-temperature Calvet Setaram Microcalorimeter considerably larger samples can be used than in an ordinary DSC. The principle of measuring heat formation during heating and cooling caused by, for example, a phase transition is equal for both these calorimetric instruments. The tests described here were partly performed at Technical University of Denmark, Department of Structural Engineering and Materials under the supervision of Dr Kurt Kielsgard Hansen, Figures O:1-O:4, and partly at the Lund Institute of Technology, Department of Building Materials under the supervision of Sture Lindmark, Figures O:5-O:10.

The freezing occurs at some degrees below zero, which depends on supercooling. In the results from the Swedish instrument, Figures O:5-O:10, the melting seems to start at some degrees above zero. The explanation for this is that the recorded temperature is not measured in the sample itself, but in the calorimeter block. This phenomenon is not seen in the results from the Danish instrument, which can be either because of some unknown difference between the two instruments, or because of a freezing point depression in the granite and limestone Öland B1 caused by small pores, Equation 2.4.1.

The results are further commented in Chapter 3.9.3.

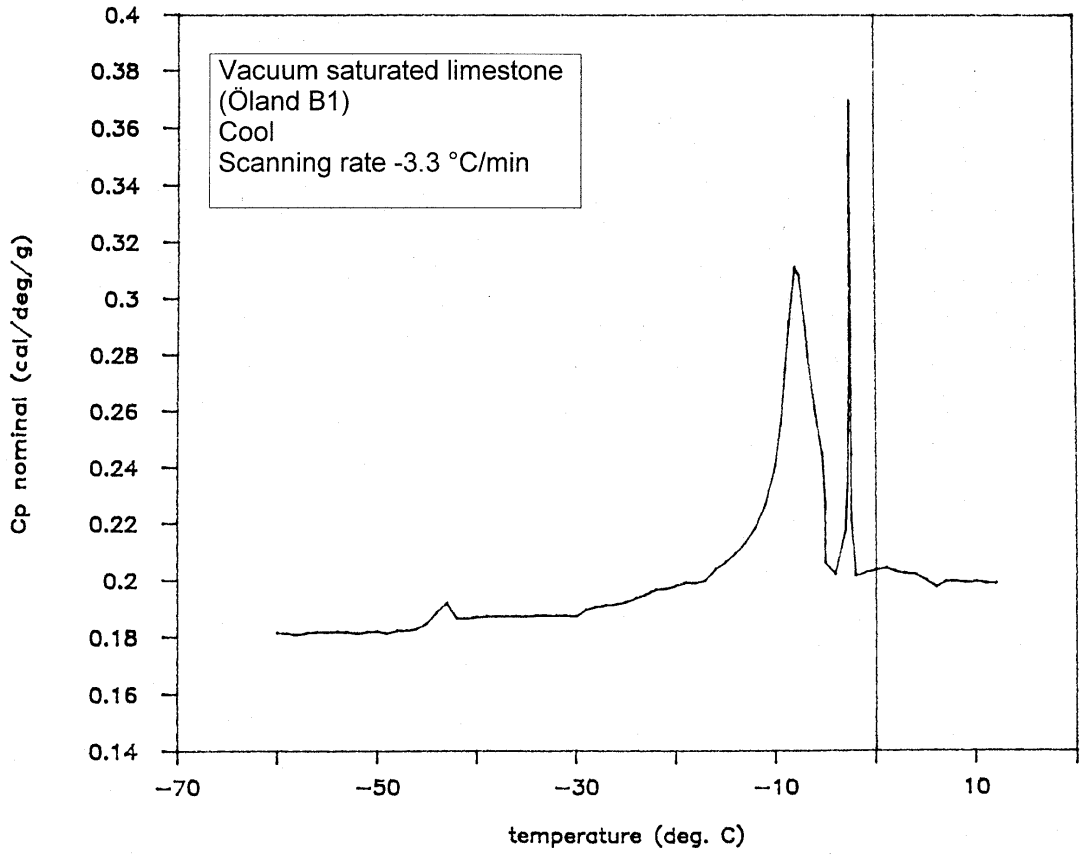

Figure O:1. Cooling of a vacuum saturated limestone Öland B1 in a Setaram calorimeter.

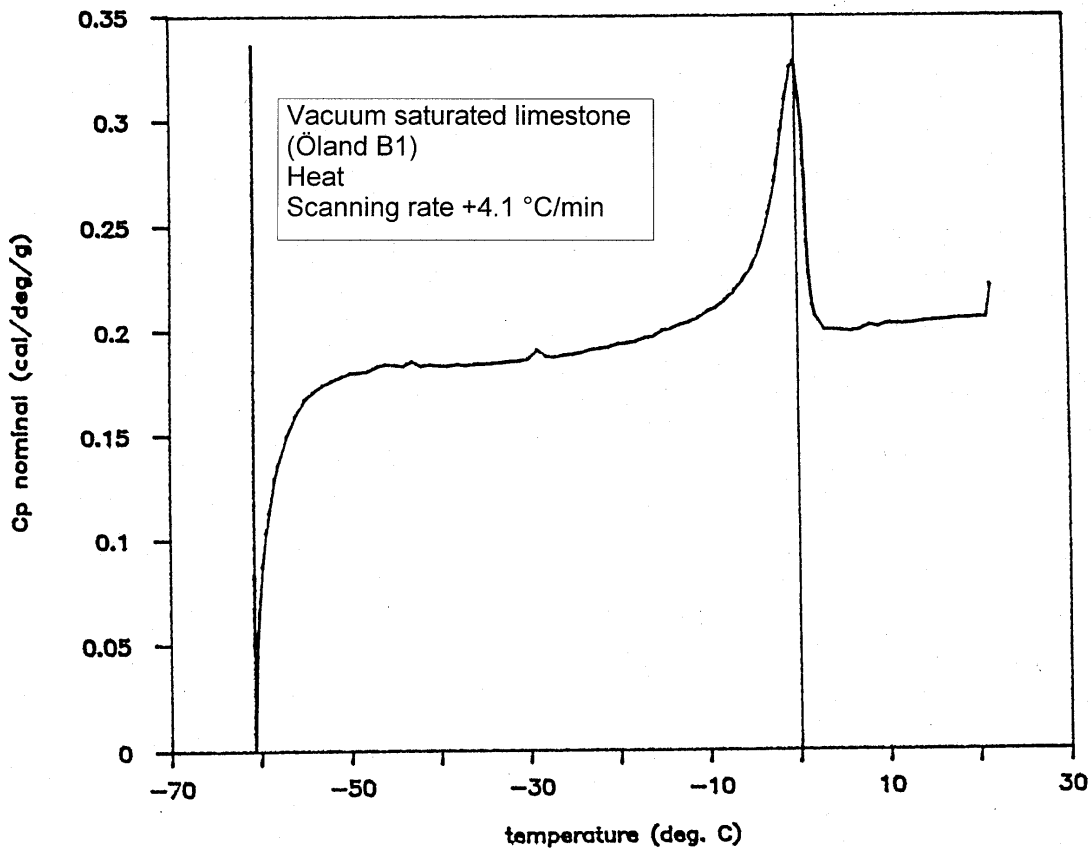

Figure O:2. Heating of a vacuum saturated limestone Öland B1 in a Setaram calorimeter.

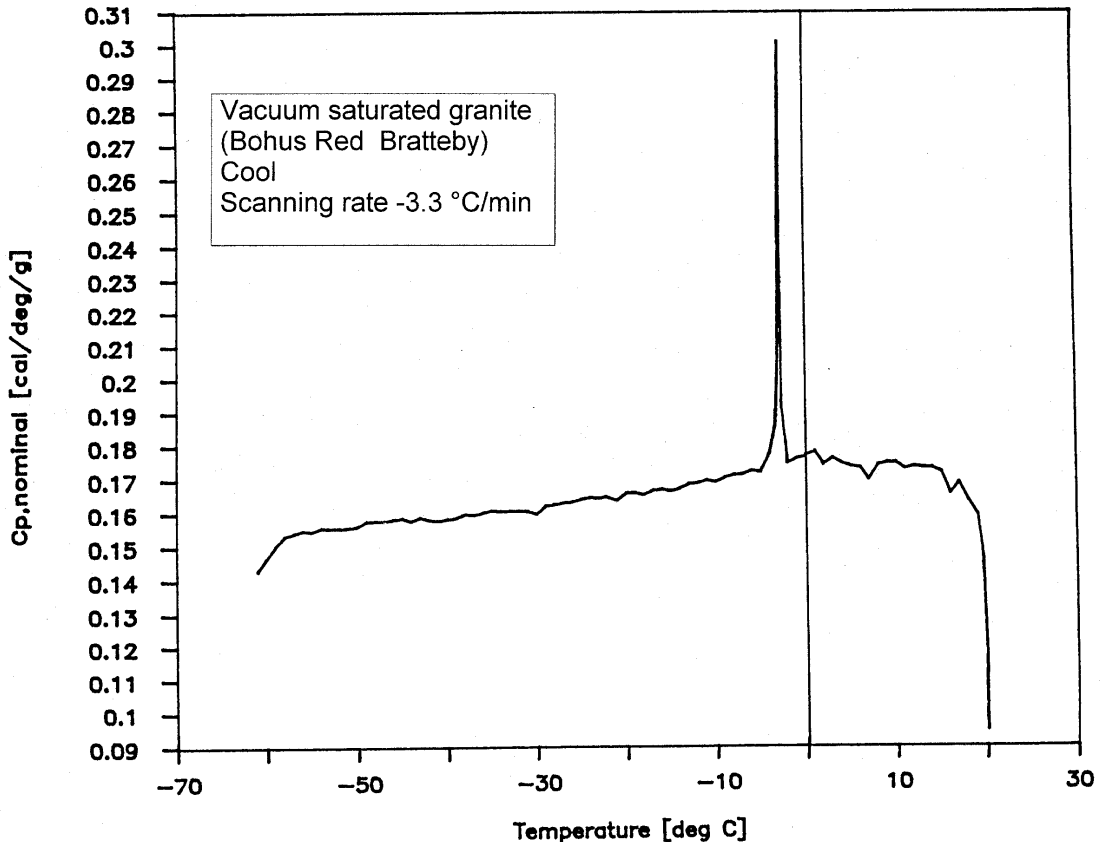

Figure O:3. Cooling of a vacuum saturated granite in a Setaram calorimeter.

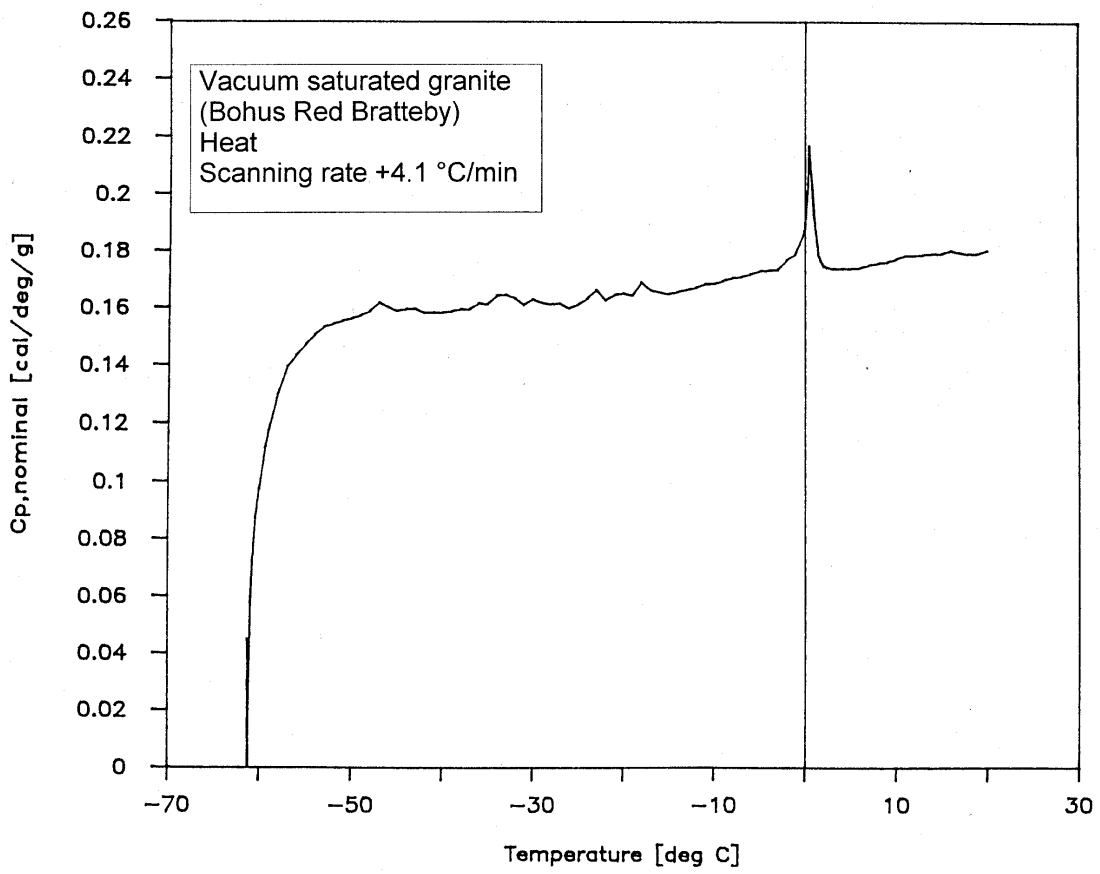

Figure O:4. Heating of a vacuum saturated granite in a Setaram calorimeter.

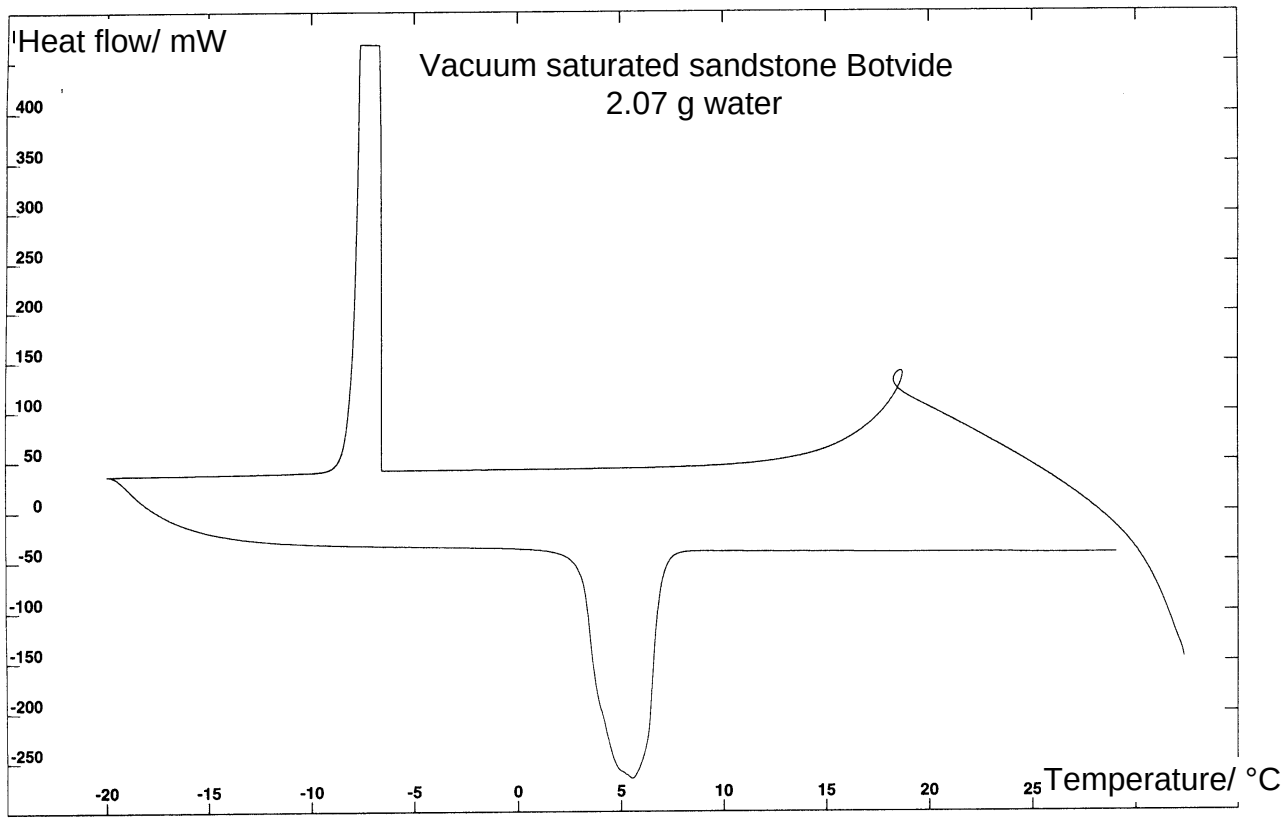

Figure O:5. Cooling of a vacuum saturated sandstone Botvide in a Setaram calorimeter.

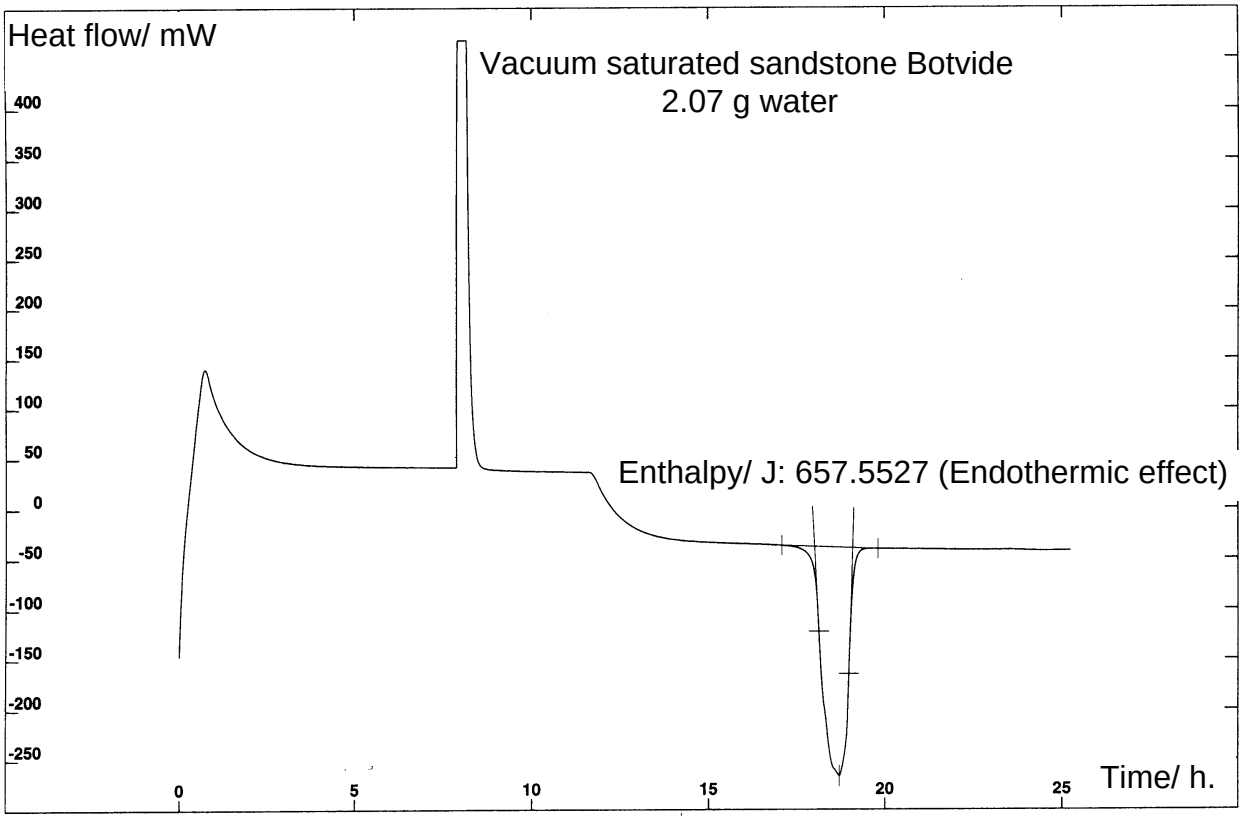

Figure O:6. Heating of a vacuum saturated sandstone Botvide in a Setaram calorimeter.

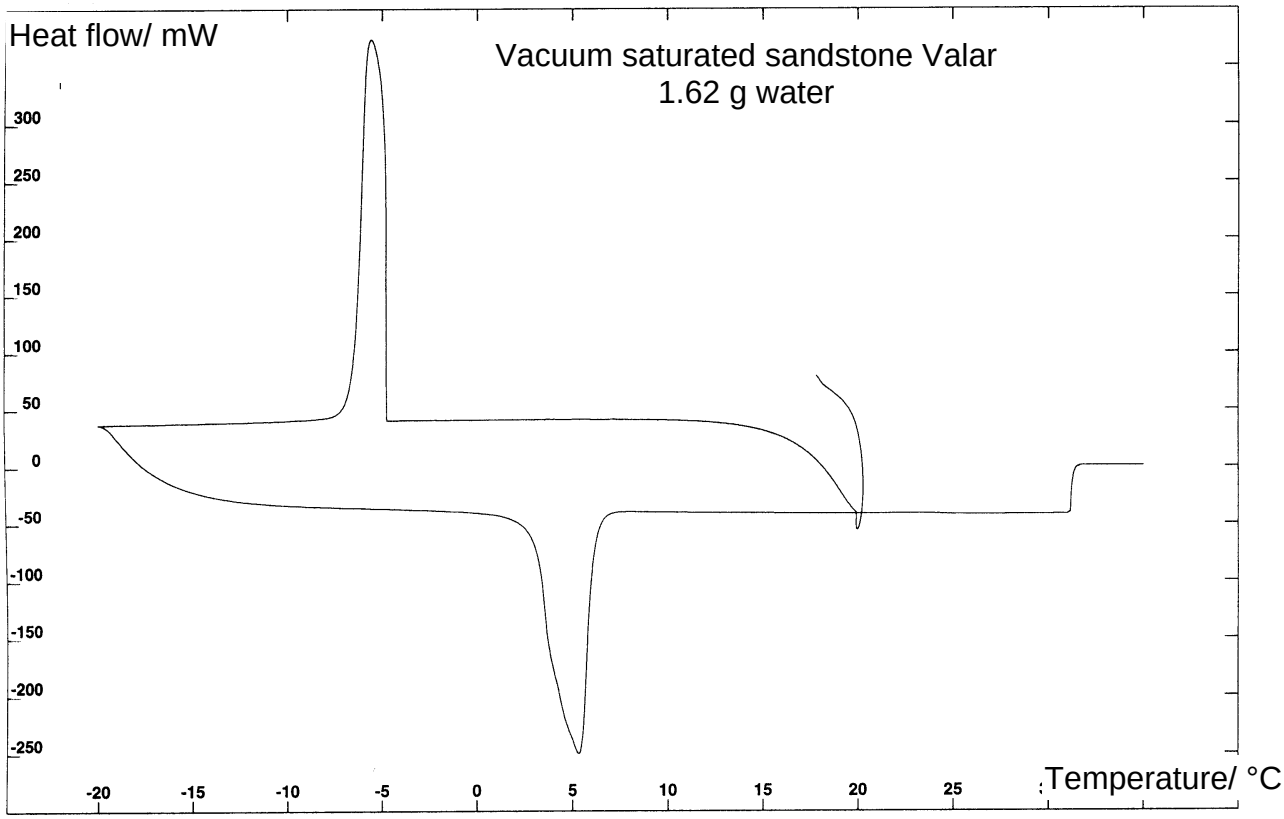

Figure O:7. Cooling of a vacuum saturated sandstone Valar in a Setaram calorimeter.

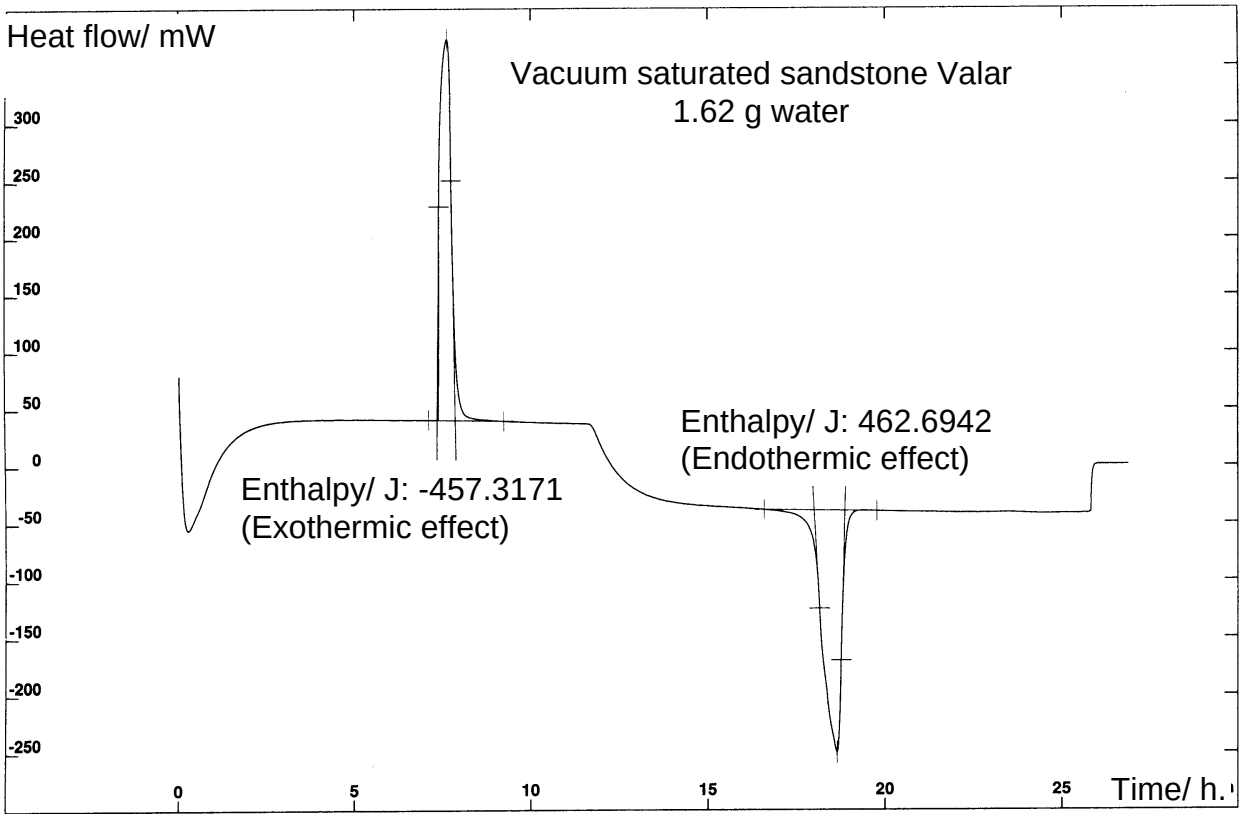

Figure O:8. Heating of a vacuum saturated sandstone Valar in a Setaram calorimeter.

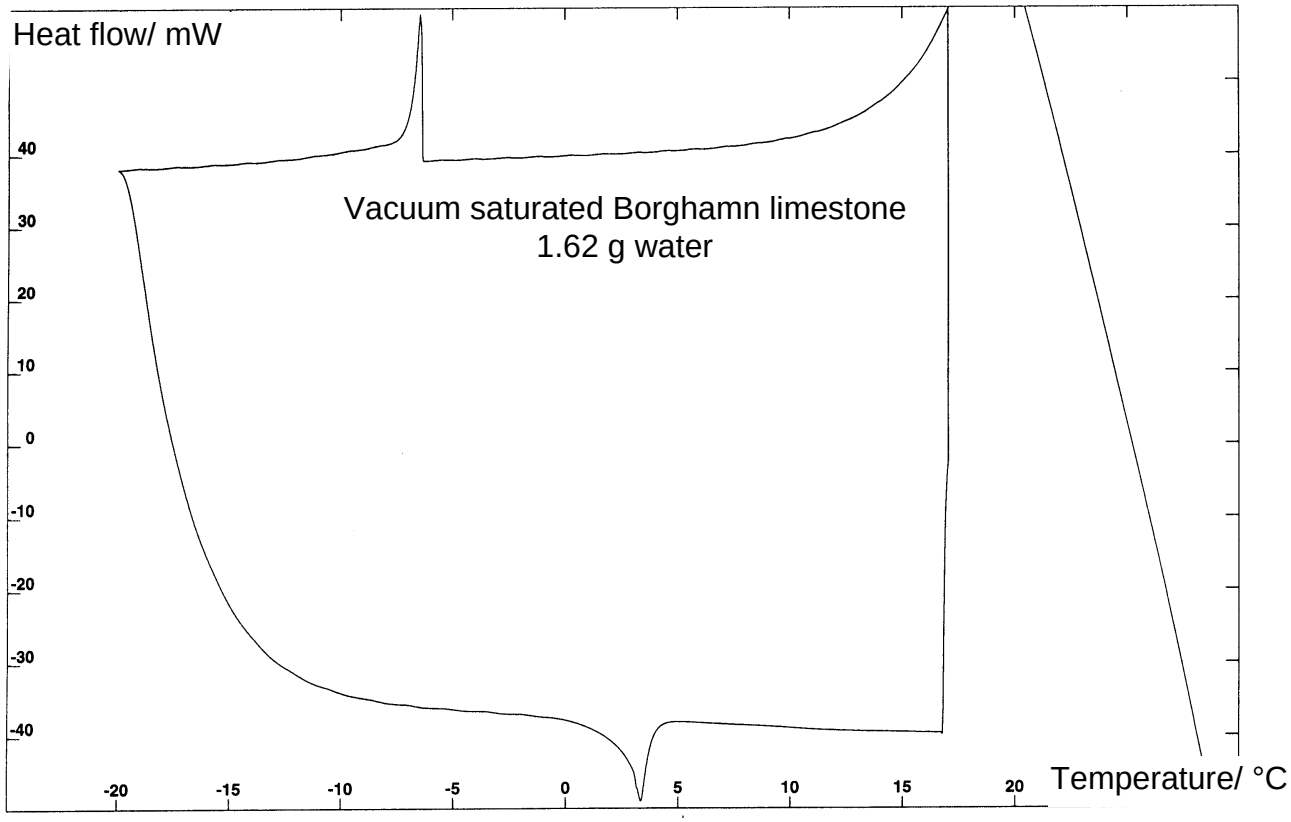

Figure O:9. Cooling of a vacuum saturated Borghamn limestone in a Setaram calorimeter.

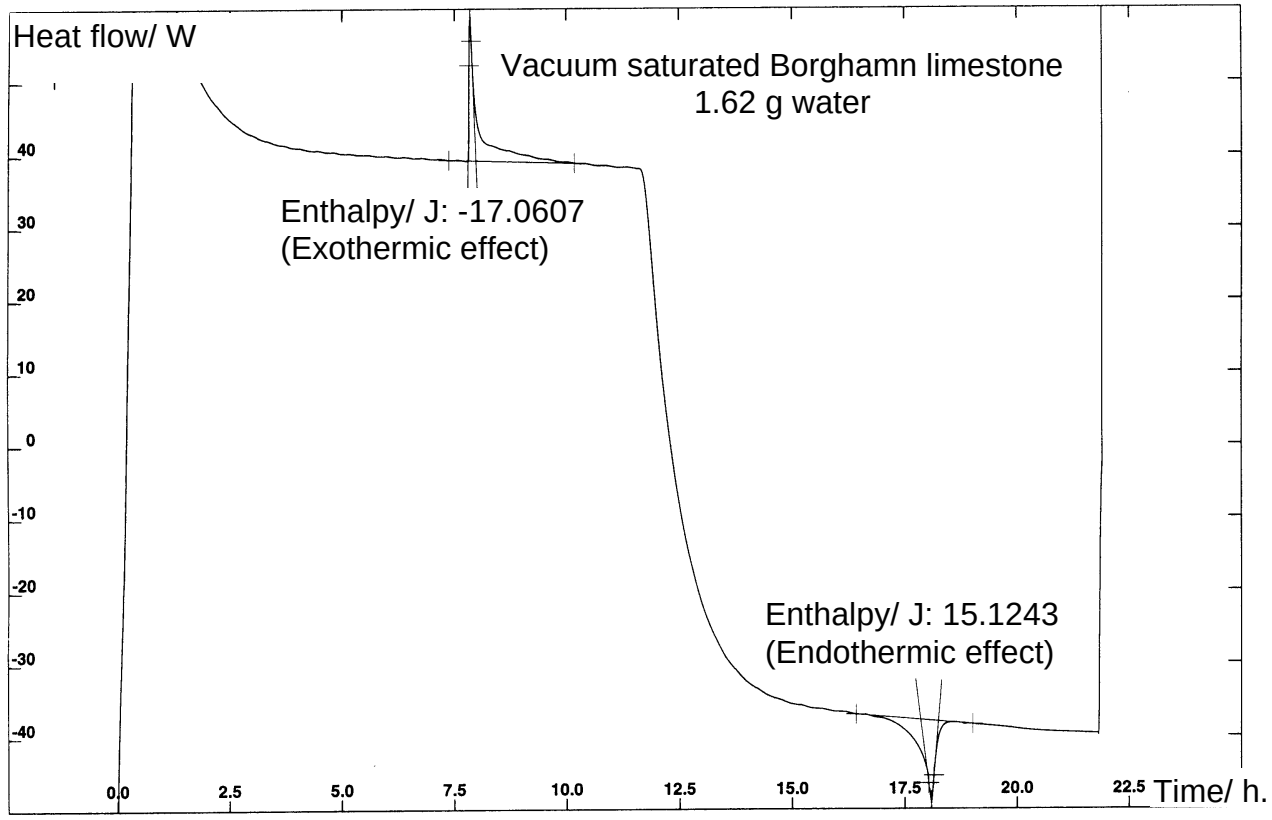

Figure O:10. Heating of a vacuum saturated Borghamn limestone in a Setaram calorimeter.

Appendix P
Tables with data from the different freeze-thaw tests

Contents

The technique for measuring the resonant frequency, the calculation of the dynamic modulus of elasticity and the correction factor *CF* are explained in Appendix G. The *S*-values are calculated as described below. The calculation method depends on the type of test. All weights in the tables are in g. For notations and units, see notation list on page ix.

Scaling test, Appendixes P1 and P2.

$$S_0 = \frac{(Q_0 - Q_{d0}) \cdot \rho_b}{Q_{d0} \cdot P \cdot \rho_w} \qquad S_n = \frac{(Q_n - Q_{dn}) \cdot \rho_b}{Q_{dn} \cdot P \cdot \rho_w} \tag{P.1}$$

Scaling test, Granite, Appendix P3.

$$S_0 = \frac{(Q_0 - Q_{dn(105)} - Q_{ds}) \cdot \rho_b}{(Q_{dn(105)} + Q_{ds}) \cdot P \cdot \rho_w} \qquad S_n = \frac{(Q_n - Q_{dn(105)}) \cdot \rho_b}{(Q_{dn(105)}) \cdot P \cdot \rho_w} \tag{P.2}$$

Scaling test, Appendix P4.

$$S_0 = \frac{(Q_0 - Q_{d0}) \cdot \rho_b}{Q_{d0} \cdot P \cdot \rho_w} \tag{P.3}$$

It was not possible to calculate S_n in the scaling tests described in Appendix P.4, due to huge weight losses. However, as can be seen, the samples were completely saturated after 19 weeks of capillary saturation before the start of the freezing and thawing. Therefore, we can assume that they were also saturated after the freeze-thaw test, that is, $S_n \approx 1$.

Dilatation test, specimens containing pure water, conditioned by vacuum saturation and drying Appendix P5, tables P5.1-P5.3.

$$S_0 = \frac{(Q_0 - Q_{d0})}{(Q_{a0} - Q_{d0})} \qquad S_n = \frac{(Q_n - Q_{dn})}{(Q_{an} - Q_{dn})} \tag{P.4}$$

Dilatation test, specimens containing salt solution, conditioned by negative pressure Appendix P5, tables P5.4-P5.9.

$$S_0 = \frac{(Q_0 - Q_{d0})}{(Q_{an} - Q_{d0})} \qquad S_n = \frac{(Q_n - Q_{dn})}{(Q_{an} - Q_{dn})} \tag{P.5}$$

Dilatation test, specimens containing salt solution, conditioned by capillary suction Appendix P5, table P5.10.

$$S_0 = \frac{(Q_0 - Q_{dn(105)})}{(Q_{an} - Q_{dn})} \qquad S_n = \frac{(Q_n - Q_{dn(105)})}{(Q_{an} - Q_{dn})} \tag{P.6}$$

The values of Q_{do} are missing, but the effects of salt in the pore system are negligable, as Q_{dn} - Q_{d0} is small even for completely saturated specimen.

S_{crit}-test, Appendix P6.

$$S_0 = \frac{(Q_0 - Q_{dn(105)})}{(Q_{a0} - Q_{dn(105)})} \qquad S_n = \frac{(Q_n - Q_{dn(105)})}{(Q_{an} - Q_{dn(105)})} \tag{P.7}$$

Appendix P1.
From Chapter 3.6.2. Unsealed multi-cycle freeze-thaw test - Scaling test, Sandstone tested in NaCl solution, and from Chapter 3.6.3 Estimation of salt content of the freeze-thaw specimens.

Letter B means sandstone Botvide.
Letter U means sandstone Uddvide.
Letter V means sandstone Valar.

The number in the letter indicates percentage by weight of the salt solution.

Table P1.1. Test series 1.

	Before freezing			After freezing, 20 cycles						
Letter	$Q_{d0(95)}$	Q_0	S_0	Q_n	$Q_{dn(95)}$	Q_{ds}	S_n	*Salt*	b_t	b_c
B0	231.102	248.4	0.701	251.44	230.252	0.686	0.862	-0.164	0	0
B2.5	230.854	248.36	0.710	249.13	228.191	3.089	0.860	0.426	0.59	0.490
B5	231.07	248.81	0.719	249.33	230.044	1.953	0.785	0.927	1.091	0.955
B10	232.059	250.32	0.737	251.01	233.484	0.564	0.703	1.989	2.153	1.919
U0	231.026	247.56	0.652	250.41	230.357	0.525	0.793	-0.144	0	0
U2.5	231.909	249.78	0.702	249.3	227.881	4.459	0.857	0.431	0.575	0.483
U5	230.935	249.56	0.735	250.07	229.616	2.349	0.812	1.03	1.174	1.008
U10	226.678	244.59	0.720	245.57	228.103	0.623	0.698	2.048	2.192	1.917
V0	247.779	262.17	0.741	265.88	247.22	0.461	0.963	-0.098	0	0
V2.5	244.533	258.34	0.720	247.15	229.46	15.213	0.984	0.14	0.238	0.221
V5	240.295	254.42	0.750	246.2	229.636	11.514	0.920	0.855	0.953	0.535
V10	236.87	251.56	0.791	248.06	232.7	5.957	0.842	1.787	1.885	1.370

Table P1.2. Test series 2.

	Before freezing			After freezing, 7 cycles						
Letter	$Q_{d0(105)}$	Q_0	S_0	Q_n	$Q_{dn(105)}$	Q_{ds}	S_n	*Salt*	b_t	b_c
B0	230.566	249.47	0.768	251.43	230.08	0.32	0.869	-0.166	0	0
B2	230.404	248.58	0.739	249.9	229.47	1.04	0.834	0.106	0.272	0.399
B4	236.814	255.94	0.757	256.94	236.62	0.82	0.805	0.626	0.792	0.819
B6	229.372	247.66	0.747	248.77	230.08	0.3	0.761	1.008	1.174	1.172
B8	232.04	249.58	0.708	250.98	232.9	0.41	0.727	1.27	1.436	1.529
B10	232.154	251.18	0.768	251.89	233.76	0.13	0.727	1.736	1.902	1.979
U0	233.975	253.45	0.759	255.79	232.71	1.085	0.904	-0.18	0	0
U2	232.911	252.37	0.761	252.34	230.5	2.57	0.864	0.159	0.339	0.411
U4	230.315	249.91	0.775	250.54	229.78	1.05	0.823	0.515	0.695	0.827
U6	231.863	251.49	0.772	252	232.68	0.21	0.757	1.027	1.207	1.214
U8	233.019	251.59	0.726	252.18	233.34	1.11	0.736	1.431	1.611	1.571
U10	232.468	251.81	0.758	252.31	234.18	0.14	0.706	1.852	2.032	1.990
V0	241.124	256.43	0.810	257.09	239.11	1.79	0.959	-0.224	0	0
V2	235.149	251.03	0.862	245.76	226.69	8.36	1.073	-0.099	0.125	0.283
V4	240.919	257.13	0.859	258.42	239.97	1.57	0.981	0.621	0.845	0.726
V6	238.455	253.29	0.794	252.64	236.97	2.28	0.844	0.795	1.019	0.908
V8	240.464	255.71	0.809	257.47	240.39	1.43	0.907	1.356	1.58	1.408
V10	237.559	251.78	0.764	253.73	238.89	0.12	0.793	1.451	1.675	1.622

Table P1.3. Test series 3.

	Before freezing					After freezing, 20 cycles					
Letter	$Q_{d0(50)}$	f_{d0}	Q_0	f_{w0}	S_0	Q_n	f_{wn}	$Q_{dn(50)}$	f_{dn}	S_n	Q_{ds}
B0	230.74	4400	249.05	2760	0.743	182.09	3920	165.93	6240	0.912	64.43
B0,5	233.19	3440	252.43	2000	0.773	231.85	2120	209.93	4040	0.978	22.93
B1,0	239.42	3420	259.12	2020	0.771	224.69	2960	204.1	5520	0.945	35.4
B1,5	240.21	3380	259.48	2040	0.752	255.93	2260	232.94	4480	0.925	7.435
B2,0	241.53	3380	261.5	2040	0.775	260.14	1620	237.3	3080	0.902	4.51
B2,5	240.12	3440	259.98	2060	0.775	259.28	1660	236.85	3080	0.887	3.54
B3,0	239.12	3500	258.58	2050	0.762	259.04	1760	236.88	3240	0.876	2.555
B3,5	241.75	3500	260.99	2020	0.746	260.37	1700	238.3	3240	0.868	4.11
U0	238.45	4040	257.33	2560	0.722	213.82	3120	195.02	5320	0.879	43.23
U0,5	237.03	4160	255.72	2560	0.719	254.78	1980	231.97	3640	0.896	5.07
U1,0	239.87	4060	259.42	2660	0.743	254.8	1820	231.64	3440	0.911	8.26
U1,5	238.09	4200	255.86	2500	0.680	253.72	1760	231.27	3720	0.885	6.96
U2,0	241.45	4140	261.12	2540	0.743	258.14	1900	235.5	3480	0.876	6.18
U2,5	240.52	4180	260.08	2540	0.741	255.08	1900	233.13	3400	0.858	7.91
U3,0	238.37	4180	257.73	2520	0.740	253.91	2000	232.41	3520	0.843	6.42
U3,5	244.82	4220	264.74	2500	0.742	262.3	2100	239.55	3720	0.866	5.8
V0	239.37	5560	255.02	3960	0.834	204.64	5280	189.38	7240	1.028	0.91
V0,5	252.41	5030	268.12	3120	0.794	231.32	2560	214.49	4360	1.001	37.79
V1,0	258.63	5220	273.62	3200	0.739	238.29	2600	222	4360	0.936	36.82
V1,5	258.9	5100	274.35	3320	0.761	244.67	2520	227.35	4440	0.972	31.8
V2,0	254.1	5180	269.57	3160	0.777	242.79	2600	225.82	4260	0.959	28.935
V2,5	251.07	4860	266.82	3080	0.800	242.76	2360	225.52	4040	0.975	26.57
V3,0	255.65	5100	270.38	3240	0.735	248.49	2600	232.48	4440	0.879	24.02
V3,5	251.54	4940	267.44	3040	0.806	248.16	2400	230.81	4480	0.959	21.97

	Calculated values					
Letter	$(f_{dn}/f_{d0})^2$	$(f_{wn}/f_{w0})^2$	CF_d	CF_w	E_{dn}/E_{d0}	E_{wn}/E_{w0}
B0	2.011	2.017	1.126	1.145	0*	0*
B0,5	1.379	1.124	1.048	1.069	0*	0*
B1,0	2.605	2.147	1.081	1.100	0*	0*
B1,5	1.757	1.227	1.018	1.035	0*	0*
B2,0	0.830	0.631	1.012	1.024	0.840	0.646
B2,5	0.802	0.649	1.009	1.020	0.809	0.663
B3,0	0.857	0.737	1.007	1.018	0.863	0.751
B3,5	0.857	0.708	1.012	1.024	0.867	0.726
U0	1.734	1.485	1.098	1.115	0*	0*
U0,5	0.766	0.598	1.011	1.030	0.774	0.616
U1,0	0.718	0.468	1.019	1.037	0.732	0.485
U1,5	0.784	0.496	1.016	1.038	0.797	0.514
U2,0	0.707	0.560	1.015	1.029	0.717	0.576
U2,5	0.662	0.560	1.021	1.033	0.675	0.578
U3,0	0.709	0.630	1.017	1.027	0.721	0.647
U3,5	0.777	0.706	1.016	1.029	0.790	0.726
V0	1.696	1.778	0.796	0.807	0*	0*
V0,5	0.751	0.673	1.078	1.094	0.810	0.737
V1,0	0.698	0.660	1.082	1.097	0.755	0.724
V1,5	0.758	0.576	1.071	1.088	0.812	0.627
V2,0	0.676	0.677	1.064	1.078	0.720	0.730
V2,5	0.691	0.587	1.059	1.073	0.732	0.630
V3,0	0.758	0.644	1.055	1.066	0.800	0.687
V3,5	0.822	0.623	1.051	1.063	0.864	0.662

* Broken sample.

Appendix P2.
From Chapter 3.6.4. Unsealed multicycle freeze-thaw test - Scaling test, Limestone tested in NaCl and Na_2SO_4 solution and sandstone Uddvide tested in Na_2SO_4-solution.

The number in the letter indicates percentage by weight of the salt solution.

Table P2.1. Limestone Öland B1 freeze-thaw-tested in NaCl solution.

	Before freezing					After freezing, 4 cycles					
Letter	$Q_{d0(105)}$	f_{d0}	Q_0	f_{w0}	S_0	Q_n	f_{wn}	$Q_{dn(105)}$	f_{dn}	S_n	Q_{ds}
K0Ca	320.44	8830	324.43	8200	0.966	324.57	8000	320.37	8720	1.018	0.01
K0.5Ca	317.22	8750	320.88	8360	0.896	287.77	7440	284.49	8140	0.895	32.67
K1Ca	288.63	8540	292.03	8120	0.914	245.73	6320	242.8	6520	0.937	45.84
K2Ca	321.16	8480	325.29	7960	0.998	240.87	6800	237.7	7740	1.035	83.49
K3Ca	309.02	8400	313.09	7840	1.022	289.26	6400	285.55	7100	1.008	23.35
K4Ca	313.66	8680	317.48	8160	0.945	314.16	7520	310.62	8200	0.885	3.21
K0Cb	273.54	7900	276.96	7440	0.970	277.07	7280	273.46	7860	1.025	5.85
K0.5Cb	310	8680	313.88	8080	0.971	275.85	5200	272	7640	1.099	36.47
K1Cb	314.94	8560	318.63	8080	0.909	276.39	6160	272.69	6920	1.053	42.2
K2Cb	306.44	8520	310.43	7920	1.011	292.19	5160	287.59	6980	1.241	18.84
K3Cb	303.29	8480	307.45	7840	1.065	268.41	4600	263.6	5540	1.416	39.43
K4Cb	315.73	8520	319.91	8000	1.028	316.99	4760	312.34	6880	1.156	3.66
	$Q_{d0(50)}$							$Q_{d0(50)}$			
Ö0C	308.87	8520	312.49	8240	0.910	312.62	8000	308.9	8320	0.935	0
Ö0.5C	309.14	8540	312.62	8120	0.874	311.64	7640	307.65	8160	1.007	1.55
Ö1C	309.35	8520	313.01	8160	0.918	312.52	6120	308.46	7600	1.022	0.99
Ö2C	287.85	8640	291.1	8080	0.876	278.12	6200	274.86	6960	0.921	13.21
Ö3C	310.37	8500	314.06	8160	0.923	307.01	5840	302.86	7600	1.064	7.7
Ö4C	301.72	8760	305.17	8120	0.888	304.77	8000	301.66	8420	0.800	0.55

Calculated values						
Letter	$(f_{dn}/f_{d0})^2$	$(f_{wn}/f_{w0})^2$	CF_d	CF_w	E_{dn}/E_{d0}	E_{wn}/E_{w0}
K0Ca	0.975	0.952	1.000	1.000	0.975	0.952
K0.5Ca	0.865	0.792	1.064	1.064	0.921	0.843
K1Ca	0.583	0.606	1.072	1.072	0.625	0.650
K2Ca	0.833	0.730	1.171	1.171	0.975	0.855
K3Ca	0.714	0.666	1.043	1.043	0.745	0.695
K4Ca	0.892	0.849	1.007	1.006	0.898	0.854
K0Cb	0.990	0.957	1.030	1.031	1.020	0.987
K0.5Cb	0.775	0.414	1.062	1.064	0.823	0.441
K1Cb	0.654	0.581	1.082	1.084	0.707	0.630
K2Cb	0.671	0.424	1.034	1.037	0.694	0.440
K3Cb	0.427	0.344	1.069	1.074	0.456	0.370
K4Cb	0.652	0.354	1.008	1.009	0.657	0.357
Ö0C	0.954	0.943	1.000	1.000	0.954	0.943
Ö0.5C	0.913	0.885	1.003	1.005	0.916	0.889
Ö1C	0.796	0.563	1.002	1.003	0.797	0.564
Ö2C	0.649	0.589	1.022	1.022	0.663	0.602
Ö3C	0.799	0.512	1.015	1.017	0.811	0.521
Ö4C	0.924	0.971	1.003	1.001	0.926	0.972

Table P2.2. Limestone Öland B1 freeze-thaw-tested in solution of $Na_2SO_4 \cdot 10H_2O$.

	Before freezing					After freezing, 20 cycles					
Letter	$Q_{d0(105)}$	f_{d0}	Q_0	f_{w0}	S_0	Q_n	f_{wn}	$Q_{dn(105)}$	f_{dn}	S_n	Q_{ds}
K0Sa	307.9	8600	312.01	7960	1.036	312.21	7320	307.64	7800	1.153	0.18
K0.5Sa	311.35	8560	315.02	8080	0.915	315.07	7320	310.97	7840	1.023	0.32
K1Sa	308.11	8920	311.86	8160	0.945	312.02	7200	307.82	8040	1.059	0.28
K2Sa	292.81	8720	296.48	8080	0.973	296.9	3160	292.61	7460	1.138	0.17
K3Sa	310.97	8600	314.85	8000	0.968	314.97	6320	310.68	7160	1.072	0.4
K4Sa	277.55	8080	281.11	7440	0.996	277.69	13400	276.7	15800	0.278	0.97
K0Sb	279.67	8000	283.22	7480	0.985	283.5	6840	279.48	7560	1.116	0.14
K0.5Sb	312.14	8720	315.74	8160	0.895	315.72	7520	311.61	8120	1.024	0.44
K1Sb	282.95	7960	286.26	7680	0.908	286.09	6840	282.43	7520	1.006	0.56
K2Sb	317.62	8400	321.67	7840	0.990	322.1	5840	317.42	7240	1.144	0.22
K3Sb	288.09	8400	291.75	7600	0.986	292.05	6280	287.91	7360	1.116	0.23
K4Sb	275.75	7920	279.33	7240	1.008	279.5	2440	275.47	5840	1.136	0.4

	Calculated values					
Letter	$(f_{dn}/f_{d0})^2$	$(f_{wn}/f_{w0})^2$	CF_d	CF_w	E_{dn}/E_{d0}	E_{wn}/E_{w0}
K0Sa	0.823	0.846	1.000	1.002	0.823	0.847
K0.5Sa	0.839	0.821	1.000	1.002	0.839	0.822
K1Sa	0.812	0.779	1.000	1.002	0.813	0.780
K2Sa	0.732	0.153	1.000	1.002	0.732	0.153
K3Sa	0.693	0.624	1.001	1.002	0.694	0.626
K4Sa	3.824	3.244	1.002	0.993	0	0
K0Sb	0.893	0.836	1.000	1.002	0.893	0.838
K0.5Sb	0.867	0.849	1.001	1.002	0.868	0.851
K1Sb	0.893	0.793	1.001	1.002	0.893	0.795
K2Sb	0.743	0.555	1.000	1.002	0.743	0.556
K3Sb	0.768	0.683	1.001	1.002	0.768	0.684
K4Sb	0.544	0.114	1.001	1.003	0.544	0.114

Table P2.3. Limestone Öland B1 freeze-thaw-tested in Na_2SO_4 solution.

	Before freezing					After freezing, 20 cycles						
Letter	$Q_{d0(50)}$	f_{d0}	Q_0	f_{w0}	S_0	Q_n	f_{wn}	$Q_{dn(50)}$	f_{dn}	S_n	Q_{ds}	$Q_{dn(105)}$
Ö0S	315.65	8820	319.09	8320	0.846	319.14	8240	315.69	8600	0.848	0.87	315.46
Ö0.5S	312.1	8840	315.61	8360	0.873	315.23	7500	311.6	8280	0.904	1.39	311.45
Ö1S	293.9	8600	297.34	8000	0.908	293.99	7500	290.26	8480	0.997	3.9	290.07
Ö2S	298.87	8600	302.12	8160	0.844	302.27	7760	297.21	8440	1.321	3.09	297.03
Ö3S	287.81	8300	291.05	7840	0.874	291.04	7360	287.79	7920	0.877	4.37	287.63
Ö4S	292.12	8320	295.51	7720	0.901	295.42	7120	292.01	7280	0.906	3.13	291.85

	Calculated values					
Letter	$(f_{dn}/f_{d0})^2$	$(f_{wn}/f_{w0})^2$	CF_d	CF_w	E_{dn}/E_{d0}	E_{wn}/E_{w0}
Ö0S	0.951	0.981	1.005	1.005	0.955	0.985
Ö0.5S	0.877	0.805	1.005	1.006	0.882	0.810
Ö1S	0.972	0.879	1.007	1.009	0.979	0.886
Ö2S	0.963	0.904	1.010	1.016	0.973	0.919
Ö3S	0.911	0.881	1.022	1.022	0.931	0.901
Ö4S	0.766	0.851	1.016	1.016	0.778	0.864

Table P2.4. Sandstone Uddvide freeze-thaw-tested in solution of $Na_2SO_4 \cdot 10H_2O$.

	Before freezing					After freezing, 20 cycles					
Letter	$Q_{d0(105)}$	f_{d0}	Q_0	f_{w0}	S_0	Q_n	f_{wn}	$Q_{dn(105)}$	f_{dn}	S_n	Q_{ds}
U0Sa	231.8	3820	250.83	2560	0.748	254.13	1920	230.99	3260	0.913	0.63
U0.5Sa	232.37	3900	251.43	2520	0.748	253.5	1960	230.84	3580	0.895	1.51
U1Sa	231.59	3980	250.61	2520	0.749	251.09	1940	228.81	3680	0.888	2.63
U2Sa	230.86	4020	250.03	2560	0.757	251.21	1640	228.85	3640	0.891	2.15
U3Sa	232.57	3940	251.79	2550	0.753	251.75	2080	229.64	4100	0.878	2.98
U4Sa	229.55	3840	248.85	2520	0.766	249.36	1740	228	3820	0.854	1.87

	Calculated values					
Letter	$(f_{dn}/f_{d0})^2$	$(f_{wn}/f_{w0})^2$	CF_d	CF_w	E_{dn}/E_{d0}	E_{wn}/E_{w0}
U0Sa	0.728	0.563	1.001	1.017	0.729	0.572
U0.5Sa	0.843	0.605	1.003	1.018	0.845	0.616
U1Sa	0.855	0.593	1.005	1.019	0.859	0.604
U2Sa	0.820	0.410	1.005	1.019	0.824	0.418
U3Sa	1.083	0.665	1.007	1.019	1.010	0.678
U4Sa	0.990	0.477	1.005	1.014	0.995	0.484

Table P2.5. Sandstone Uddvide freeze-thaw-tested in Na_2SO_4 solution.

	Before freezing					After freezing, 20 cycles						
Letter	$Q_{d0(50)}$	f_{d0}	Q_0	f_{w0}	S_0	Q_n	f_{wn}	$Q_{dn(50)}$	f_{dn}	S_n	Q_{ds}	$Q_{dn(105)}$
U0	224.27	4040	241.33	2660	0.693	245	2320	223.93	3680	0.858	2.31	223.79
U0.5	221.34	4080	238.07	2640	0.689	241.05	1820	220.46	3440	0.851	2.14	220.29
U1	226.18	4080	243.27	2660	0.689	246.91	1960	226.01	3680	0.843	2.15	225.92
U2	225.11	4140	242.76	2640	0.715	245.49	2260	224.58	4000	0.849	1.78	224.46
U3	223.38	4180	241.34	2780	0.733	243.79	2020	222.94	3960	0.852	3.35	222.85
U4	224.46	4200	242.81	2680	0.745	244.82	1500	225.81	3560	0.767	3.61	225.63

	Calculated values					
Letter	$(f_{dn}/f_{d0})^2$	$(f_{wn}/f_{w0})^2$	CF_d	CF_w	E_{dn}/E_{d0}	E_{wn}/E_{w0}
U0	0.830	0.761	1.014	1.031	0.841	0.784
U0.5	0.711	0.475	1.010	1.027	0.718	0.488
U1	0.814	0.543	1.013	1.029	0.824	0.559
U2	0.934	0.733	1.009	1.023	0.942	0.750
U3	0.898	0.528	1.020	1.032	0.915	0.545
U4	0.718	0.313	1.030	1.032	0.740	0.323

Table P2.6. Borghamn limestone freeze-thaw-tested in NaCl solution.

	Before freezing					After freezing, 20 cycles						
Letter	$Q_{d0(50)}$	f_{d0}	Q_0	f_{w0}	S_0	Q_n	f_{wn}	$Q_{dn(50)}$	f_{dn}	S_n	Q_{ds}	$Q_{dn(105)}$
0Ca	277.455	8880	278.3	8840	0.463	278.46	8500	277.45	8700	0.554	1.42	277.29
0Cb	277.21	9080	278.09	8840	0.483	278.15	8700	277.19	8900	0.527	1.07	277.06
0.5Ca	288.68	9240	289.4	9240	0.380	288.71	8560	287.84	8720	0.460	0.76	287.66
0.5Cb	279.22	9180	280.05	9120	0.452	280.14	8800	279.2	8800	0.512	1.53	279.06
1Ca	279.16	9120	280.21	8960	0.572	265.45	8000	264.2	8440	0.720	15.95	264.05
1Cb	279.51	8880	280.86	8600	0.735	279.94	8640	278.59	8560	0.737	1.67	278.4
2Ca	270.795	8740	272.4	8680	0.902	269.3	8240	267.82	8440	0.841	4.52	267.62
2Cb	280.48	9220	281.42	9160	0.510	281.58	8900	280.9	8900	0.368	0.2	280.56
3Ca	280.76	9200	281.7	9040	0.509	280.51	8400	279.39	8640	0.610	2.36	279.21
3Cb	283.36	8680	284.92	8400	0.838	285.08	7900	283.44	8300	0.880	2.16	283.23
4Ca	289.39	9160	290.45	9000	0.557	290.6	8720	289.46	8880	0.599	0.98	289.29
4Cb	286.37	9220	287.16	9120	0.420	287.29	8800	286.45	8800	0.446	0.3	286.23

	Calculated values					
Letter	$(f_{dn}/f_{d0})^2$	$(f_{wn}/f_{w0})^2$	CF_d	CF_w	E_{dn}/E_{d0}	E_{wn}/E_{w0}
0Ca	0.960	0.925	1.007	1.008	0.967	0.932
0Cb	0.961	0.969	1.005	1.006	0.966	0.974
0.5Ca	0.891	0.858	1.001	1.001	0.891	0.859
0.5Cb	0.919	0.931	1.008	1.008	0.926	0.939
1Ca	0.856	0.797	1.026	1.027	0.879	0.819
1Cb	0.929	1.009	1.005	1.005	0.934	1.014
2Ca	0.933	0.901	1.012	1.011	0.943	0.911
2Cb	0.932	0.944	1.002	1.002	0.934	0.946
3Ca	0.882	0.863	1.007	1.008	0.888	0.870
3Cb	0.914	0.884	1.011	1.011	0.925	0.895
4Ca	0.940	0.939	1.005	1.005	0.945	0.944
4Cb	0.911	0.931	1.002	1.002	0.913	0.933

Table P2.7. Borghamn limestone freeze-thaw-tested in solution of $Na_2SO_4 \cdot 10H_2O$.

	Before freezing					After freezing, 20 cycles						
Letter	$Q_{d0(50)}$	f_{d0}	Q_0	f_{w0}	S_0	Q_n	f_{wn}	$Q_{dn(50)}$	f_{dn}	S_n	Q_{ds}	$Q_{dn(105)}$
0Ca	284.69	9240	285.68	9080	0.529	285.83	8400	284.6	8640	0.658	0.18	284.53
0Cb	270.33	8820	271.34	8680	0.568	271.32	8360	270.28	8480	0.585	0.2	270.11
0.5Ca	264.22	8760	265.15	8720	0.536	265.07	8500	264.12	8480	0.547	0.15	264
0.5Cb	284.76	9340	285.54	9160	0.417	285.59	8900	284.67	8920	0.492	0.3	284.46
1Ca	280.86	9120	281.73	9080	0.471	281.81	8800	280.77	8800	0.564	0.21	280.59
1Cb	267.66	8930	268.53	8740	0.495	268.59	8560	267.6	8500	0.563	1.64	267.44
2Ca	279.375	9140	280.4	8880	0.558	280.45	8680	279.33	8720	0.610	0.27	279.14
2Cb	273.08	9020	274.15	8680	0.596	273.66	8400	272.51	8500	0.642	1.81	272.33
3Ca	287.26	9020	288.1	9040	0.445	288.18	8500	287.08	8400	0.583	0.69	286.97
3Cb	276.67	9020	277.8	8800	0.621	277.69	8560	276.33	8640	0.749	1.6	276.23
4Ca	283.97	9180	284.72	8960	0.402	284.85	8960	284.02	8880	0.445	2.99	283.84
4Cb	285.59	9280	286.37	9240	0.416	286.48	8800	285.6	8960	0.469	1.65	285.38

	Calculated values					
Letter	$(f_{dn}/f_{d0})^2$	$(f_{wn}/f_{w0})^2$	CF_d	CF_w	E_{dn}/E_{d0}	E_{wn}/E_{w0}
0Ca	0.874	0.856	1.001	1.001	0.875	0.857
0Cb	0.924	0.928	1.001	1.001	0.925	0.928
0.5Ca	0.937	0.950	1.000	1.000	0.937	0.951
0.5Cb	0.912	0.944	1.001	1.002	0.913	0.946
1Ca	0.931	0.939	1.001	1.001	0.932	0.941
1Cb	0.906	0.959	1.008	1.008	0.913	0.967
2Ca	0.910	0.955	1.001	1.002	0.911	0.957
2Cb	0.888	0.937	1.007	1.007	0.894	0.943
3Ca	0.867	0.884	1.003	1.004	0.870	0.887
3Cb	0.918	0.946	1.007	1.008	0.924	0.953
4Ca	0.936	1.000	1.015	1.016	0.950	1.016
4Cb	0.932	0.907	1.008	1.009	0.940	0.915

Table P2.8. Borghamn limestone freeze-thaw-tested in Na_2SO_4 solution.

	Before freezing					After freezing, 20 cycles						
Letter	$Q_{d0(50)}$	f_{d0}	Q_0	f_{w0}	S_0	Q_n	f_{wn}	$Q_{dn(50)}$	f_{dn}	S_n	Q_{ds}	$Q_{dn(105)}$
B0	277.49	9100	278.4	8880	0.499	278.48	8240	277.45	8700	0.565	1.85	277.3
B0.5	271.51	9100	272.84	8780	0.745	272.74	8800	271.38	8760	0.763	0.54	271.23
B1	287.54	8880	288.91	8640	0.725	288.99	8600	287.63	8900	0.719	1	287.42
B2	268.46	8780	270.02	8720	0.884	270.09	8480	268.49	8640	0.907	3.2	268.31
B3	271.18	8980	271.86	8960	0.382	271.98	8560	271.16	8720	0.460	2.07	271.01
B4	282.75	9080	283.58	9120	0.447	283.81	8900	282.71	8680	0.592	2.74	282.52

	Calculated values					
Letter	$(f_{dn}/f_{d0})^2$	$(f_{wn}/f_{w0})^2$	CF_d	CF_w	E_{dn}/E_{d0}	E_{wn}/E_{w0}
B0	0.914	0.861	1.009	1.010	0.922	0.869
B0.5	0.927	1.005	1.002	1.002	0.929	1.007
B1	1.005	0.991	1.005	1.005	1.010	0.996
B2	0.968	0.946	1.016	1.016	0.984	0.961
B3	0.943	0.913	1.010	1.011	0.953	0.923
B4	0.914	0.952	1.014	1.015	0.926	0.966

Appendix P3.
From Chapter 3.6.5. Unsealed multicycle freeze-thaw test - Scaling test, Granite tested in solutions of NaCl and Na_2SO_4.

First part of letter: S means 2% Na_2SO_4 solution.
First part of letter: C means 2% NaCl solution.
First part of letter: H means pure water.
Second part of letter: V means vacuum saturated.
Second part of letter: C means capillary saturated for 10 days.
Letter D is a dummy specimen with a drilled hole for temperature measurement.

Table P3.1. Granite

	Before freezing					After freezing, 35 cycles						
Letter	$Q_{d0(50)}$	f_{d0}	Q_0	f_{w0}	S_0	Q_n	f_{wn}	$Q_{dn(50)}$	f_{dn}	S_n	Q_{ds}	$Q_{dn(50)}+Q_{ds}$
SV	304.09	9720	304.46	10380	0.764	304.41	9800	304.02	9660	0.813	0.085	303.825
CV	304.7	9600	305.04	9820	0.915	305.04	9720	304.64	9360	0.943	0.02	304.36
SC	307.32	9220	307.65	9580	0.783	307.59	9560	307.18	9300	0.839	0.1	306.98
CC	298.86	9200	299.19	9660	0.947	299.18	9840	298.78	9440	0.947	0.01	298.51
HV	303.97	9680	304.31	10060	0.848	304.35	10120	303.9	10000	0.966	0.045	303.655
HC	333.7	9600	334.12	10060	0.810	334.09	9960	333.64	9680	0.861	0.07	333.41
CCD	293.14	8920	293.53	9460		293.41	9280	292.75	8680		0.04	292.6

	Calculated values					
Letter	$(f_{dn}/f_{d0})^2$	$(f_{wn}/f_{w0})^2$	CF_d	CF_w	E_{dn}/E_{d0}	E_{wn}/E_{w0}
SV	0.988	0.891	1.000	1.000	0.988	0.892
CV	0.951	0.980	1.000	1.000	0.951	0.980
SC	1.017	0.996	1.000	1.000	1.017	0.996
CC	1.053	1.038	1.000	1.000	1.053	1.038
HV	1.067	1.012	1.000	1.000	1.067	1.012
HC	1.017	0.980	1.000	1.000	1.017	0.980
CCD	0.947	0.962	0.999	1.000	0.946	0.962

Appendix P4.
From Chapter 3.6.6. Unsealed multicycle freeze-thaw test - Scaling test, test with different internal and external salt concentrations.

Letter i*ayb* means internal concentration of *a* percentage by weight and external concentration of *b* percentage by weight.

The prisms were sometimes so badly scaled that it was not possible to calculate the resonant frequency.

Table P4.1. Sandstone Valar tested in NaCl solution.

	Before freezing					14 cycles					
Letter	$Q_{d0(105)}$	f_{d0}	Q_0	f_{w0}	S_0	Q_n	f_{wn}	Q_{ds}	$(f_{wn}/f_{w0})^2$	CF_w	E_{wn}/E_{w0}
i0y0	257.73	4280	277.57	2960	0.982	277.73	2440	0.46	0.680	1.003	0.682
i0y0.25	255.06	4300	274.96	2960	0.995	256.02	1600	17.32	0.292	1.036	0.303
i0y0.5	256.55	4300	276.56	3120	0.995	263.76	1400	11.54	0.201	1.023	0.206
i0y1	251.6	5200	270.83	3560	0.975	253.49	1840	19.23	0.267	1.054	0.281
i0.25y0	247.48	4040	266.9	2960	1.001	263.83	2140	3.27	0.523	1.008	0.527
i0.25y0.25	254.14	4320	274	2840	0.997	252.25	1580	20.13	0.310	1.042	0.323
i0.25y0.5	257.5	4180	277.51	3160	0.991	269.63	1380	8.4	0.191	1.023	0.195
i0.25y1	252.48	4260	272.25	2880	0.999	254.28	900	18.38	0.098	1.046	0.102
i0.5y0	255.8	5040	275.67	3440	0.991	271.18	2640	4.74	0.589	1.012	0.596
i0.5y0.25	248.89	4040	268.4	2800	1.000	264.18	1740	4.81	0.386	1.013	0.391
i0.5y0.5	252.34	5180	272.4	3320	1.014	257.49	2460	14.81	0.549	1.035	0.568
i0.5y1	255.65	4320	275.56	3000	0.994	257.16	1120	17.74	0.139	1.041	0.145
i1y0	251.71	5200	271.07	3480	0.981	266.05	2840	5.29	0.666	1.013	0.675
i1y0.25	253.53	4360	272.97	2480	0.978	268.67	1700	6.04	0.470	1.021	0.480
i1y0.5	246.1	4220	265.45	3280	1.003	261.79	2400	4.65	0.535	1.014	0.543
i1y1	250.7	5280	270.22	3440	0.993	258.53	2260	11.95	0.432	1.029	0.444

	23 cycles						
Letter	Q_n	f_{wn}	Q_{ds}	$Q_{ds}(cum)$	$(f_{wn}/f_{w0})^2$	CF_w	E_{wn}/E_{w0}
i0y0	277.67	2060	0.74	1.2	0.484	1.005	0.487
i0y0.25	234.92	2280	19.9	37.22	0.593	0.966	0.573
i0y0.5	236.29	1720	26.66	38.2	0.304	1.008	0.306
i0y1	234.14	1520	19.32	38.55	0.182	0.974	0.178
i0.25y0	263.86	1780	0.64	3.91	0.362	0.992	0.359
i0.25y0.25	239.02	1200	13.11	33.24	0.179	0.945	0.169
i0.25y0.5	259.12	4480	11.09	19.49	2.010	0.999	2.008
i0.25y1	191.13		58.23	76.61		1.021	
i0.5y0	269.42	2340	2.04	6.78	0.463	0.989	0.458
i0.5y0.25	213.44	2420	46.86	51.67	0.747	1.071	0.800
i0.5y0.5	242.04	1940	15.75	30.56	0.341	0.979	0.334
i0.5y1	227.38		28.34	46.08		0.984	
i1y0	263.47	2640	2.72	8.01	0.576	0.988	0.569
i1y0.25	247.91	5800	19.85	25.89	5.470	1.026	5.613
i1y0.5	243.76	1960	18.13	22.78	0.357	1.027	0.367
i1y1	238.84	1740	18.33	30.28	0.256	0.989	0.253

Table P4.1. Sandstone Valar tested in NaCl solution.

	31 cycles						
Letter	Q_n	f_{wn}	Q_{ds}	$Q_{ds}(cum)$	$(f_{wn}/f_{w0})^2$	CF_w	E_{wn}/E_{w0}
i0y0	277.81	1860	0.32	1.06	0.395	1.003	0.396
i0y0.25	170.61		59.02	78.92		0.908	
i0y0.5	145.94		82.04	108.7		0.909	
i0y1	202.94	1100	28.32	47.64	0.095	0.894	0.085
i0.25y0	263.74	1500	0.88	1.52	0.257	0.993	0.255
i0.25y0.25	175.84	1680	58.6	71.71	0.350	0.936	0.328
i0.25y0.5	152.19	2360	97.47	108.56	0.558	1.059	0.591
i0.25y1			171.81	230.04			
i0.5y0	267.98	2180	2.07	4.11	0.402	0.984	0.395
i0.5y0.25	171.63	2000	40.13	86.99	0.510	0.823	0.420
i0.5y0.5	215.03	1580	24.96	40.71	0.226	0.921	0.209
i0.5y1			206.75	235.09			
i1y0	259.69	2400	4.1	6.82	0.476	0.982	0.467
i1y0.25	171.5	3000	70.02	89.87	1.463	0.992	1.452
i1y0.5	199.23	1620	41.33	59.46	0.244	0.974	0.238
i1y1	208.98	1340	27.15	45.48	0.152	0.915	0.139

Table P4.2. Sandstone Valar tested in Na_2SO_4 solution.

	Before freezing					23 cycles					
Letter	$Q_{d0(105)}$	f_{d0}	Q_{w0}	f_{w0}	S_0	Q_n	f_{wn}	Q_{ds}	$(f_{wn}/f_{w0})^2$	CF_w	E_{wn}/E_{w0}
i0y0	256.97	4020	276.85	2840	0.987	277.09	1960	1.31	0.476	1.009	0.480
i0y0.25	250.95	5140	270.51	3320	0.994	253.82	2120	17.37	0.408	1.044	0.426
i0y0.5	254.88	4240	274.34	2920	0.974	264.78	1860	10.86	0.406	1.031	0.418
i0y1	257.96	4340	277.75	3000	0.979	269.41	2160	9.7	0.518	1.029	0.533
i0.25y0	266.37	4440	286.98	2880	0.987	282.2	2560	5.31	0.790	1.015	0.802
i0.25y0.25	247.55	4240	267.05	2840	1.005	252.54	2400	14.79	0.714	1.035	0.739
i0.25y0.5	261.17	4260	281.71	2920	1.003	265.76	2320	15.21	0.631	1.036	0.654
i0.25y1	261.37	4340	281.7	2960	0.992	274.72	2080	8.37	0.494	1.026	0.507
i0.5y0	256.39	5100	276	3440	0.976	275.44	2720	1.69	0.625	1.008	0.630
i0.5y0.25	253.14	4100	272.65	2880	0.983	259.24	2220	13.86	0.594	1.035	0.615
i0.5y0.5	253.89	5100	273.83	3480	1.002	260.93	2720	13.16	0.611	1.033	0.631
i0.5y1	255.03	4300	274.75	3000	0.987	253.29	2300	21.16	0.588	1.050	0.617
i1y0	251.41	5040	271.04	3440	0.996	264.22	2600	7.59	0.571	1.021	0.583
i1y0.25	254.08	5020	273.8	3400	0.990	253.92	2800	19.47	0.678	1.045	0.709
i1y0.5	254.52	4340	274.54	2920	1.004	229.7	2760	42.7	0.893	1.096	0.979
i1y1	254.84	5040	274.9	3440	1.004	258.83	2600	16.26	0.571	1.040	0.594

Table P4.2. Sandstone Valar tested in Na_2SO_4 solution.

	38 cycles						
Letter	Q_n	f_{wn}	Q_{ds}	$Q_{ds}(cum)$	$(f_{wn}/f_{w0})^2$	CF_w	E_{wn}/E_{w0}
i0y0	277.67	2060	0.74	2.05	0.526	1.007	0.530
i0y0.25	234.92	2280	19.9	37.27	0.472	0.982	0.463
i0y0.5	236.29	1720	26.66	37.52	0.347	1.016	0.353
i0y1	234.14	1520	19.32	29.02	0.257	0.949	0.244
i0.25y0	263.86	1780	0.64	5.95	0.382	0.923	0.353
i0.25y0.25	239.02	1200	13.11	27.9	0.179	0.970	0.173
i0.25y0.5	259.12	4480	11.09	26.3	2.354	0.984	2.317
i0.25y1	191.13		58.23	66.6		0.987	
i0.5y0	269.42	2340	2.04	3.73	0.463	0.988	0.457
i0.5y0.25	213.44	2420	46.86	60.72	0.706	1.054	0.744
i0.5y0.5	242.04	1940	15.75	28.91	0.311	0.973	0.303
i0.5y1	227.38		28.34	49.5		0.987	
i1y0	263.47	2640	2.72	10.31	0.589	0.988	0.582
i1y0.25	247.91	5800	19.85	39.32	2.910	1.023	2.977
i1y0.5	243.76	1960	18.13	60.83	0.451	0.993	0.447
i1y1	238.84	1740	18.33	34.59	0.256	0.972	0.249

	52 cycles						
Letter	Q_n	f_{wn}	Q_{ds}	$Q_{ds}(cum)$	$(f_{wn}/f_{w0})^2$	CF_w	E_{wn}/E_{w0}
i0y0	236.91		4.6	5.34		0.880	
i0y0.25	236.51	1440	10.99	30.89	0.188	0.935	0.176
i0y0.5	217.35	1700	34.75	61.41	0.339	0.985	0.334
i0y1	220.1	1760	35.62	54.94	0.344	0.991	0.341
i0.25y0	279.7	1640	1.13	1.77	0.324	0.981	0.318
i0.25y0.25	220.11	1960	22.12	35.23	0.476	0.945	0.450
i0.25y0.5	220.2	2360	15.66	26.75	0.653	0.860	0.562
i0.25y1	204.13	1520	23.5	81.73	0.264	0.838	0.221
i0.5y0	273.89	2080	1.72	3.76	0.366	1.003	0.367
i0.5y0.25	196.48	2600	29.76	76.62	0.815	0.867	0.707
i0.5y0.5	232.48	2020	17.72	33.47	0.337	0.947	0.319
i0.5y1	184.16	2440	30.29	58.63	0.662	0.810	0.536
i1y0	257.7	2040	5.07	7.79	0.352	0.980	0.345
i1y0.25	234.17	2020	10.38	30.23	0.353	0.911	0.322
i1y0.5	164.1	3000	23.55	41.68	1.056	0.691	0.730
i1y1	217.57	1700	29.61	47.94	0.244	0.952	0.232

Table P4.3. Limestone Öland B1 tested in NaCl solution.

	Before freezing					3 cycles					
Letter	$Q_{d0(105)}$	f_{d0}	Q_0	f_{w0}	S_0 [1]	Q_n	f_{wn}	Q_{ds}	$(f_{wn}/f_{w0})^2$	CF_w	E_{wn}/E_{w0}
i0y0	305.59	8024	310.2	8000	1.171	310.23	7840	0.08	0.960	1.001	0.961
i0y0.25	266.69	8144	270.64	6720	1.150	247.12		22.56		1.026	
i0y0.5	303.63	8184	307.66	8160	1.030	305.5	5920	4.66	0.526	1.017	0.535
i0y1	305.68	8408	309.89	8080	1.069	280.41		29.61		1.056	
i0.25y0	297.84	8184	302.67	7680	1.259	302.68	7680	0.06	1.000	1.000	1.000
i0.25y0.25	300.65	8416	304.75	7920	1.058	304.31	7760	0.57	0.960	1.001	0.961
i0.25y0.5	295.58	8440	299.91	8000	1.137	284.74	7840	15.32	0.960	1.027	0.987
i0.25y1	305.91	8456	310.65	8080	1.203	287.97		22.63		1.042	
i0.5y0	305.56	8464	310.54	7920	1.265	310.52	7840	0.01	0.980	1.000	0.980
i0.5y0.25	297.37	8480	301.84	8000	1.167	295.55	7200	6.48	0.810	1.012	0.820
i0.5y0.5	300.72	8240	305.32	7840	1.187	301.11	7360	4.4	0.881	1.009	0.889
i0.5y1	304.25	8336	308.48	8080	1.079	305.52	7680	3.16	0.903	1.006	0.909
i1y0	296.96	8408	301.25	7680	1.121	301.25	7760	0.01	1.021	1.000	1.021
i1y0.25	302.26	8320	306.84	7760	1.176	306.9	7600	0.07	0.959	1.001	0.960
i1y0.5	305.05	8456	309.13	7920	1.038	300.75	8120	8.29	1.051	1.015	1.067
i1y1	306.91	8440	311.32	8000	1.115	278.73	8600	32.3	1.156	1.060	1.225

	4 cycles						
Letter	Q_n	f_{wn}	Q_{ds}	$Q_{ds}(cum)$	$(f_{wn}/f_{w0})^2$	CF_w	E_{wn}/E_{w0}
i0y0	310.24	7920	0.03	0.11	0.980	1.000	0.980
i0y0.25	242.84		4.62	27.18		0.919	
i0y0.5	285.15	12400	18.35	23.01	2.309	1.019	2.353
i0y1	275.18	10800	5.15	34.76	1.787	0.912	1.629
i0.25y0	302.68	7520			0.959	1.000	0.959
i0.25y0.25	304.62	7680	0.02	0.59	0.940	1.000	0.940
i0.25y0.5	279.2	7440	5.33	20.65	0.865	0.957	0.827
i0.25y1	274.86	8880	12.86	35.49	1.208	0.945	1.142
i0.5y0	310.51	7360			0.864	1.000	0.864
i0.5y0.25	279.36	11000	15.13	21.61	1.891	1.000	1.891
i0.5y0.5	290.64	6560	10.07	14.47	0.700	1.002	0.702
i0.5y1	305.26	7760	0.27	3.43	0.922	0.991	0.914
i1y0	301.22	7680	0	0.01	1.000	1.000	1.000
i1y0.25	306.68	7680	0.17	0.24	0.979	1.000	0.980
i1y0.5	300.76	8160	0.01	8.3	1.062	0.973	1.033
i1y1	276.65	8480	1.99	34.29	1.124	0.898	1.009

[1] One possible reason why the calculated degrees of saturation are higher than 1, which is of course theoretically impossible, is that the porosity and density of the particular piece of stone used in this test were somewhat different than in the piece of stone used for measurement of porosity and density.

Table P4.3. Limestone Öland B1 tested in NaCl solution.

	7 cycles						
Letter	Q_n	f_{wn}	Q_{ds}	$Q_{ds}(cum)$	$(f_{wn}/f_{w0})^2$	CF_w	E_{wn}/E_{w0}
i0y0	310.24	7840	0.1	0.13	0.960	1.001	0.961
i0y0.25	162.62		78.8	83.42		0.924	
i0y0.5	233.28	6400	50.56	68.91	0.615	0.992	0.610
i0y1	196.51	9600	75.11	80.26	1.412	0.955	1.348
i0.25y0	302.68	7520	0.12	0.12	0.959	1.001	0.959
i0.25y0.25	304.14	7760	0.22	0.24	0.960	0.999	0.959
i0.25y0.5	262.85	8960	15.78	21.11	1.254	0.951	1.192
i0.25y1	191.86	11400	81.4	94.26	1.991	0.965	1.921
i0.5y0	310.51	7760	0.07	0.07	0.960	1.000	0.960
i0.5y0.25	229.56	10800	48.86	63.99	1.823	0.986	1.796
i0.5y0.5	252.52	8080	37.25	47.32	1.062	1.006	1.068
i0.5y1	304.85	7840	0.54	0.81	0.941	0.991	0.933
i1y0	301.22	7680	0.1	0.1	1.000	1.000	1.000
i1y0.25	279.25	7760	26.91	27.08	1.000	1.047	1.047
i1y0.5	300.66	8320	0.14	0.15	1.104	0.973	1.074
i1y1	276.57	8000	0.44	2.43	1.000	0.890	0.890

	10 cycles						
Letter	Q_n	f_{wn}	Q_{ds}	$Q_{ds}(cum)$	$(f_{wn}/f_{w0})^2$	CF_w	E_{wn}/E_{w0}
i0y0	310.26	7520	0.07	78.87	0.884	1.001	0.884
i0y0.25	147.78		14.78	65.34		0.589	
i0y0.5	130.02		101.66	176.77		0.747	
i0y1	160.96		34.83	34.95		0.623	
i0.25y0	302.65	7680	0.04	0.26	1.000	1.000	1.000
i0.25y0.25	300.09	7680	4.03	19.81	0.940	1.005	0.945
i0.25y0.5	248.1	10400	14.52	95.92	1.690	0.891	1.506
i0.25y1	179.21	12000	12.15	12.22	2.206	0.614	1.354
i0.5y0	310.5	7760	0.02	48.88	0.960	1.000	0.960
i0.5y0.25	216.52	11000	12.86	50.11	1.891	0.766	1.449
i0.5y0.5	252.23	8000	0.31	0.85	1.041	0.827	0.862
i0.5y1	223.17	10000	80.47	80.57	1.532	1.124	1.722
i1y0	301.22	7760	0.03	26.94	1.021	1.000	1.021
i1y0.25	243.34	10000	35.22	35.36	1.661	0.954	1.584
i1y0.5	286.32	8160	14.24	14.68	1.062	0.996	1.058
i1y1	252.98	8800	23.18	23.18	1.210	0.916	1.109

Table P4.4. Limestone Öland B1 tested in Na_2SO_4 solution.

	Before freezing					23 cycles					
Letter	$Q_{d0(105)}$	f_{d0}	Q_0	f_{w0}	S_0 [1]	Q_n	f_{wn}	Q_{ds}	$(f_{wn}/f_{w0})^2$	CF_w	E_{wn}/E_{w0}
i0y0	299.75	8456	304.46	7760	1.220	304.79	6240	0.24	0.647	1.002	0.648
i0y0.25	302.2	8296	306.26	7680	1.043	291.85	7520	14.51	0.959	1.027	0.984
i0y0.5	305.48	8360	309.75	7680	1.085	303.04	6960	7.05	0.821	1.014	0.833
i0y1	306.65	8424	310.8	8160	1.050	306.71	8080	4.22	0.980	1.008	0.989
i0.25y0	299.34	8408	303.39	7600	1.050	303.4	7600	0.18	1.000	1.001	1.001
i0.25y0.25	304.72	8392	309.26	7920	1.156	309.19	7200	0.32	0.826	1.001	0.828
i0.25y0.5	309.24	8360	313.55	7920	1.082	313.55	7360	0.34	0.864	1.002	0.865
i0.25y1	294.12	8256	298.23	7920	1.085	289.45	7600	8.97	0.921	1.016	0.936
i0.5y0	304.53	8432	309.02	7840	1.144	309	7360	0.2	0.881	1.001	0.882
i0.5y0.25	309	8252	313.15	8000	1.042	309.78	7680	3.51	0.922	1.007	0.928
i0.5y0.5	305.24	8456	309.87	8000	1.177	309.03	7560	1.04	0.893	1.003	0.895
i0.5y1	299.53	8304	303.85	7840	1.119	300.57	7440	3.58	0.901	1.007	0.907
i1y0	296.51	8344	300.83	8000	1.131	300.85	7840	0.13	0.960	1.001	0.961
i1y0.25	298.66	8240	303.31	7920	1.208	291.99	7840	11.18	0.980	1.019	0.999
i1y0.5	306.5	8400	310.7	8000	1.064	310.67	8000	0.12	1.000	1.001	1.001
i1y1	299.52	8328	304.07	8000	1.179	301.28	7440	2.94	0.865	1.006	0.870

	38 cycles						
Letter	Q_n	f_{wn}	Q_{ds}	$Q_{ds}(cum)$	$(f_{wn}/f_{w0})^2$	CF_w	E_{wn}/E_{w0}
i0y0	302.16	5920	2.82	3.06	0.582	1.007	0.586
i0y0.25	285.76	7520	6.2	20.71	0.959	0.963	0.923
i0y0.5	302.62	7100	0.65	7.7	0.855	0.980	0.838
i0y1	306.58	7440	0.43	4.65	0.831	0.989	0.822
i0.25y0	303.46	7280	0.21		0.918	1.001	0.919
i0.25y0.25	301.89	6720	7.44	7.76	0.720	1.014	0.730
i0.25y0.5	306.82	6880	6.82	7.16	0.755	1.013	0.765
i0.25y1	289.39	7440	0.21	9.18	0.882	0.971	0.857
i0.5y0	309	6960	0.21		0.788	1.001	0.789
i0.5y0.25	309.43	7280	0.6	4.11	0.828	0.991	0.821
i0.5y0.5	307.06	7360	2.14	3.18	0.846	1.002	0.848
i0.5y1	300.71	7360	0.22	3.8	0.881	0.991	0.873
i1y0	300.8	7440	0.2	0.33	0.865	1.001	0.866
i1y0.25	289.87	7520	2.36	13.54	0.902	0.967	0.872
i1y0.5	310.7	7760	0.2	0.32	0.941	1.001	0.942
i1y1	298.97	7360	2.45	5.39	0.846	0.996	0.843

[1] One possible reason why the calculated degrees of saturation are higher than 1, which is of course theoretically impossible, is that the porosity and density of the particular piece of stone used in this test were somewhat different than in the piece of stone used for measurement of porosity and density.

Table P4.4. Limestone Öland B1 tested in Na_2SO_4 solution.

	52 cycles						
Letter	Q_n	f_{wn}	Q_{ds}	$Q_{ds}(cum)$	$(f_{wn}/f_{w0})^2$	CF_w	E_{wn}/E_{w0}
i0y0	302.1	6800	0.15	2.97	0.768	0.993	0.763
i0y0.25	285.11	7120	0.68	6.88	0.859	0.934	0.803
i0y0.5	302.54	6720	0.13	0.78	0.766	0.977	0.748
i0y1	300.62	7360	5.93	6.36	0.814	0.997	0.811
i0.25y0	303.39	7200	0.14	0.35	0.898	1.001	0.898
i0.25y0.25	301.13	6480	1	8.44	0.669	0.979	0.655
i0.25y0.5	304.52	6320	2.41	9.23	0.637	0.983	0.626
i0.25y1	288.42	7280	1.18	1.39	0.845	0.973	0.822
i0.5y0	309	6960	0.12	0.33	0.788	1.001	0.789
i0.5y0.25	309.11	6880	0.48	1.08	0.740	0.990	0.732
i0.5y0.5	300.09	6880	6.86	9	0.740	1.003	0.742
i0.5y1	298.95	7200	1.8	2.02	0.843	0.993	0.837
i1y0	300.69	6880	0.27	0.47	0.740	1.001	0.740
i1y0.25	289.86	6400	0.25	2.61	0.653	0.957	0.625
i1y0.5	310.5	7600	0.3	0.5	0.903	1.001	0.903
i1y1	298.26	7040	0.76	3.21	0.774	0.985	0.763

Appendix P5. From Chapter 3.7. Sealed single-cycle freeze-thaw tests - Dilatation tests

Table P5.1. Sandstone Botvide tested in pure water.

	Before freezing							
Letter	$Q_{d0(105°)}$	f_{d0}	Q_{a0}	Q_{w0}	Q_0	f_{w0}	S_0	V_0
B31	136.47	1900	151.06	85.69	146.58	1160	0.693	65.37
B32	141.88	2040	157.29	89.2	153.36	1280	0.745	68.09
B33	137.74	2000	152.57	86.63	149.78	1200	0.812	65.94
B34	138.03	1950	152.89	86.79	150.82	1170	0.861	66.1
B35	140.7	2130	155.64	88.45	154.41	1260	0.918	67.19
B36	135.69	1890	150.17	85.31	150.01	1100	0.989	64.86

	After freezing							
Letter	Q_n	f_{wn}	$Q_{dn(105°)}$	f_{dn}	Q_{an}	Q_{wn}	S_n	V_n
B31	146.39	1140	136.38	1920	151.06	85.68	0.682	65.38
B32	153.29	1200	141.81	1980	157.3	89.03	0.741	68.27
B33	149.62	1140	137.67	1940	152.49	86.52	0.806	65.97
B34	150.65	1070	137.97	1890	152.87	86.56	0.851	66.31
B35	154.24	1140	140.55	2040	155.61	88.25	0.909	67.36
B36	149.81	960	135.63	1660	150.17	85.13	0.975	65.04

	Calculated values						*perm.*	*max.*
Letter	$(f_{dn}/f_{d0})^2$	$(f_{wn}/f_{w0})^2$	CF_d	CF_w	E_{dn}/E_{d0}	E_{wn}/E_{w0}	*dil.(‰)*	*dil.(‰)*
B31	1.021	0.966	0.999	0.999	1.020	0.965	-0.023	-0.015
B32	0.942	0.879	1.000	1.000	0.942	0.879	0	-0.117
B33	0.941	0.903	0.999	0.999	0.940	0.902	0.053	0.035
B34	0.939	0.836	1.000	0.999	0.939	0.835	0.096	0.170
B35	0.917	0.819	0.999	0.999	0.916	0.818	0.167	0.345
B36	0.771	0.762	1.000	0.999	0.771	0.761	0.315	0.616

Table P5.2. Sandstone Uddvide tested in pure water.

	Before freezing							
Letter	$Q_{d0(105°)}$	f_{d0}	Q_{a0}	Q_{w0}	Q_0	f_{w0}	S_0	V_0
U21	134.87	2000	150.34	84.78	145.57	1200	0.692	65.56
U22	134.95	1810	150.65	84.78	147.21	1160	0.781	65.87
U23	139.13	1920	155.14	87.49	152.28	1220	0.821	67.65
U24	135.78	1950	151.43	85.42	149.4	1200	0.870	66.01
U25	135.24	1920	150.52	85.04	149.32	1220	0.921	65.48
U26	138.15	1910	153.88	86.78	153.72	1220	0.990	67.1

	After freezing							
Letter	Q_n	f_{wn}	$Q_{dn(105°)}$	f_{dn}	Q_{an}	Q_{wn}	S_n	V_n
U21	145.17	1160	134.79	1900	150.33	84.57	0.668	65.76
U22	147.03	1140	134.89	1860	150.61	84.64	0.772	65.97
U23	152.08	1240	139.09	1900	155.1	87.23	0.811	67.87
U24	149.09	1180	135.7	1890	151.4	85.11	0.853	66.29
U25	148.91	1100	135.14	1800	150.62	84.78	0.890	65.84
U26	153.51	1060	138.08	1840	153.89	86.64	0.976	67.25

Table P5.2. Sandstone Uddvide tested in pure water.

	Calculated values						*perm.*	*max.*
Letter	$(f_{dn}/f_{d0})^2$	$(f_{wn}/f_{w0})^2$	CF_d	CF_w	E_{dn}/E_{d0}	E_{wn}/E_{w0}	*dil.(‰)*	*dil.(‰)*
U21	0.903	0.934	0.999	0.997	0.902	0.932	-0.013	-0.123
U22	1.056	0.966	1.000	0.999	1.056	0.965	0.003	-0.045
U23	0.979	1.033	1.000	0.999	0.979	1.032	0.006	-0.015
U24	0.939	0.967	0.999	0.998	0.939	0.965	0.041	0.097
U25	0.879	0.813	0.999	0.997	0.878	0.811	0.100	0.226
U26	0.928	0.755	0.999	0.999	0.928	0.754	0.238	0.470

Table P5.3. Sandstone Valar tested in pure water.

	Before freezing							
Letter	$Q_{d0(105°)}$	f_{d0}	Q_{a0}	Q_{w0}	Q_0	f_{w0}	S_0	V_0
V31	134.14	2290	143.98	84.45	141.48	1400	0.746	59.53
V32	146.6	2880	153.41	92.39	152.04	2480	0.799	61.02
V33	133.9	2280	143.84	84.35	142.36	1420	0.851	59.49
V34	132.37	2280	142.29	83.38	141.29	1380	0.899	58.91
V35	128.03	2520	134.94	80.69	134.65	2040	0.958	54.25
V36	131.95	2240	142	83.165	142	1450	1	58.835

Table P5.3. Sandstone Valar tested in pure water.

	After freezing							
Letter	Q_n	f_{wn}	$Q_{dn(105°)}$	f_{dn}	Q_{an}	Q_{wn}	S_n	V_n
V31	141.43	1340	134.04	2140	143.88	84.49	0.751	59.39
V32	151.97	2420	146.51	2660	153.34	92.405	0.799	60.935
V33	142.31	1380	133.79	2220	143.74	84.36	0.856	59.38
V34	141.18	1320	132.26	1120	142.2	83.41	0.897	58.79
V35	134.59	1880	127.96	2280	134.94	80.71	0.950	54.23
V36	141.86	1300	131.84	2060	142	83.12	0.986	58.88

Table P5.3. Sandstone Valar tested in pure water.

	Calculated values						*perm.*	*max.*
Letter	$(f_{dn}/f_{d0})^2$	$(f_{wn}/f_{w0})^2$	CF_d	CF_w	E_{dn}/E_{d0}	E_{wn}/E_{w0}	*dil.(‰)*	*dil.(‰)*
V31	0.873	0.916	0.999	1.000	0.873	0.916	0.014	-0.252
V32	0.853	0.952	0.999	1.000	0.853	0.952	0.014	0.000
V33	0.948	0.944	0.999	1.000	0.947	0.944	0.018	-0.193
V34	0.241	0.915	0.999	0.999	0.241	0.914	-0.029	-0.023
V35	0.819	0.849	0.999	1.000	0.818	0.849	0.076	0.162
V36	0.846	0.804	0.999	0.999	0.845	0.803	0.217	0.417

In Tables P5.4 - P5.10 below:

Letter B means sandstone Botvide.
Letter U means sandstone Uddvide.
Letter V means sandstone Valar.
Letter X means sandstone X:1.
Letter K means limestone Öland B1.

The number in the letter indicates percent by weight of salt solution.

Letter C means NaCl-solution.
Letter S means solution of $Na_2SO_4 \cdot 10H_2O$.

Table P5.4. Samples submerged in solution for 1 day.

	$Q_{dn(105°)}$	f_{dn}	Q_{an}	Q_{wn}	S^1	*perm. dil. (‰)*	*max. dil. (‰)*
B0.5C	125.47	1480	138.76	78.73	0.698	0.008	-0.266
U0.5C	123.79	1860	136.39	77.63	0.691	0.016	-0.116
V0.5C	136.57	2520	143.32	86.04	0.45	0.014	-0.088
B1.0C	121.09	1480	133.92	76.03	0.705	-0.006	-0.208
U1.0C	126.04	1780	139.04	79.01	0.701	0	-0.185
V1.0C	122.76	2000	132.27	77.41	0.676	0.008	-0.273
B0.5S	125.48	1600	138.63	78.67	0.695	-0.006	-0.254
U0.5S	123.73	1740	136.63	77.63	0.974	-0.008	-0.231
V0.5S	144.84	2680	150.42	91.38	0.278	-0.031	-0.116
B1.0S	127.96	1460	141.47	80.46	0.695	0.002	-0.113
U1.0S	123.11	1760	135.81	77.23	0.711	0.002	0.203
V1.0S	122.6	2040	132.38	77.16	0.7	-0.004	-0.051

[1] Calculated before data loss.

Table P5.5. Samples submerged in solution for 7 days.

	Q_n	$Q_{dn(105°)}$	f_{dn}	Q_{an}	Q_{wn}	S_n	*perm. dil. (‰)*	*max. dil. (‰)*
B0.5C	138.56	127.45	1400	140.95	79.48	0.823	0.029	-0.069
U0.5C	134	123.39	1740	136.04	77.5	0.839	0.016	-0.028
V0.5C	134.81	126.97	2200	136.73	80.12	0.803	0.012	-0.254
B1.0C	136.43	125.83	1520	139.13	79.05	0.797	0.006	-0.150
U1.0C	135.44	125.02	1890	138.06	78.5	0.799	0.018	-0.023
V1.0C	132.27	124.45	2060	134.35	78.39	0.790	-0.002	-0.208
B0.5S	140.35	129.2	1500	143.04	81.01	0.806	0.039	-0.070
U0.5S	126.04	116.19	1820	128.22	72.89	0.819	0.006	-0.012
V0.5S	138.16	130.01	2100	140.1	81.92	0.808	0.006	-0.039
B1.0S	139.43	128.31	1460	141.93	80.52	0.816	0.053	0
U1.0S	133.37	122.5	1700	135.62	76.76	0.829	0.014	0
V1.0S	144.55	142.14	2960	145.54	89.77	0.709	0.002	-0.243

Table P5.6. Samples submerged in solution for 21 days.

	Before freezing			After freezing							Calculated values		
Letter	Q_0	f_{w0}	S_0	Q_n	f_{wn}	$Q_{dn}(105°)$	f_{dn}	Q_{an}	Q_{wn}	S_n	$(f_{wn}/f_{w0})^{2}$''	CF_w	E_{wn}/E_{w0}
B0.5C	137.07	860	0.894	136.85	820	125.15	1480	138.48	78.62	0.878	0.909	0.998	0.908
U0.5C	138.15	1200	0.902	137.9	1100	126.29	1800	139.44	79.3	0.883	0.840	0.998	0.839
V0.5C	133.82	1340	0.892	133.66	1320	125.14	2140	134.87	79	0.876	0.970	0.999	0.969
B1.0C	140.68	1000	0.874	140.42	980	128.71	1800	142.4	80.68	0.855	0.960	0.998	0.959
U1.0C	137.21	1120	0.873	137.09	1060	125.56	1830	138.91	78.67	0.864	0.896	0.999	0.895
V1.0C	135.81	1400	0.903	135.63	1320	127.18	2200	136.74	80.14	0.884	0.889	0.999	0.888
B0.5S	140.1	860	0.896	139.92	820	128.06	1520	141.5	80.31	0.882	0.909	0.999	0.908
U0.5S	135.3	1120	0.899	135.08	1030	123.53	1830	136.62	77.54	0.882	0.846	0.998	0.844
V0.5S	127.81	1220	0.898	127.83	1160	118.94	1880	128.82	74.95	0.900	0.904	1.000	0.904
B1.0S	133.87	820	0.888	133.62	770	122.19	1505	135.34	76.76	0.869	0.882	0.998	0.880
U1.0S	135.97	1120	0.918	135.75	1070	124.32	1820	137.01	77.97	0.901	0.913	0.998	0.911
V1.0S	148.42	3000	0.789	148.23	3000	145.61	2960	149.17	91.9	0.736	1.000	0.999	0.999

Letter	*perm. dil. (‰)*	*max. dil. (‰)*
B0.5C	0.014	0.062
U0.5C	0.045	0.069
V0.5C	0.031	0.118
B1.0C	-0.084	0.040
U1.0C	0.022	0.077
V1.0C	-0.016	0.113
B0.5S	0.094	0.092
U0.5S	0.063	0.067
V0.5S	0.006	-0.042
B1.0S	0.112	0.162
U1.0S	0.059	0.035
V1.0S	0.053	0.054

Table P5.7. Samples submerged in solution for 3 months.

	Before freezing			After freezing							Calculated values		
Letter	Q_0	f_{w0}	S_0	Q_n	f_{wn}	$Q_{dn(105°)}$	f_{dn}	Q_{an}	Q_{wn}	S_n	$(f_{wn}/f_{w0})^{2}$''	CF_w	E_{wn}/E_{w0}
B0.5C	142.57	860	1	142.32	760	128.77	1360	142.47	80.79	0.989	0.781	0.998	0.780
U0.5C	137.75	1000	0.995	137.52	830	124.72	1540	137.82	78.24	0.977	0.689	0.998	0.688
V0.5C	130.86	1440	0.985	130.74	1220	121.39	2060	131	76.54	0.973	0.718	0.999	0.717
B1.0C	139.56	880	0.988	139.41	770	126.26	1440	139.72	79.19	0.977	0.766	0.999	0.765
U1.0C	136.41	1100	0.997	136.25	920	123.66	1680	136.45	77.55	0.984	0.700	0.999	0.699
V1.0C	146.32	1720	0.984	146.17	1540	136.7	2300	146.48	86.11	0.968	0.802	0.999	0.801
B0.5S	139.35	980	0.998	139.22	880	126.25	1580	139.37	79.22	0.989	0.806	0.999	0.806
U0.5S	141.44	1040	0.996	141.29	870	128.12	1600	141.5	80.34	0.984	0.700	0.999	0.699
V0.5S	133.26	1420	0.995	133.1	1200	123.18	1920	133.31	77.59	0.979	0.714	0.999	0.713
B1.0S	138.5	830	0.995	138.38	740	125.2	1400	138.57	78.59	0.986	0.795	0.999	0.794
U1.0S	125.73	1880	0.992	125.62	870	113.88	1520	125.82	71.49	0.983	0.214	0.999	0.214
V1.0S	141.72	1420	0.992	141.54	1260	131.38	2020	141.8	82.83	0.975	0.787	0.999	0.786

Letter	*perm. dil. (‰)*	*max. dil. (‰)*
B0.5C	0.650	1.214
U0.5C	0.582	0.965
V0.5C	0.359	0.617
B1.0C	0.654	1.175
U1.0C	0.474	0.789
V1.0C	0.270	0.506
B0.5S	0.513	1.154
U0.5S	0.515	0.850
V0.5S	0.372	0.632
B1.0S	0.492	0.896
U1.0S	0.623	1.030
V1.0S	0.325	0.652

Table P5.8. Samples evacuated to about 280 mbar.

	Before freezing						After freezing						
Letter	$Q_{d0(105°)}$	f_{d0}	Q_{w0}	Q_0	f_{w0}	S_0	Q_n	f_{wn}	$Q_{dn(105°)}$	f_{dn}	Q_{an}	Q_{wn}	S_n
B0.5C	125.73	1620	78.31	138.72	990	0.968	138.47	960	125.73	1650	139.15	78.84	0.949
U0.5C	125.1	1660	77.87	137.52	1110	0.960	137.3	1040	125.09	1680	138.04	78.44	0.943
V0.5C	146.46	2280	91.37	156.59	1300	0.923	156.4	1290	146.45	2240	157.44	92.16	0.905
X0.5C	145.99	2680	91.02	156.21	1980	0.932	156.03	1920	145.99	2680	156.96	91.65	0.915
B1.0C	127.28	1660	79.17	139.99	950	0.942	139.74	1000	127.37	1700	140.77	79.86	0.923
U1.0C	125.29	1760	77.96	137.71	1080	0.935	137.56	1040	125.38	1720	138.57	78.58	0.923
V1.0C	143.96	2300	89.55	153.83	1240	0.899	153.71	1260	144.03	2180	154.94	90.51	0.887
X1.0C	144.95	2920	90.2	155.06	2080	0.928	154.87	2020	145.02	2860	155.85	91.11	0.910
B0.5S	124.13	1440	77.73	137.29	840	0.984	137.12	730	124.14	1410	137.51	77.86	0.971
U0.5S	123.12	1755	77.05	135.9	1080	0.985	135.71	900	123.13	1620	136.09	77.21	0.971
V0.5S	142.62	2320	89.27	153.57	1300	0.961	153.41	1260	142.62	2160	154.02	89.68	0.946
X0.5S	145	2840	90.52	155.4	1960	0.948	155.33	1840	145.01	2560	155.97	91.03	0.942
B1.0S	127.38	1640	79.61	140.87	1020	0.981	140.71	900	127.49	1600	141.13	79.92	0.969
U1.0S	123.62	1620	77.24	136.5	1020	0.989	136.33	880	123.73	1620	136.64	77.49	0.976
V1.0S	148.55	2400	93.03	159.3	1370	0.957	159.16	1260	148.62	2270	159.78	93.47	0.944
X1.0S	143.03	2840	89.26	153.19	2000	0.956	153.04	1920	143.1	2720	153.66	89.77	0.941

	Calculated values							*perm.*	*max.*
Letter	$(f_{dn}/f_{d0})^2$	$(f_{wn}/f_{w0})^2$	CF_d	CF_w	E_{dn}/E_{d0}	E_{wn}/E_{w0}	Q_{dn}-Q_{d0}	*dil. (‰)*	*dil. (‰)*
B0.5C	1.037	0.940	1.000	0.998	1.037	0.939	0	0.135	0.310
U0.5C	1.024	0.878	1.000	0.998	1.024	0.876	-0.01	0.149	0.290
V0.5C	0.965	0.985	1.000	0.999	0.965	0.983	-0.01	0	0.216
X0.5C	1.000	0.940	1.000	0.999	1	0.939	0	0.010	-0.031
B1.0C	1.049	1.108	1.001	0.998	1.050	1.106	0.09	0.092	0.243
U1.0C	0.955	0.927	1.001	0.999	0.956	0.926	0.09	0.090	0.189
V1.0C	0.898	1.033	1.000	0.999	0.899	1.032	0.07	0.016	-0.237
X1.0C	0.959	0.943	1.000	0.999	0.960	0.942	0.07	0	-0.031
B0.5S	0.959	0.755	1.000	0.999	0.959	0.754	0.01	0.539	0.964
U0.5S	0.852	0.694	1.000	0.999	0.852	0.693	0.01	0.313	0.549
V0.5S	0.867	0.939	1.000	0.999	0.867	0.938	0	0.094	0.185
X0.5S	0.813	0.881	1.000	1	0.813	0.881	0.01	0	0.093
B1.0S	0.952	0.779	1.001	0.999	0.953	0.778	0.11	0.317	0.587
U1.0S	1.000	0.744	1.001	0.999	1.001	0.743	0.11	0.390	0.555
V1.0S	0.895	0.846	1.000	0.999	0.895	0.845	0.07	0.059	0.108
X1.0S	0.917	0.922	1.000	0.999	0.918	0.921	0.07	0.006	0.031

Table P5.9. Samples evacuated to about 250 mbar.

	Before freezing						After freezing						
Letter	$Q_{d0(105°)}$	f_{d0}	Q_{w0}	Q_0	f_{w0}	S_0	Q_n	f_{wn}	$Q_{dn(105°)}$	f_{dn}	Q_{an}	Q_{wn}	S_n
B0.5C	126.69	1680	79.31	139.82	1020	0.996	139.63	900	126.66	1600	139.87	79.58	0.982
U0.5C	124.79	1690	78.1	137.76	1020	0.989	137.56	900	124.77	1620	137.9	78.33	0.974
V0.5C	144.43	2300	90.36	154.81	1360	0.955	154.67	1260	144.38	2220	155.3	90.87	0.942
X0.5C	146.81	2720	91.85	157.47	2000	0.966	157.37	1920	146.75	2640	157.84	92.27	0.958
B1.0C	126.99	1640	79.24	140.19	1010	0.972	140.08	940	127.05	1630	140.57	79.7	0.964
U1.0C	118.52	1730	73.76	130.32	1100	0.945	130.36	1000	118.57	1680	131.01	74.45	0.948
V1.0C	137.39	2240	85.83	147.4	1400	0.919	147.39	1270	137.4	2220	148.28	86.65	0.918
X1.0C	146.59	2760	91.3	156.76	2040	0.925	156.87	1960	146.6	2720	157.59	91.96	0.934
B0.5S	125.29	1720	78.05	137.95	1000	0.950	138.04	940	125.25	1630	138.61	78.49	0.957
U0.5S	115.68	1680	72.12	127.46	1070	0.946	127.53	960	115.64	1680	128.13	72.52	0.952
V0.5S	144.59	2280	90.12	155.19	1290	0.915	155.14	1260	144.54	2210	156.17	90.98	0.911
X0.5S	148.43	2880	92.41	158.71	2080	0.924	158.65	1980	148.38	2860	159.56	93.23	0.919
B1.0S	126.88	1640	79.57	140.38	1000	1	140.2	920	126.93	1580	140.35	79.58	0.989
U1.0S	126.98	1790	79.53	139.73	1000	0.976	139.89	930	127.03	1740	140.04	79.62	0.988
V1.0S	143.44	2160	89.77	154.09	1320	0.953	153.92	1140	143.41	1940	154.61	90.25	0.938
X1.0S	146.3	2840	91.56	156.97	2080	0.966	156.9	1960	146.29	2680	157.34	91.64	0.960

	Calculated values							*perm.*	*max.*
Letter	$(f_{dn}/f_{d0})^2$	$(f_{wn}/f_{w0})^2$	CF_d	CF_w	E_{dn}/E_{d0}	E_{wn}/E_{w0}	Q_{dn}-Q_{d0}	*dil. (‰)*	*dil. (‰)*
B0.5C	0.907	0.779	1.000	0.999	0.907	0.777	-0.03	0.343	0.678
U0.5C	0.919	0.779	1.000	0.999	0.919	0.777	-0.02	0.472	0.772
V0.5C	0.932	0.858	1.000	0.999	0.931	0.858	-0.05	0.090	0.148
X0.5C	0.942	0.922	1.000	0.999	0.942	0.921	-0.06	0.016	0.135
B1.0C	0.988	0.866	1.000	0.999	0.988	0.866	0.06	0.174	0.382
U1.0C	0.943	0.826	1.000	1.000	0.943	0.827	0.05	0.114	0.263
V1.0C	0.982	0.823	1.000	1.000	0.982	0.823	0.01	0.041	0.000
X1.0C	0.971	0.923	1.000	1.001	0.971	0.924	0.01	0.006	0.023
B0.5S	0.898	0.884	1.000	1.001	0.898	0.884	-0.04	0.198	0.418
U0.5S	1.000	0.805	1.000	1.001	1	0.805	-0.04	0.237	0.445
V0.5S	0.940	0.954	1.000	1.000	0.939	0.954	-0.05	0.014	-0.130
X0.5S	0.986	0.906	1.000	1.000	0.986	0.906	-0.05	0.010	-0.031
B1.0S	0.928	0.846	1.000	0.999	0.929	0.845	0.05	0.419	0.763
U1.0S	0.945	0.865	1.000	1.001	0.945	0.866	0.05	0.439	0.761
V1.0S	0.807	0.746	1.000	0.999	0.807	0.745	-0.03	0.157	0.095
X1.0S	0.890	0.888	1.000	1.000	0.890	0.888	-0.01	0.035	0.208

Table P5.10. Samples evacuated to about 1 mbar (vacuum).

	Before freezing					After freezing							
Letter	$Q_{d0(105°)}$	f_{d0}	Q_{w0}	Q_0	f_{w0}	Q_n	f_{wn}	$Q_{dn(105°)}$	f_{dn}	Q_{an}	Q_{wn}	S_n	V_n
B0.5C	124.09	1440	77.97	137.21	800	136.97	750	124.13	1420	137.18	77.92	0.984	59.26
U0.5C	123.93	1700	77.84	136.51	1120	136.32	915	123.96	1600	136.52	77.79	0.984	58.73
V0.5C	134.98	2120	85.03	145.39	1300	145.08	1140	135.01	2070	145.3	84.93	0.979	60.37
X0.5C	145.03	2680	91.19	155.83	2020	155.38	1900	145.07	2640	155.9	91.18	0.952	64.72
K0.5C	169	3960	107.25	170.78	3880	170.69	3760	169.01	4000	170.94	107.25	0.870	63.69
B1.0C	129.01	1720	81.17	142.65	1060	142.4	930	129.18	1680	142.7	80.96	0.978	61.74
U1.0C	127.29	1780	80.02	140.49	1000	140.24	880	127.41	1600	140.46	79.87	0.983	60.59
V1.0C	132.73	2200	83.66	143.48	1380	143.21	1180	132.82	2080	143.42	83.63	0.980	59.79
X1.0C	147.01	2720	92.48	158.21	2000	157.93	1780	147.09	2620	158.04	92.29	0.990	65.75
K0.5S	167.54	3960	106.31	169.39	3840	169.24	3800	167.56	3960	169.35	106.21	0.939	63.14
B0.5S	127.96	1450	80.46	141.72	840	141.52	740	127.98	1400	141.47	80.28	1	61.19
U0.5S	125.78	1720	79.03	139.13	1050	138.94	860	125.78	1550	138.88	78.88	1	60
V0.5S	138.58	2240	87.31	149.27	1340	149.13	1180	138.52	2120	149.15	87.09	0.998	62.06
X0.5S	148.05	2850	93.04	159.13	2080	158.94	1840	147.97	2800	159.26	93.08	0.972	66.18
K0.5S	176.72	4040	112.09	178.61	3960	178.47	3840	176.7	4080	178.61	112.08	0.927	66.53
B1.0S	126.83	1500	79.77	140.44	840	140.27	730	126.89	1400	140.28	79.57	0.999	60.71
U1.0S	116.43	1660	73.23	128.91	1020	128.72	840	116.48	1520	128.74	73.07	0.998	55.67
V1.0S	144.85	2300	91.27	155.99	1420	155.8	1180	144.84	2120	155.91	91.15	0.990	64.76
X1.0S	149.59	2800	94.09	160.94	2050	160.74	1800	149.61	2720	160.68	93.92	1	66.76
K1.0S	169.68	4000	107.63	171.44	3880	171.44	3840	169.64	4040	171.38	107.62	1	63.76

	Calculated values							*perm.*	*max.*
Letter	$(f_{dn}/f_{d0})^2$	$(f_{wn}/f_{w0})^2$	CF_d	CF_w	E_{dn}/E_{d0}	E_{wn}/E_{w0}	Q_{dn}-Q_{d0}	*dil. (‰)*	*dil. (‰)*
B0.5C	0.972	0.879	1.000	0.998	0.973	0.877	0.04	0.609	1.133
U0.5C	0.886	0.667	1.000	0.999	0.886	0.667	0.03	0.449	0.761
V0.5C	0.953	0.769	1.000	0.998	0.954	0.767	0.03	0.227	0.533
X0.5C	0.970	0.885	1.000	0.997	0.971	0.882	0.04	0.061	0.254
K0.5C	1.020	0.939	1.000	0.999	1.020	0.939	0.01	0	0.13
B1.0C	0.954	0.770	1.001	0.998	0.955	0.768	0.17	0.384	0.702
U1.0C	0.808	0.774	1.001	0.998	0.809	0.773	0.12	0.541	0.879
V1.0C	0.894	0.731	1.001	0.998	0.894	0.730	0.09	0.339	0.694
X1.0C	0.928	0.792	1.001	0.998	0.928	0.791	0.08	0.108	0.370
K0.5S	1.000	0.979	1.000	0.999	1.000	0.978	0.02	0.06	0.11
B0.5S	0.932	0.776	1.000	0.999	0.932	0.775	0.02	0.739	1.308
U0.5S	0.812	0.671	1.000	0.999	0.812	0.670	0	0.658	1.066
V0.5S	0.896	0.775	1.000	0.999	0.895	0.775	-0.06	0.359	0.711
X0.5S	0.965	0.783	0.999	0.999	0.965	0.782	-0.08	0.347	0.457
K0.5S	1.020	0.940	1.000	0.999	1.020	0.940	-0.02	0.07	0.17
B1.0S	0.871	0.755	1.000	0.999	0.872	0.754	0.06	0.752	1.357
U1.0S	0.838	0.678	1.000	0.999	0.839	0.677	0.05	0.580	0.964
V1.0S	0.850	0.691	1.000	0.999	0.850	0.690	-0.01	0.388	0.754
X1.0S	0.944	0.771	1.000	0.999	0.944	0.770	0.02	0.145	0.513
K1.0S	1.020	0.979	1.000	1.000	1.020	0.979	-0.04	0.09	0.15

Appendix P6.
From Chapter 3.8. Sealed multicycle freeze-thaw test - S_{crit}-test.

Table P6.1. Sandstone Botvide.

	Before freezing							
Letter	$Q_{d0(50°)}$	f_{d0}	Q_{a0}	Q_{w0}	Q_0	f_{w0}	S_0	V_0
B1	140.29	2160	155.72	87.73	149.4	1240	0.594	67.99
B2	137.53	1980	152.57	85.97	147.37	1160	0.659	66.6
B3	137.67	1960	152.61	86.08	148.21	1180	0.709	66.53
B4	141	2060	156.37	88.18	151.95	1170	0.715	68.19
B5	143.65	2060	159.35	89.82	155.14	1180	0.734	69.53
B6	147.65	2100	163.58	92.31	159.74	1200	0.761	71.27
B7	137.68	1980	152.56	86.09	149.24	1180	0.779	66.47
B8	141.07	2040	156.45	88.22	153.35	1180	0.800	68.23
B9	138.78	2000	153.76	86.74	151.13	1170	0.827	67.02
B10	139.74	2000	154.57	87.33	152.2	1180	0.843	67.24
B11	131.72	1920	145.99	82.36	144.16	1140	0.873	63.63
B12	138.38	2080	153.41	86.5	151.23	1240	0.857	66.91
B13	140.29	2040	155.28	87.69	153.88	1180	0.908	67.59
B14	140.33	2080	155.59	87.7	154.82	1220	0.950	67.89
B15	137.25	2040	152.18	85.8	152.18	1210	1.000	66.38

	After freezing							
Letter	Q_n	f_{wn}	$Q_{dn(105°)}$	f_{dn}	Q_{an}	Q_{wn}	S_n	V_n
B1	149.01	1260	140.16	2080	155.71	87.68	0.569	68.03
B2	147.03	1180	137.32	1920	152.42	85.9	0.643	66.52
B3	147.85	1200	137.49	1880	152.57	86.01	0.687	66.56
B4	151.58	1180	140.88	1920	156.37	88.13	0.691	68.24
B5	154.71	1200	143.5	1980	159.36	89.78	0.707	69.58
B6	159.25	1200	147.52	1920	163.53	92.275	0.733	71.255
B7	148.77	1180	137.53	1900	152.49	86.06	0.751	66.43
B8	152.85	1160	140.94	1960	156.42	88.16	0.769	68.26
B9	150.6	1160	138.53	1940	153.67	86.65	0.797	67.02
B10	151.56	1120	139.47	1900	154.55	87.24	0.802	67.31
B11	143.59	1080	131.57	1840	145.94	82.28	0.836	63.66
B12	150.66	1220	138.21	2020	153.39	86.45	0.820	66.94
B13	153.41	1120	140.02	1900	155.19	87.58	0.883	67.61
B14	154.36	1040	140.1	1800	155.62	87.64	0.919	67.98
B15	151.92	850	137.05	1560	152.37	85.74	0.971	66.63

	Calculated values					
Letter	$(f_{dn}/f_{d0})^2$	$(f_{wn}/f_{w0})^2$	CF_d	CF_w	E_{dn}/E_{d0}	E_{wn}/E_{w0}
B1	0.927	1.033	0.999	0.997	0.926	1.030
B2	0.940	1.035	0.998	0.998	0.939	1.032
B3	0.920	1.034	0.999	0.998	0.919	1.032
B4	0.869	1.017	0.999	0.998	0.868	1.015
B5	0.924	1.034	0.999	0.997	0.923	1.031
B6	0.836	1.000	0.999	0.997	0.835	0.997
B7	0.921	1.000	0.999	0.997	0.920	0.997
B8	0.923	0.966	0.999	0.997	0.922	0.963
B9	0.941	0.983	0.998	0.996	0.939	0.980
B10	0.903	0.901	0.998	0.996	0.901	0.897
B11	0.918	0.898	0.999	0.996	0.917	0.894
B12	0.943	0.968	0.999	0.996	0.942	0.964
B13	0.867	0.901	0.998	0.997	0.866	0.898
B14	0.749	0.727	0.998	0.997	0.748	0.725
B15	0.585	0.493	0.999	0.998	0.584	0.493

Table P6.2. Sandstone Uddvide.

	Before freezing							
Letter	$Q_{d0(50°)}$	f_{d0}	Q_{a0}	Q_{w0}	Q_0	f_{w0}	S_0	V_0
U1	140.46	2040	156.77	87.81	150.26	1280	0.606	68.96
U2	140.49	2080	156.89	87.82	151.03	1300	0.647	69.07
U3	139.19	2040	155.33	87.01	150.46	1220	0.702	68.32
U4	135.37	2160	151.17	84.6	146.41	1260	0.703	66.57
U5	134.82	2040	150.5	84.27	146.4	1260	0.742	66.23
U6	138.18	2160	154.31	86.37	150.21	1280	0.748	67.94
U7	135.88	2080	151.68	84.96	148.25	1220	0.785	66.72
U8	133.21	2000	148.88	83.245	145.66	1180	0.797	65.635
U9	139.48	2160	155.68	87.17	152.85	1300	0.827	68.51
U10	136.12	2000	151.98	85.05	149.55	1240	0.849	66.93
U11	134.63	2040	150.29	84.15	148.08	1220	0.861	66.14
U12	137.3	1960	153.07	85.84	151.42	1240	0.897	67.23
U13	137.8	1920	153.88	86.14	152.43	1220	0.911	67.74
U14	136.3	2040	152.16	85.22	151.48	1240	0.958	66.94
U15	133.17	1880	148.75	83.25	148.75	1180	1.000	65.5

	After freezing							
Letter	Q_n	f_{wn}	$Q_{dn(105°)}$	f_{dn}	Q_{an}	Q_{wn}	S_n	V_n
U1	149.87	1300	140.24	1960	156.63	87.73	0.588	68.9
U2	150.67	1310	140.28	1980	156.74	87.75	0.631	68.99
U3	150.04	1240	138.99	2000	155.2	86.93	0.682	68.27
U4	146.02	1280	135.17	2040	151.05	84.52	0.683	66.53
U5	146.06	1280	134.59	2040	150.39	84.18	0.726	66.21
U6	149.87	1280	138.02	2040	154.28	86.32	0.729	67.96
U7	147.9	1240	135.7	1900	151.58	84.87	0.768	66.71
U8	145.27	1270	132.98	2020	148.73	83.16	0.780	65.57
U9	152.47	1260	139.29	2060	155.64	87.12	0.806	68.52
U10	149.13	1240	135.89	2000	151.89	84.98	0.828	66.91
U11	147.71	1200	134.41	1950	150.27	84.08	0.839	66.19
U12	150.7	1150	137.12	1880	153.02	85.77	0.854	67.25
U13	152.06	1120	137.58	1780	153.81	86.07	0.892	67.74
U14	151.12	1040	136.1	1740	152.18	85.15	0.934	67.03
U15	148.51	860	133.01	1460	148.9	83.2	0.975	65.7

	Calculated values					
Letter	$(f_{dn}/f_{d0})^2$	$(f_{wn}/f_{w0})^2$	CF_d	CF_w	E_{dn}/E_{d0}	E_{wn}/E_{w0}
U1	0.923	1.031	0.998	0.997	0.922	1.029
U2	0.906	1.015	0.999	0.998	0.905	1.013
U3	0.961	1.033	0.999	0.997	0.960	1.030
U4	0.892	1.032	0.999	0.997	0.891	1.029
U5	1.000	1.032	0.998	0.998	0.998	1.030
U6	0.892	1.000	0.999	0.998	0.891	0.998
U7	0.834	1.033	0.999	0.998	0.833	1.031
U8	1.020	1.158	0.998	0.997	1.018	1.155
U9	0.910	0.939	0.999	0.998	0.908	0.937
U10	1.000	1.000	0.998	0.997	0.998	0.997
U11	0.914	0.967	0.998	0.998	0.912	0.965
U12	0.920	0.860	0.999	0.995	0.919	0.856
U13	0.859	0.843	0.998	0.998	0.858	0.841
U14	0.728	0.703	0.999	0.998	0.726	0.702
U15	0.603	0.531	0.999	0.998	0.602	0.530

Table P6.3. Sandstone Valar.

	Before freezing							
Letter	$Q_{d0(50°)}$	f_{d0}	Q_{a0}	Q_{w0}	Q_0	f_{w0}	S_0	V_0
1	137.03	2400	146.17	86.06	144.12	1680	0.778	60.11
2	144.67	2400	155.39	90.88	152.95	1520	0.776	64.51
3	145.46	2560	155.18	91.34	153.01	1840	0.780	63.84
4	153.63	3760	158.57	96.62	157.48	3360	0.784	61.95
5	147.5	2400	158.58	92.65	156.63	1520	0.826	65.93
6	143.06	2600	153.31	89.845	151.76	1840	0.851	63.465
7	136.62	2320	146.57	85.82	145.27	1520	0.872	60.75
8	142.61	2340	153.37	89.57	152.09	1520	0.883	63.8
9	138.08	2360	148.78	86.7	147.88	1440	0.917	62.08
10	138.15	2480	147.27	86.76	146.54	1760	0.921	60.51
11	143.65	2400	154.15	90.23	153.55	1520	0.944	63.92
12	142.38	2400	152.89	89.45	152.4	1600	0.954	63.44
13	161.72	3600	165.63	101.75	165.38	3560	0.938	63.88
14	160.33	3640	164.29	100.86	163.06	3500	0.699	63.43
15	144.06	2360	154.82	90.51	155.04	1600	1.020	64.31

	After freezing							
Letter	Q_n	f_{wn}	$Q_{dn(105°)}$	f_{dn}	Q_{an}	Q_{wn}	S_n	V_n
1	143.9	1660	136.92	2320	146.15	86.05	0.756	60.1
2	152.715	1500	144.49	2320	155.38	90.85	0.755	64.53
3	152.785	1780	145.31	2440	155.18	91.315	0.757	63.865
4	157.335	3040	153.52	3040	158.55	96.59	0.758	61.96
5	156.435	1490	147.35	2360	158.53	92.63	0.813	65.9
6	151.515	1770	142.93	2360	153.38	89.815	0.822	63.565
7	145.07	1400	136.44	2200	146.6	85.78	0.849	60.82
8	151.935	1440	142.43	2320	153.39	89.55	0.867	63.84
9	147.74	1400	137.93	2240	148.79	86.66	0.903	62.13
10	146.325	1760	138.01	2400	147.26	86.74	0.899	60.52
11	153.34	1500	143.49	2280	154.19	90.195	0.921	63.995
12	152.225	1330	142.2	2200	152.98	89.425	0.930	63.555
13	165.1	3040	161.6	3120	165.61	101.725	0.873	63.885
14	163.855	3080	160.2	3120	164.27	100.845	0.898	63.425
15	154.87	1120	143.87	1960	155.14	90.47	0.976	64.67

	Calculated values					
Letter	$(f_{dn}/f_{d0})^2$	$(f_{wn}/f_{w0})^2$	CF_d	CF_w	E_{dn}/E_{d0}	E_{wn}/E_{w0}
1	0.934	0.976	0.999	0.998	0.934	0.975
2	0.934	0.974	0.999	0.998	0.933	0.972
3	0.908	0.936	0.999	0.999	0.908	0.934
4	0.654	0.819	0.999	0.999	0.653	0.818
5	0.967	0.961	0.999	0.999	0.966	0.960
6	0.824	0.925	0.999	0.998	0.823	0.924
7	0.899	0.848	0.999	0.999	0.898	0.847
8	0.983	0.898	0.999	0.999	0.982	0.897
9	0.901	0.945	0.999	0.999	0.900	0.944
10	0.937	1.000	0.999	0.999	0.936	0.999
11	0.903	0.974	0.999	0.999	0.901	0.973
12	0.840	0.691	0.999	0.999	0.839	0.690
13	0.751	0.729	0.999	0.998	0.751	0.728
14	0.735	0.774	0.999	1.005	0.734	0.778
15	0.690	0.490	0.999	0.999	0.689	0.489

In Table P6.4 below:

Letter G means granite Bohus Red Bratteby.
Letter K means limestone Öland B1.
Letter V means that the specimens were vacuum saturated with pure water.
Letter S means that the specimens were vacuum saturated with a 2% solution of $Na_2SO_4 \cdot 10H_2O$.

Table P6.4. Granite and limestone.

	Before freezing							
Letter	$Q_{d0(50°)}$	f_{d0}	Q_{a0}	Q_{w0}	Q_0	f_{w0}	S_0	V_0
GV1	179.44	5040	179.64	111.95	179.6	5040	0.886	67.69
GV2	182.97	5040	183.21	114.17	183.13	5040	0.795	69.04
GS1	185.25	5100			185.45	5280	1.474*	
GS2	181.57	5120			181.75	5280	0.786*	
KV1	177.16	4080	179.56	112.15	179.47	3920	0.965	67.41
KV2	177.53	4040	179.83	112.37	179.71	3960	0.951	67.46
KS1	178.95	4120			181.16	3800	1.024*	
KS2	176.43	4080			178.52	3840	0.977*	

	After freezing							
Letter	Q_n	f_{wn}	$Q_{dn(105°)}$	f_{dn}	Q_{an}	Q_{wn}	S_n	V_n
GV1	179.55	4920	179.29	4640	179.7	111.93	0.634	67.77
GV2	183.08	4960	182.82	4640	183.24	114.14	0.619	69.1
GS1	185.39	5040	184.82	**			1.333*	
GS2	181.7	4880	181.42	4720			0.667*	
KV1	179.44	3880	176.98	4000	179.57	112.11	0.950	67.46
KV2	179.61	4000	177.37	4080	179.86	112.35	0.900	67.51
KS1	181.08	3920	178.8	4020			0.990*	
KS2	178.47	4000	176.3	4040			0.955*	

Calculated values					
$(f_{dn}/f_{d0})^2$	$(f_{wn}/f_{w0})^2$	CF_d	CF_w	E_{dn}/E_{d0}	E_{wn}/E_{w0}
0.848	0.953	0.999	1.000	0.847	0.953
0.848	0.969	0.999	1.000	0.847	0.968
	0.911	0.998	1.000		0.911
0.850	0.854	0.999	1.000	0.849	0.854
0.961	0.980	0.999	1.000	0.960	0.980
1.020	1.020	0.999	0.999	1.019	1.020
0.952	1.064	0.999	1.000	0.951	1.064
0.980	1.085	0.999	1.000	0.980	1.085

* S is calculated according to Equation P.2, with $Q_{ds} = 0$.
** The sample was broken by accident.